Study of the size and distribution of landslides in the Zagros mountains (Iran)

Ghazipour, Neda

UNIVERSITE DE GENEVE

FACULTÉ DES SCIENCES

Département de Sciences de la Terre

Director: Prof. Costanza Bonadonna
Co-director: Dr. Guy Simpson

Study of the Size and Distribution of Landslides in the Zagros Mountains (Iran)

THÈSE

Présentée à la Faculté des Sciences de l'Université de Genève pour obtenir le grade de Docteur ès sciences, mention Sciences de la Terre

par

Neda Ghazipour

de

Tabriz (Iran)

These N°

4806

GENÈVE

Section des sciences de la Terre

2015

ABSTRACT

This study investigates the size distribution of large mass movements in the seismically active Zagros mountain belt (southwest Iran) using a new inventory developed in this project. I have identified and documented 335 large landslides detectable in Google Earth™ images. Geometrical measurements and geological information on landslides were extracted from a digital elevation model with a 30m resolution and 140 geological maps at a 1:100000 scale.

Individual landslides have volumes ranging from 10^4 to 3×10^{10} m^3 and cover areas ranging from 10^3 to 10^8 m^2. The relationship between landslide volumes (V_L) and areas (A_L) is well described by a power law of the form $V_L = A_L^{\alpha}$ where α = 1.49 over five orders of magnitude of A_L and seven orders of magnitude of V_L. The cumulative volume distribution of the largest slope failures (about 50%) are well describe by an inverse power law of the form $N_L = 10^{7.3} V_L^{-0.675}$ for $V_L \geq 3.2\times10^7 m^3$.

I show that the frequency-size (i.e. volume) distribution is heavy tailed, following a power law for the largest landslides (>10^7 m^3) with a scaling exponent β = 1.51. Non power law behaviour for smaller landslides is probably an artefact due to the relatively low resolution nature of the data, such that we are essentially missing many small landslides.

Comparison of the results with other published datasets shows that the Zagros landslides are truly large and show similar scaling behaviour to that observed in other regions, especially to datasets where landslides are relatively large (deep seated) and occur in relatively resistant materials (e.g. consolidated rocks, as opposed to soil).

I investigated twelve factors using Principal Component Analysis (PCA) to determine the role and relative importance of landslide causatives (i.e. geological, geomorphological and physical factors). The results reveal that the combination of parameters that control the frequency of landslides (i.e., fluvial channels, active faults and folds) are different from those factors controlling their size (i.e., topographic relief, elevation and slope). Some factors like lithological type and dip direction affect both landslide volume and frequency.

The spatial pattern of landslides shows that the size of landslides is larger in the northern part of the Zagros region and decreases towards the south and east, while they are more abundant in the southeast and their frequency decreases towards the north and west. I conclude that the larger size of landslides in the western part of the Zagros is a result of the high elevation, high topographic relief and extensive outcrops of carbonate rock in this region. In comparison, the eastern part of the Zagros has more frequent small landslides due to the presence of less consolidated (evaporite) rocks. Finally, I speculate that the giant landslides of the Zagros were most likely triggered by enhanced precipitation during the early-mid Holocene rather than by large earthquakes.

RÉSUMÉ

Cette étude a pour objet la répartition des instabilités de versants de grande ampleur dans la chaîne du Zagros (Iran du Sud-Ouest), qui est active sismiquement. Un nouvel inventaire a été réalisé dans le cadre de ce projet. Au total 335 instabilités de grand volume reconnaissables sur les images Google Earth™ ont été recensées. Les données sur la géométrie, les mensurations et la géologie des instabilités ont été extraites d'un modèle numérique d'altitude d'une résolution de 30 m et de 140 cartes géologiques à l'échelle 1:100000.

Les instabilités de versant montrent des volumes compris entre 10^4 et 3×10^{10} m^3 et occupent des surfaces allant de 10^3 à 10^8 m^2. La relation entre le volume (V_L) des instabilités et leur surface (A_L) est bien décrite par une loi de puissance de forme $V_L = A_L^{\alpha}$ où α = 1.49 à travers cinq ordres de grandeur de A_L et sept ordres de grandeur de V_L. La distribution en volume cumulé des plus grandes instabilités (environ 50% d'entre elles) est bien décrite par une loi de puissance de forme $N_L = 10^{7.3} V_L^{-0.675}$ pour $V_L \geq 3.2\times10^7$ m^3.

Le diagramme de distribution de la fréquence de taille des instabilités (c.-à-d. de leur volume) suit une loi de puissance avec une constante de proportionnalité β = 1.51 pour les instabilités majeures (> 10^7 m^3), mais présente une queue importante. Le fait que la distribution des instabilités de plus faible volume ne suit pas une loi de puissance résulte probablement d'un biais d'échantillonnage, la faible résolution des données ne permettant pas de les détecter toutes.

La comparaison des résultats obtenus avec d'autres bases de données publiées met en évidence que les instabilités sont de très grand volume dans le Zagros et qu'elles montrent des distributions de tailles similaires à celles observées dans d'autres regions. L'analogie est particulièrement bonne avec les regions où les instabilités de versant sont de grande taille (avec une surface de glissement profonde) et affectent des lithologies relativement compétentes (p. ex. des roches consolidées plutôt que des sols).

Une analyse en composante principale (ACP) basée sur douze paramètres a été réalisée afin de determiner l'importance relative de différents facteurs de prédisposition aux instabilités (c.-à-d. les facteurs géologiques, géomorphologiques et physiques). Les résultats démontrent que la combinaison des paramètres qui contrôlent la fréquence des instabilités (c.-à-d. les incisions fluviatiles, les failles actives et les plis) est différente de celle qui contrôle leur taille (c.à.d. le relief topographique, l'altitude et la pente). Certains facteurs comme le type lithologique et le pendage des couches influencent à la fois le volume et la fréquence des instabilités.

La répartition spatiale des instabilités de versant montre que les leur taille est plus importante dans la partie Nord du Zagros et qu'elle diminue en direction du Sud et de l'Est. Les instabilités sont par contre plus nombreuses dans le Sud-Ouest et leur fréquence diminue en direction du Nord et de l'Ouest. On peut en conclure que la grande taille des instabilités dans la partie occidentale du Zagros est corrélée avec l'altitude élevée, le relief très accidenté et la grande proportion de calcaires affleurants dans cette région. En comparaison, la partie orientale du Zagros présente une plus grande fréquence d'instabilités de plus petite taille en raison de la présence de roches moins résistantes (évaporites). Il est également postulé que les instabilités de versant "géantes" du Zagros ont été déclenchées par l'augmentation des précipitations durant l'Holocène inférieur et moyen plutôt que par des tremblements de terre majeurs.

ACKNOWLEDGMENT

Foremost, I would like to express my deepest thanks to my advisor, Dr. Guy Simpson for giving me the opportunity to work with him and for his guidance throughout my Ph.D. His patience, encouragement, and immense knowledge were key motivations throughout my PhD. I would also like to thank Dr. Katja Petrini, for her encouragement and emotional support during difficult times.

I would like to thank Prof. Costanza Bonadonna, Dr. Mario Sartori, and Dr. Marc-Henri Derron for their valuable comments and suggestions and for letting me benefit from their knowledge. I am very thankful for their efforts and the time they spent serving on my committee.

I am grateful to Dr. Stéphanie Girardclos, Dr.Corine Frischknecht, Dr. Marc-Henri Derronand Dr. Jamshid Hassan Zadehfor and Dr. Irene Manzella for their valuable advice and suggestions that have inspired me new research directions.

My deepest gratitude goes to Mortaza Pirouz, who taught me Petrel software to create 3D model of landslides, Seyed Abolfazl Hosseini, who consulted me for identifying percentage of each lithology in each geological formation and Gholamhossein Bagheri for his help and comments on my script.

This dissertation would not have been possible without emotional support of my parents. Words cannot express how grateful I am to my father, (Rashid Ghazipour) my mother (Nasrin Pour Ramezan Nejad) and my husband (Mortaza Pirouz), all of the sacrifices that you've made on my behalf. Thanks for believing in me, I can't thank you enough for encouraging me throughout this experience. I wish to dedicate this thesis to my family.

I also had the great pleasure of meeting Prof. Urs Schaltegger, Prof. Rosanna Martini, Prof. Daniel Ariztegui, Dr. Elias Samankassou and Mrs. Sofia Saldana.

Lucia Dominguez, Camille Thomas, Haseeb Zia, Antonio Benventi, Eduardo Rossi, Federico Brogi, Stefano Pollastri, Mahmoud Leila, Gholamhossein Bagheri for being good friends and their support and encourage especially when I have been far from my family.

I am thankful to my officemates for being friendly and welcoming and creating a positive working environment Fiona Burns, Valentin Chesnel, Antoine De Haller, Azarm Farzam , Caroline Bouvet de Maisonneuve.

I would like to thank Ali Farzam, Sedigheh Beygom Farzam and Azarm Farzam for making unforgettable moments in some beautiful places in Switzerland.

I also would like to thanks Gholamhossein Bagheri and Pari Asadi, for enjoyable times that we have had together during these years. I have greatly enjoyed the opportunity to be with you.

Last but not least, I have been very privileged to get to know and to collaborate with many other great people who became friends over the last several years at the University of Geneva. My gratitude goes to my friends and colleagues of the Maraîchers building, especially Chloé Pretet, Mélanie Gretz, Jeremy Ragusa, Katrina Kremer, Matar N'Diaye, Lina Ospina-Ostios, Arnoud Slootman, Valentin Chesnel, Jennifer Fischer, Agathe Martignier, Eric Herrwagen, Erika Baldessin, Jorn Wotzlaw and Ryan Cochrane.

Neda Ghazipour

Geneva, 2015

Table of contents

Chapter1: Introduction

Chapter 2: Size distribution of landslides in the Zagros mountain belt

Chapter 3: Spatial Pattern of landslides

Chapter 4: Factors controlling the spatial distribution of landslides in the Zagros region

Chapter 5: Multivariate analysis of landslide sizes in the Zagros region

Chapter 6: Discussion and Conclusion

List of appendix

List of references

List of Figures

Chapter 1: Introduction

Chapter 2: Size distribution of landslides in the Zagros mountain belt

Chapter 3: Spatial pattern of landslides

Chapter 4: Factors controlling the spatial distribution of landslides in the Zagros region

Chapter 5: Multivariate analysis of landslide size in the Zagros region

Chapter 6: Discussion and Conclusion

List of Tables

Chapter 2: Size distribution of landslides in the Zagros mountain belt

Chapter 3: Spatial pattern of landslides

Chapter 5: Multivariate analysis of landslide size in the Zagros region

List of Appendix

Chapter 1

INTRODUCTION

Landslides are a complex natural phenomenon forming a serious risk to humans living in regions where significant local relief coincides with large populations (Brabb and Harrod, 1989; Brabb, 1991; Alexander, 2004). They also play an important role in the surface evolution of mountain belts by redistributing mass from more elevated to less elevated regions (Densmore et al., 1997; Stark and Hovius, 2001; Malamud et al., 2004; Korup et al., 2007; Hewitt et al., 2008; Korup et al., 2010; Guzzetti et al., 2012). In many countries, landslides are a first order risk (due to economic losses and fatalities) comparable with earthquakes, floods and windstorms (Schuster and Fleming, 1986; Turner and Schuster, 1996; Guzzetti et al., 1999a; Hart, 2004). Worldwide landslide fatalities and related costs are rising as a result of increasing populations due to expansion of human settlements into increasingly hazardous terrains (Alexander, 1993; Hart, 2004) in both developing and industrial countries. Fatalities associated with mass movements are high in developing and third world countries (Shah, 1983; Alexander, 1993; Charman and Griffiths, 1993; Hart, 2004), whereas economic losses are more severe in the industrialised world (Schuster and Fleming, 1986; Guzzetti et al., 1999). In either case, the impact of landsides is strongly governed by the volume or mass of material displaced and/or by how many landslides of each size occur.

The primary aim of this study is to better understand the size and frequency of landslides in active mountain belts, using the Zagros as an example. To achieve this goal we need to analyse large landslides where these features are well exposed and can be accurately measured (because of lower limit of resolution of DEM data). This study also investigates the various primary factors that might be important in controlling the size and frequency of the observed slope instabilities.

One result of this study is the generation of a new landslide inventory for the Zagros that focuses on landslides with volumes exceeding 10^4 m^3. This medium to large inventory mostly includes either slides (slumps, rockslides, debris slides and earth slides) or complex mass movements, based on the classification scheme proposed by the British Geological Survey (Varnes, 1978; Cruden and Varnes, 1996; Hungr et al., 2013).

These kind of inventories are valuable for assessing the distribution and patterns of landslides in a particular region. They can be used to show the location of old failures and areas where mass failures are more frequent. However, these inventories are not suitable for identifying the location of new failures but they help to prepare a risk and/or hazard map. The statistical assessment of existing landslides assumes that the prediction of future landslide areas can be assessed by measuring the combination of variables that have led to past events (Ohlmacher and Davis, 2003; Lee and Pradhan, 2006; Legorreta Paulin, 2007).

1.1 LANDSLIDES IN IRAN

Landslides are one of the most common and significant natural hazards in Iran. However, there is a severe lack of precise information about landslides for most parts of the country. Previous studies estimated an average annual cost of landslide damage at around 190 million US dollars (Komak panah et al., 1994). Only a small percentage of the countrys' area has been investigated in landslide inventories and landslide susceptibility maps (e.g. Tehran, Southern Caspian sea, Lorestan)("www.iiees.ac.ir/iiees/geo/geo_tech1.html" ; Safavi and Mirsaneii, 2009; Babakan et al., 2009), and very little advantage of this knowledge has been used to reduce hazards of this phenomenon in Iran.

The distribution and nature of landslides in Iran is poorly understood, due to lack of systematic investigations. There are only a handful of published master and doctoral theses (Alimohammadi, 2005; Shayan, 2006; Babakan et al., 2009; Rajabi et al., 2011; Shirani and Seif, 2012). In 1996 a project was initiated by the ministry of Jihad-e-Sazandegi to develop a list of the landslides in Iran to establish their extent and significance. In the first stage, the database was compiled from field observation. Database compilation continued using aerial photograph. The most significant landslides were selected for field observation and their detailed information was recorded. During the ten years between 1996 and 2006 detailed information on 4420 landslides with different sizes have been recorded. These mass failures caused 185 fatalities and their damages are estimated at about 14 million dollars ("landslide.ir"). In addition, the location of 14200 events were recognized on aerial photographs and recorded on topographic maps. Of the total number of records, only 782 landslides were located in the Zagros region (Fig. 1.1).

1.2 LANDSLIDE INVENTORY OF THE ZAGROS REGION

The Zagros is one of the most famous and well-studied geological provinces in the world, in terms of its rich hydrocarbon reserves and extreme seismic activity. However the nature and distribution of landslides in the Zagros are poorly understood. The Zagros has numerous pre-historic landslides (e.g. Seimareh and Gahar landslides) but they have never been the subject of a uniform and systematic study.

A review of published literature and reports reveals that research on landslides within the Zagros region has focused mostly on using remote sensing imagery (unpublished data "Forests, range and watershed management organization of Iran"). Previous regional studies were limited to zonation and geotechnical hazard mapping of the Lorestan province (unpublished data, "www.iiees.ac.ir/iiees/geo/geo_tech1.html"). An inventory of landslides exists in the Lorestan province and in some parts of the Fars province ("Forests, range and watershed management organization of Iran") (Fig.1.1).

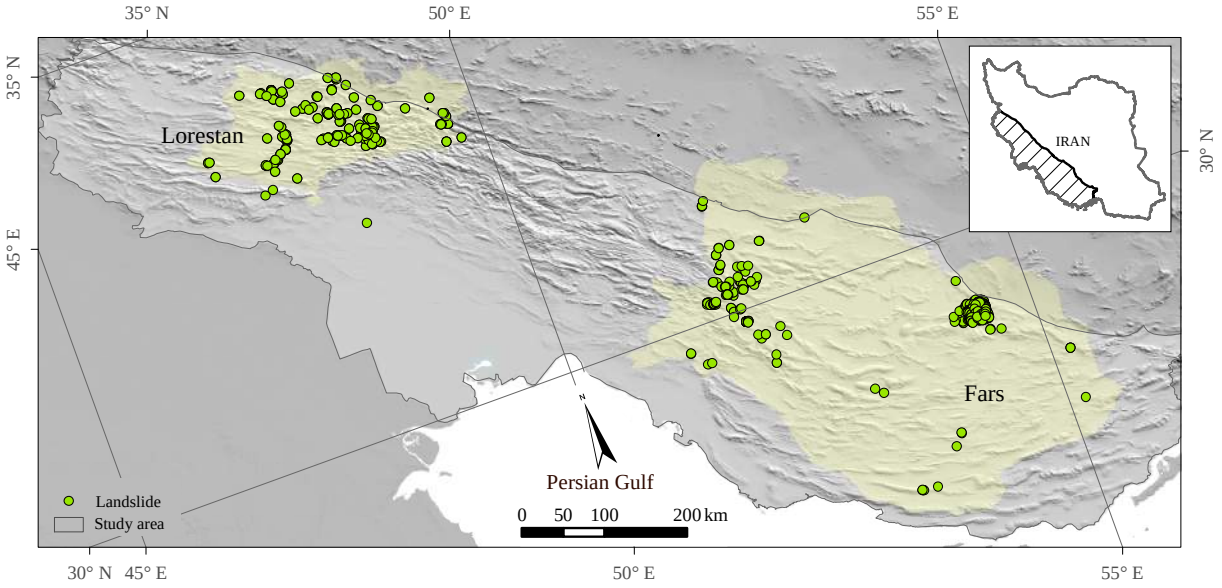

Fig.1.1 Previously recorded landslides of the Zagros region N_L= 782. Data from the Forests, range and watershed management of Iran (1996 - 2010).

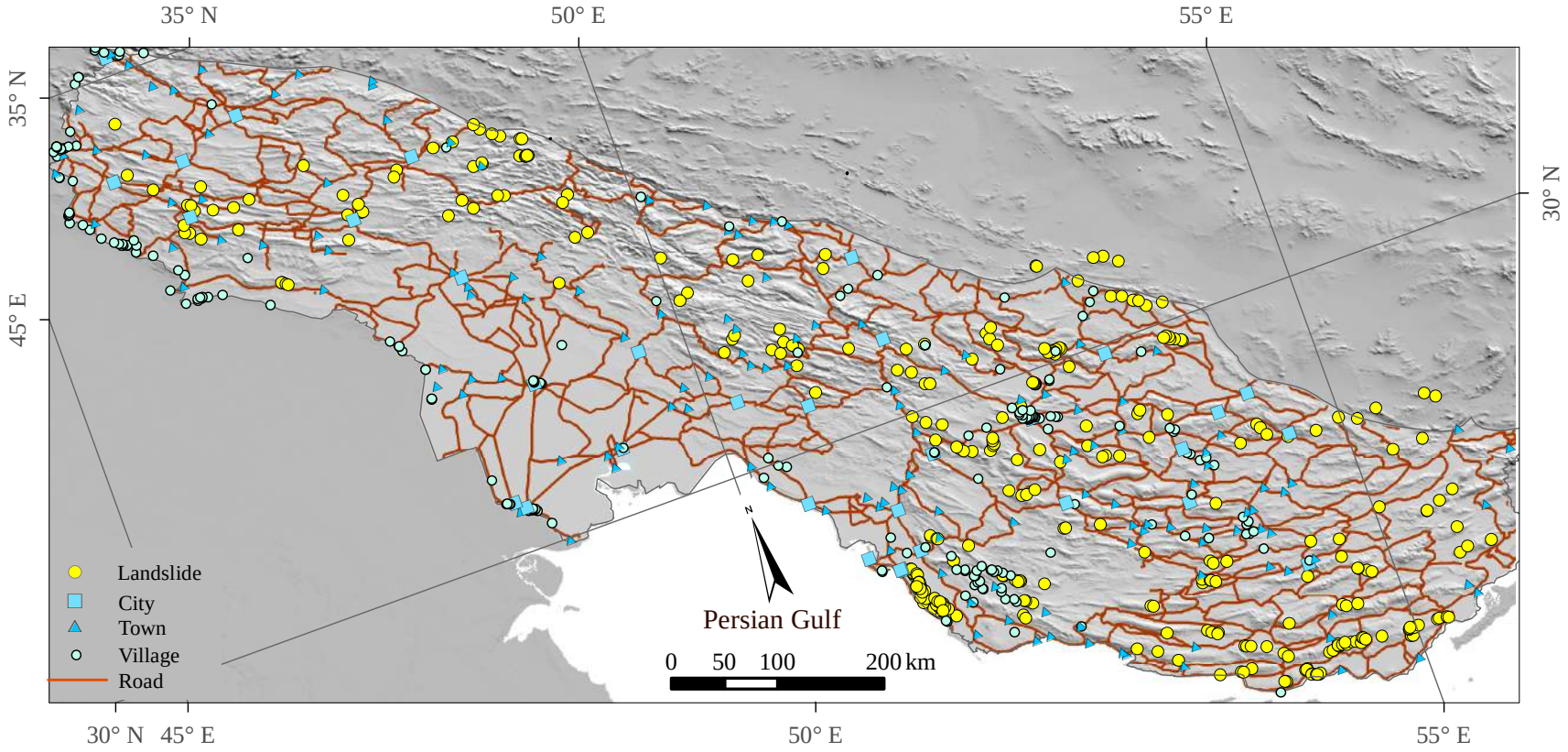

Fig. 1.2. Distribution of large landslides (>10^4 m^3) in the Zagros region and location of settlements and main roads.

There are some individual studies at the watershed scale or of single mass movements in the Zagros region (Harrison and Falcon, 1938; Shoaei et al., 1998; Shayan, 2006; Rajabi et al., 2011; Roberts and Evans, 2013; Othman and Gloaguen, 2013).

In the Zagros region, a fatal event occurred in April 1998 due to mass failure in cretaceous limestones following heavy rainfall. This dramatic landslide buried the Abikar village and killed all fifty-five habitants (Bolourchi and Ansari, 1998). Many other settlements and infrastructures are under constant threat from slope instabilities in this mountainous area (Fig. 1.2). These examples highlight the importance of study landslides in this region.

1.3 Examples of Zagros landslides

Some examples of distinct landslide features of deep seated rock avalanches and earth slides that were identified in the Zagros are illustrated in this section. Ground features of these movements include source areas and/or accumulation zones. Two examples of the largest landslides observed in the field and in Google Earth images are presented in Figures 1.3 and 1.4. Fig. 1.3A shows a satellite image of the Seymareh rock avalanche and Fig 1.3B shows its field picture. The landslide excavation area is 15.5 km wide across slope and 7.5 km long down slope (see Fig. 1.3A). The debris is composed of angular limestone ranging from fine soil to large boulders (25m×10m×8m) (see Fig 1.3B). As already mentioned, because of the 15 km run out of this huge rock avalanche, the boundary of debris is not recognisable in the field but its indicators are completely clear from remote sensing. A Google Earth view of a complex landslide is shown in Fig. 1.4A and its field picture is represented in Fig. 1.4B. In the case of large deep seated landslides, such as these two examples, it is important to establish the exact boundary of the mass movement. This is because an error in mapping the boundary could significantly influence the volume measurement.

Another example of pre-historic landslides (unknown age) is observed in Gahar where two landslides blocked a valley to form a natural lake Fig. 1.5. Fig. 1.5A and B show the Google Earth view of these landslides, along with a field photo. The volume of the northern landslide was measured to be 3×10^7 m^3 while the southern landslide was measured to be 5.5×10^7 m^3. A lot of ancient landslides are detected close to cities and villages in the Zagros region. Fig. 1.6A and 1.6B show a debris slide that is a part of a complex landslide that is located 800 m east of the Sepid Dasht town. Other examples of towns and villages that are located close to large landslides are Dashtak, Bakan, Eydooni, Kalani and Dasgte Barm in the Fars province, Dorud in the Lorestan province, Sheikh habil and Arand in the Kohkiluye- Boyerahmad province, and Sarghale in the Chahar Mahal va Bakhtiari province.

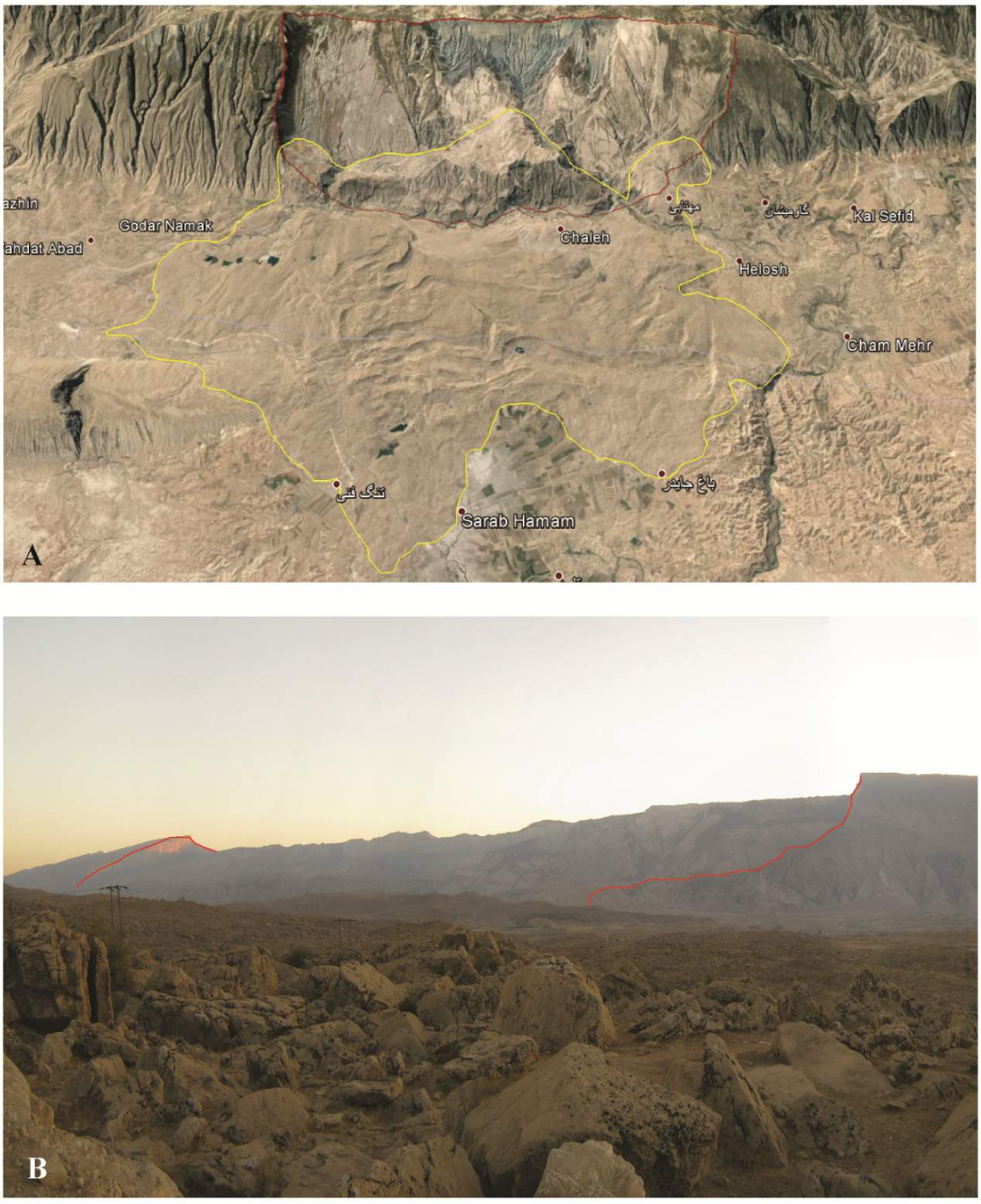

Fig. 1.3. An example of the Seymareh rock avalanche (panel A and B) (33° 00' 15.23" N, 47° 36' 40.87" E) in the Zagros region.

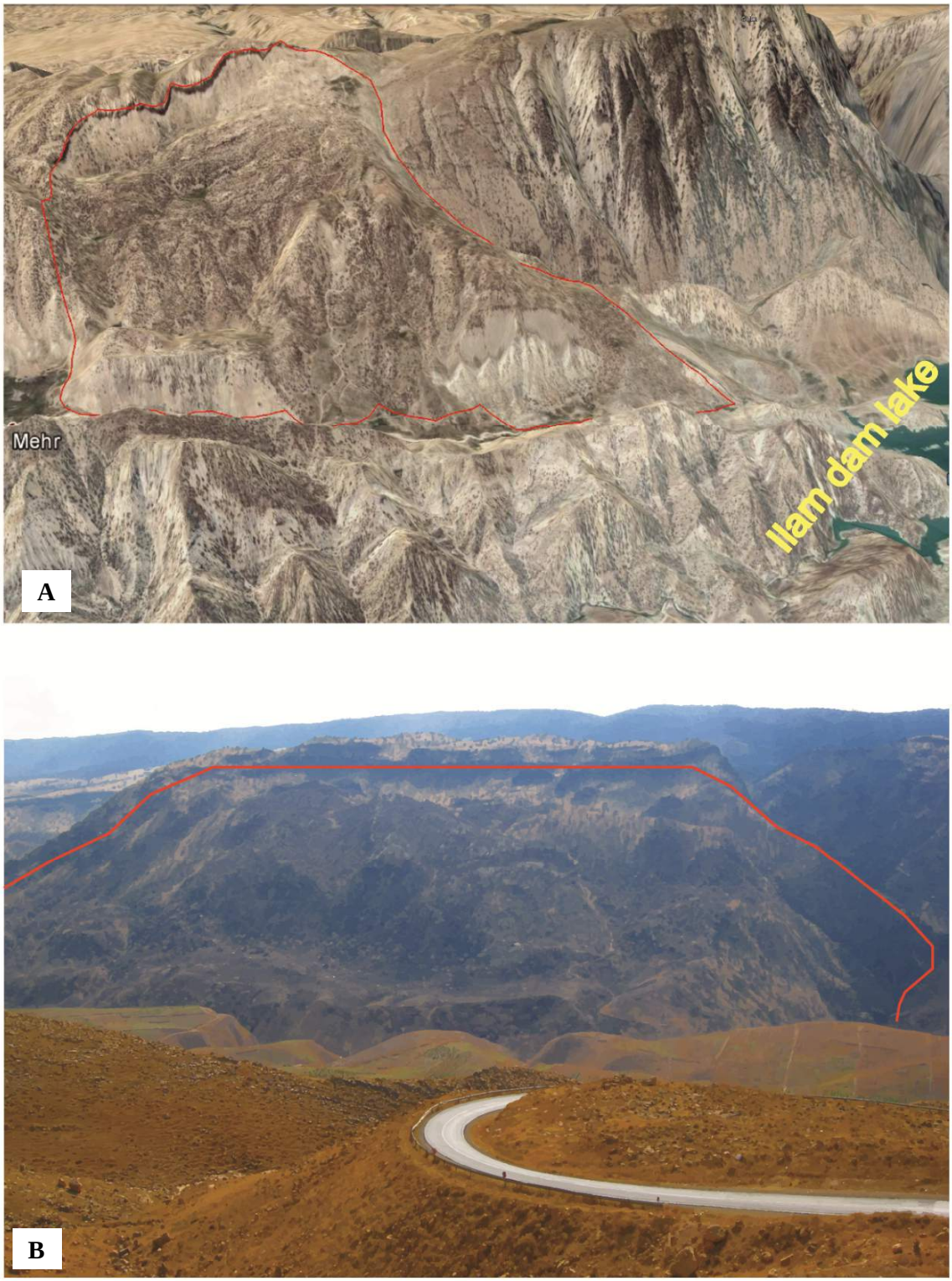

Fig. 1.4. An example of a complex landslide (panel A and B) (33° 26' 03.63" N, 46° 26' 25.68" E) in the Zagros region. Lack of vegetation in this region makes it suitable for investigation by remote sensing.

Fig. 1.5. Panels A and B represent a Google earth image and a field picture of the Gahar barrier lake, respectively (see above). Two landslides deposits are observed on (identified with red polygons) (33° 18' 54.16" N, 49° 16' 15.47" E) (33° 18' 42.13" N, 49° 17' 02.89" E) from scars located on both sides of the valley. The lake is 2.5 km long and 500 m wide.

Fig. 1.6. Panel A represents a Google Earth image and a field picture (B) of a landslide that is located east of the Sepid Dasht town, (33° 13' 00.57" N, 48° 53' 48.78" E) in the Lorestan province.

1.4 Study area

The Zagros mountain chain that is the focus of this study is situated in southwest Iran. It extends for more than 1500 km from the border of Iran in the west to the Strait of Hormuz in the east. The Zagros is a 200 - 300 km wide belt bordered to the northeast by the Main Zagros Reverse Fault (MZRF) and to the southeast by the Zagros Foredeep Fault (ZFF) (Fig. 1.7).

The Zagros consists mainly of continental margin and foreland basin sedimentary rocks including mainly carbonate, marl, sandstone, evaporite and conglomerate (Colman-Sadd, 1978; Alavi, 2004; Pirouz, 2013) but also includes volcanic and metamorphic rocks (Fig. 1.8).

1.4.1 Brief introduction to tectonics of the Zagros

The Zagros is one of the most seismically active belts of Asia, with frequent earthquakes of up to Mw 7.0 (Fig. 1.9). This seismic activity results from the collision of the Eurasian and Iranian lithospheric plates, which are currently converging at rates exceeding 20 mm/year (McClusky et al., 2003; Vernant et al., 2004; Bayer et al., 2006; Walpersdorf et al., 2006). The rate of convergence and its angle is heterogeneous along the fold thrust belt (Chu and Gordon, 1998; McClusky et al., 2003) (Fig. 1.10). It increases from the north-western Zagros to the south-eastern part of the region (Vernant et al., 2004).

The change in convergence rate coincides with the N-S Kazerun fault (see Fig. 1.10) that separates the Zagros into two different deformation zones (Walpersdorf et al., 2006; Berberian, 1995; Talebian and Jackson, 2004; Authemayou et al., 2005). Not only are the general structures and intensity of deformation significantly different on both sides of the Kazerun fault but the distribution of sedimentary rocks also varies between these regions (Pirouz, 2013). The Zagros region has been divided into three main geological provinces that are known as the Fars, Khuzestan and Lorestan provinces from east to west (Berberian, 1995).

1.4.2 Morphology and topography of the Zagros

The Zagros has maximum and mean elevations of 4400 and 1070 m, respectively. The elevation is generally highest in the north and decreases towards the south and east (Fig. 1.11). The Fars region has a maximum elevation of 2000 meters, whereas the western part of the Zagros has the highest elevation of the region. The two highest peaks of the Zagros mountain belt, Zard-kuh and Dena that reach more than 4000 m above sea level, are located in the western part of the Zagros region. Local relief in the Zagros ranges between 0 and 2900 m with an average of 840 meters (see chapter 4). This high relief is the result of active thrusting and folding of the sedimentary sequence (Fig. 1.12). Figure 1.12 clearly show that high relief areas are mostly localized in the western Zagros and are less developed in the Fars region. Topographic slopes range from 5° to more than 60° averaged over a horizontal area of 240 × 240 m, with steep gradients localized mainly along the flanks of anticlines and river valleys (Fig. 1.13).

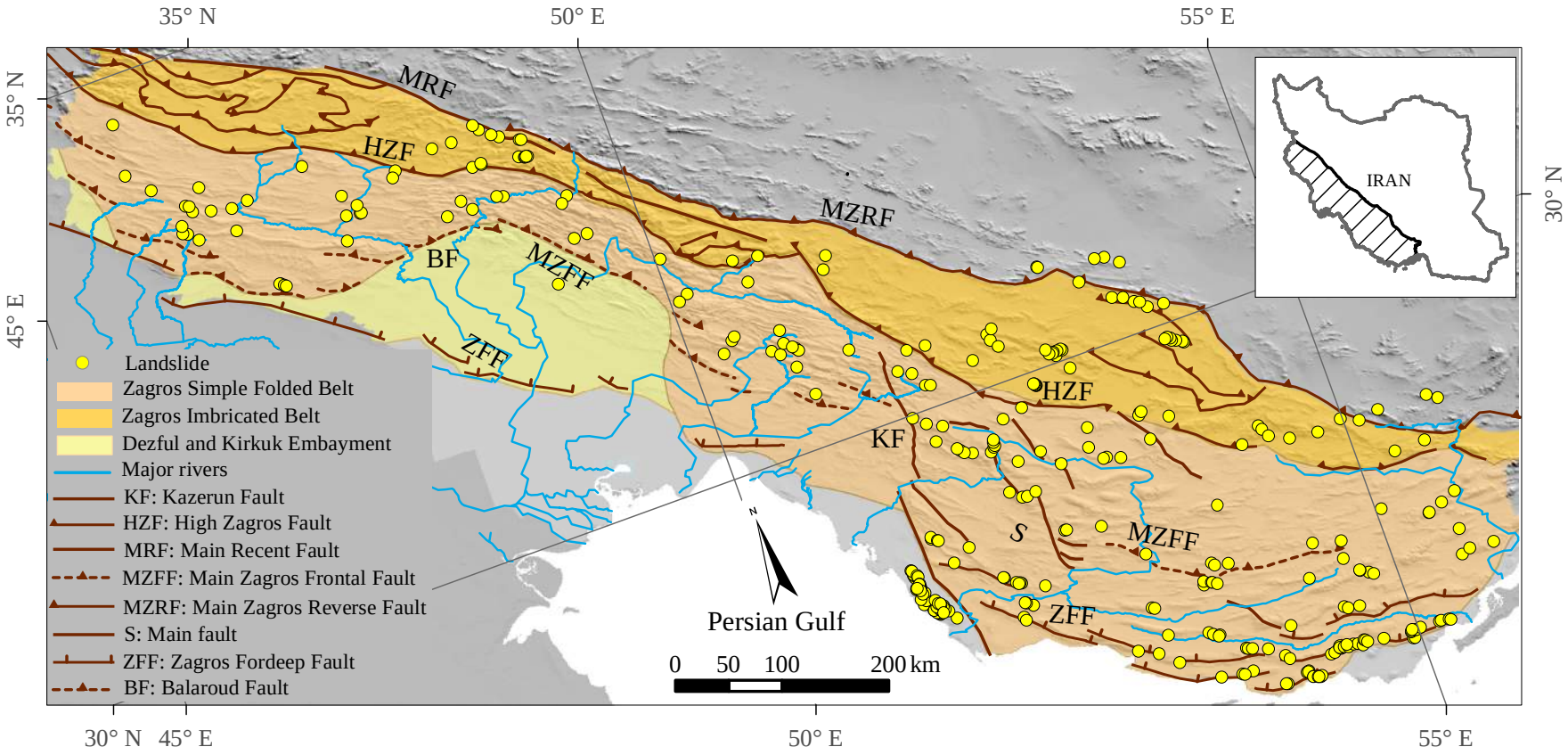

Fig. 1.7. Study area comprising the Zagros region in south west Iran, showing the location of 335 large landslides investigated in this thesis.

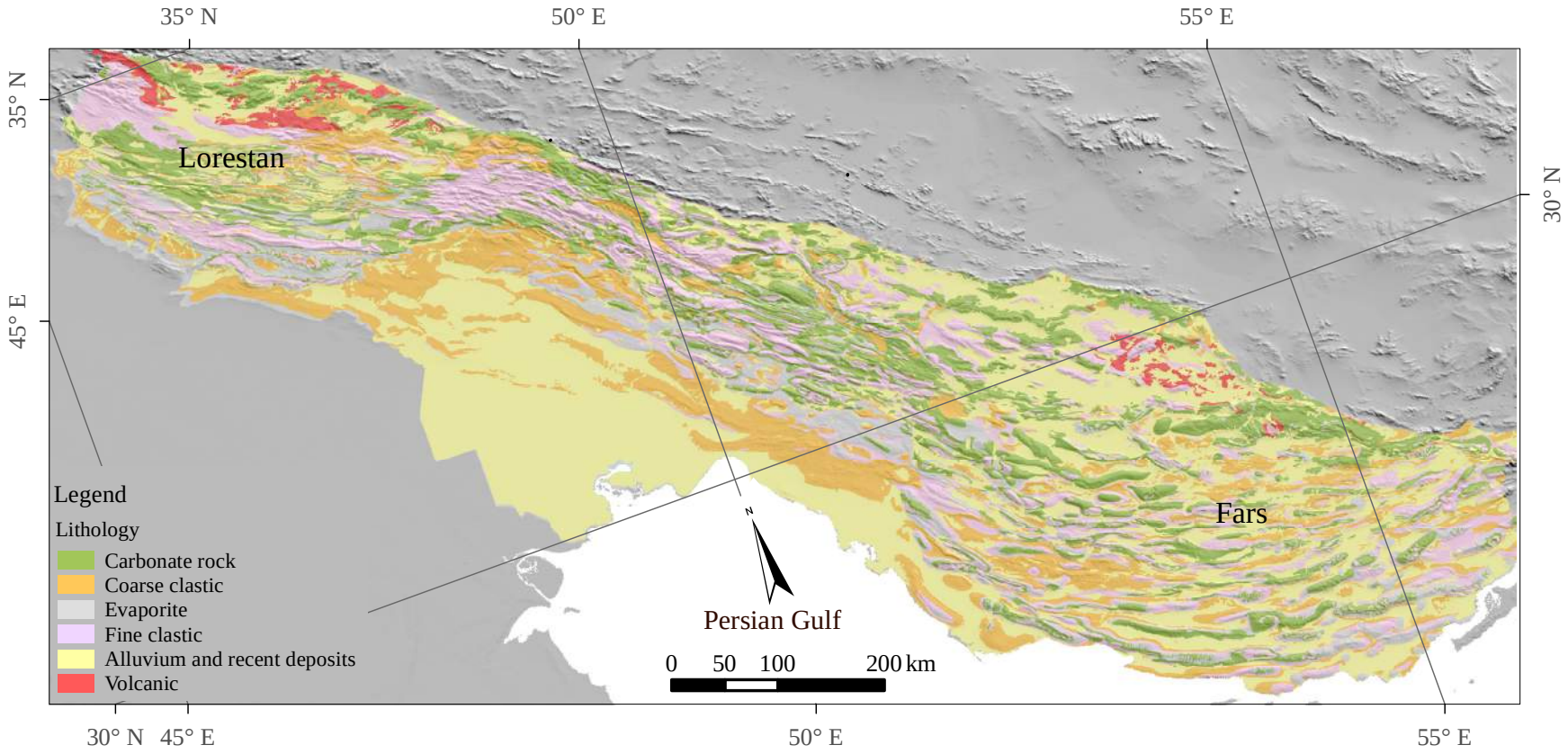

Fig. 1.8. Distribution of the 6 main lithologies in the study area.

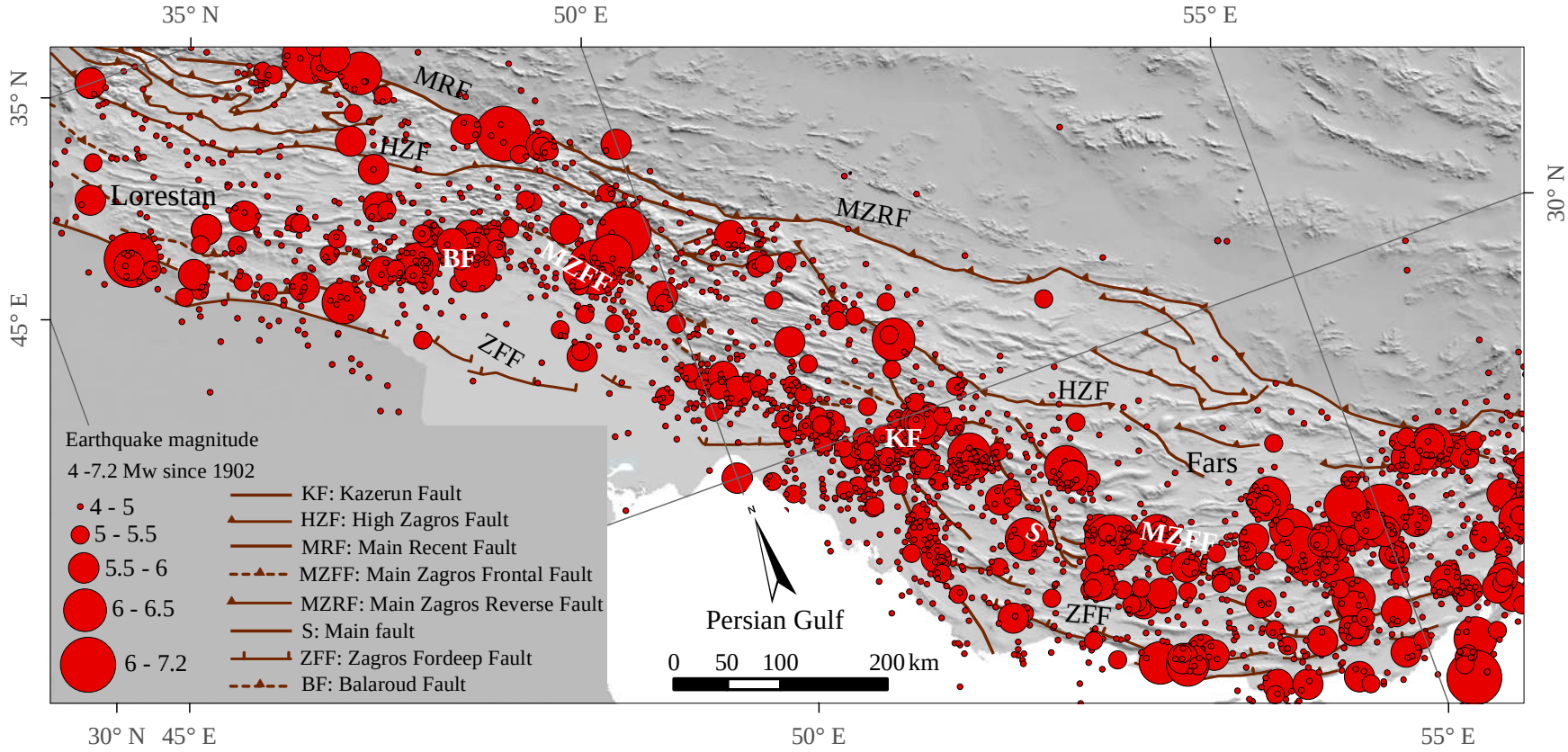

Fig. 1.9. Distribution of more than 2500 epicentres of earthquakes greater than M_w = 4 that have been recorded since 1902 ("www.iiees.ac.ir/iiees/geo/geo_tech1.html").

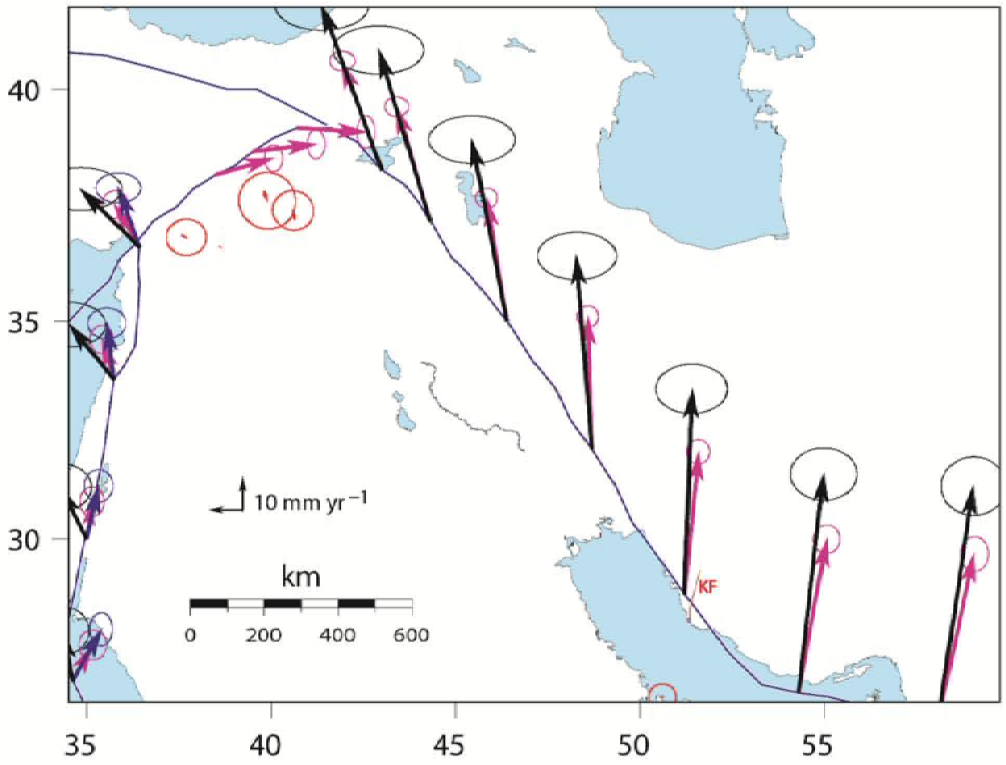

Fig. 1.10. GPS horizontal velocities and their 95 percent confidence ellipses. Red arrows represent results of McClusky (2003), black arrows shows results from Chu & Gordon (1998) for a 3 Myr average. KF represent Kazerun fault.

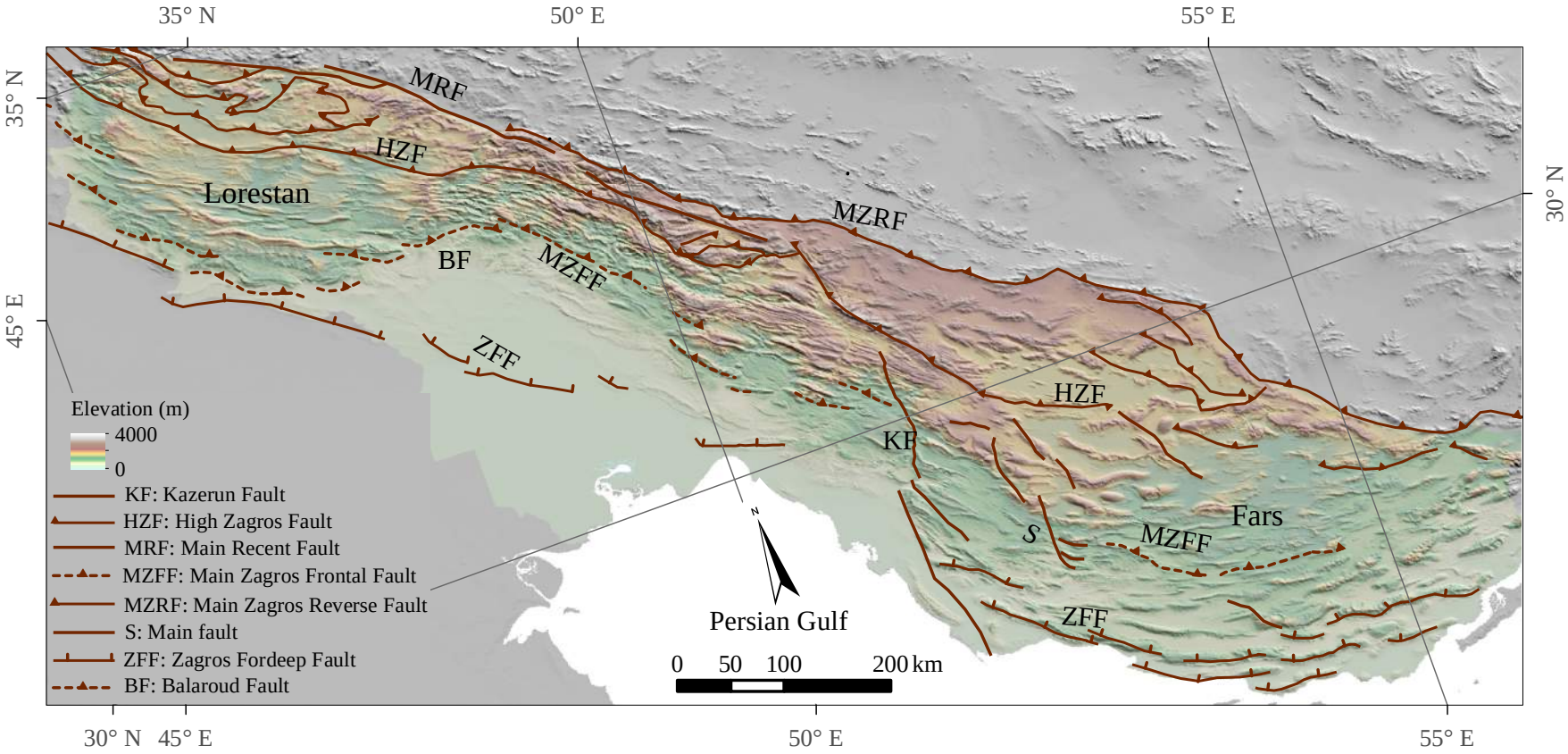

Fig. 1.11. Shaded topography of the Zagros mountain belt.

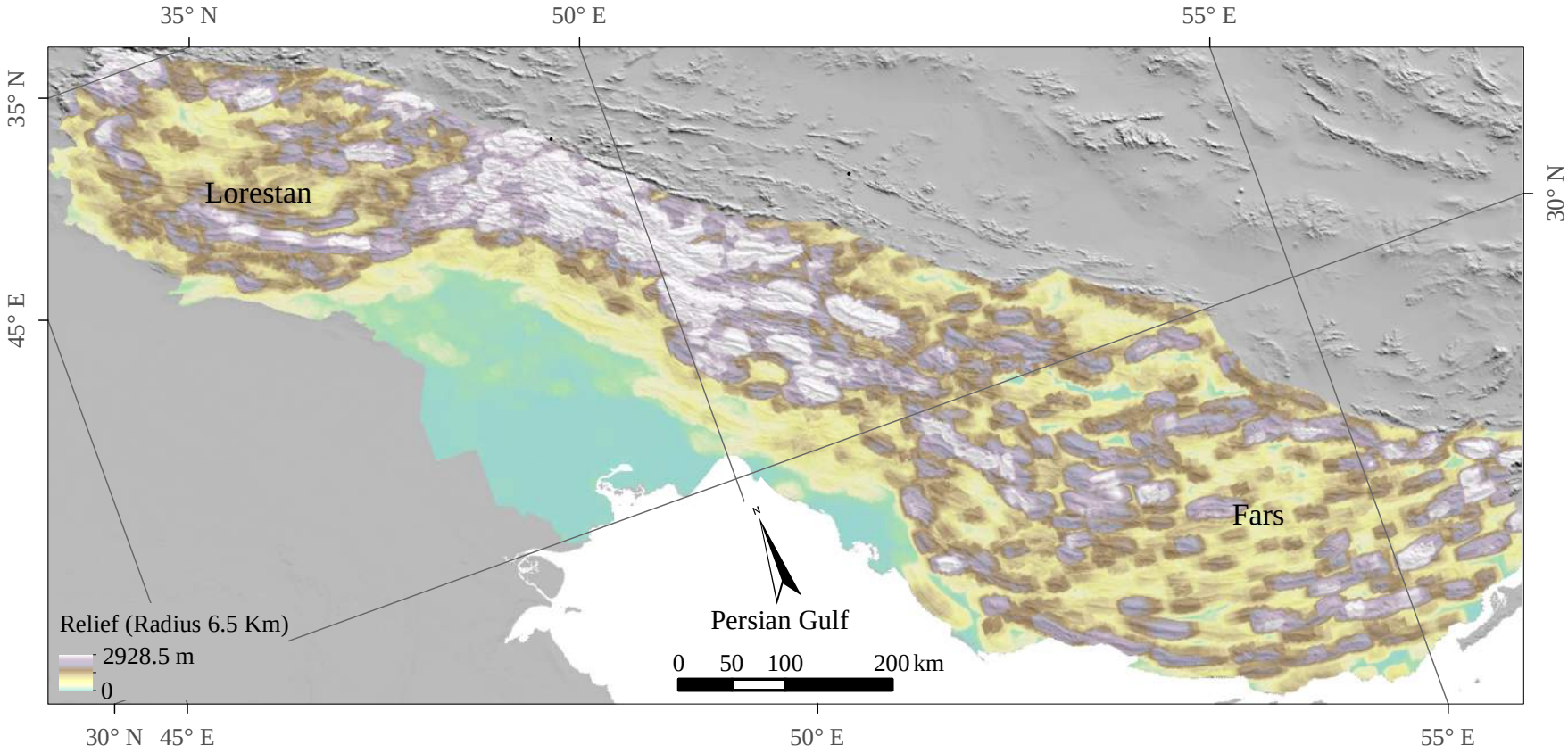

Fig. 1.12. Topographic relief for the Zagros mountain belt, calculated as an average within a 6.5 km radius circle (see chapter 4).

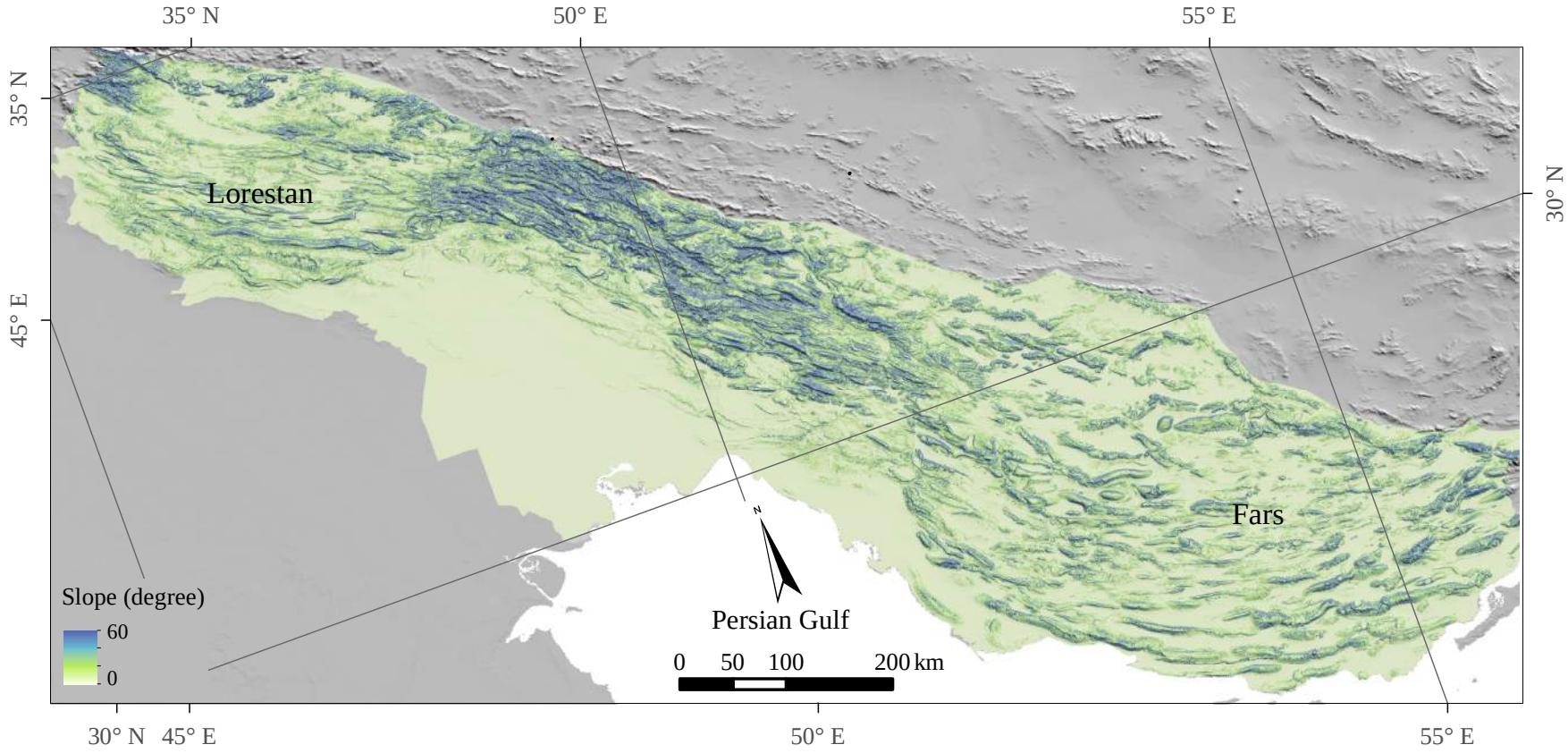

Fig. 1.13. Slope (as an angle) of topography, computed as an average over a 240 × 240 m area.

1.4.3 Climate of the Zagros

Today the Zagros mountain belt is mostly dominated by an arid or semiarid climate with annual precipitation of ~ 350 mm, with most precipitation falling during winter and spring. Small glaciers are presently observed in the Zagros Mountains above 4000 m (Ferrigno, 1988). Glaciers were probably considerably more widespread during Quaternary glacial periods when the snow line was 600 - 800 m lower than the present level and the temperature pattern was similar to that observed today but 4 to 5 ℃ lower (Bobek, 1963).

1.5 Importance of a landslide study in the Zagros region

The Zagros region was selected as case study because it is ideal for the study of landslides since it is relatively arid and has sparse vegetation cover. The region contains numerous historical and prehistoric (probably mostly Holocene) landslides, many of which have been mapped as such on published geological maps and that are obvious on satellite images. The Zagros also contains the Seymareh landslide (Harrison and Falcon, 1938; Shoaei et al., 1998; Shayan, 2006) one of the world's largest subaerial landslides with a volume of 32 km^3, a width of about 5 km and a runout distance of about 10 - 15 km. Some investigations and evidence demonstrate that the age of this pre-historical landslide dates back to 10 - 11 thousand years ago (Shoaei et al., 1998; Harrison and Falcon, 1938; Watson and Wright, 1969). The Gahar landslide is another ancient landslide in the Zagros region that formed a natural lake. The volume of this landslide has been estimated at about 25.38 million cubic meters (Yarahmadi et al., 2012), that is 50 percent smaller than our calculation in this study. Unfortunately, there are not sufficient dating studies to constrain the age of the Gahar landslide (Alipoor et al., 2012).

1.6 Aims and scientific objectives

This study intends to gain a better understanding of the distribution of large landslides and their statistical characteristics / behaviour within the Zagros region. Characterizing the location of large landslides that coincide with human settlements will highlight vulnerable areas and it can be used for planning and land use management for existing and expanding human settlements.

To achieve this aim, 9 research tasks were defined:

1. Identify large landslides (>$10^4 m^3$), characterize their extent and map them.

2. Measure landslides volume within a three dimensional model.

3. Collect available geological and geomorphological information on individual landslides.

4. Investigate the size-frequency characteristics of landslides.

5. Investigate the pattern of geographic distribution of landslides.

6. Identify the most significant parameters that control the size and frequency of landslides.

7. Investigate the probable trigger mechanisms of large landslides.

8. Compare the landslide inventory of the Zagros to other existing inventories.

9. Define the extent of the areas susceptible to frequent and large volume landslides that coincide with human settlements.

1.7 Thesis structure

The thesis is presented in six chapters. The present chapter provides an introduction and an overview of previous research, objectives and a summary of the geological and climatic context.

Chapter 2 presents a new method used to measure volume of landslides and the resulting frequency-volume statistics.

Chapter 3 presents results of two statistical methods used to examine the spatial distribution of landslides.

Chapter 4 describes a preliminary statistical analysis of the factors controlling the spatial distribution of landslides frequency and size within the Zagros region. A discussion of the probable trigger mechanisms of landslides is also presented.

Chapter 5 presents a principal component analysis applied to the Zagros landslide database that has been performed to determine the most relevant variables that control the volume of landslides.

Chapter 6 gives conclusions of this thesis, defines the extent of susceptible areas where frequent and large

volume landslides coincide with human settlements and makes suggestions for future work.

Chapter 2

SIZE DISTRIBUTION OF LANDSLIDES IN THE ZAGROS MOUNTAIN BELT

Paper submitted to Geological society of America.

2.1 INTRODUCTION

This study has investigated large landslides in the Zagros region, based mainly on a digital Elevation Model (DEM) with a 30 m resolution combined with Google Earth™ images and field investigation. In doing so, I present a new landslide inventory for the Zagros mountain belt of southwest Iran. This is the first study of this nature in the Zagros region. This inventory is geomorphological in the sense that there is no control on the age of the investigated landslides. The Zagros region is ideal for a study of this nature since it is relatively arid and has sparse vegetation cover. As already mentioned in chapter 1, the Zagros region contains many historical and prehistoric landslides that are obvious on satellite images. We focus on landslides that are relatively unaffected by erosion or sedimentation following mass movement. Because of this, most landslides are probably late Quaternary or Holocene in age. This study covers a large region and includes landslides (deposits and scars) with areas (A_L) that span 5 orders of magnitude between $10^3 < A_L < 10^8 m^2$. Due to previous studies (Malamud et al., 2004) this inventory is incomplete because it does not include small landslides ($<10^4 m^3$) and could be extended in the future.

This chapter presents an overview of the spatial distribution of landslides, an investigation of the area-volume scaling and a study of the probability density distribution of landslide volumes. Comparison of this database results with other published datasets shows that the Zagros landslides are truly large ($10^4 m^3$ to $10^{10} m^3$) and show similar scaling behaviour to that observed in other regions, especially to datasets where landslides are relatively large and occur in relatively resistant materials (e.g. consolidated rocks, as opposed to soil).

2.2 METHODOLOGY

The location and geomorphometric characteristics of the landslide inventory were obtained using the following procedure:

1. 2075 landslides were initially located on the basis of 140 1:100000 scale geological maps published by either the Geological Survey of Iran or the National Iranian Oil Company (Fig. 2.1). Fig. 2.2 illustrates the geological maps that have been used in this study.

2. Landslides were checked using satellite images (15 - 30 m per pixel) in Google Earth. Landslides that could not be clearly identified were eliminated from further investigation. The visual imagery was followed by field checking. Approximately 50% of the landslides (160 landslides) were checked in the field. Based on the satellite image interpretation and field mapping, 283 additional landslides were identified.

3. Boundaries of slide deposits and scarps were digitised on the basis of 1:25000 ASTER DEM's using the Petrel software. Of the 2358 initially located events, only 335

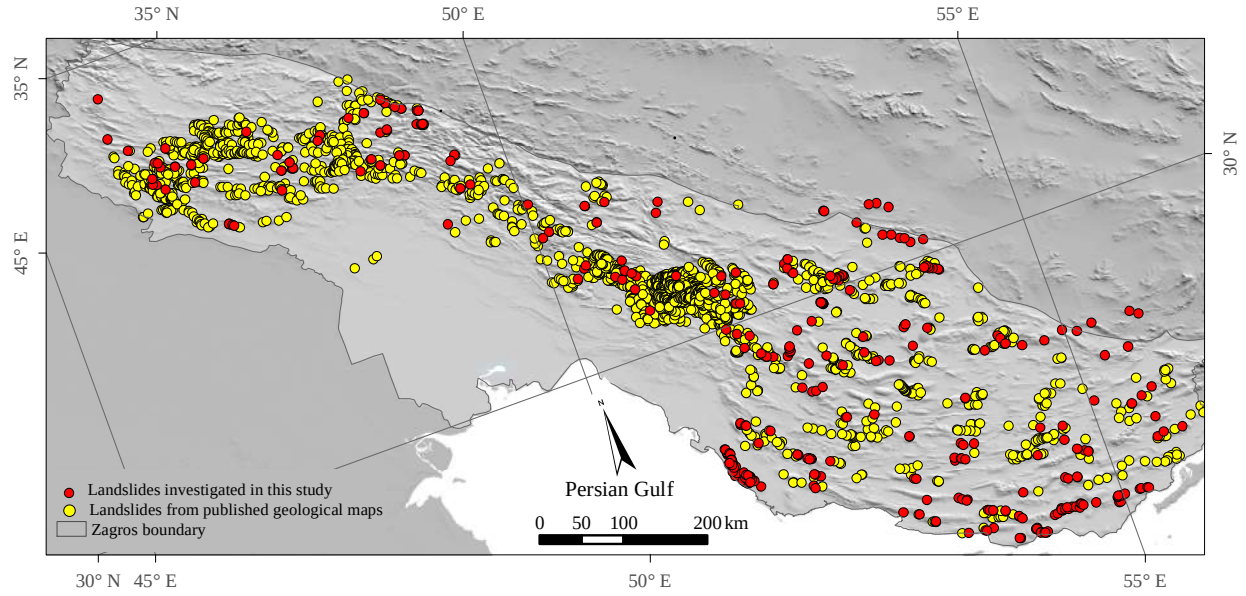

Fig. 2.1. 2075 landslides location on 1:100000 scale geological maps are shown as yellow dots. The red dots show 335 landslides for which I obtained volume measurements through this study.

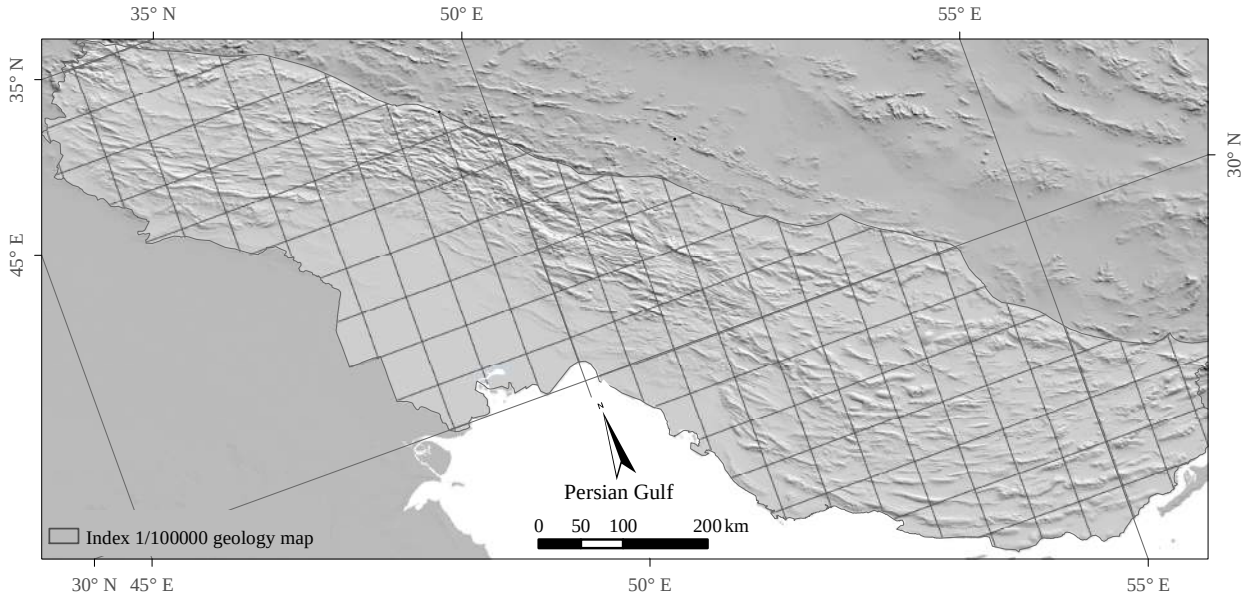

Fig. 2.2. Index of geological map at a 1:100000 scale. The quarters show the location of 140 geological maps that were initially used in this study.

landslides were retained for further volume and area calculation (see Fig. 2.1, red dots). Fig. 2.3 shows some examples of investigated landslides illustrated in 3D view using Petrel.

4. Landslide volumes were calculated in Petrel by computing the volume between the modern (observed) topography (Fig 2.4A) and a reconstructed surface intended to represent the pre-slide topography (Fig 2.4B). In some cases with short runout distances where all or part of the slide mass remained within the source area, we assumed the slide surface to be described by the lower part of an ellipsoid (Xie et al., 2003).The processes involved in the volume measurements using petrel are presented for two different landslides (with long and short runout distances) in Fig. 2.4 and 2.5.

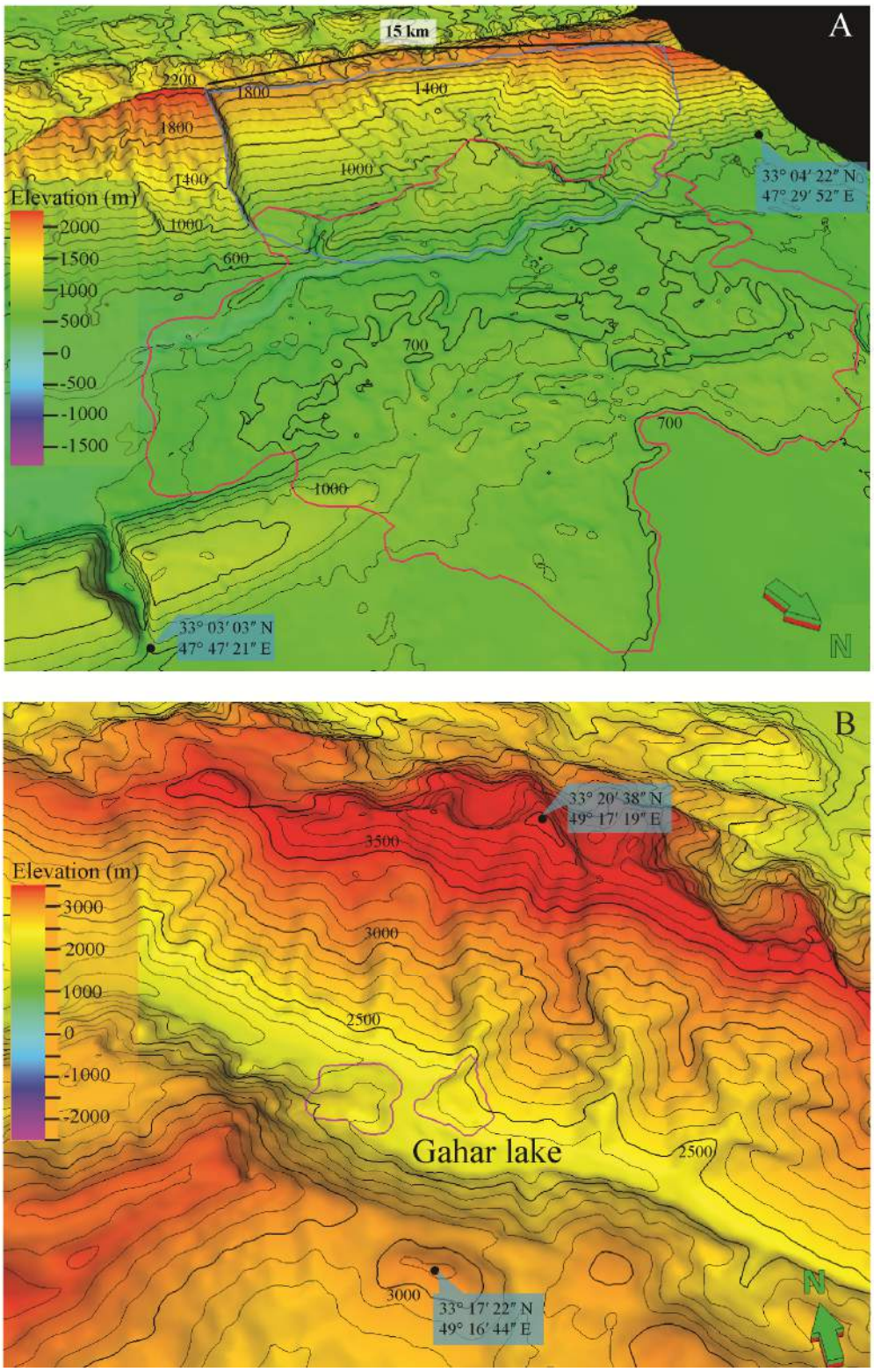

Fig. 2.3. The modern topography of landslides as seen in digital elevation models within Petrel. (A) The source area of the Seymareh rock avalanche is shown with a blue polygon, the debris is shown with a red polygon. (B) Debris of two landslides that formed Gahar Lake are shown with red polygons.

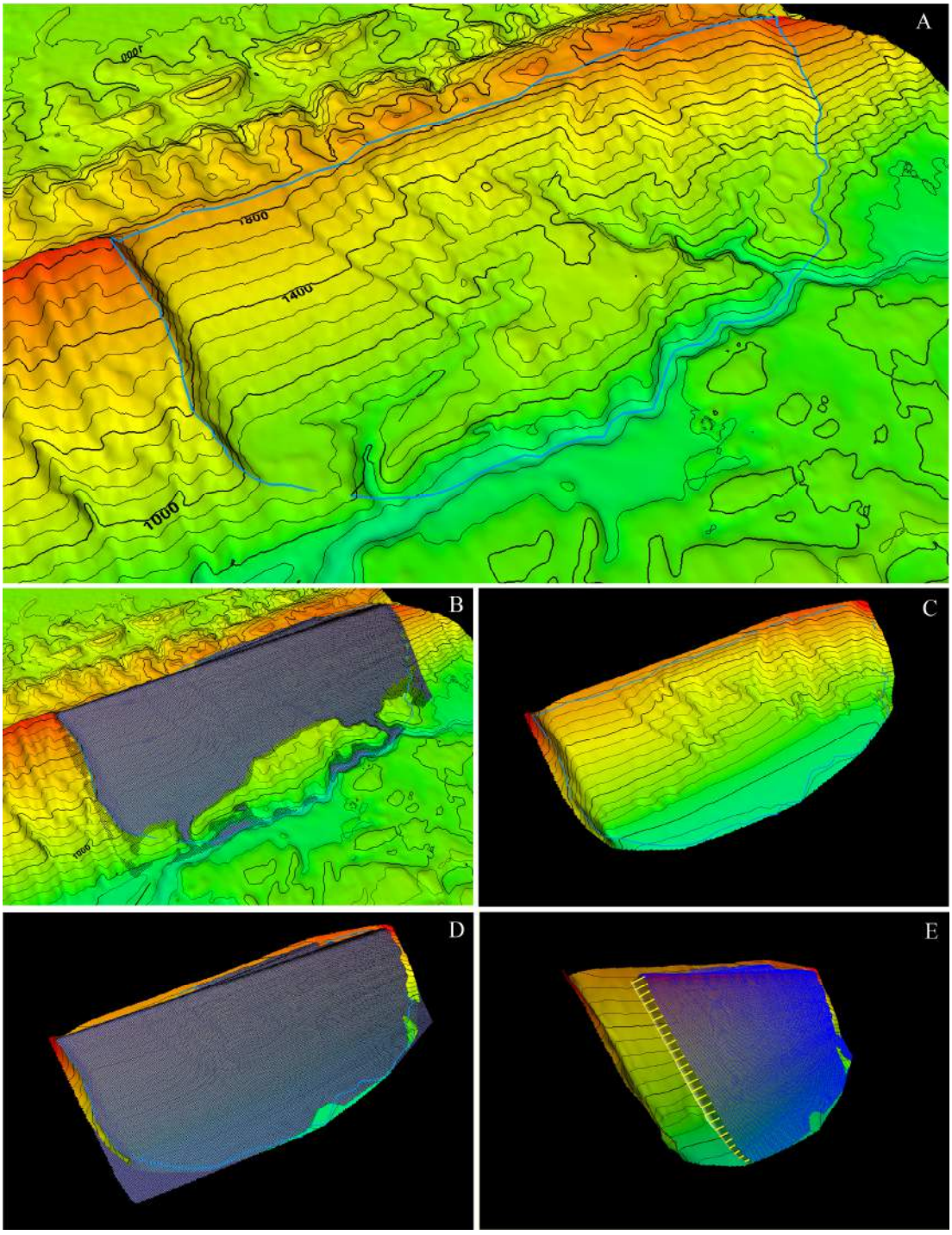

Fig. 2.4. (A) Modern topography in the source part of the Seymareh landslide where part of the slide mass remained in the source area. The dark blue surface in panel B shows the reconstructed surface that represents the pre-slide surface. To calculate volume of the landslide, the buried part of the sliding surface was reconstructed (panel C). (D) Sliding surface and pre-slide surface of the Seymareh landslide. (E) The volume of landslide were calculated by computing the volume between these two surfaces inside the boundary of the landslide.

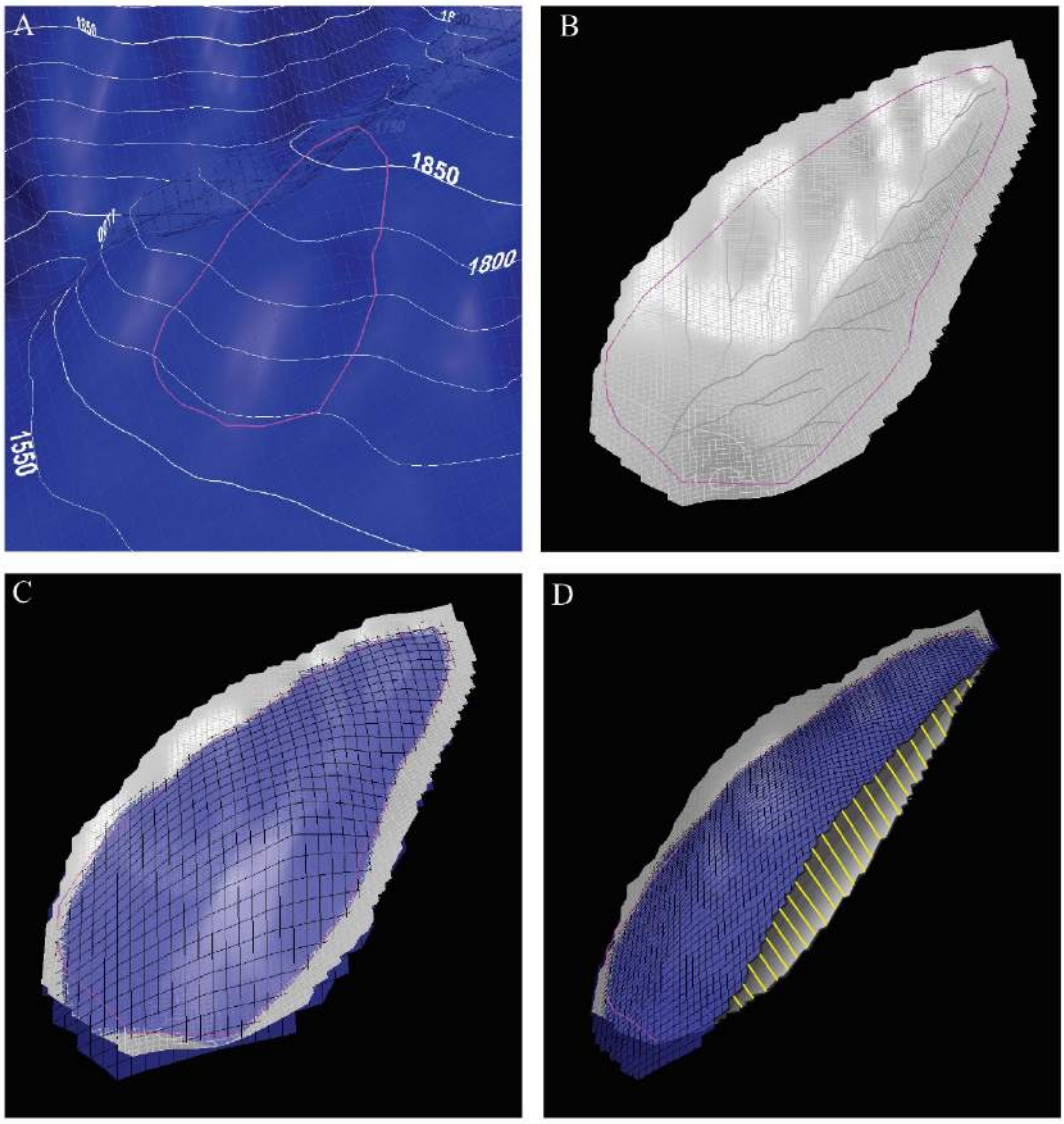

Fig. 2.5. Example where part of the slide mass remains in the source area, In this case after detecting the boundary of mass movement (A), the sliding surface is reconstructed assuming the shape is given by the lower part of an ellipsoid (Xie et al., 2003) (B). Panel (C) shows the combined slide surface and the modern topography. Panel (D) shows the landslide volume, computed as the difference between the modern topography and the reconstructed slide surface.

2.3 RESULTS

Fig. 2.6 shows the relationship between landslide volume and landslide surface area in logarithmic coordinates for our entire dataset. The data fall on a straight line (R^2 = 0.96) that is well described by a power law of the form:

$$V_L = 0.042\ A_L^{1.4929} \qquad \text{(Eq2.1)}$$

The error on the scaling exponent α is ±0.002. This power law expression can obviously be used to estimate the volume of individual landslides when the surface area of the slope failure is known but the volume is difficult to measure (Eq 2.1).

The vertical and horizontal error of the DEM data is considered in volume measurements. The upper and lower error for each individual landslide measurement is assumed to lie between 5 and 30% depending on the shape of landslide. The upper error on the volume

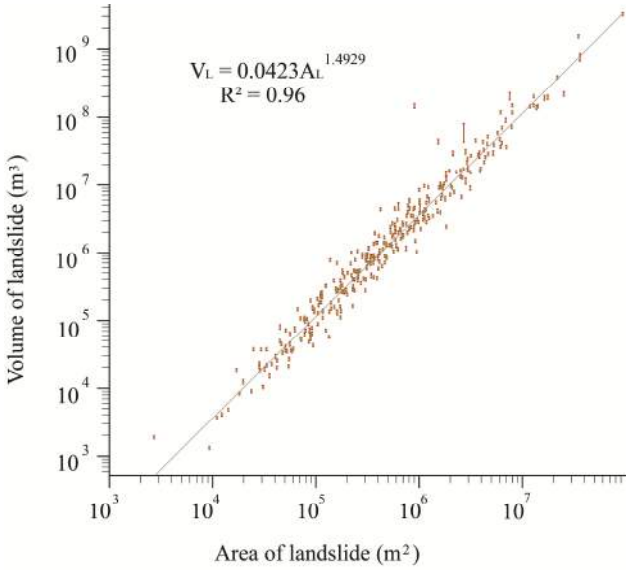

Fig. 2.6. The volume versus area of 335 Zagros landslides in logarithmic coordinates. The black line shows a linear regression. Error bars are shown for each landslide

estimations are considered to be maximum because some may have basal slide surface deeper than assumed when fitting a polynomial to the slide base. (Fig.2.6).

A histogram of the landslide database (Fig.2.7) reveals a highly skewed distribution with a heavy tail, indicating that the population is dominated by numerous small volume landslides ($<10^7 m^3$) and relatively few large volume landslides, as often observed in other studies (Stark and Hovius, 2001; Xie et al., 2003; Malamud et al., 2004a; Newman, 2005; White et al., 2008; Brunetti et al., 2009; Guzzetti et al., 2009a).

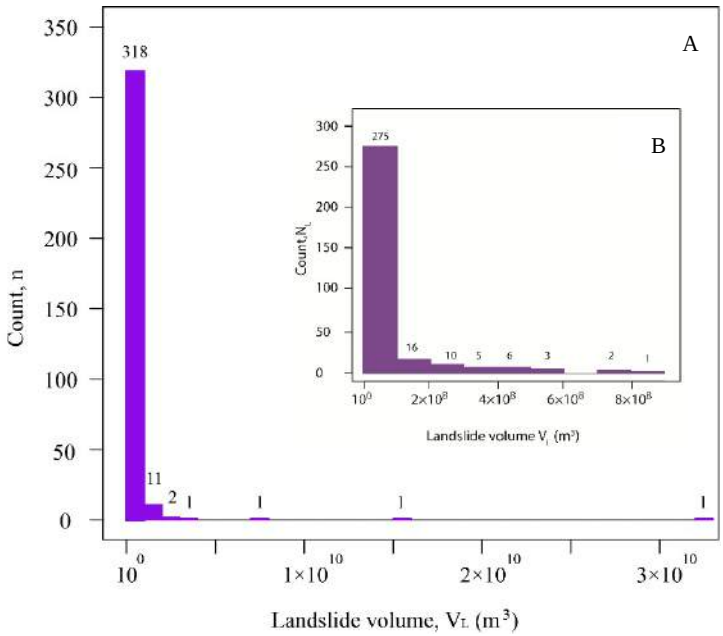

Fig. 2.7. A) Histogram showing the frequency of 335 Zagros landslides as a function of landslide volume on linear coordinates ($1.3\times10^4 m^3$ – $3.2\times10^{10} m^3$) and B) Presents frequency of 318 landslides ($1.3\times10^4 m^3$–$8.8\times10^8 m^3$). The bin size determined by Sturges' rule.

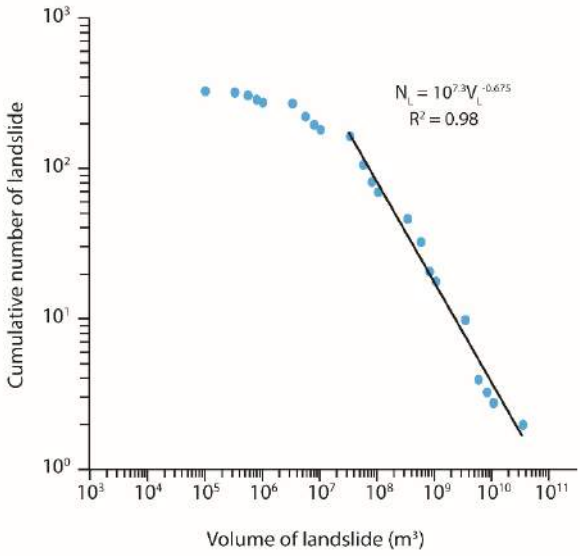

Fig. 2.8. Cumulative volume distribution of 335 landslides in the Zagros mountain belt. The line is a linear regression to landslides with volumes in the range 3.2×10^7 - 3.2×10^{10} m^3.

When our landslide data are plotted as a cumulative distribution (Fig. 2.8), it can be seen that the largest landslides (3.2×10^7 - 3.2×10^{10} m^3), comprising 167 landslides or about 50% of the dataset are well described by the power law (Stark and Hovius, 2001):

$$N_L = 10^{7.3} V_L^{-0.675} \qquad \text{(Eq 2.2)}$$

The volume distribution deviates from a power-law for volumes smaller than about $3.2\times10^7 m^3$. We believe this roll-over behaviour is most likely to be caused by a systematic under sampling of the smallest landslides (Stark and Hovius, 2001) rather than some physical lower limit on landslide volume (Burroughs and Tebbens, 2001). This is considered the most likely explanation because of the relatively low resolution of the DEM (30 m) and the large area of

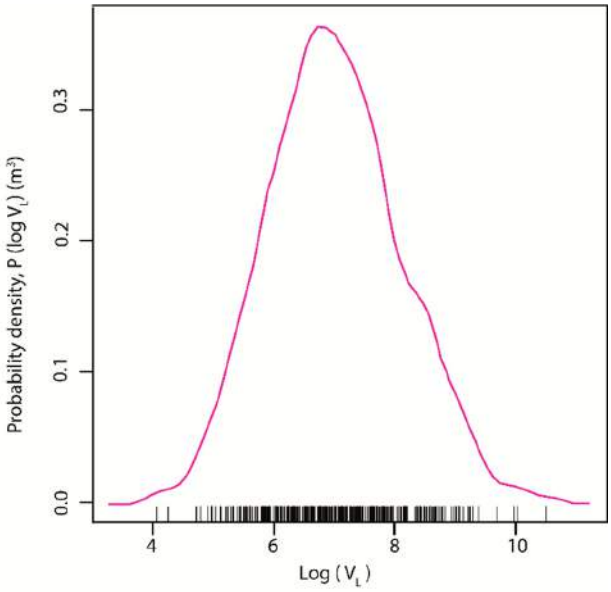

Fig. 2.9. Probability density of the logarithm of landslide volume as a function of log V_L shown in linear coordinates.

our investigation (322000 km^2). If true, it would mean we are missing more than 2000 landslides between volumes 1.3×10^4 and 3.2×10^7 m^3.

In order to facilitate comparison between the Zagros landslides and other published datasets (presented in the next section), the probability density function of landslide volume has also been computed. To compute the probability density, a kernel density estimation (KDE) is adopted that we performed using a script written in R developed by (Brunetti et al., 2009). An optimally smoothed curve is obtained using a Gaussian kernel with a band width of 0.25. The probability density log V_L obtained through the KDE (Fig. 2.9) is smooth and approaches a symmetrical shape with a maxima at $10^{6.8}$m^3.

Since we are interested in the probability density of landslide volumes, we transformed P ($log\ V_L$) to P (V_L) while satisfying the normalization condition (see for example Brunetti et al., 2009). The result of the transformed $P(V_L)$ as a function of V_L is shown in Fig. 2.10. Once again, the large volume at the end of the distribution can be fit with a power law (Keefer, 1994; Hovius et al., 1997; Stark and Hovius, 2001):

$$P\ (V_L) = 885.3\ V_L^{-1.51} \qquad \text{(Eq 2.3)}$$

where P (V_L) is the non-cumulative probability density for a landslide of volume V_L and β is the non-cumulative power-law scaling exponent that has a value of about 1.51.

2.4 COMPARISON WITH OTHER DATABASES

Empirical relationships of 12 previously published datasets linking A_L to V_L along with the new relationship determined in this study are shown in Fig. 2.11 (see also Table 2.1). Most data show a linear trend on logarithmic coordinates, indicating power law scaling between landslide volume and surface area (Simonett, 1967; Rice et al., 1969; Rice and Foggin, 1971; Abele, 1974; Innes, 1983; Whitehouse, 1983; Martin et al., 2002; Haflidason et al., 2005; Korup, 2005a; Ten Brink et al., 2006; Katz et al., 2008; Guzzetti et al., 2009a) with exponents ranging from 0.88 to 1.95. The smaller exponents tend to be associated either with relatively small-volume datasets (<3.2×10^7m^3) (Rice et al., 1969; Larsen and Torres-Sanchez, 1998; Martin et al., 2002; Brunetti et al., 2009) or with shallow landslides (e.g., soil slide, debris slide, and debris flow; curve names Ng, Sc, St, Cj, Ca, Bc and Nw). The Zagros landslides clearly fall on the same general trend as the other datasets with relatively large exponents α=1.49, which is typical for deep-seated bedrock failures (Abele, 1974; Whitehouse, 1983; Haflidason et al., 2005; Korup, 2005b; Ten Brink et al., 2006; Galli et al., 2008; Larsen et al., 2010).

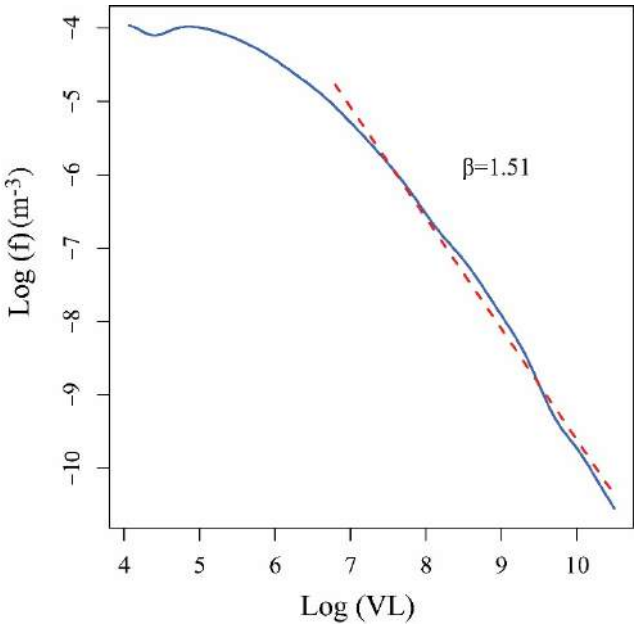

Fig. 2.10. Logarithm of the probability density of landslide volume, f = P (V_L) as a function of the logarithm of landslide volume. The fit shows a linear regression yielding a scaling exponent β=1.51.

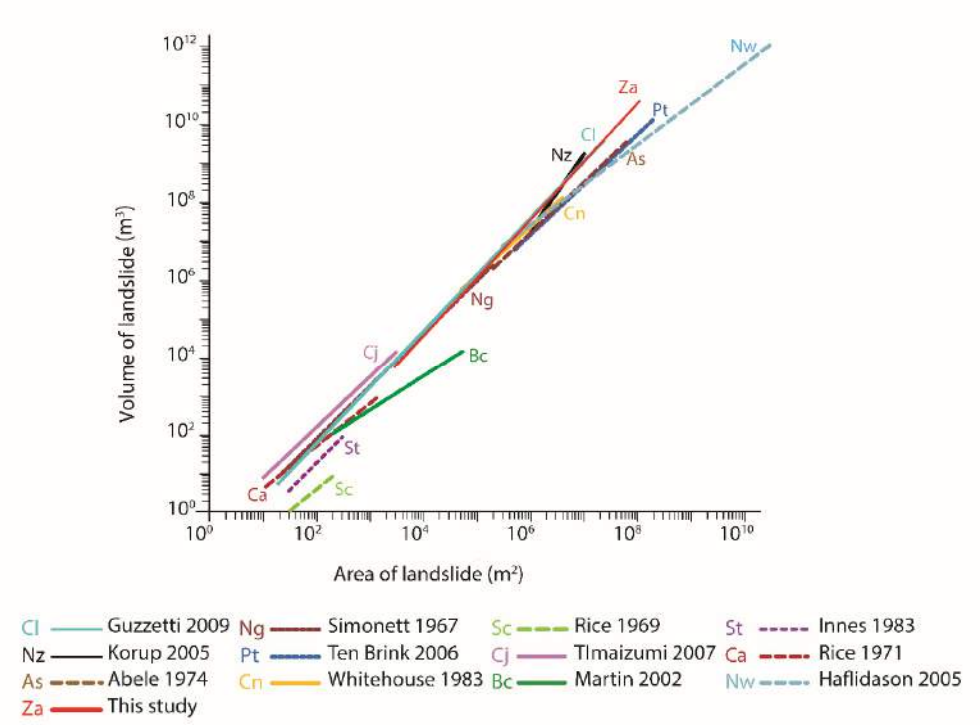

Fig. 2.11. Comparison of the Zagros landslide volume-area relationship (red line) with 12 published datasets (modified after Guzzetti et al.,2009). See Table 2.1 for more details.

Table 2.1. Empirical relationships linking landslide area A_L to landslide volume V_L shown in Fig. 2.11

ID	Dataset	N	Equation	Slope $\beta\pm\varepsilon$ [a]	Source
Za	Zagros, Iran	335	$V_L=0.042\ A_L^{1.4929}$	1.5±0	This study (Eq. 2.1)
Bc	British Columbia	615	$V_L=1.0359\ A_L^{0.88}$	-	Martin et al. (2002)
Nw	Storegga, Norway	65	$V_L=17.136\ A_L^{1.0322}$	-	Haflidason et al. (2005)
St	Scottish Highlands	30	$V_L=0.0329\ A_L^{1.3852}$	-	Innes (1983)
Nz	W-S Alps, New Zealand	23	$V_L=0.00004\ A_L^{1.95}$	-	Korup (2005)
Pt	Puerto Rico	160	$V_L=0.263\ A_L^{1.292}$	-	Uri S. ten Brink (2006)
Cj	Central Japan	51	$V_L=0.39\ A_L^{1.31}$	-	Imaizumi and Sidle (2007)
Ca	South California	37	$V_L=0.328\ A_L^{1.104}$	-	Rice and Foggin (1971)
As	Alps	53	$V_L=0.242\ A_L^{1.307}$	-	Abele (1974)
Cn	Central S Alps, New Zealand	45	$V_L=0.769\ A_L^{1.25}$	-	Whitehouse (1983)
Ci	Central Italy	677	$V_L=0.074\ A_L^{1.45}$	-	FaustoGuzzetti (2009)
Ng	New Guinea	207	$V_L=0.1479\ A_L^{1.368}$	1.2±0	Simonett (1967)
Sc	South California	29	$V_L=0.234\ A_L^{1.11}$	-	Rice et al. (1969)

[a] $\mathcal{E}$=0.0 indicates that the error Ɛ is smaller than 0.05, and $\mathcal{E}$ =0.1 indicates that the error is $0.05 \leq \mathcal{E} \leq 0.09$.

Table 2.2 Characteristics of 14 landslide datasets (modified from Brunetti et al., 2009). Some of the datasets are complete (e.g., It, Gf, Pr, Uk, Us), while others are incomplete (e.g., Ng, In, Db, Sl, Wn, Sm, Nv, Vl, Mn, Za) (Malamud et al., 2004).

ID	Dataset	N	Slope $\beta \pm \varepsilon$ [a]	Source
Za	Zagros, Iran	335	1.5±0	This study (Eq. 2.1)
Ng	New Guinea	207	1.2±0	Simonett (1967)
Db	Debris flow	46	1.3±0	Iverson (1997) and Iverson et al. (1998)
Sl	World slide	404	1.5±0.1	Guzzetti et al. (2009)
Wn	Washington, USA	20	1.3±0	Baum et al. (2000)
Uk	Peat slides, Shetland Is., UK	17	1.6±0.1	Dykes and Warburton (2008)
Sm	Submarine	43	1±0.1	Hampton et al. (1996) and Legros (2002)
Nv	Non volcanic	153	1.1±0	Erismann and Abele (2001) and Legros (2002)
Vl	Volcanic	55	1.1±0.1	Hayashi and Self (1992) and Legros (2002)
Mn	Mars-Moon	28	1±0	McEwen (1989) and Legros (2002)
Pr	Puerto Rico, USA	1019	1.9±0	Larsen and Torres-S´anchez (1996 and 1998)
It	Umbria-Marche, central Italy	133	1.3±0	Antonini et al. (2002)
Gf	Grenoble, France	105	1.2±0	Dussauge-Peisser et al. (2002) and Dussauge et al. (2003)
Us	Yosemite, USA	379	1.3±0	Wieczorek et al. (1992)
In	Himalaya, India	338	1.5±0	Barnard et al. (2001)

[a] ε=0.0 indicates that the error ε is smaller than 0.05, and ε =0.1 indicates that the error is $0.05 \leq \varepsilon \leq 0.09$

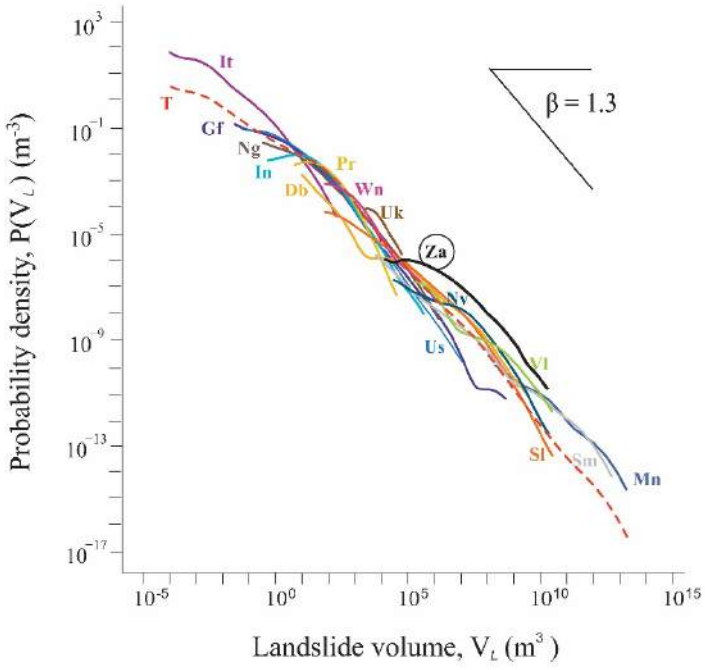

Fig. 2.12 Probability density of landslide volumes as a function of landslide volume, shown in logarithmic coordinates. Za refers to the Zagros data base. Letters refer to database ID in table 2.2. T (red dashed line) refers to the combined dataset (modified from Brunetti et al., 2009).

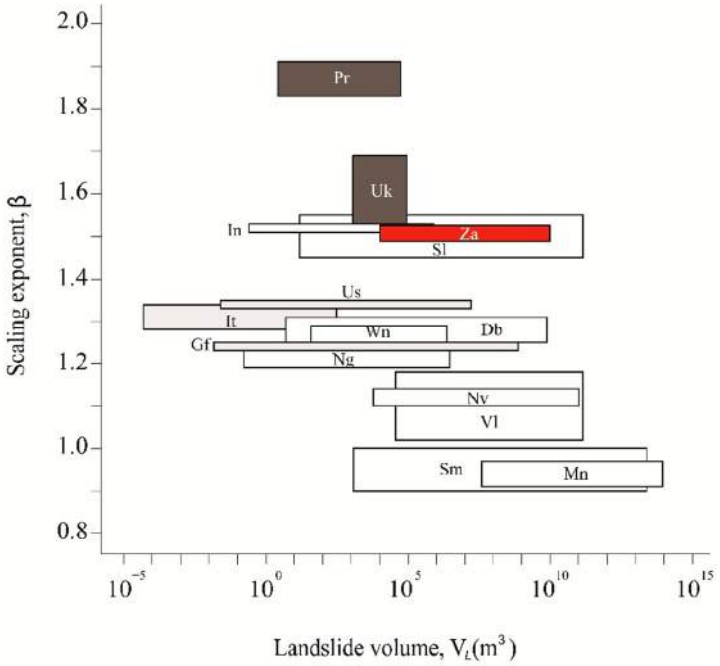

Fig 2.13. Power law scaling exponent β for different landslide volumes from a range of different studies (modified from Brunetti et al., 2009). The Zagros landslides are illustrated in red. Rock falls are shown in light gray, slides are in dark gray, while other landslide types are in white. Abbreviations refer to dataset ID in table 2.2.

Fig. 2.12 shows a comparison between the probability density of the volumes for the Zagros landslides, along with other published datasets on logarithmic coordinates (Table 2.2) (Simonett, 1967; Rice and Foggin, 1971; McEwen, 1989; Wieczorek et al., 1992; Hayashi and Self, 1992; Larsen and Torres-Sanchez, 1996; Hampton et al., 1996; Iverson, 1997; Iverson et al., 1998; Larsen and Torres-Sanchez, 1998; Baum et al., 2000; Erismann and Abele, 2001; Legros, 2002; Barnard et al., 2001; Dussauge-Peisser et al., 2002; Dussauge et al., 2003; Antonini et al., 2002; Dykes and Warburton, 2008; Guzzetti et al., 2009a). Most data fall on a similar shaped curve, indicating power law scaling as noted earlier. The scaling exponent β for the combined dataset is approximately 1.3, while the Zagros has a value of 1.51 (see Fig. 2.10). Almost all databases exhibit rollover in the probability density of landslides towards their smaller volumes (Pelletier, 1997; Stark and Hovius, 2001; Guzzetti et al., 2002; Brardinoni and Church, 2004; Malamud et al., 2004b; VanDen Eeckhaut et al., 2007), while those that more closely approximate true power law behaviour appear to be dominated by rock falls (Brunetti et al., 2009)

Fig. 2.13 summarises the variability of the scaling exponents as a function of landslide volume. Differences in the scaling exponents of the density distributions possibly reflect different landslide types and different materials (Densmore et al., 1998; Brunetti et al., 2009). Most slide mass failures have scaling exponents in the range $1.5<\beta<1.9$ (which includes the range of variability in the Zagros), while rock falls typically show lower values in the range $1.1<\beta<1.4$. These results are consistent with numerical simulations which show that landslides with less consolidated material have a higher exponent compared to stronger material (Densmore et al., 1998). We conclude that the high scaling exponent for the Zagros database reflects the type of materials involved in mass failure, which often includes thick consolidated formations (e.g., Asmari carbonates) above unconsolidated units (e.g., Pabdeh shale/marl). This combination appears favourable for the formation of relatively large, deep-seated mass movements.

2.5 Conclusion

We have created for the first time a database containing the volumes and areas of 335 landslides in the Zagros mountain belt. The volume measurement were performed by using a new method in the three dimensional environment of the petrel software. Analysis of this database shows power law scaling

between landslide volume and area with a scaling exponent of α=1.491, similar to observed in other studies. This study proposes that the scaling exponent is mainly related to the thickness of landslides (i.e the shape) rather than any specific physical process. The cumulative number of landslide volumes also shows a power-law distribution. The fit of the data deviates from a power-law for volume smaller than about $3.2\times10^{7}m^{3}$.We propose this is probably an artefact due to a systematic under sampling of the smallest landslides linked to the low resolution of the data that is used in this study. We also investigated the probability distribution of the Zagros landslides spanning six orders of magnitude in volume ($10^{4}<V_{L}<10^{10}m^{3}$). The landslide volume with the highest probability of occurrence is approximately 10^{7} m^{3}. These results advance the understanding of the statistics of landslide volumes in the Zagros region, and can contribute to the validation of computer models of landslide sizes, landslide hazard, erosion and sediment flux within landscapes dominated by landslides.

Chapter 3

SPATIAL PATTERN OF LANDSLIDES

3.1 INTRODUCTION

The spatial patterns of geographical events are the result of physical or geomorphological processes on earth's surface (Lee and Wong, 2001). Any spatial distribution of events within a defined area will create a pattern. Geographic patterns range from completely clustered at one extreme to completely dispersed at the other (Mitchell, 2005) (Fig. 3.1). A pattern that falls between these extremes is called random (Lee and Wong, 2001; Mitchell, 2005). In this chapter the spatial pattern of landslides across the Zagros mountain belt is measured to quantify the degree of randomness versus clustering. This can lead to a better understanding of the processes that produced such patterns (Burt and Barber, 1996).

3.2 IDENTIFYING PATTERNS STATISTICALLY

One way of identifying spatial patterns in a landslide dataset is to display their location on a map (Fig. 3.2). The other way is to use statistics to find out whether the distributions of landslides are clustered, dispersed, or random.

To measure the pattern of landslides statistically two methods were used: nearest neighbour and quadrate analyses. Nearest neighbour analysis is a measure of how similar the observed mean distance is to the expected mean distance for a random distribution (Lee and Wong, 2001). Quadrate analysis counts the number of features per unit area and examines how the density of the features changes over space. Quadrate analysis doesn't consider the proximity of features to each other or their arrangement in relation to each other (Lee and Wong, 2001; Mitchell, 2005)

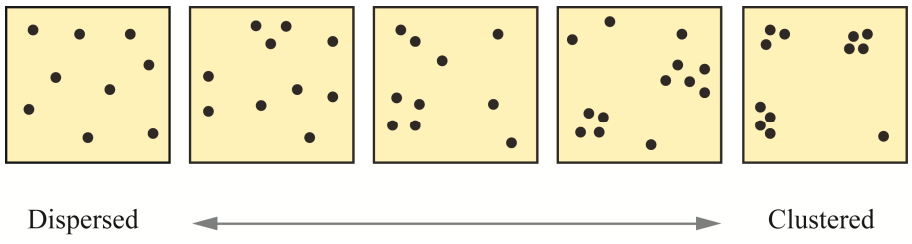

Fig. 3.1. Different patterns measurable by the nearest neighbour index based on the average distance from each feature to its nearest neighbour (modified from Mitchell, 2005).

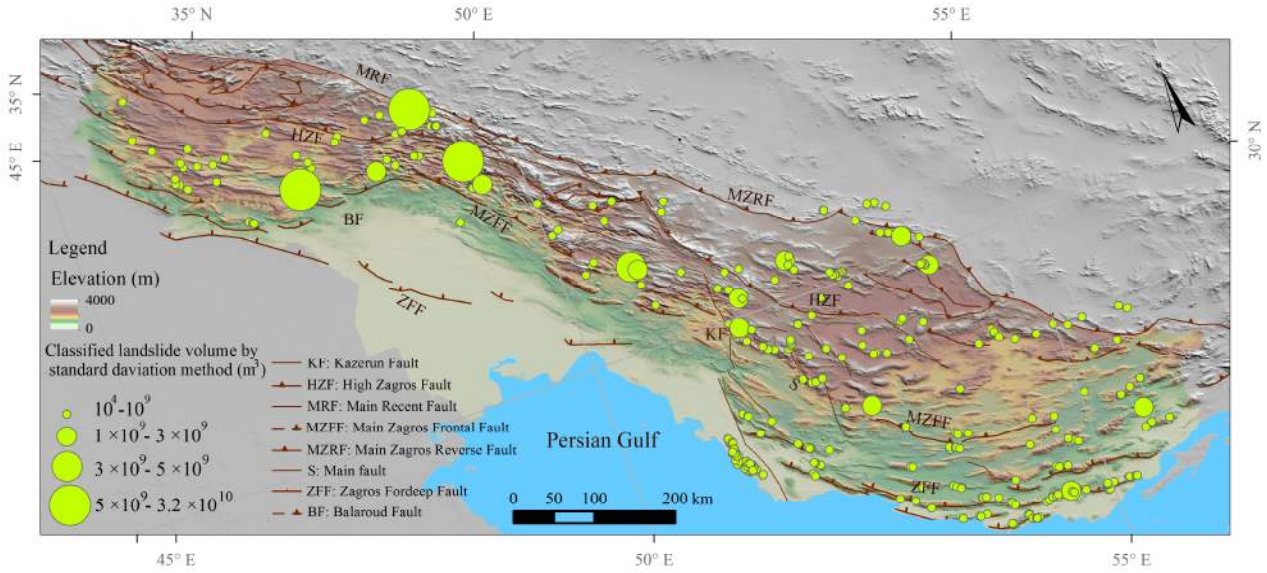

Fig. 3.2. Distribution of landslide classed in terms of volume in the Zagros mountain belt.

To determine the pattern of a landslide distribution, statistics incorporates the distance between features (e.g., landslides), measured as the straight-line distance between the x and y coordinates of the features. Although measuring the distance between point features is clear (since they have a unique centroid), measuring the distance between features with an area is more difficult. In this study, I consider the centroid-to-centroid distance (Fig. 3.3B), rather than the distance separating adjacent slide polygons (Fig. 3.3A).

3.2.1 NEAREST NEIGHBOUR INDEX

The nearest neighbour index (Clark and Evans, 1954) is a distance statistical method that has been used in many different fields for a wide variety of problems (Cressie, 1991). It is also implemented in Arc GIS for pattern recognition. The nearest neighbour index measures the similarity of the mean distance of features to the expected mean distance that would be expected on the basis of chance. Results of nearest neighbour index helps to identify clustering or randomness of features and it also considers the relationship between features and captures the pattern of the features.

3.2.2 OBSERVED MEAN DISTANCE

To calculate the nearest neighbour index first, the

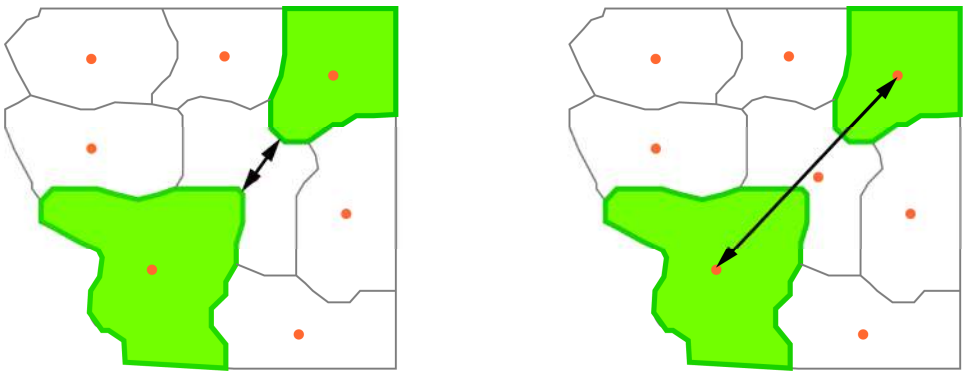

Fig. 3.3. Two methods for quantifying the distance between different features containing an area. (A) The distance is the closest distance separating the polygons, while in (B) it is the distance separating the polygon centroid (modified from Mitchell, 2005).

nearest neighbour distance is calculated. For each point the distance from each feature to all other features in the dataset is measured, and then the shortest distance is selected as a nearest neighbour to the feature. Then, the mean distance for the observed distribution of features is calculated by the sum of the distances divided by the number of features (Bailey and Gatrell, 1998; Ebdon, 1985; Mitchell, 2005):

$$\bar{d}_o = \frac{\sum_{i=1}^{n} c_i}{n} \qquad \text{(Eq. 3.1)}$$

where $\bar{d}_o$ is the observed mean distance, c_i is distance to each feature`s nearest neighbours and n is number of features.

In theory, the mean distance for a completely clustered distribution is 0. This means that all points are at the same location so the distance between each point and its nearest neighbour is 0. In the Zagros landslides dataset with 335 landslide events, the observed mean distance obtained from Eq 3.1 is 7421.3 meters.

3.2.3 EXPECTED MEAN DISTANCE

For a completely dispersed distribution, the mean distance is the inverse of the square root of the number of points divided by the areal extent of the study area (Clark and Evans, 1954). The expected mean distance can be computed as:

$$\bar{d}_e = \frac{0.5}{\sqrt{N/A}} \qquad \text{(Eq. 3.2)}$$

where $\bar{d}_e$ is the expected mean distance for a random distribution, N is number of features and A is the area of the study area. The mean distance for a random distribution is between the values for a completely clustered and a completely dispersed distributions (0 and 1, respectively).

The expected mean distance calculated from Eq 3.2 for the area influenced by landslides in the Zagros ($172.3 \times 10^9 m^2$) is equal to 11341.8 meters.

3.2.3.1 CALCULATING THE NEAREST NEIGHBOUR INDEX

To calculate the nearest neighbour index, one subtracts the mean distance for an expected random distribution from the mean distance for the observed distribution (Witherick et al., 1998; Mitchell, 2005):

$$d = \bar{d}_o - \bar{d}_e \qquad \text{(Eq. 3.3)}$$

where d is the nearest neighbour index, $\bar{d}_e$ is the expected mean distance for an expected random distribution and $\bar{d}_o$ is the mean distance for the observed distribution.

If the observed and expected means are equal, the difference is 0, meaning that the observed distribution is random. Nearest neighbour indices of less than 0 represent clustered distributions (Table 3.1). The nearest neighbour of the Zagros dataset is equal to -3920 that reveals a clustered distribution.

Another way of showing the nearest neighbour index is to calculate the ratio between the two mean distances. Dividing the observed mean distance by the expected mean distance for a random distribution (Mitchell, 2005; Smith, 2010):

$$r = \frac{\bar{d}_o}{\bar{d}_e} \qquad \text{(Eq. 3.4)}$$

Table 3.1. Nearest neighbour index (modified from Mitchell, 2005)

Pattern	*Ratio*	*Difference*
Clustered	R<1	D < 0
Random	R=1	D = 0
Dispersed	R>1	D > 0

If the means are the same, the ratio is 1 and the observed distribution can be considered random. If the expected mean is greater than the observed mean, the ratio is less than 1 and the observed distribution is clustered. The closer the value to 0 (the value for a completely clustered pattern), the more clustered the pattern. If the expected mean is less than the observed mean, the difference is greater than 1 and the observed distribution is dispersed (Table 3.1). The ratio obtained from Eq. 3.4 for the Zagros landslide dataset is equal to 0.65, suggesting that the landslide distribution exhibits clustering. Details of nearest neighbour index for the Zagros landslides are reported in Fig. 3.4.

3.2.3.2 TESTING THE RESULTS OF THE NEAREST NEIGHBOUR INDEX

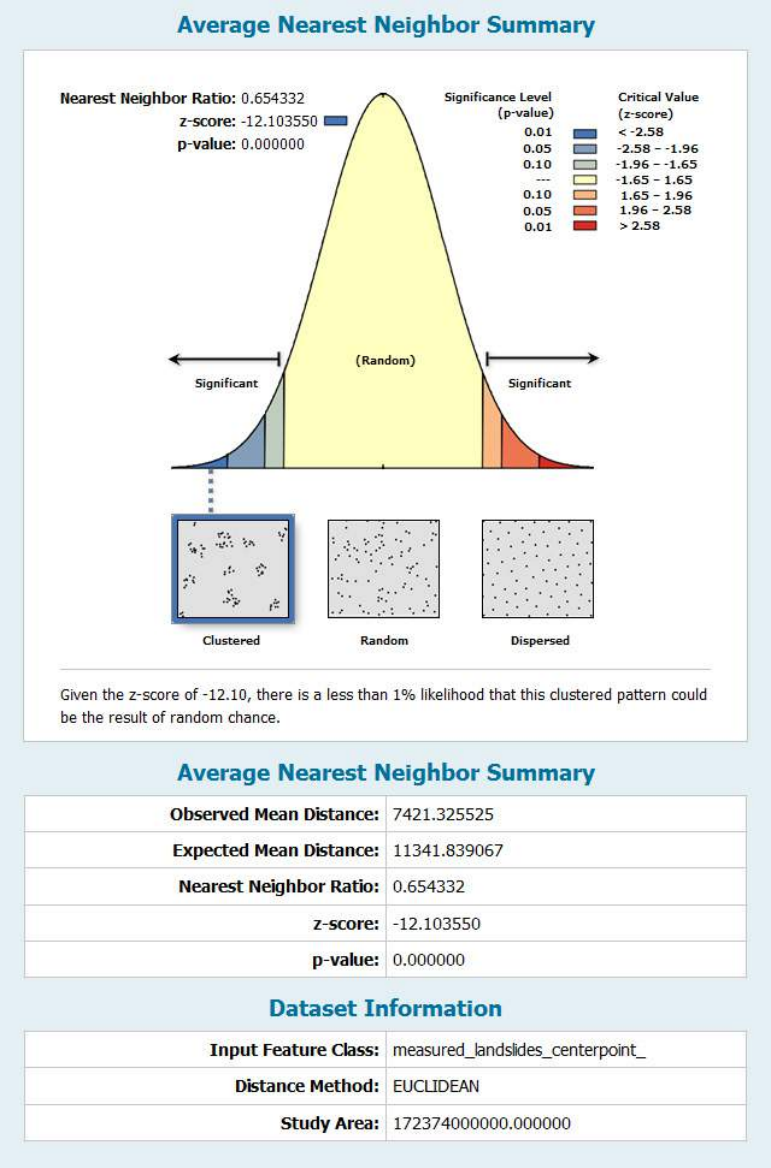

Fig. 3.4. Graphical summary of average nearest neighbor calculations of the Zagros landslide database.

Here, the statistical significance of the results of the nearest neighbour calculations is tested using the Z-score test. The null hypothesis is that the features are randomly distributed. The Z-score test divides the difference between the observed and expected values by the standard error (Lee and Wong, 2001; Mitchell, 2005):

$$Z = \frac{\bar{d}_o - \bar{d}_e}{\mathrm{SE}} \qquad \text{(Eq. 3.5)}$$

where Z is the Z-score, $\bar{d}_e$ is the expected mean distance for a completely random distribution, $\bar{d}_o$ is the observed mean distance and SE is the standard error.

The standard error (*SE*) measures the distribution of mean distances around their average value. This is equivalent to the standard deviation of the mean distance for the full set of features divided by the square root of the number of features (Bailey and Gatrell, 1998; Mitchell, 2005). The standard error is calculated from:

$$SE = \frac{0.26136}{\sqrt{n^2/A}} \qquad \text{(Eq. 4.6)}$$

where n is the number of features and A (m^3) is the areal extent of the features.

The concept of standard error is based on using a circle divided into equal sectors and finding the number of features, given a hypothetical random distribution in any given sector. The value 0.26136 is a constant derived from the radius of the circle (Bailey and Gatrell, 1998).

Since the difference is positive if the observed mean distance is greater than the expected mean distance, a positive Z-score indicates a dispersed pattern; conversely, the difference is negative if the observed mean distance is less than the expected mean distance; hence a negative z score indicates a clustered pattern. At a confidence level of 95% the Z-score would have to be greater than 1.96 or less than -1.96 to be statistically significant. The Z-score for the Zagros landslide dataset is equal to -12.103 (Fig. 3.4) indicating that the null hypothesis must be rejected and that the clustered landslide pattern is statistically significant in the Zagros region.

3.3 DENSITY OF LANDSLIDES

An alternative measure of the landslide pattern can be obtained by computing the density of landslides (Earickson and Harlin, 1994; Mitchell, 2005). To

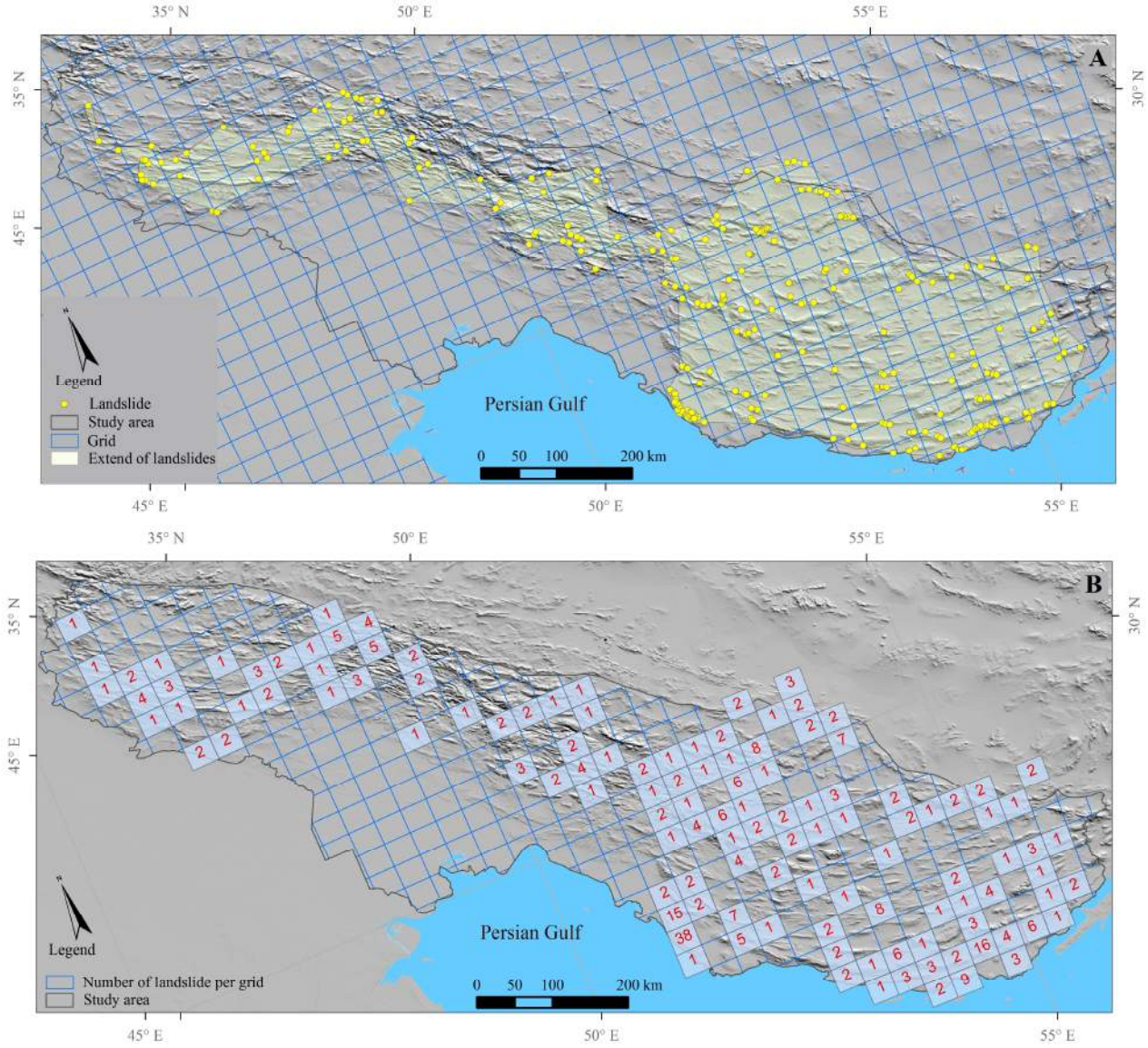

Fig. 3.5. Calculation of landslide density using *quadrate analysis* within Arc GIS (A) Centre point of landslides is overlaid by a grid of square cells of equal size. (B) The numbers inside cells represents the counts of landslides inside each cell.

identify the density of landslides within the study area, *quadrate analysis* is used within Arc GIS software. In this method the study area is overlain with equal-sized quadrangles. The number of landslides in each quadrant is counted and this value is compared with the number expected from a random distribution. If most of the landslides are located in fewer areas than expected and more areas than expected remain blank, the landslides form a clustered distribution. Results of this method helps to evaluate density distribution of geographical events but proximity of features to each other, or their relative arrangement is not considered as do the nearest neighbour index.

The quadrant size depends on the size of the study area and will affect the patterns that are identified. The aim is to choose a suitable size to be large enough to capture any pattern but not too large to obscure the pattern. Based on the statistical investigation (Ebdon, 1985; Getis, 1991; Getis and Ord, 1992; Mitchell, 2005), a reasonable size is twice the size of the mean area per event, which is simply the area of the study area divided by the length of one side of the square calculated by taking the square root of the result:

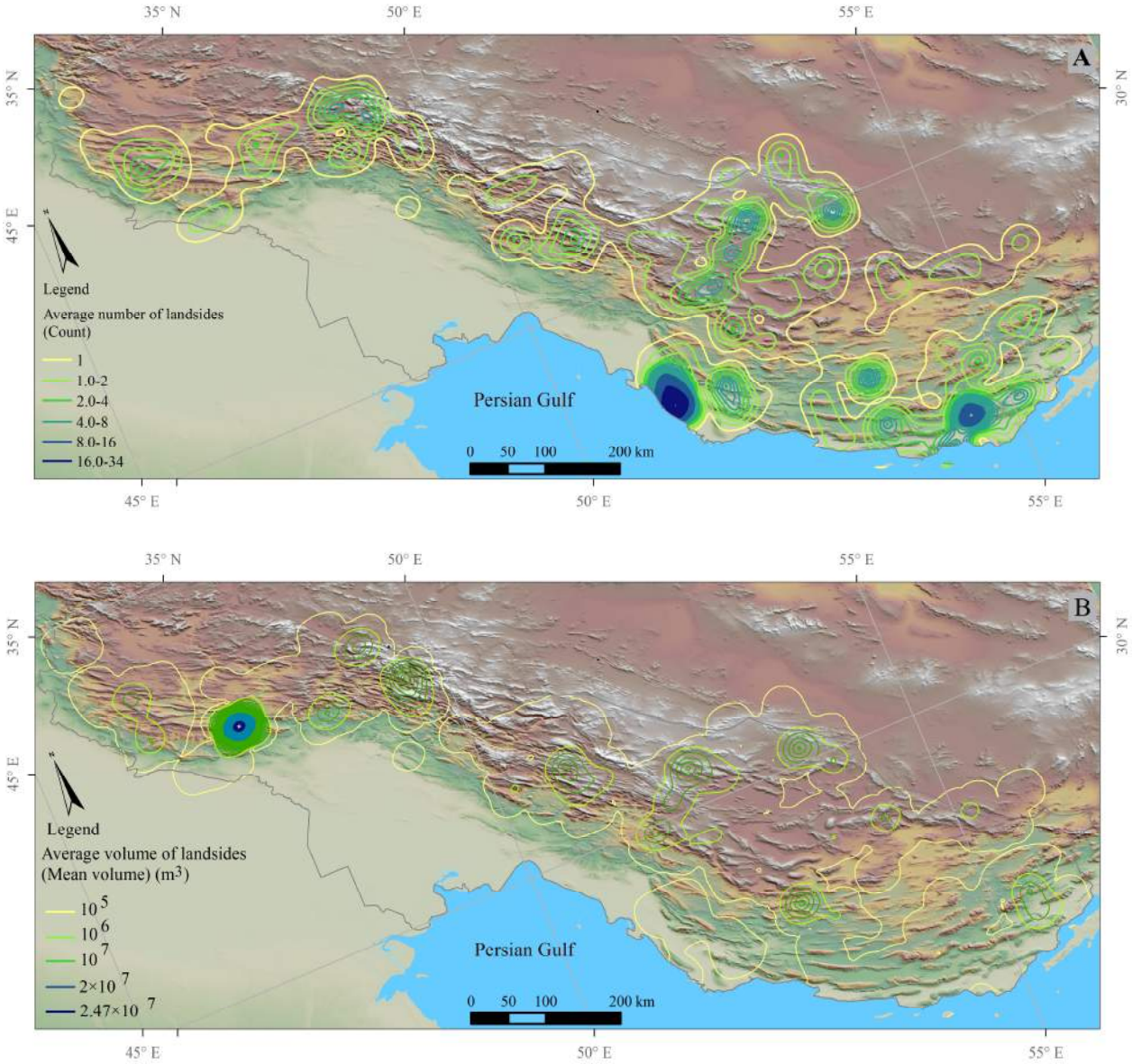

Fig. 3.6. Results of landslide density calculations for the Zagros using *quadrate analysis* within Arc GIS (A) Contours with different colours represent similar density of landslides. (B) Contours represent density of average volume of landslides.

$$I = \sqrt{2 \times {}^{A}/_{N}} \qquad \text{(Eq. 3.7)}$$

where I is the length of a side of a quadrate, A is the extent of the study area and N is the number of features. The area that covers the extent of all landslides is equal to 172,374 km^2, and (N) is equal to 335 events, the mean area per point is 514 km^2, the area of each quad is 1029 km^2, and the length of a quadrangle side is 32.07 km (Fig. 3.5.A). Then, the number of landslide centre points per unit area is counted (Fig. 3.5.B).

To represent the distribution of landslides, I interpolated the values of the centre points of events (i.e., landslides). The density of landslides frequency is shown in Fig. 3.6.A and the volume density of landslides is represented in Fig. 3.6.B. The distribution of landslides is clearly not uniform across the Zagros mountain belt. Landslides are more abundant in the southeast of the study area and decrease towards the northeast (Fig 3.6A). However, the size of landslides (volume of the displaced material) is larger in the northern part of the area and decreases toward the south and east (Fig 3.6B). The mean volume of landslides in the western Zagros is 9 times larger than in the eastern Zagros whereas the abundance of landslide in the eastern part of the region is 3.5 times more than in the western part of the region.

3.4 CONCLUSION

The spatial distribution of landslides investigated as a part of this study display a statistically significant clustered pattern. Identifying these clustered regions may be useful in that there could be geographical associations with other variables that can be identified. Mapping the locations of large landslides concentrations may help identify causes of instability.

Primary results reveal that the frequency of landslides close to the coast line is probably related to the extent of low strength lithologies in the southern part of the study area (Pirouz, 2013). Dating studies in the Zagros region show that these formations are younger and therefore are probably less consolidated (Pirouz et al., 2011). This will be discussed in more detail in Chapter 4.

Chapter 4

Factors controlling the spatial distribution of landslides in the Zagros region

4.1 Introduction

The susceptibility of a slope to failure and the spatial distribution of landslides is a consequence of the interaction of different causative factors including geological, morphological and physical processes (Alcántara-Ayala and Goudie, 2010). In this chapter, twelve potential causative factors are investigated (e.g., topographic relief, lithology, slope) in order to better understand why the studied landslides occur where they are and which factors control their size. Answering these questions will let us characterize the spatial distribution of landslides in the Zagros region. All landslide causative factors that have investigated in this study can be divided into 4 main categories including: 1) topographical factors (i.e., elevation, relief, curvature, aspect, slope, Pre slope), 2) geological factors (i.e., lithology), 3) geological process (i.e., basement faulting, surface faulting and folding), 4) surface process (i.e., fluvial channel incision) that here considered as river and main stream incision. Some of these causative factors such as topographical relief can be produced by geological process, such as faulting and folding, or can result from surface processes (e.g., river incision) (Bishop et al., 2003) or a combination of both. These natural factors are considered to make a slope potentially gravitationally unstable, triggering a landslide (Miller et al., 2010; Chen and Duan, 2014).

In this chapter, analysis of the landslide distribution will highlight some of the factors that have been controlling size and abundance of the landslides in the Zagros region. The results allow the possible identification of those combinations of geological and/or geomorphological parameters that makes hill slopes more susceptible for failure. The triggering factors behind the landslide distribution such as earthquake and climate are also briefly discussed in this Chapter.

4.2 Control on the spatial distribution of landslides

Numerous elements can affect slope failure and interact in complex ways (Varnes and Slopes, 1984). In this study, twelve possible causative factors of landslide are measured at a regional scale. This will enable us to (1) identify relationships of these variables with the location of landslides and (2) to recognize factors controlling the volume of material that is involved in landslide activity and the frequency of mass failures. The causative factors are divided into four main categories that include topographical factors, geological factors, geological process and surface process.

4.2.1 Topographical and morphological factors

4.2.1.1. Elevation

Because landslides are ultimately driven by gravity, it could be expected that on hillslopes they are somehow correlated with elevation. In addition, highly elevated areas may experience more rainfall, lower temperatures and longer periods of snow cover, all of which could influence landsliding (Pinet and Souriau, 1988; Coe et al., 2004; Miller, 2007). The elevation in the Zagros ranges from 0 m at the coastline to nearly 4400 m on Dena peak (the highest mountain), with a mean elevation of 1070 m (Fig. 4.1A). A topographic profile between the Main Zagros Reverse Fault and the Zagros Fordeep Fault

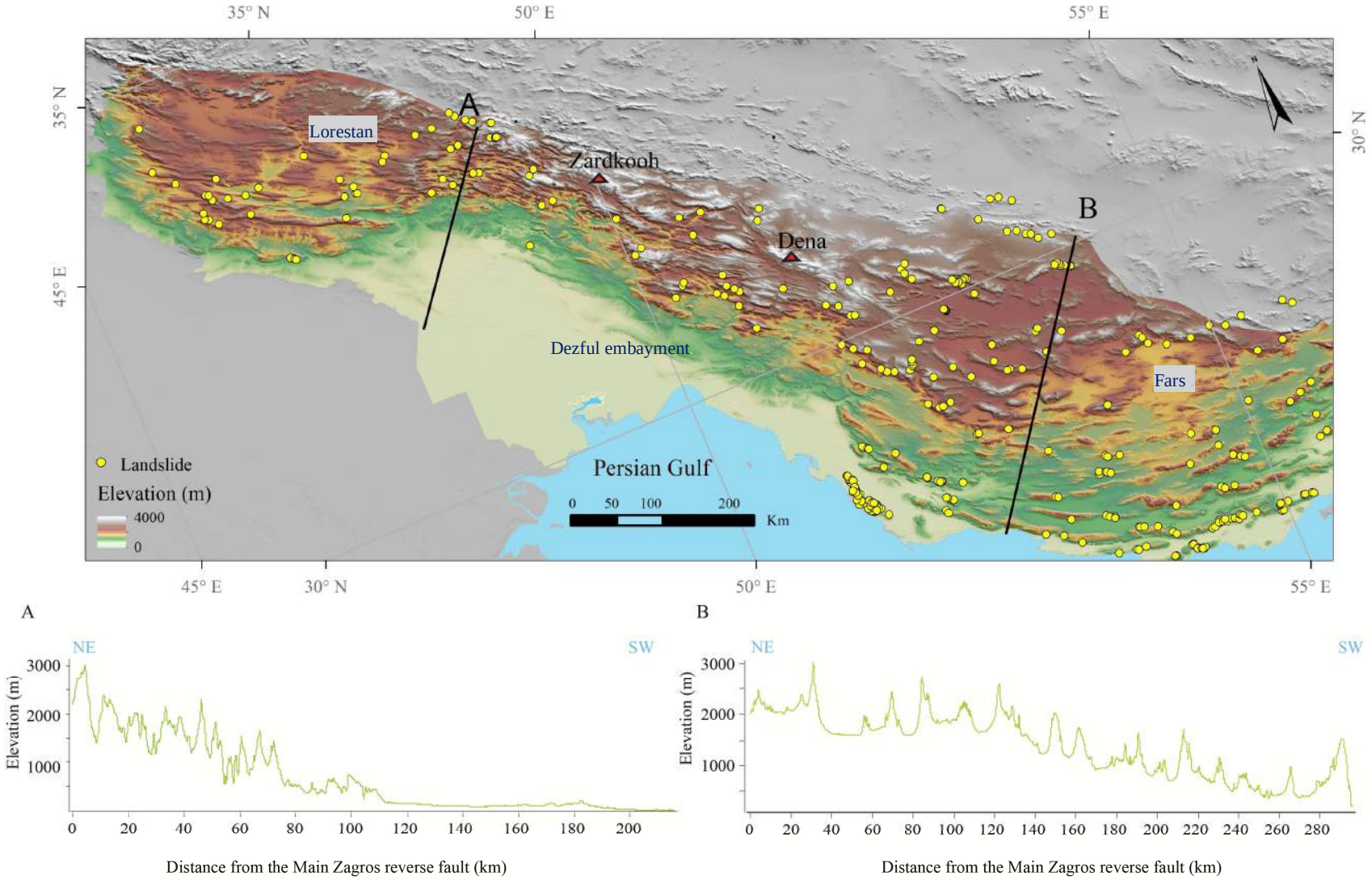

Fig. 4.1. A) Map of distribution of mean elevation derived from a DEM (resolution 30m) along with two elevation profiles.

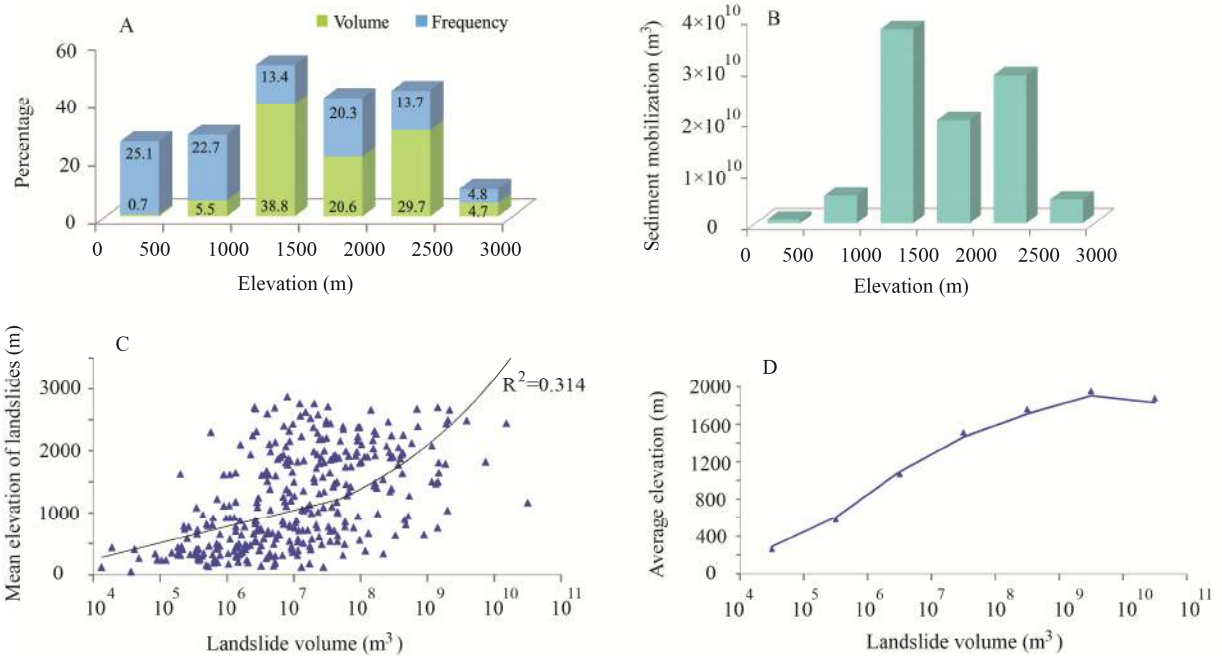

Fig. 4.2. A) Percentage of volume and frequency of large landslides (V > 10^4 m^3) versus mean elevation. B) Sediment productions of large landslides versus mean elevation, computed following Reid and Page (2002). C) Relationship between mean elevation and landslides volume (blue dots are mean elevation of landslides and black line is power fit of landslides mean elevation). D) Average of mean elevation in different volume classes.

shows that elevation increases northward (Fig 4.1A and B). The Dezful embayment in the south has low relief and low elevation (section line A in Fig 4.1). From the north-eastern limit of the Dezful embayment (Lorestan region), the topography climbs from the plains to the highest elevations near the Main Zagros reverse fault (Allen et al., 2013). Section line B in Fig 4.1 shows that the elevation profile across the Fars region is much more uniform than in the Lorestan region. The Fars profile shows a steady climb from the coast to about 180 km northward, after which the average slope decreases (Allen et al., 2013).

By plotting the landslide frequency versus elevation, we can see that 47.4% of landslides by frequency occur in the elevation range 1000 - 2500 m, while the same elevation interval accounts for 89.1% of landslides in terms of volume (Fig. 4.2.A). The amount of sediment produced by landslides is highest between 1000 and 1500 m elevation (Fig. 4.2.B). The volume of sediment mobilized was calculated here by multiplying the frequency of landslides in each relief interval by the average volume in that interval (Reid and Page, 2002).

Fig. 4.2.C illustrates the relationship between volume and mean elevation of large landslides in the Zagros mountain belt; the plot shows considerable variability, but an overall tendency for larger volume landslides to occur at higher elevations. The average elevation of landslides within different volume intervals is shown in Fig. 4.2.D. This graph shows a rough positive relationship between mean elevation and landslide volume up to elevation of about 1880 m, with a slight decrease thereafter.

4.2.1.2. RELIEF

General topographic relief of the Zagros region is the result of tectonics and surface processes. Local relief is generated by concurrent basement faulting and folding of sedimentary cover rocks (Jackson, 1980; McQuarrie, 2004), and river incision. The presence of a thick incompetent layer of basal salt causes low topography and relatively low relief in the eastern part of the region (Fars) compared to the western part (Lorestan) (Pirouz et al., 2011). River erosion also forms high relief along major rivers valleys in the western part of the region (Lorestan), especially where rivers cross fold axes, whereas in the eastern part of the region (Fars) they pass around the anticlines and are mostly parallel with fold axes.

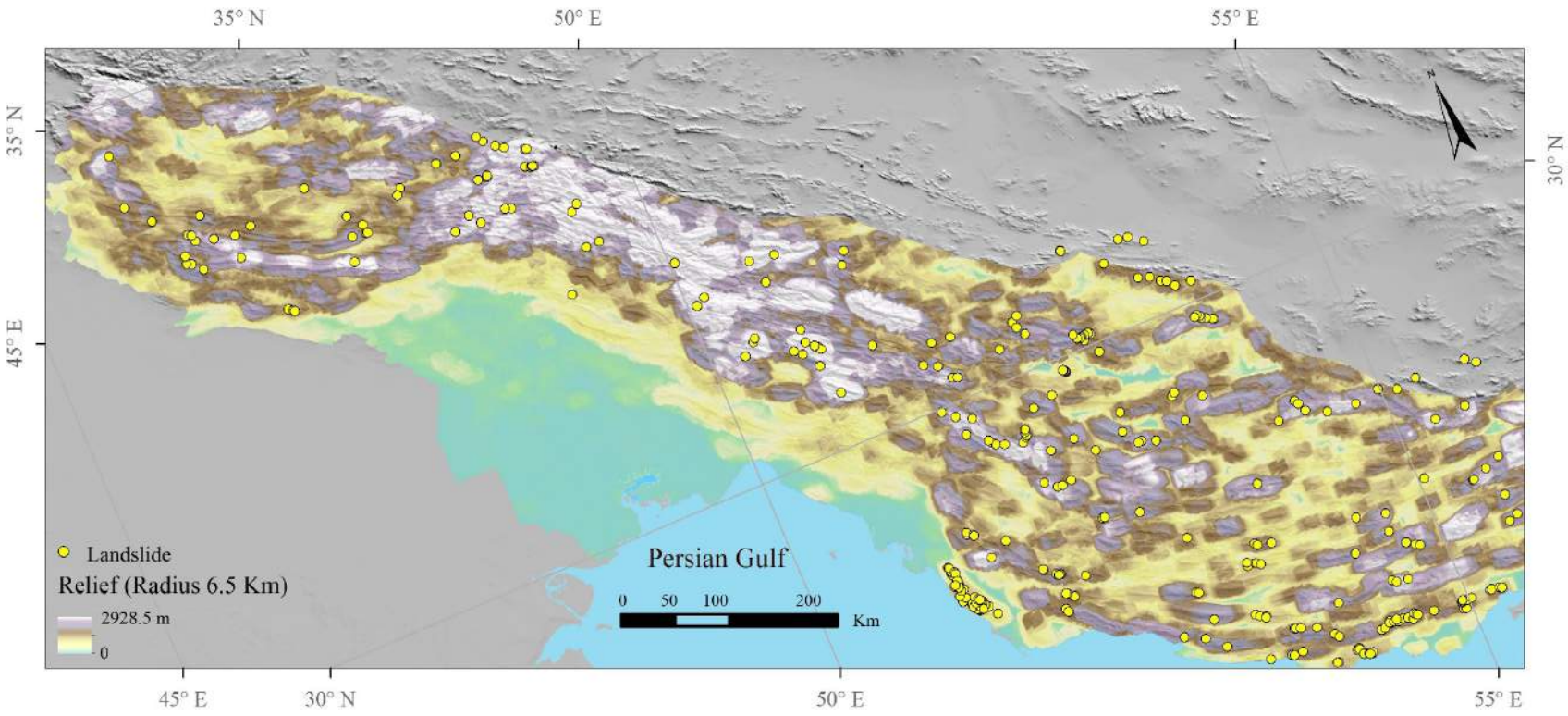

Fig. 4.3. Topographic relief of the Zagros and distribution of landslides in the study area.

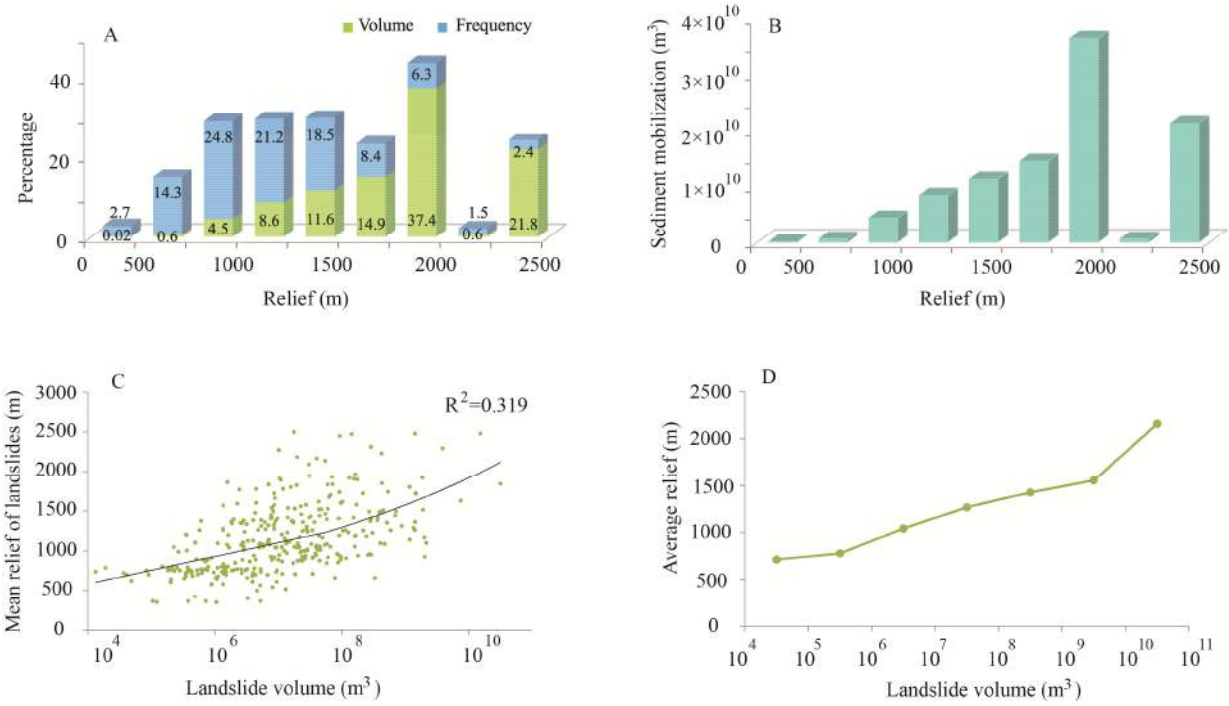

Fig. 4.4. A) Percentage of volume and frequency of large landslides (V> 10^4 m^3) in mean local relief. B) Sediment production from large landslides in mean local relief, computed following Reid and Page (2002). C) Relationship between mean local relief and landslide volume (green dots are mean local relief of landslides and black line is power fit of landslides mean relief. D) Average of mean relief as a function of landslide volume.

Topographic relief is defined as the difference in elevation within a certain limited area (Montgomery and Brandon, 2002; Wang et al., 2013). In this study, we quantified the relief within a circle with a 6.5 km radius (Fig. 4.3). This distance is equivalent to the standard deviation of measured landslides areas and it is large enough to span the large fold structures characteristic of the Zagros (Takezawa et al., 2012). To calculate the relief of each landslide individually, the focal statistic extension in Arc GIS software is used and the mean relief of landslide polygon areas is calculated. 78.8% of landslides (in terms of frequency) have local relief ranging from 500 - 1500 m, while 74.7% of landslides volume is located in relief between 1500 - 2500 m (Fig. 4.4A). The amount of sediment produced by landslides within a relief class is a function of their volume and frequency (Reid and Page, 2002). This measure shows a significant increase in sediment mobilization due to landslides in higher relief (Fig. 4.4B). Fig. 4.4C shows the relationship between volume and local relief of landslides in the Zagros mountain belt.

The average relief of landslides in different volume intervals is shown in Fig. 4.4D; this data shows larger volume landslides occurred in high relief areas, through the correlation coefficient is poor (R^2=0.319).

4.2.1 TOPOGRAPHIC CURVATURE

Curvature is a measure of how the slope of a surface changes in space. The curvature is potentially an important parameter influencing the distribution of landslides since it controls whether water flowing over the surface will diverge (convex) or converge (concave). (Hack and Goodlett, 1960; Reneau and Dietrich, 1987). The curvature of a surface is also potentially important in controlling intensity of seismic shaking, since ground seismic accelerations are often accentuated along ridges (Bouchon, 1973; Davis and West, 1973; Geli et al., 1988).

Curvature is defined as the second derivative of the surface (i.e. the slope of the slope) (Zevenbergen and Thorne, 1987; Moore et al., 1991; “ArcGIS Desktop”) and can be routinely computed within Arc GIS software using zonal statistics. Plan curvature is perpendicular to the direction of the maximum slope that influences on convergence and divergence of flow (“ArcGIS Blog”). The measured mean curvature corresponds to the curvature of the slide surface upon

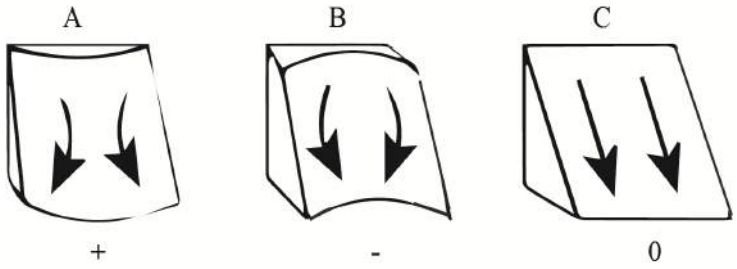

Fig. 4.5. The slopes with positive curvature (a), negative curvature (b) and zero curvature (c) ("ArcGIS Blog").

which landslides moved, since most of the investigated landslides are slides. Results show that the mean curvature varies from -0.72 to 0.40, while the minimum and maximum curvatures (representing extreme relief) ranges between -12.2 to 10.2. A positive value indicates that the surface is upwardly convex whereas a negative value indicates that the surface is upwardly concave, and a value of zero indicates that the surface is planar (Ohlmacher, 2007) (Fig. 4.5).

Fig. 4.6A demonstrates that 83% of landslides in terms of frequency and 92.2% of landslide by volume occurred on surfaces with a curvature between -0.2 and 0, indicating that most landslides slipped on a flat or slightly concave surface. Analysis of sediment mobilization in Fig. 4.6B shows that 97.2% of landslides by volume in this dataset moved on surfaces with curvature values between -0.3 to 0.

4.2.1.4. DIP DIRECTION

The aspect of a slope can influence landslide generation, since differently directed slopes are exposed to differences in solar radiation, prevailing weather, moisture retention and vegetation, which may affect soil strength and pore fluid pressures (e.g., Wieczorek et al., 1997). In the Zagros fold thrust belt the dominant aspect of hillslope is perpendicular to the general trends of the folds. To investigate the relationship between landslide frequency and slope aspect, the DEM was used to calculate the aspect of each landslide using the zonal statistic extension of Arc GIS software.

Results show that the landslide frequency is relatively low on slopes directed northwest-southeast while it increases with the orientation angle, reaching a maximum for northeast-southwest directions (Fig. 4.7).

Fig. 4.8A demonstrates that 35.2% of landslides by frequency and almost 59% of the total volume of landslides are located on northeast directed slopes. The southwest direction contains almost 33% of landslides by frequency and almost 22% of the total volume of landslides. Most sediment discharge linked to landslides in the study area is from the NE, SW, and NW directions, respectively, while other directions contain only 4.2% of landslides by volume (Fig. 4.8B).

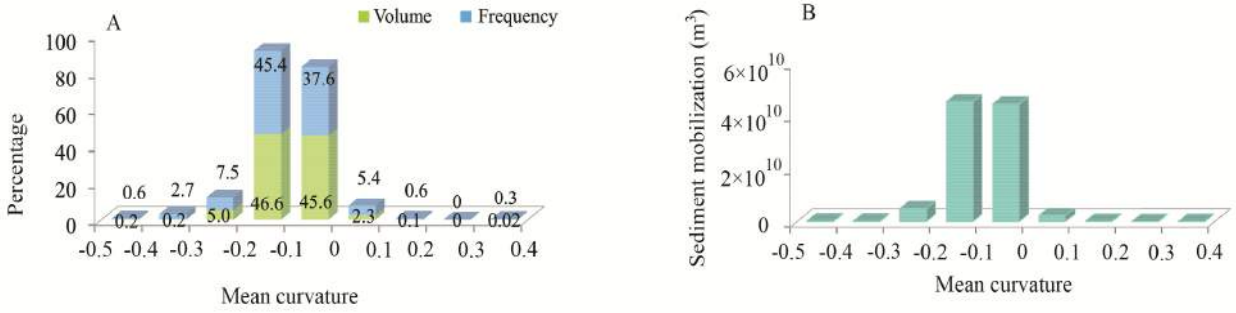

Fig. 4.6. A) Percentage of frequency and volume of landslides versus mean curvature. B) The amount of sediment mobilised by landsliding for different mean curvature classes.

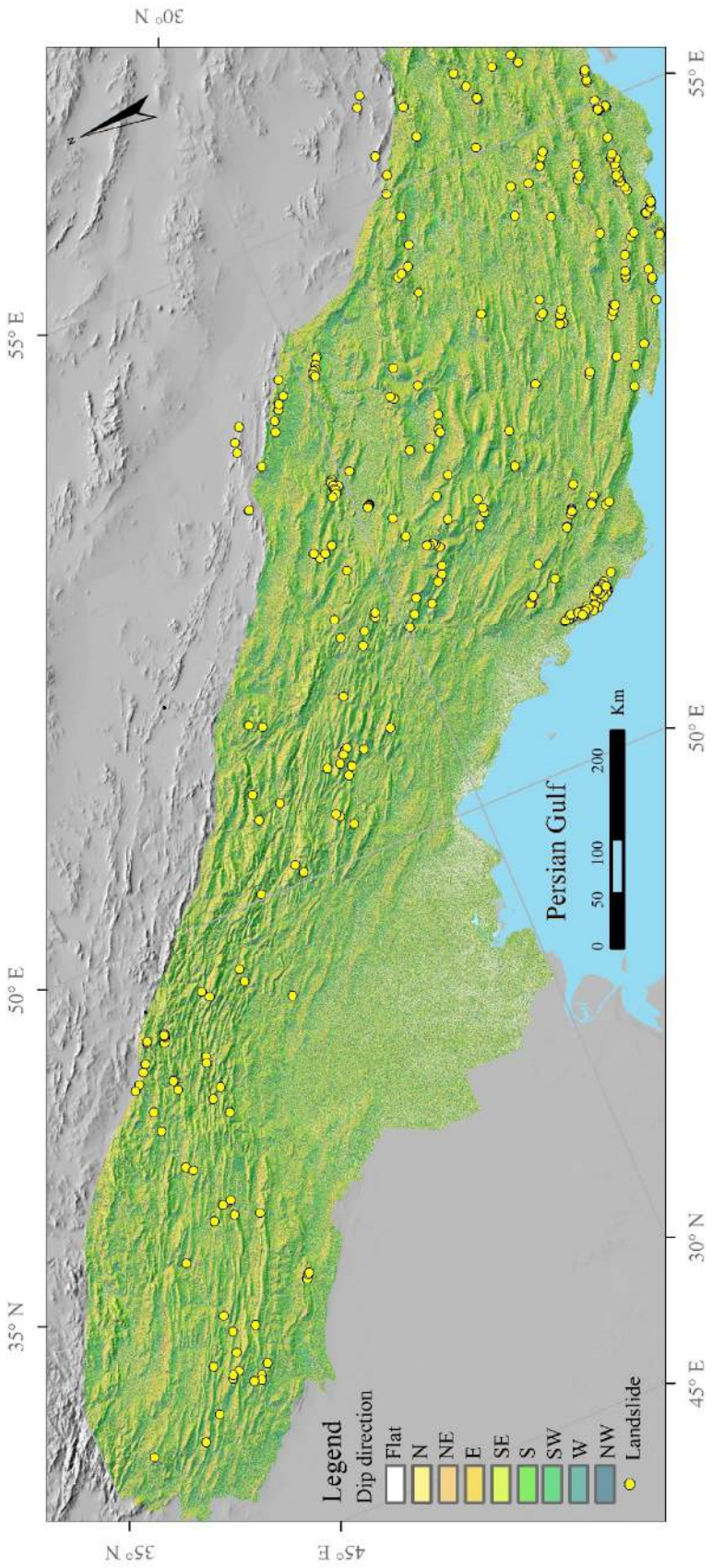

Fig. 4.7. Map showing the dip direction of topographic slopes along with landslide locations in the Zagros. Northeast and southwest directed slopes are dominant.

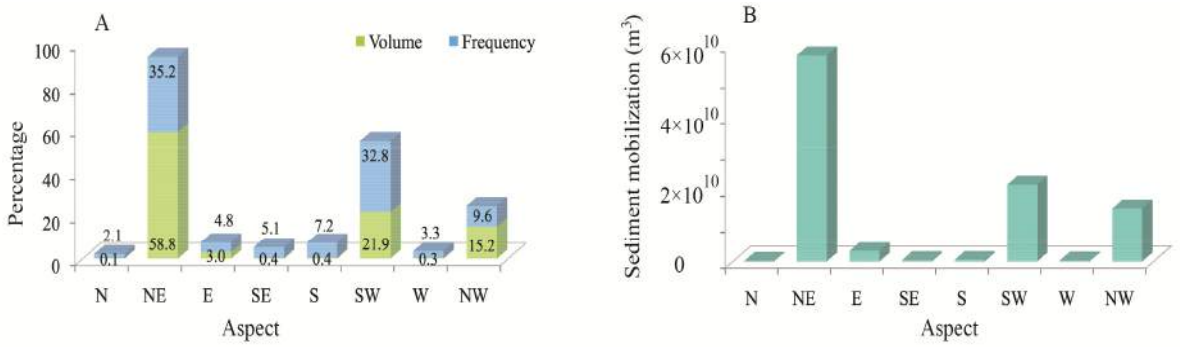

Fig. 4.8. A) Percentage of volume and frequency of large landslides ($V > 10^4$ m^3) in different directions. B) Sediment productions of large landslides in different directions.

4.2.1.5. SLOPE AND PRE-SLOPE

The slope of the topography is likely to have an important control on gravitational mass failure (Larsen and Torres-Sanchez, 1998; Dai and Lee, 2002). The slope is determined by both the rock strength and the operating erosive processes, but the actual controls are poorly understood and can be complicated. For example, many steep slopes in competent rocks are more stable than gentle slopes within weak material (Varnes and Slopes, 1984).

Mass movements will continue until a stable slope is achieved (Prellwitz et al., 1994). The actual mean slope of landslide should therefore indicate a stable condition. The mean slope of the landslide is calculated as an average of all cells in the slope raster that belong to the same landslide polygon (Fig. 4.9A and C).

While the pre-slope is also estimated here, defined as the slope prior to mass failure. Slopes were computed as an average, obtained at the scale of the entire landslide. The pre-slopes (S_p) of the landslides is computed individually as arctan of elevation range divided by the horizontal distance from the scarp and toe of the depleted area (Fig. 4.9B).

$$S_p = \arctan(\Delta Z / \Delta d) \qquad \text{Eq. 4.1}$$

where ΔZ is the maximum change in elevation between the top and bottom of a slide and Δd is the horizontal distance between the top and base taken in the direction of the maximum gradient (Fig. 4.9B).

All landslides in our database have slopes of less than 50° (Fig. 4.10). We are unable to resolve slopes >45° which essentially means we ignore rockfalls (N Ghazipour, 2007; Chen et al., 2008). The pre-slope of 75.5% of landslides by frequency and 96.4% of the total volume of landslide was between 5° to 25° (Fig. 4.11.A). The amount of sediment discharge linked to landslides is greatest for slopes between 5° and 15°; that means 84% of the total volume of sediment moved by landslides were located in pre-slopes with less than 15 degrees (Fig. 4.11.B). Fig. 4.11.C shows that there is a poor correlation between the volume of landslides and their pre slope. The average pre slope of landslides versus different volume intervals is shown in Fig. 4.11.D; larger volume landslides tend to occur on more gentle slopes, on average.

The slope of 86.5% of landslides by frequency and 83.3% of the total volume of landslides occur between 10° and 25° (Fig. 4.11.E). The amount of sediment mobilised by landsliding is a maximum in the slope range 15° - 25°, which includes 67.4% of the total volume of sediment that moved by landslides (Fig. 4.11.F). Fig. 4.11.G shows a poor relationship between volume and the slope of landslides. The volume of landsides is independent of the average slope (Fig. 4.11.H).

Comparison of diagrams A and E in Fig. 4.11 shows that the mean slope of landslides is generally steeper than the pre-slope. This is probably due to the steep head scarps and sidewalls of landslides.

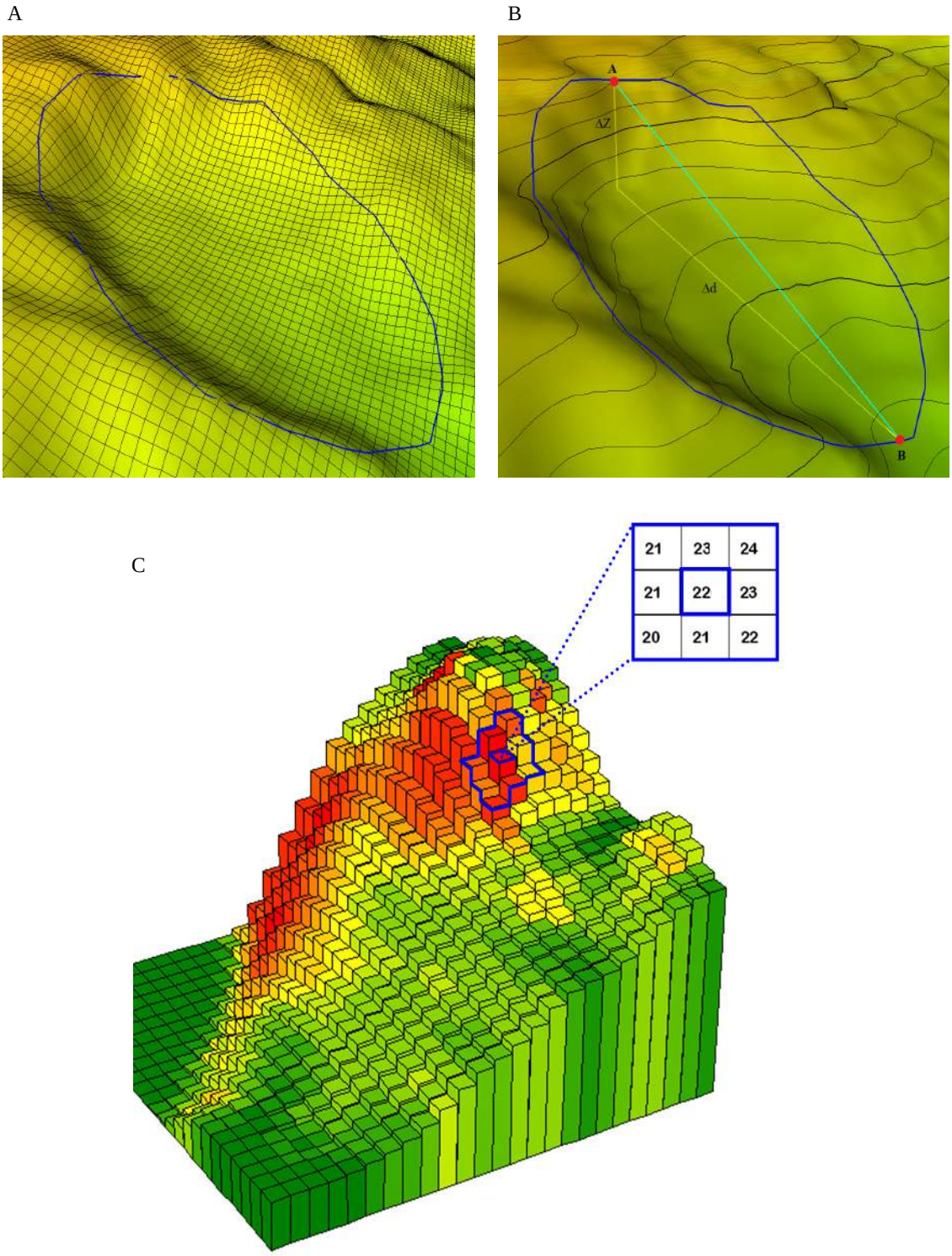

Fig. 4.9. A) Elevation surface and the grid of raster layer of a landslide polygon. B) Pre slope is computed from the elevation difference between two point A and B divided by the horizontal distance between two points. C) The mean slope value of the landslide polygon is calculated from cells value inside the polygon by using Zonal statistic extension in ArcGIS (Berry and Mattie, 2005).

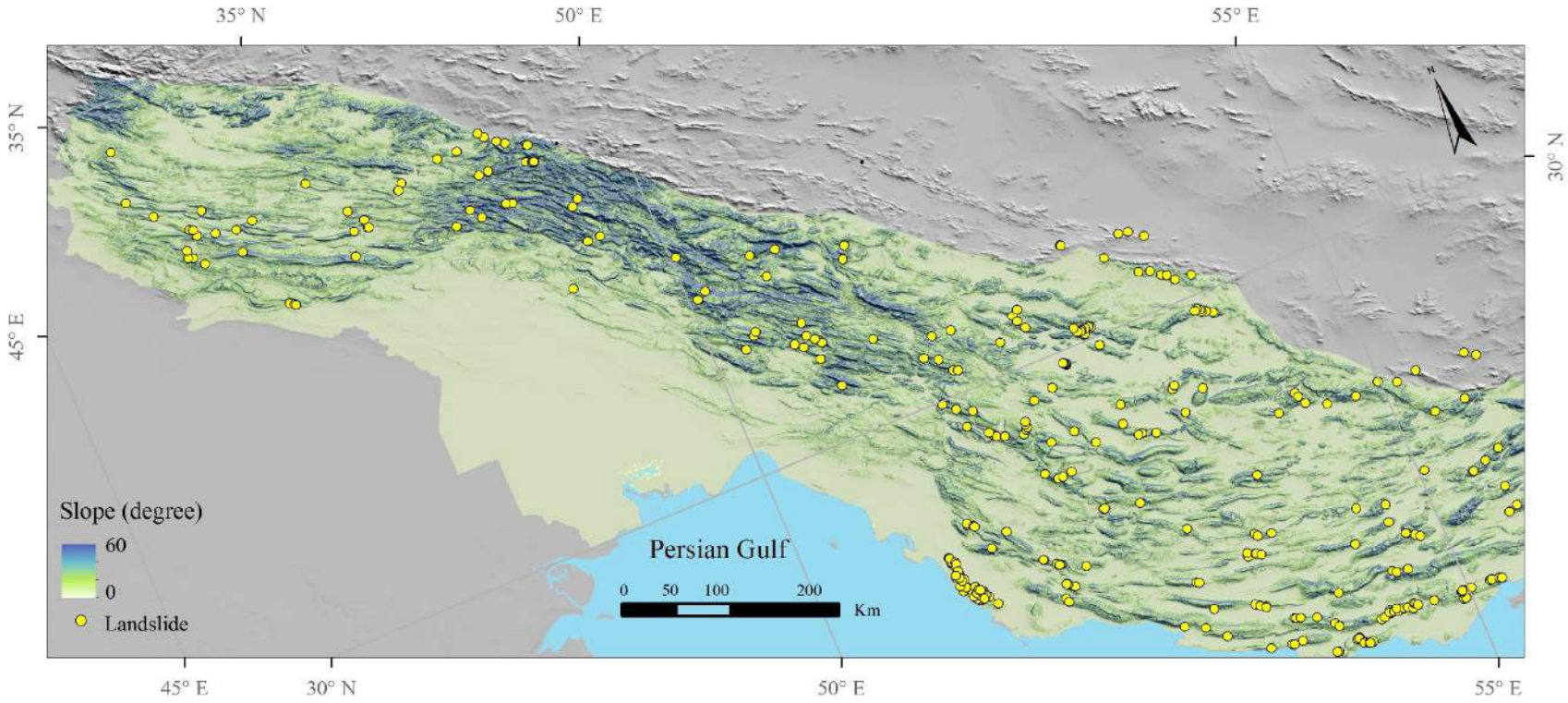

Fig. 4.10. Map showing landslide locations and the magnitude of the topographic slope derived from the DEM with resolution 30 m × 30 m.

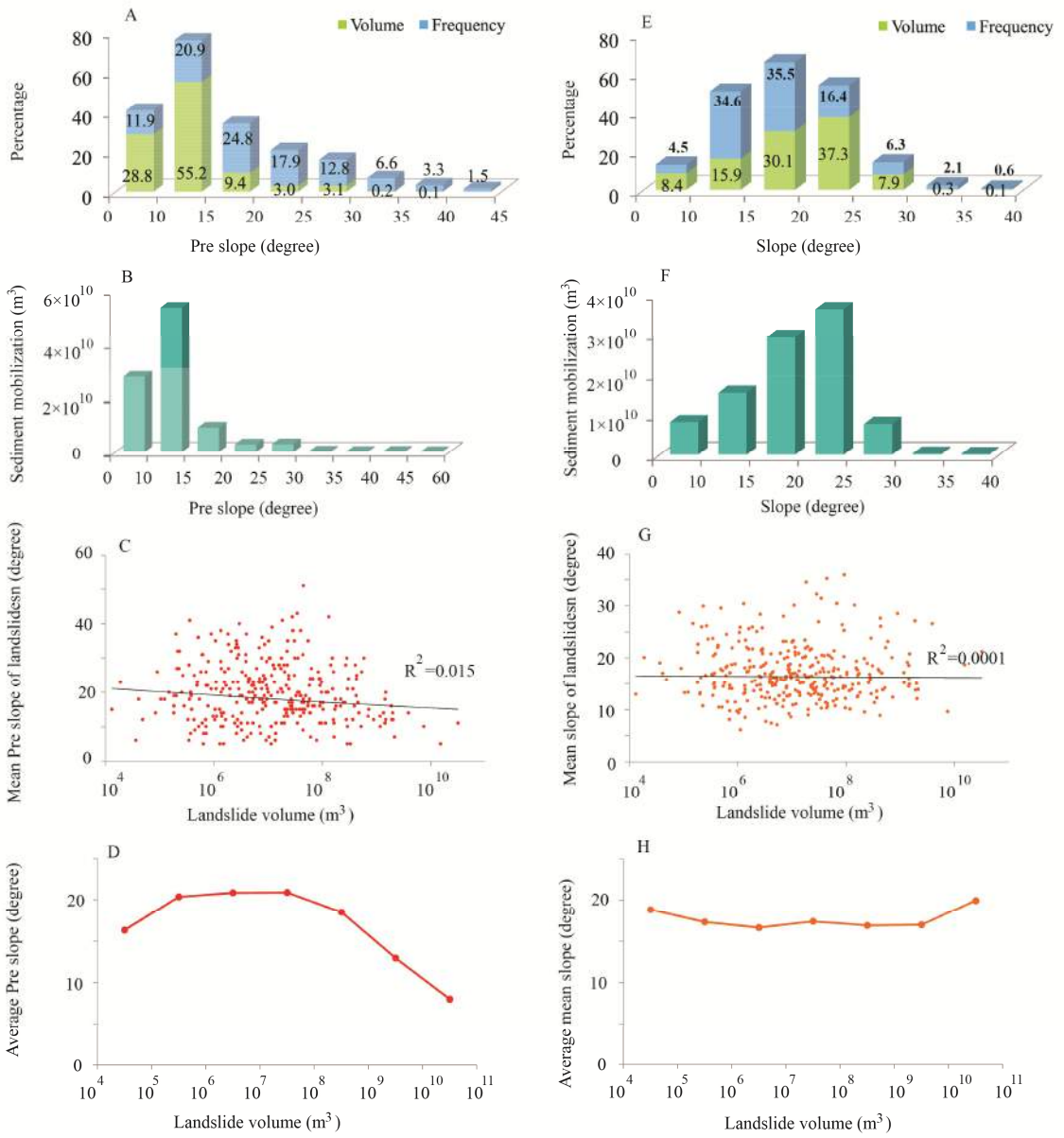

Fig. 4.11. A) Percentage of volume and frequency of large landslides (V > 10 ^{4} m^3) versus pre slope classes. B) Sediment productions of large landslides versus pre slope angles. C) Relationship between pre slope and landslides volume (red dots are pre slope of landslides and black line is power fit of data. D) Average of pre slope versus volume classes. E) Percentage of volume and frequency of large landslides (V > 10 ^{4} m^3) versus mean slope classes. F) Sediment productions of large landslides versus mean slope angles. G) Relationship between mean slope and landslides volume (red dots are mean slope of landslides and black line is power fit of data). H) Average of slope degree versus volume classes.

4.2.2 GEOLOGICAL FACTORS

4.2.2.1 LITHOLOGY

To identify the lithology involved in each landslide, geological maps published by the Geological Survey of Iran and National Iranian Oil Company have been used at 1/100000 and 1/250000 scale. Studied landslides are located entirely within the sedimentary series. Sedimentary rocks have been divided into 4 main lithological associations, which exhibit broadly different mechanical behaviour. These are carbonates, coarse clastics, evaporites, fine grained clastics and alluvium (Fig. 4.12). Carbonate rocks are more resistant than other sedimentary rocks and are usually associated with the highest peaks (Dena and Zardkuh peaks) in the Zagros mountain belt. Alternatively, coarse clastic rocks like sandstones and conglomerates are less resistant than carbonates, but

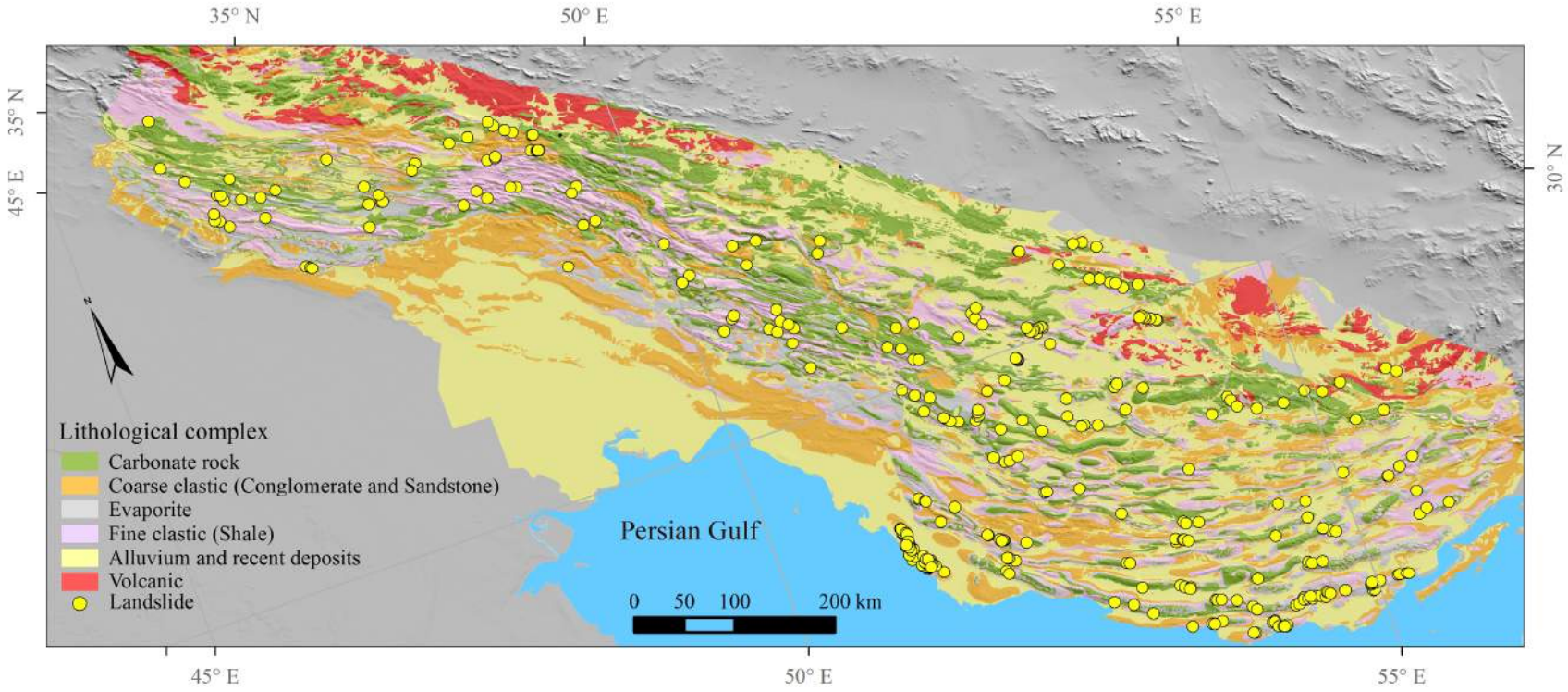

Fig. 4.12. Studied landslides are entirely within the sedimentary series, including carbonates, coarse clastics, evaporites and fine clastics.

more resistant than fine clastic rocks (e.g., mudstone and siltstone). The weakest and most easily eroded rocks in the study area are evaporites including gypsum and salt. Successions most prone to landslides in the Zagros are characterized by an alternation of weak and relatively resistant rocks (e.g., evaporites and carbonates). It is important to emphasize that because the distribution of the main lithologies in the Zagros changes laterally and vertically, deformation and erosion play an important role on the distribution of these lithologies (Pirouz et al., 2011). Fine clastics and evaporite rocks are thick and have more outcrops in the south eastern (Fars) of the Zagros region. The fine clastics thickness are remarkably thin or absent in the northern and western parts of the Zagros region, while the carbonate rocks have more outcrops in north west part of the region (Lorestan)(Pirouz et al., 2011).

This part of the study has been carried out using Arc GIS. To quantify the lithology as a variable for statistical analysis, the percentage of each lithology in each landslide polygon is estimated from the source area of mass failure. The lithology of each landslide is represented as a percentage in four columns: carbonate, coarse clastic, fine clastic and evaporite.

Fig. 4.13A shows that 74.5% of landslides by volume occurred in carbonate rocks and almost 17% of landslides occurred in fine clastic rocks. Coarse clastic and evaporite rocks contain 8% of landslides-

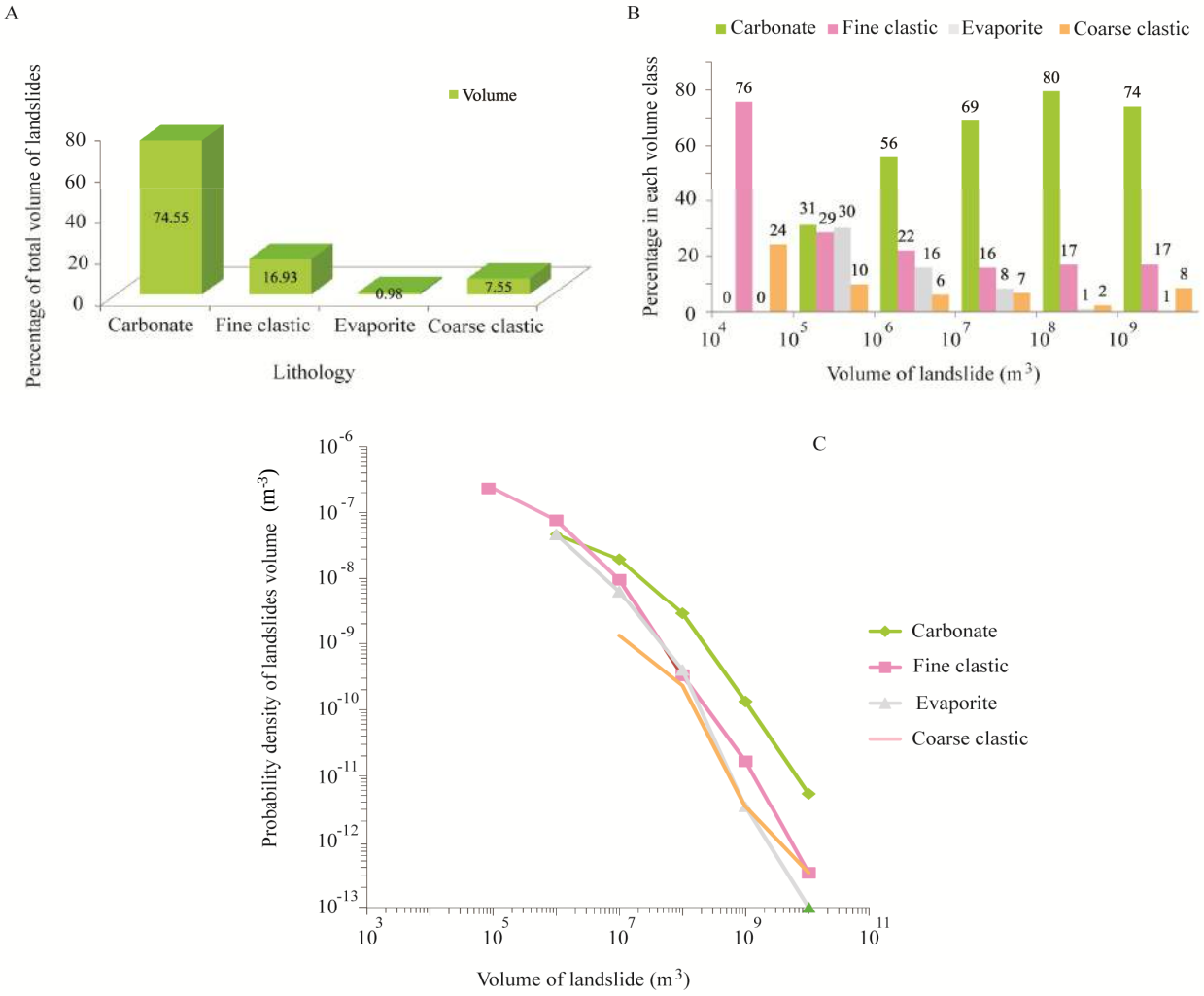

Fig. 4.13. A) Percentage of landslide volume within four different lithologies. B) Percentage of four lithologies in volume classes. C) Probability density of volume of landslides in four lithologies.

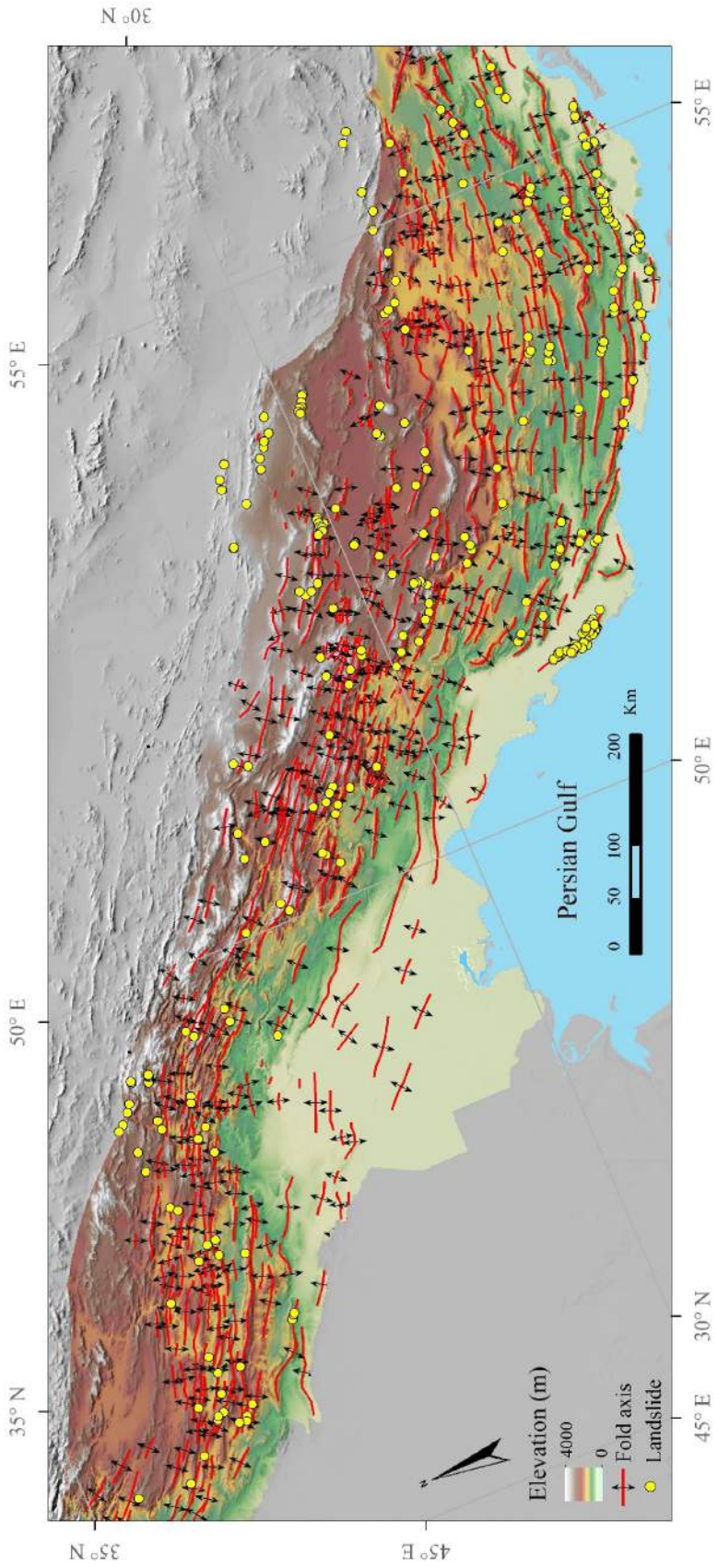

Fig. 4.14. Map showing the distribution of fold axes and landslides in the study area.

by volume. Fig. 4.13B shows the percentage of four different lithologies in different volume classes. Less resistance rocks contain smaller volume mass failures while, high strength rocks contain larger volume landslides. The probability density of landslides in four lithologies is shown in Fig. 4.13C. The data can be fit with a law of the form:

$$P(V_L)=1/N_{TL}\times\delta N_L/\delta V_L \qquad (4.1)$$

where N_{TL} is the total number of landslides, δV_L is the bin width, and δN_L is the number of landslide with volume between V_L and $V_L+\delta V_L$ (Malamud et al., 2004). Bin width increases with increasing volume, so that bin widths are approximately equal in logarithmic coordinates. Fig. 4.13C shows that the largest landslides ($V_L>10^7 m^3$) are most probable in carbonate rocks while smaller volume of landslides ($V_L<10^7 m^3$) are most common in fine clastics.

4.2.3. GEOLOGICAL STRUCTURE

4.2.3.1. FOLDS

The Zagros fold thrust belt is characterized by many elongate, nearly symmetrical folds with low aspect ratios (width to length ratio) that formed in response to regional shortening (Ramsey et al., 2008). The Zagros folds are associated with considerable elevation and relief, as illustrated in sections 4.2.1.1 and 4.2.1.2. However, relief may also be linked to other factors (e.g. river incision) that may be independent of folds. In this section, the relationship between folds and landslides is investigated by focusing on the distance to fold axes, not topographic measures. To quantify this relationship, we have digitized fold traces using geological maps and satellite images in the Arc GIS environment (Fig. 4.14) and investigated the nearest distance between fold axes and landslides. Fig. 4.15A demonstrates that 80.6% of landslides by frequency and 85% of total volume of landslides are located within 5 km of a fold axis. Fig. 4.15B shows that sediment mobilized by

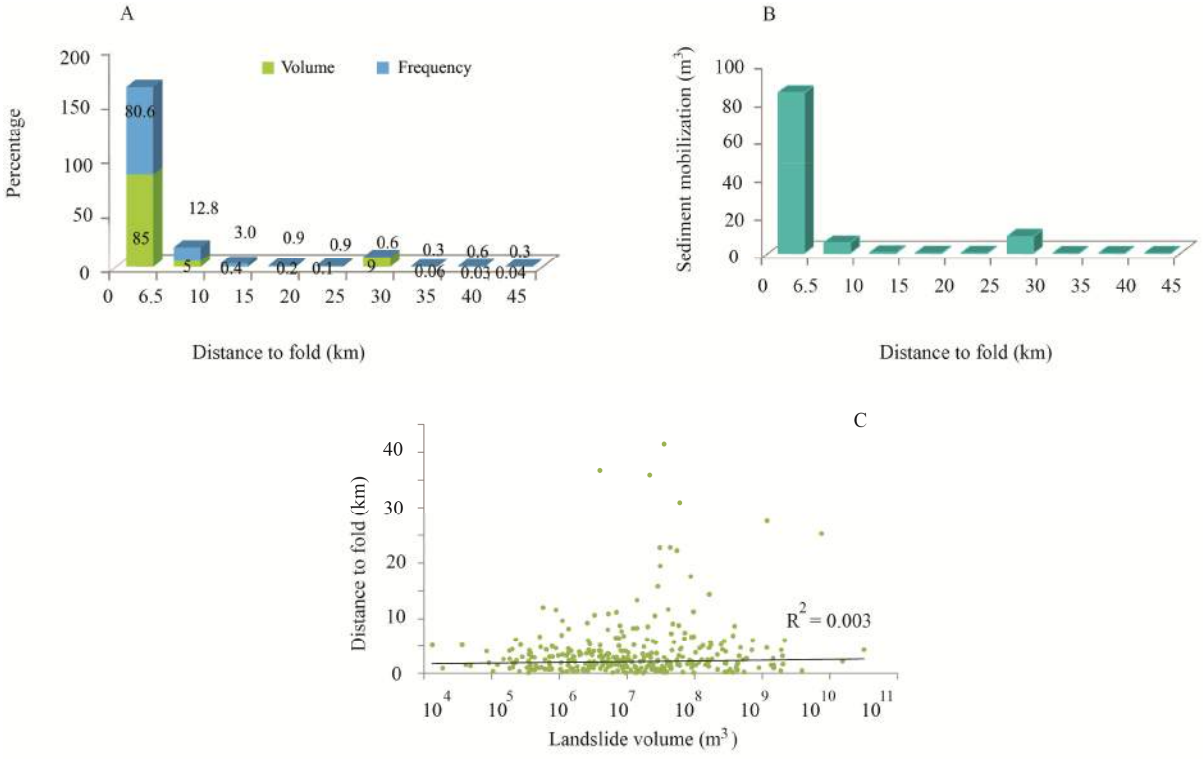

Fig. 4.15. A) Percentage of volume and frequency of large landslides ($V > 10^4 m^3$) versus distance to fold axes. B) Sediment productions of large landslides versus distance to fold axes. C) Relationship between distance to fold axes and landslides volume (black line is power fit of landslides distance to folds axes).

landslides occurs almost entirely within 5 km of a folds axis. There is no relationship between landslides volume and distance to a fold because almost all of the landslides are located on fold limbs Fig. 4.15C.

4.2.3.2. FAULTS

Although the Zagros is best known for its spectacular folding and faulting, especially within the basement (McQuarrie, 2004). Basement faults are deeply rooted faults that cut old crystalline rocks with Precambrian age. These faults are typically reactivated throughout the Cenozoic and in some case are clearly active today (since they modify the present day topography). To determine whether they play a role in controlling the landslide distribution, we have quantified the distance between landslides and major basement faults (Fig. 4.16) and surface fault ruptures (Fig. 4.17).

Fig. 4.18A shows that 82.4% of the volume of landslides and 77.4% of landslides by frequency occurred within 40 km of a basement fault. The frequency and volume of landslides have a strong inverse correlation with the distance from basement faults. Sediment mobilization mostly occurred close to basement faults (Fig. 4.18B). The relationship between landslide volume and the average distance to basement faults (Fig. 4.18C) indicates that landslides are largest close to basement faults. This relation could indicate a link between fault induced fracturing and/or seismic shaking and landsliding (J. S. Scheingross, 2013).

Almost 92% of landslides in the Zagros in terms of frequency and 97% of landslides by volume occur within a short distance, only about 10 km, from recent surface fault ruptures (Jibson et al., 2004). The volume of landslides doesn’t show any correlation with distance to recent faults, most occurring within 10 km (Fig. 4.18D). Sediment mobilization therefore also occurred mostly within 10 km of active faults (Fig. 4.18E). The relationship between landslide volume and average distance to faults (Fig. 4.18F) seems to indicate that the volume of landslides is independent of the distance to faults.

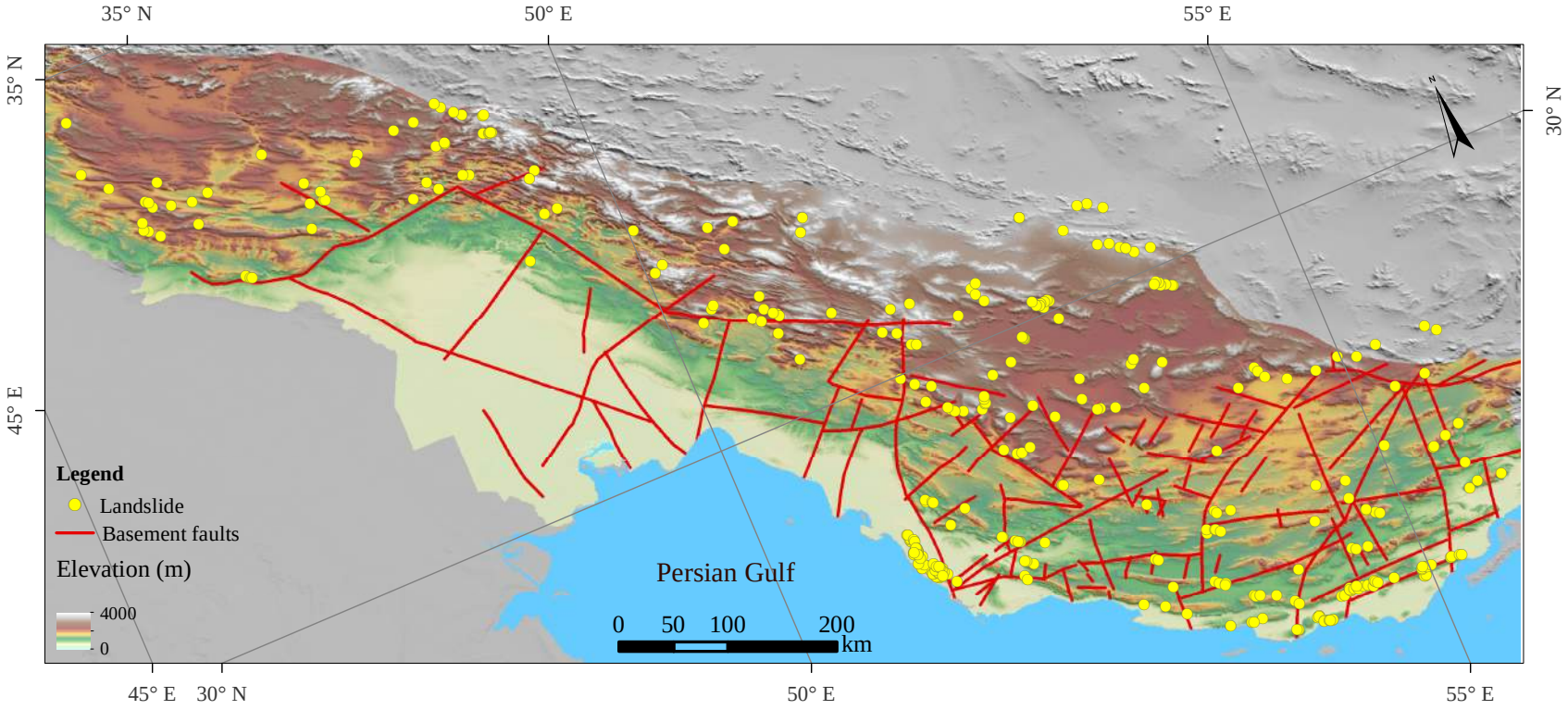

Fig. 4.16. Distribution of basement faults and landslides in the study area.

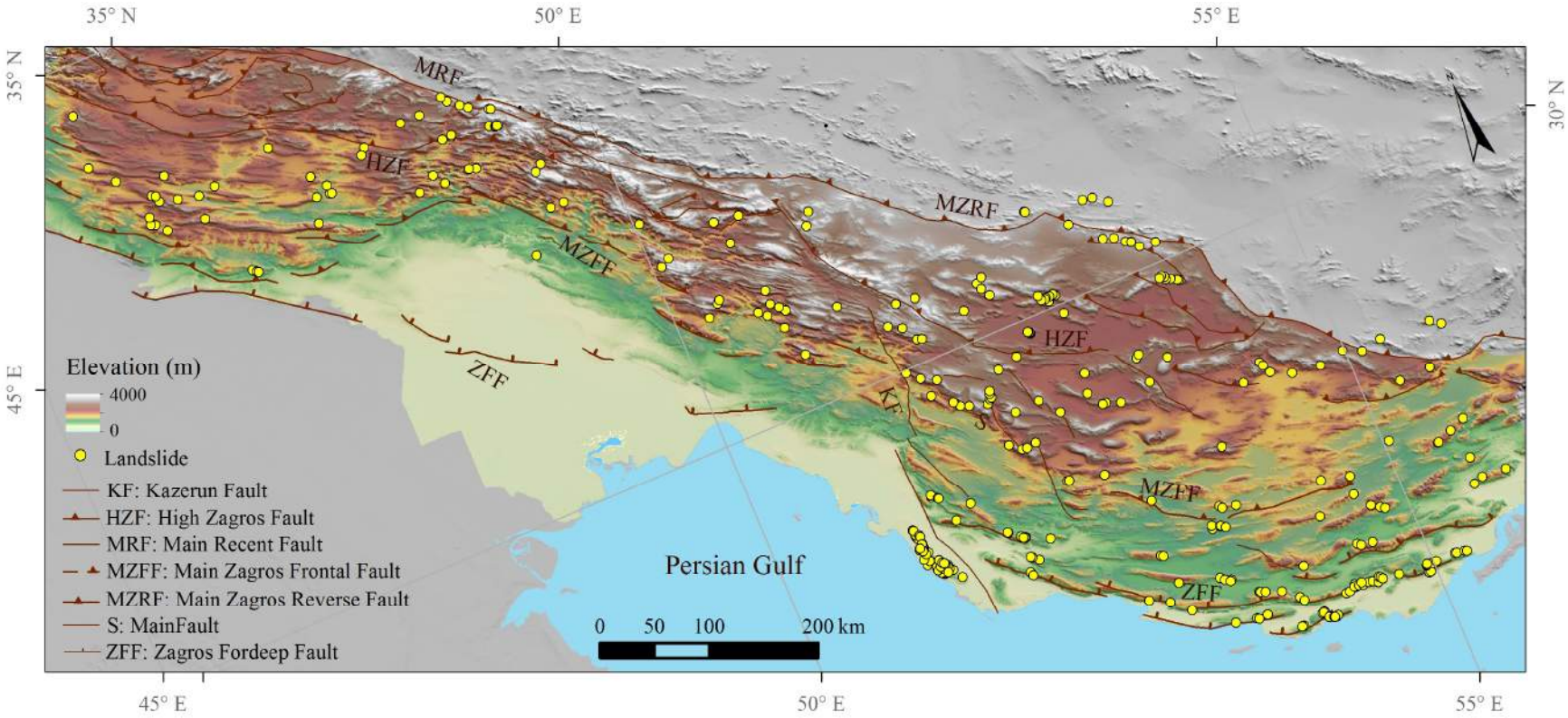

Fig. 4.17. Distribution of active surface faults and landslides in the Zagros mountain belt.

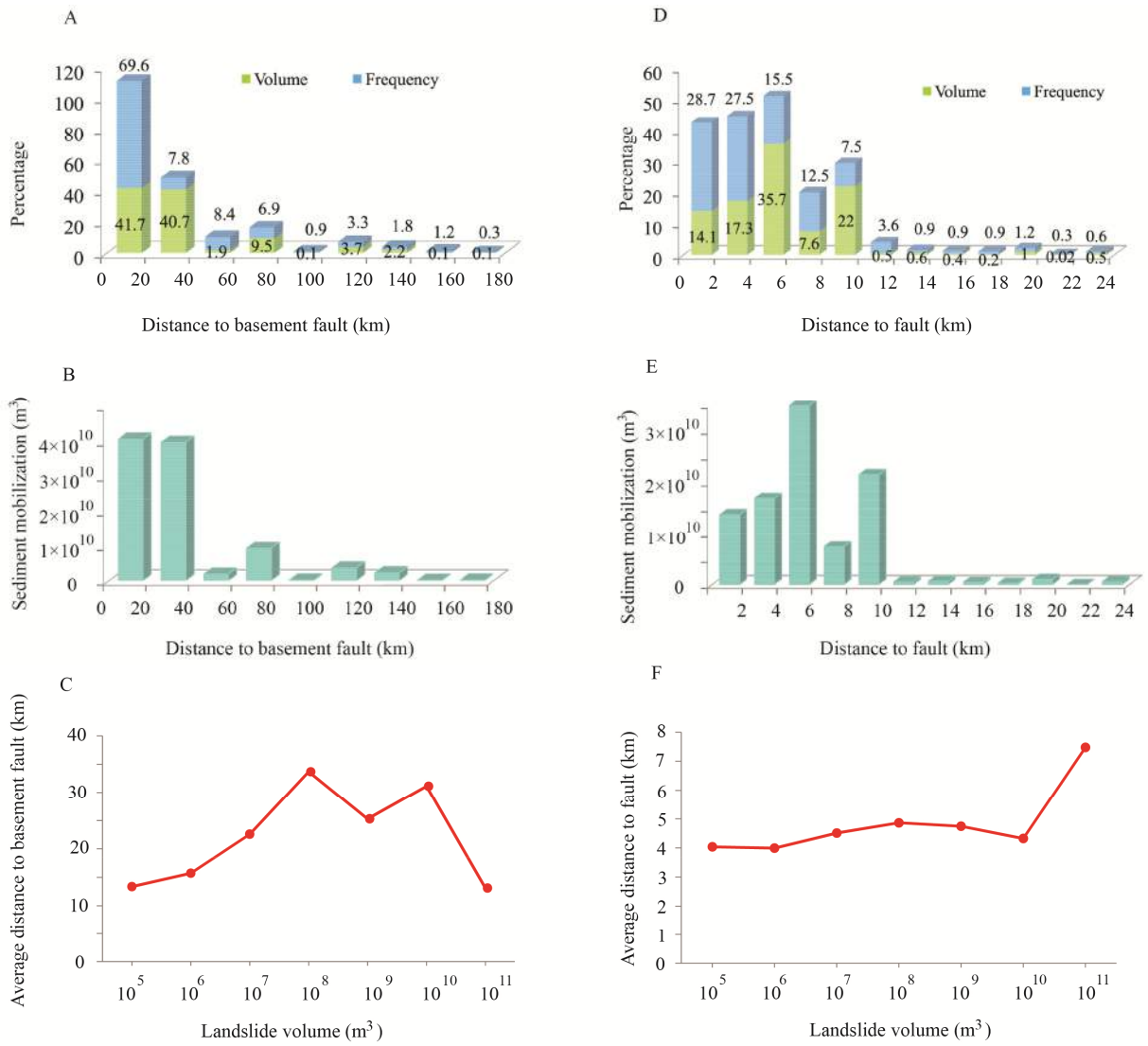

Fig. 4.18. A) Volume and frequency of landslides versus distance to basement faults. B) Sediment mobilization versus distance to basement faults. C) Relationship between landslide volume and average distance to basement faults. D) Volume and frequency of landslides versus distance to active fault. E) Sediment mobilization versus distance to faults. F) Relationship between landslide volume and average distance to faults.

4.2.3 SURFACE PROCESSES

4.2.4.1. FLUVIAL SYSTEM

Water from rainfall runoff and snow melt accumulates in drainage systems on Earth's surface and ultimately results in incised fluvial networks. These drainage systems and their related incision are potentially important in influencing landslides (Azañón et al., 2005; Moeyersons et al., 2010; Lacoste et al., 2011) since they locally enhance the relief and surface slopes (Korup et al., 2010) and modulate the pore pressure state of the surrounding slopes. Indeed, river incision has been suggested to have caused the massive Seymareh landslide (Shoaei et al 1998). To better understand the importance of these effects within the Zagros, I have analysed the relationship between the measured landslides and either the distance to a drainage axis or to an actual river valley (Fig. 4.19).

Note that drainage axes and rivers are separately distinguished because whereas the drainage network only represents a theoretical fluvial network, the

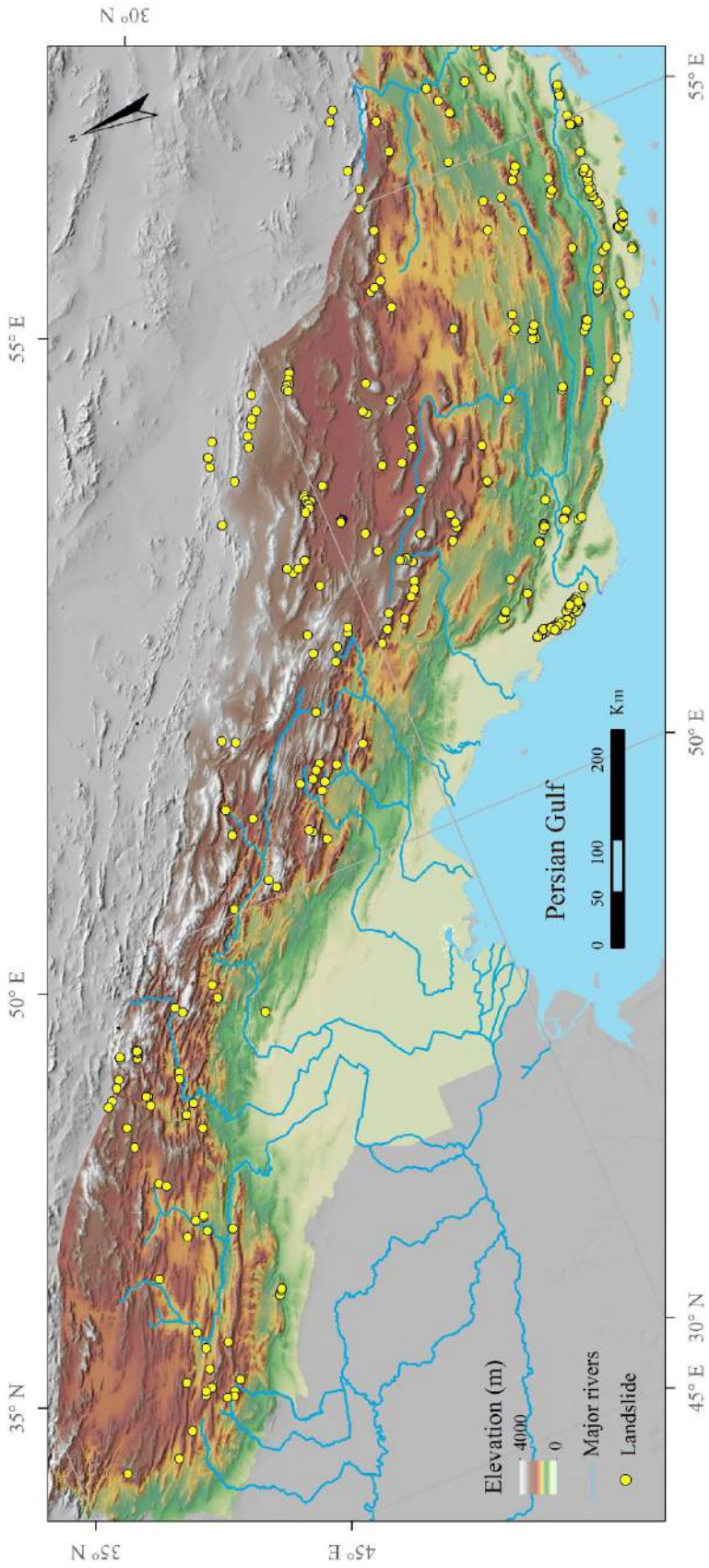

Fig. 4.19. Distribution of major rivers and landslides in the study area.

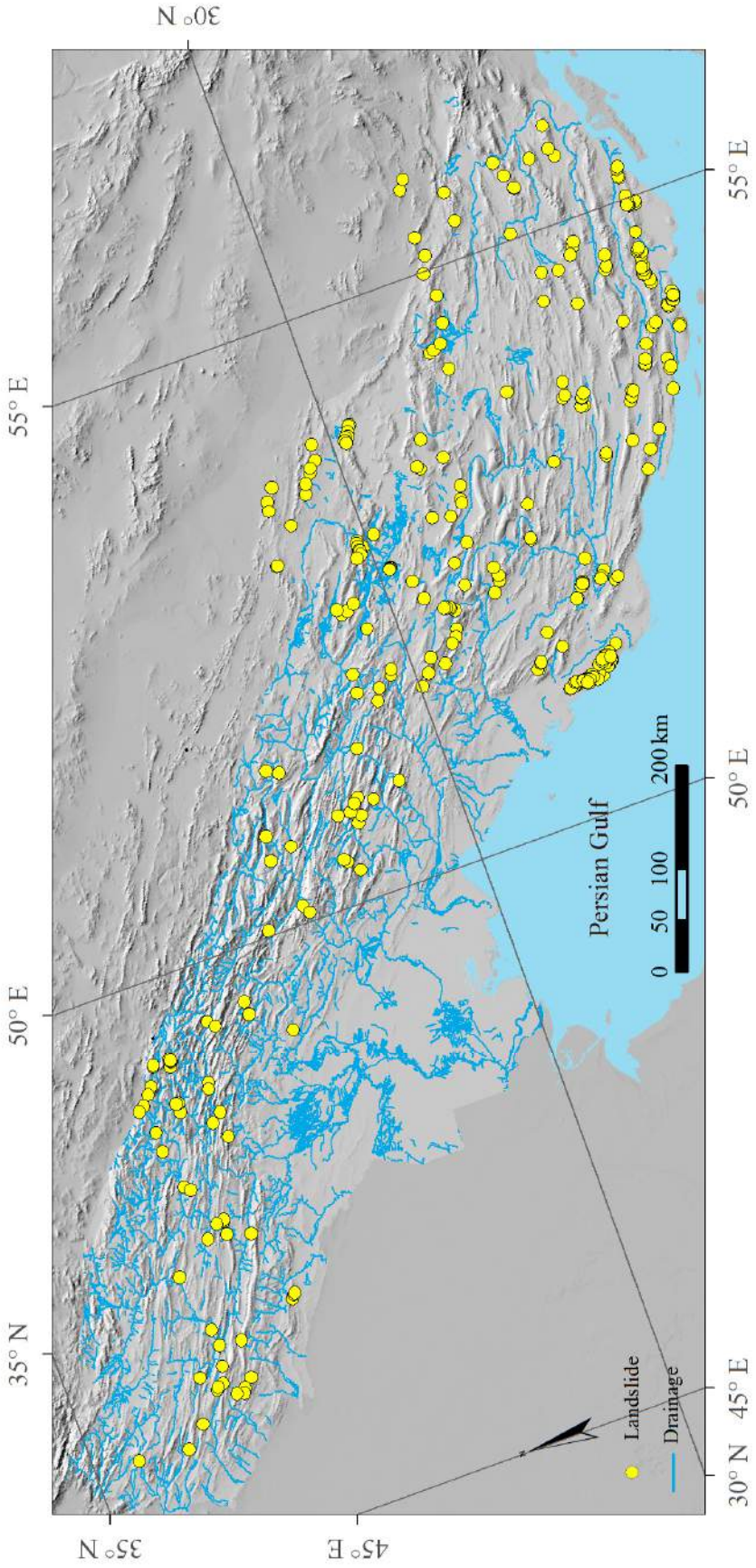

Fig. 4.20. Distribution of main drainage and landslides in the study area.

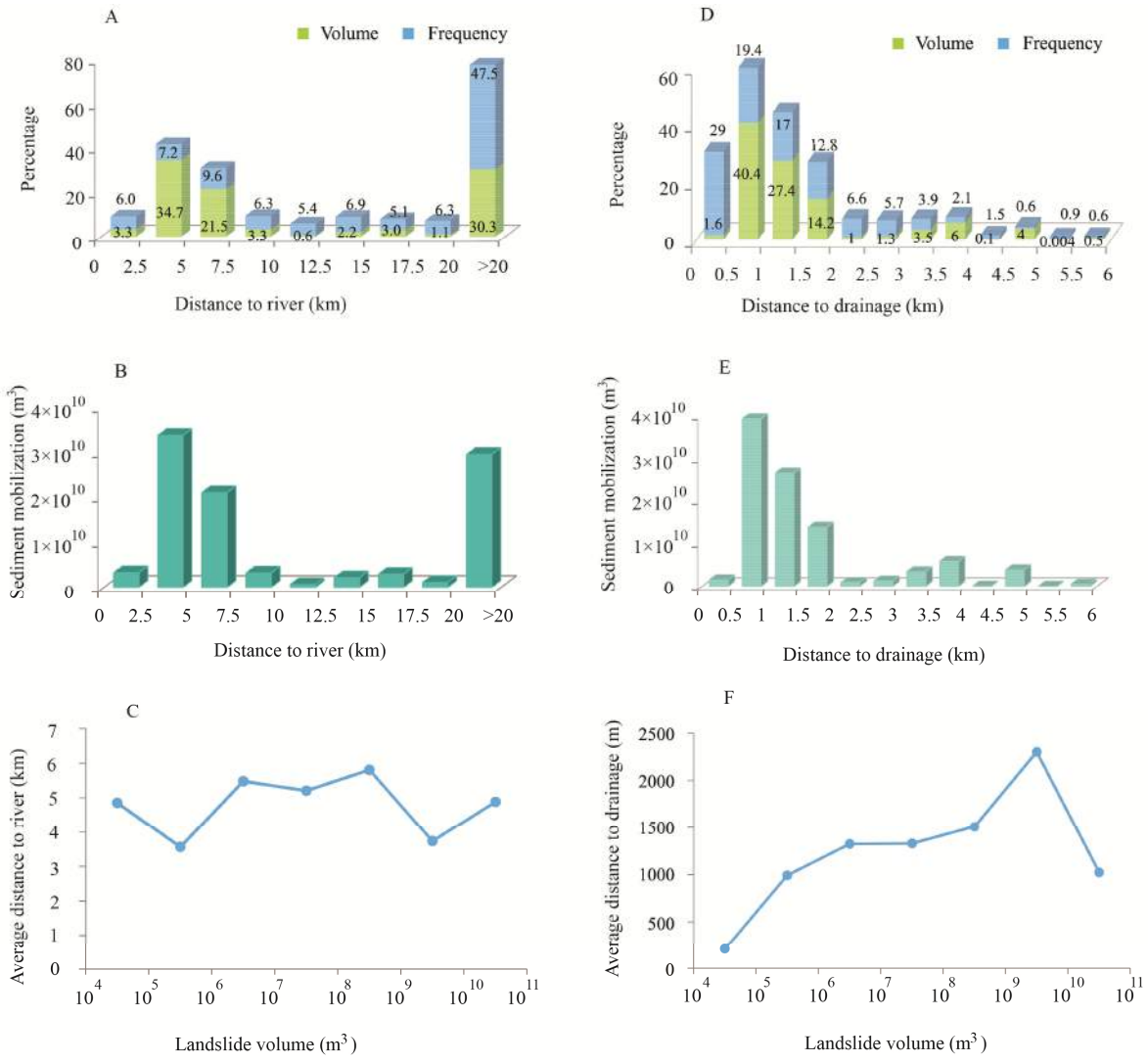

Fig. 4.21. A) Percentage of frequency and volume of landslides versus distance to a river. B) The amount of sediment linked to landsliding versus distance to the nearest river. C) The average distance to a river at different landslide volume classes. D) Percentage of frequency and volume of landslides with distance to drainage. E) The amount of sediment moved as a function of distance to drainage. F) The average distance to drainage in different landslide volume classes.

rivers incisions occur only where sufficient stream power exists to cause significant erosion.

Results show that 59.5% of landslides by volume and 22.8% of landslides in terms of frequency are located less than 7.5 km from rivers. Fig. 4.20B shows that the amount of sediment discharge linked to landslides is greatest between 2.5 and 7.5 km from rivers. The relationship between landslide volume and average distance to river shows that there is no relationship between landslides size and distance to rivers (Fig. 4.20C).

Fig. 4.20 shows distribution of drainage and landslides in the Zagros region. Fig. 4.21D shows that 84.6% of the volume of landslides and 84.8% of the frequency of landslides occurred within 2.5 km of a drainage axis. The frequency of landslides has strong inverse correlation with the distance to drainage (Fig. 4.21D). Sediment mobilization mostly occurred within 2 km of a drainage axis (Fig. 4.21E). The relationship between landslide volume and average distance to drainage is represented in Fig. 4.21F. The volume of landslides has slight direct correlation with distance to drainage. At small distance, there are more frequent landslides with small magnitude while at

greater distances there are fewer landslides with large magnitude.

4.3 SUMMARY OF ANALYSES

Preliminary analysis shows that the parameters that have a meaningful relationship with the frequency of landslides are not necessarily the same as those parameters that have meaningful relationship with the magnitude (size) of landslides. The Frequency of landslides in the Zagros region is controlled by the location of the folds, faults and the fluvial drainage system. The size of landslides is controlled by topographic relief, elevation and slope. Some parameters such as lithology and dip directions affect on both the frequency and the size of landslides in this region.

4.4. PROBABLE TRIGGER OF LANDSLIDES IN THE ZAGROS REGION

The occurrence of landslides is usually a direct response to one or more triggers (e.g., volcanic eruption, earthquake, rainfall, rapid snow melt).

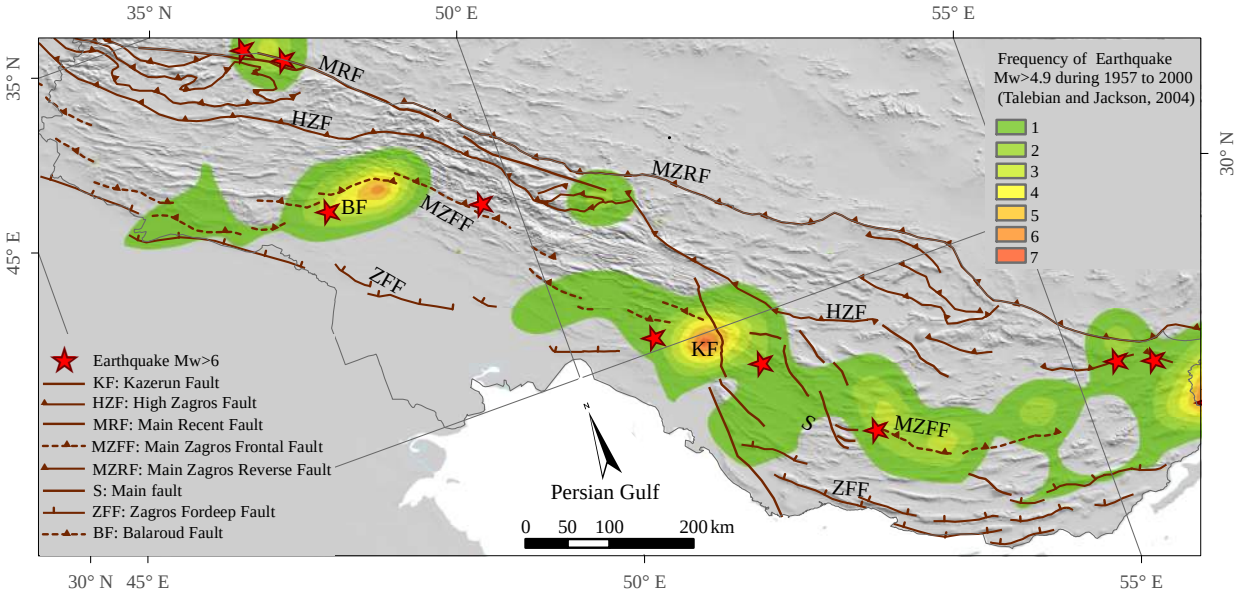

Fig. 4.22. Frequency of earthquakes represented with polygons along with the largest earthquakes shown with stars.

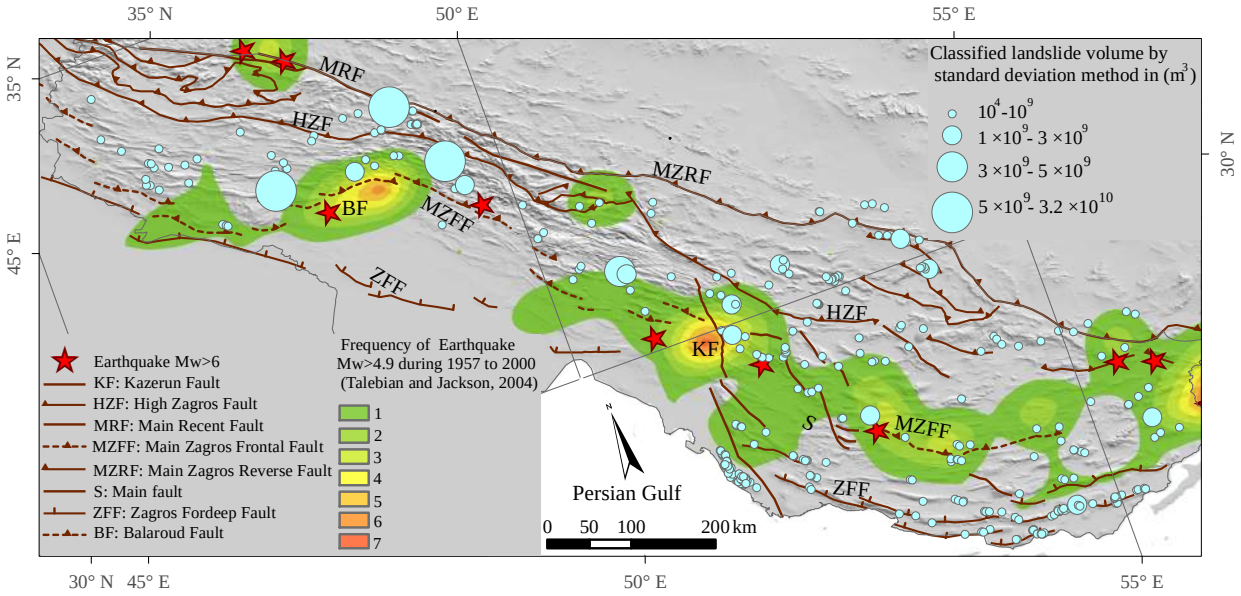

Fig. 4.23. Frequency of earthquakes represented with polygons and the landslides are shown with dots.

Precipitation and earthquakes are the most common triggers for slope failures (Richard Dixon Oldham, 1899; Keefer, 1984; Keefer, 1994; Harp and Jibson, 1996). In the Zagros fold thrust belt I consider in more detail two main triggers mechanisms: earthquakes and rainfall.

4.4.1. SEISMICITY OF THE ZAGROS AND THE LINK WITH LANDSLIDES

The Zagros is a mountain belt undergoing active continental collision. It accommodates roughly half of the 25 mm year^{-1} of convergence between the Arabian and Eurasian plates (Talebian and Jackson, 2004; Tatar et al., 2004) and is a site for intense seismicity. The seismicity of the Zagros is mostly spread over the entire region, extending from the coast line to about 180 km inland (Talebian and Jackson, 2004). The magnitude of historical earthquakes rarely exceeds M_w = 6.5 (Fig. 4.22). Most large earthquakes originate beneath the sedimentary cover (i.e., in the basement below the Hormuz salt) and are rarely associated with surface rupture (Talebian and Jackson, 2004). Focal mechanisms mostly show reverse faulting with strikes parallel to fold axes observed at the surface. Reverse faulting is most active in the low topography near the SW edge of the belt, while the higher topography is dominated by strike-slip faulting (Talebian and Jackson, 2004).

The presence of large earthquakes in the recent century and the absence of large historical landslides may indicate that landslides in the Zagros are triggered by some mechanism other than earthquakes. However, this interpretation remains speculative because the landslides are of unknown age and because we have no way of knowing whether the magnitude of the present day earthquakes is representative of those that occurred in the past.

The distribution of medium to large magnitude earthquakes (Tatar et al., 2004) and large landslides is shown in Fig 4.23. Landslides are more frequent in the seismically active mountainous regions, but no large landslides have occurred in the areas affected by frequent historical earthquakes since 1957. This is probably because giant landslides require a large earthquake (possibly M_w >7.5), not frequent moderate ones.

Keefer (1994) investigated the relationship between earthquake moment magnitude and the volume of triggered landslides (Fig. 4.24). According to this study, a landslide like the Seymareh with a volume of 32 km^3 would require a M_w = 9 earthquake. This earthquake is considerably bigger than any historical earthquake in the Zagros. I therefore tentatively propose that it is unlikely that earthquakes are the main trigger mechanism for (at least the large) Zagros landslides.

Dating landslide events would help to evaluate relevant triggers such as earthquakes and climate impacts. Our poor knowledge about the age of landslide events, except one which highlights an age of 10000-11000 years, Seymareh landslide, and short time frame of recorded large earthquakes with no failure event make it complicate to link landslide inventory either to earthquake events or climatic impacts.

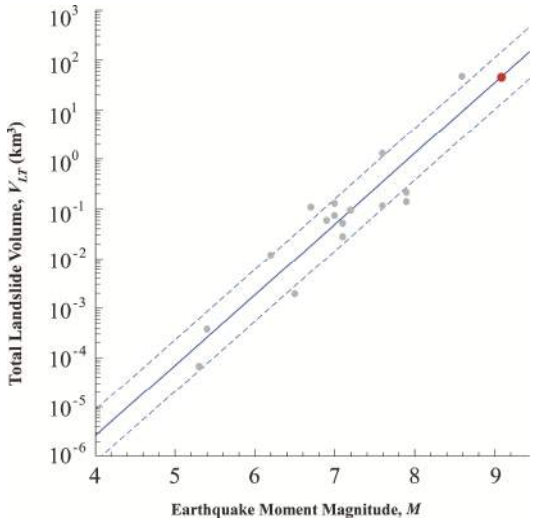

Fig. 4.24. Relationship between the volumes of landslides triggered by an earthquake and the earthquake's moment magnitude, modified after Keefer (1994). The gray dots are 16 landslides from Keefer (1994). The red dot is the volume of the Seymareh

4.4.2. CLIMATE CHANGE AND LANDSLIDES

While the parameters that trigger landslides are complex, it is obvious that climate influences the occurrence of landslides. Water (mainly derived by precipitation, but also originating from snow melt) is the principle component that connects landslides to climate, while other potentially important factors include changes in temperature, intensity of rainfall (Beniston et al., 2011).

The modern climate of the Zagros region is typically Mediterranean (Ferrigno, 1988) with the temperature and the amount of precipitation varying extremely throughout the region and through time. The Zagros Mountains contain five small glaciers on the northern slopes of Zard Kuh at an elevation of 4268 m and the snowline is normally located at around 3900 m (Grunert et al., 1978). The annual precipitation rates ranges between 30 to 250 mm in the east and along the Persian Gulf coastline (Kharazipour, 2008), to 250 mm in the outer foothill and to more than 1000 mm in the highest part of the range in the western Zagros mountains (Wright, 1961; Kharazipour, 2008). The average annual temperature is about 25°C at the coastline (Khoshbakht, 2006) and decreases to 11.5°C as elevation rises towards the central Zagros (e.g. Shaher-e-kord). During the winter, the average temperature decreases to 17°C along the coast and to less than -30°C on the mountain summits.

A series of climate changes occurred in the northern hemisphere during the Holocene. Generally, three temperature substages are recorded during this period: an early cool stage about 10000 years B.P., a middle climate optimum stage between 9000 to 4000 B.P. when the average global temperature reached its maximum during the Holocene, and a late cooling stage that contains the Little Ice Ages about 1300 years B.P. (Fig. 4.25) (Dansgaard et al., 1969; Schönwiese, 1995). The rates of these climate changes varied considerably depending on the location.

Holocene environmental conditions in the Zagros are mostly obtained from lake cores (Zaribar and Mirabad lakes) in northwest part of the Zagros (Van Zeist, 1967; Stevens et al., 2006; Stevens et al., 2001; Griffiths et al., 2001). Palynological studies show that during the late Pleistocene - early Holocene (11000 to 8000 years ago) this region experienced significant changes in climate with relatively more rainfall and humid conditions (Van Zeist, 1967; Jones et al., 2013) compared to the late Holocene climate state. Other paleoclimate studies indicates wet phases in the Upper Pleistocene and Lower Holocene occurred in the eastern Mediterranean (Wagner and Geyh, 1999), south-east Sahara (Pachur and Hoelzmann, 1991; Hoelzmann et al., 2004), Afghanistan (Pias, 1972), Arabian peninsula (Nettleton and Chadwick, 1996), northern Oman (Burns et al., 1998; Fleitmann, 2001; Fleitmann et al., 2003) and northern and western parts of Iran (Kehl, 2009). Also palynological analysis of

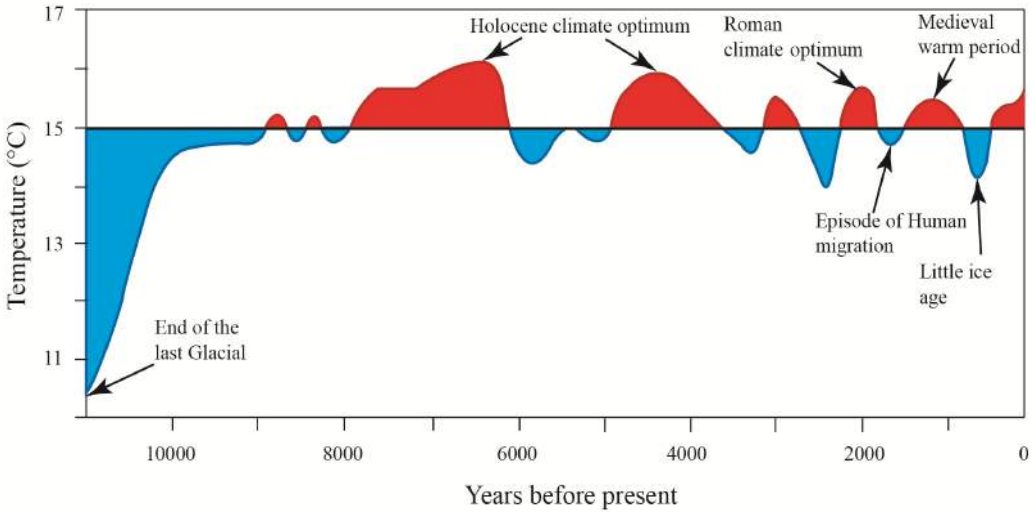

Fig. 4.25. Average temperatures of the northern hemisphere during the past 11000 years obtained on the bases of ice core Oxygen isotope analysis and greenhouse gas concentration (modified after Dansgaard et al., 1969; Schönwiese, 1995).

lake cores in the eastern Iraqi desert by (Al-Rawi et al., 2005) indicates a pluvial peak between 9000-6000 years B.P.

The younger Dryas interval (12800 - 11500 years ago) that was during the last glacial termination, was a major cold climatic event during the transition from the glacial period into the present Holocene interglacial (Berger, 1990; Muscheler et al., 2008; Pearce et al., 2013). Afterwards ice sheets began melting, and the Sahara and Arabian deserts covered with vegetation (Singer and Avery, 2007). The earth entered into conditions that were much warmer and moister than today. In the Middle East, the highest lake levels were recorded in the period 11000 - 6000 yeas B.P (Al-Rawi et al., 2005).

We suspect that enhanced precipitation during the early-mid Holocene was the main trigger responsible for many landslides in the study area. Many of the large Zagros landslides occurred when the thick carbonate rocks (Asmari limestone) slid off fine clastics (Pabdeh Gurpi marls). This situation would be favoured by rapid drainage of surface runoff water in the carbonates and generation of high pore fluid pressures in the underlying low permeability marls, which is likely to have occurred following extreme rainfall events and during anomalously wet periods. This hypothesis is consistent with radiocarbon dates for the largest Zagros landslide (the Seymareh) which took place 10000 to 11000 years B.P. More dating studies on landslides in the future are required to test this hypothesis.

Furthermore combination of two triggers (earthquake and climatic impact) increase probability of mass failure. For instance, a small earthquake could possibly trigger very larger landslides during a heavy rainstorm to compare with the same event in a dry condition (Faris and Wang, 2014). By considering that, there is no record of a large landslide in the last century, dry condition, for such a seismically active region. This may highlights a probability of occurring landslide events during a wet climatic condition.

4.5. CONCLUSION

The analysis carried out in this study shows that there is no single clear controlling factor that controls the spatial distribution of landslides in the Zagros region but a combination of these factors confined their distribution. Controlling factors on the frequency of landslides are different from those controlling factors on the size of landslides. Our results reveal that the frequency distribution of landslides increases close to parameters that generate topographic relief (i.e., fluvial channel, active faults and folds). They also occurred mostly on concave slip surfaces. The size distribution of landslides is strongly correlated with average topographic relief and average elevation, but is also influenced by the slope distribution. Lithology and dip direction affect both landslide volume and frequency. We find no clear evidence that landslides were triggered by earthquakes with magnitude of $M_w \leq 7$, and speculate that many landslides may have occurred during a wet period during the mid-Holocene. More detail studies are needed to confirm these initial findings about the trigger of large landslides in the Zagros region.

Chapter 5

MULTIVARIATE ANALYSIS OF LANDSLIDE SIZES IN THE ZAGROS REGION

5.1 INTRODUCTION

Statistical assessment of the recorded data in a landslide inventory makes it possible to gain a better understanding of the factors that control the distribution of landslides. A statistical approach assumes that the prediction of future landslides can be assessed by finding the combination of variables that have led to previous landslides (Ohlmacher and Davis, 2003; Legorreta Paulin, 2007). In this study, different statistical methods have been used to identify (1) how the data is distributed (i.e. frequency distribution, Q-Q plot and normality test), (2) how the variables are correlated with each other (i.e. linear correlation) and (3) probable correlations between causative factors and the volumes of landslides (i.e. correlation test). In addition, we investigate what parameters determine the size of individual landslides in the Zagros region. For this purpose, we investigate our database using Principal Component Analysis. A combination of direct mapping and indirect statistics is useful to extract the underlying causes of clustering. This method is applied separately in the western (Lorestan) and eastern sides (Fars) of the region due to different patterns of landslides in these two areas (as it mentioned in chapter 3).

5.2 STATISTICS OF INVENTORY AND IDENTIFICATION METHOD

Many factors influence the distribution of landslides but there are probably only a few variables that control their occurrence. In this study twelve variables that affect the landslide distribution at a regional scale have been measured (as presented in the previous chapter). In addition to these variables (e.i. elevation, relief, topographic curvature, dip direction, slope, pre-slope, lithology, distance to fold axis, distance to surface fault, distance to basement faults, distance to main river, distance to drainage), each record of landslide in the database consists of three characteristic landslide measures: volume, area and landslide type.

To identify relationships of these variables and landslide characteristics, a statistical method is needed. The assessment of data for normality of samples is essential as it dictates the type of analysis that has to be used. The normal distribution of data shows that data is parametric while a skewed distribution shows that data is non-parametric. The distribution of data has been investigated by two methods (Frequency distribution of landslides and Normal probability plot). The distribution is then tested for Normality.

5.2.1 FREQUENCY DISTRIBUTION OF LANDSLIDES

The frequency distribution of variables is represented by histograms in Fig. 5.1. The bin width of histograms is computed by Sturges method. The red line shows the mean of the data. Non-numeric parameters (e.g. slide type and dip direction) are ignored. Almost all of the variables show non parametric distributions, except mean relief and mean curvature. The Q-Q plot is the other method that is used in assessing the distribution of data more precisely.

5.2.2 NORMAL PROBABILITY PLOT

The method for assessing normality of data is the quantile-quantile plot (Q-Q plot). In this method, normality of data distributions measures similarity of the distribution of data with a normal distribution. For normal data the points that are plotted in a Q-Q plot form an approximate straight line. Results of the Q-Q plots shown in Fig. 5.2 reveals that the variables are non-parametric. To determine if a dataset is well modelled by a normal distribution the normality test (Shapiro-Wilk test) is used.

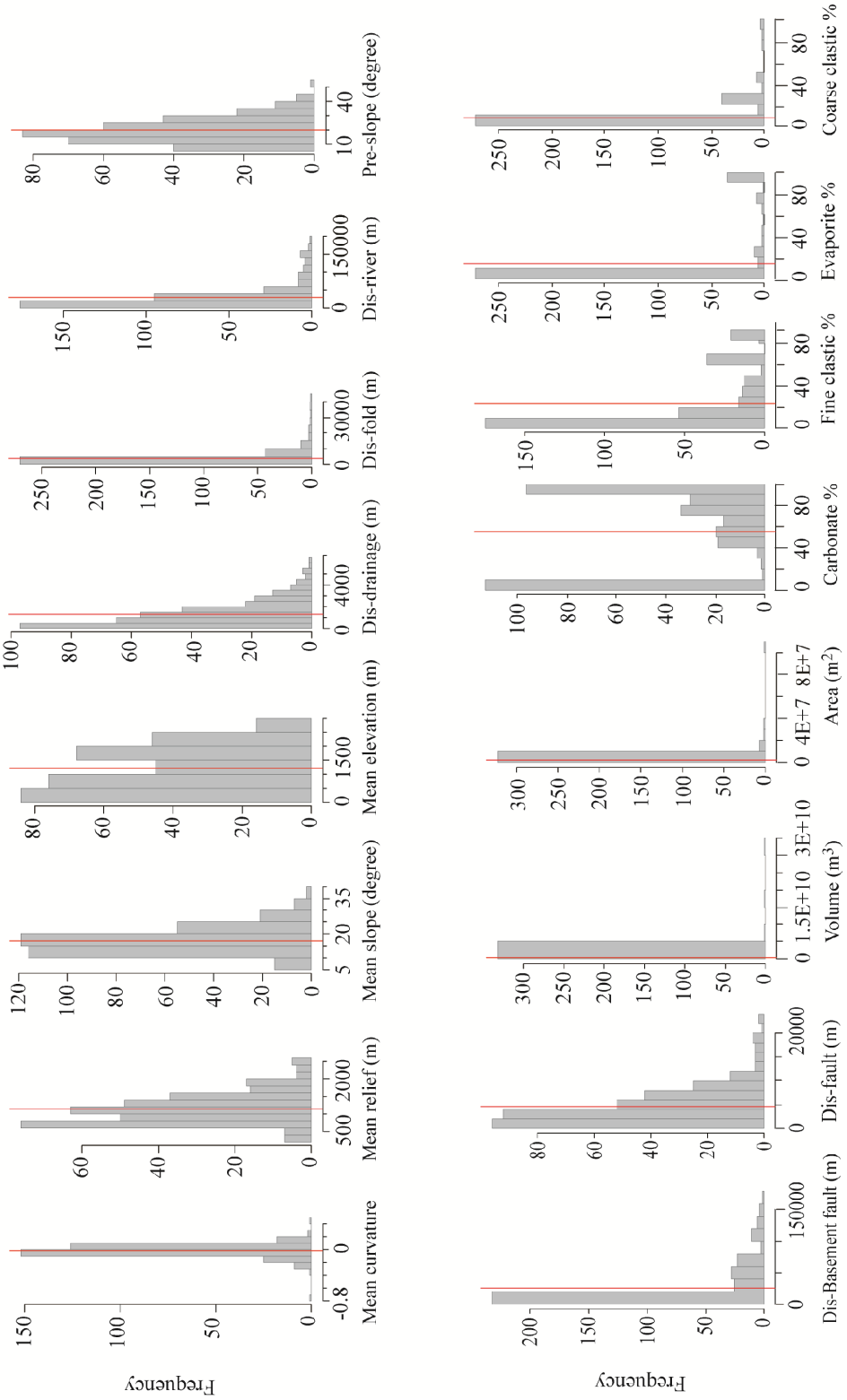

Fig. 5. 1. Frequency distributions of the landslide-control variables.

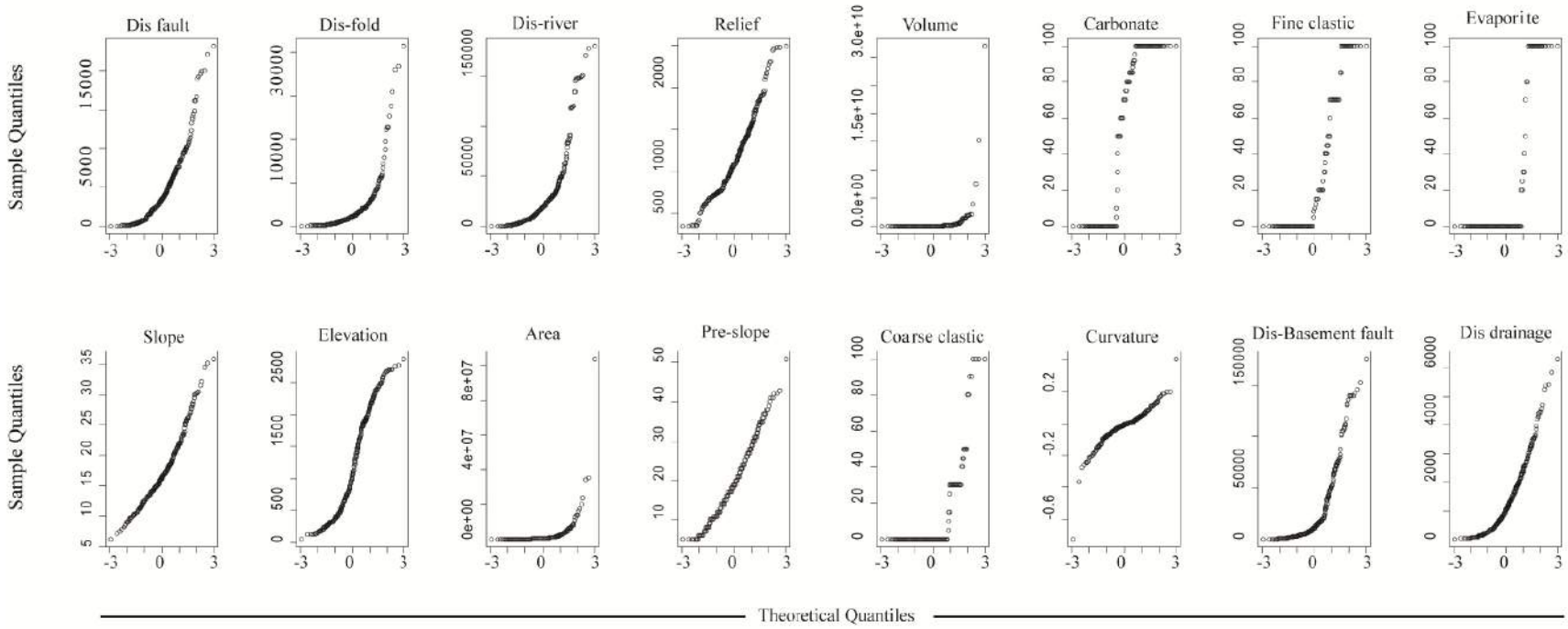

Fig. 5. 2. Quantile-quantile plots (Q-Q plot) show normality of data distributions, measuring similarity of the distributions relative to a theoretical normal distribution. The vertical axis represents sample quantiles, the vertical axis represents theoretical quantiles.

5.2.3 NORMALITY TEST

The Shapiro test is a way to find normality of variables for sample sizes smaller than 2000 (Shapiro and Wilk, 1965; Royston, 1982). In the Shapiro test, the null hypothesis is that the population is normally distributed. If the p-value is less than the chosen P-value, then the null hypothesis is rejected. The test rejects the hypothesis of normality when the P-value is less than or equal to 0.05 (or 5%). Failing the normality test allows to state with 95% confidence that the data does not fit a normal distribution and the variable is non parametric. The results are represented in the table 5.1 and confirm that all variables in this dataset are non parametric.

Table 5.1. Result of Shapiro test

No	Variables	P-Value
1	Volume	2.2E-16
2	Carbonate	2.2E-16
3	Fine clastic	2.2E-16
4	Evaporite	2.2E-16
5	Coarse clastic	2.2E-16
6	Mean curvature	7.7E-16
7	Dis Basement fault	2.2E-16
8	Dis drainage	6.7E-16
9	Dis fault	2.2E-16
10	Dis fold	2.2E-16
11	Dis river	2.2E-16
12	Pre- slope	1.3E-05
13	Mean relief	6.5E-09
14	Mean slope	1.1E-08
15	Mean elevation	2.9E-11
16	Area	2.2E-16

5.2.4 LINEAR CORRELATION OF VARIABLES

The correlation analysis is applied to measure a potential linear relationship between two variables. The result ranges from -1 to +1 and is independent of the units of measurement. A value near 0 indicates little correlation between attributes; a value near +1 indicates a high level of positive correlation and value near -1 indicates a high level of negative correlation. Results of the correlation analysis are shown in table 5.2. The correlations of table 5.2 show that two variables volume and area show strong correlation with one another, as could be expected. Carbonates have a relatively good correlation with mean elevation. Mean relief and mean elevation also show a moderate correlation with one another. In addition carbonate and fine clastics show a good negative correlation. The rest of the variables demonstrate weak or very weak linear correlations.

Since we are interested in the correlation between volume and the other variables, correlation analysis of the volume versus the rest of the variables in the dataset have been tested. Results of the correlation test reveal if the correlation is real or random. If the P value is less than 0.05 and a correlation number is close to 1, then a real correlation between variables is confirmed. Results for the Zagros inventory are shown in table 5.3. The only variable that shows a real correlation with the volume of landslides is area which has a P-value of less than 0.05 and a correlation number close to 1. Of the remaining variables, relief exhibit some correlation with the volume of landslides while pre-slope and the amount of evaporite rocks have negative correlations with the volume of mass failures.

	Volume	Carbonate	Fine clastic	Evaporite	Coarse clastic	Mean curvature	Dis Basement	Dis drainage	Dis fault	Dis fold	Dis river	Pre- slope	Mean relief	Mean slope	Mean elevation	Area
Volume	1															
Carbonate	0.07	1														
Fine clastic	-0.03	-0.60	1													
Evaporite	-0.06	-0.48	-0.29	1												
Coarse clastic	0.00	-0.42	0.17	-0.18	1											
Mean curvature	0.00	-0.12	0.11	0.01	0.08	1										
Dis Basement fau	0.01	0.26	-0.15	-0.25	0.11	0.01	1									
Dis drainage	0.03	0.15	-0.13	0.04	-0.19	-0.05	0.08	1								
Dis fault	0.04	0.06	0.07	-0.16	0.03	0.06	-0.03	0.06	1							
Dis fold	0.04	0.15	-0.14	-0.12	0.13	-0.07	0.28	-0.02	-0.08	1						
Dis river	-0.03	0.19	-0.10	-0.19	0.07	0.01	0.80	0.09	-0.01	0.22	1					
Pre- slope	-0.14	0.09	-0.14	0.07	-0.07	0.00	0.05	0.12	0.08	0.01	0.11	1				
Mean relief	0.21	0.28	-0.25	-0.08	-0.08	-0.03	0.04	0.14	0.08	0.10	-0.06	0.11	1			
Mean slope	0.04	-0.04	0.02	0.09	-0.09	0.03	-0.11	0.20	0.10	-0.07	-0.12	0.25	0.21	1		
Mean elevation	0.09	0.56	-0.34	-0.35	-0.09	-0.10	0.55	0.18	0.04	0.26	0.47	0.16	0.53	0.01	1	
Area	0.95	0.13	-0.06	-0.10	-0.01	-0.02	0.06	0.08	0.04	0.06	0.02	-0.17	0.26	0.02	0.17	1

Table 5.2. Linear correlation analysis results. Red colours shows positive correlation and purple colours shows negative correlation.

Table 5.3. Results of correlation test between volume and other variables.

Variables	P-value	Correlation
Area	2.20E-16	0.95
Mean relief	8.47E-05	0.21
Mean elevation	0.09	0.09
Carbonate	0.21	0.07
Dis.fault	0.45	0.04
Mean slope	0.46	0.04
Dis.fold	0.48	0.04
Dis.drainage	0.62	0.03
Dis Basement fault	0.92	0.01
Mean curvature	0.93	0.005
Coarse clastic	0.98	0.001
Fine clastic	0.58	-0.03
Dis.river	0.58	-0.03
Evaporite	0.28	-0.06
Pre.slope	0.01	-0.14

5.3 Principle component analysis of the Zagros inventory

Principal component analysis (PCA) is a multivariate statistical technique that enables a dataset to be described in terms of a reduced number of variables, which are linear combinations of the pre-existing variables (Carrara et al., 1999; Baeza and Corominas, 2001). The goals of PCA are to: (1) extract the most important information from the data table (2) compress the size of the data set by keeping only the important information (3) simplify the description of the data set and (4) analyse the structure of the observations and the variables. PCA reduces the dimensionality of a dataset by finding a new set of variables, smaller than the original dataset and retains most information of samples. The new variables are called principal components. The number of components that extracted into PCA is less or equal to the number of observed variables. In most studies, because only the first few components account for meaningful amounts of variance, only these first few components are retained for further interpretation (Hatcher and O'Rourke, 2013). The later components normally account for trivial variance. The most important step in PCA is to determine meaningful components that should be retained for interpretation.

Here, principal component analysis has been applied on all numeric parameters except area (instead volume is used to represent the size of landslides). The dataset includes 15 variables shown in table 5.4

5.3.1 Determining components to retain

Four criteria are commonly used to determine the meaningful components. This section will describe these four criteria to determine retained components for the landslide dataset of the Zagros mountain belt.

5.3.1.1 The eigenvalue- one

The (Kaiser, 1960) rule is the most often used method to determine the number of components to retain, that is based on inception of the correlation matrix eigenvalues. In this method, only the components that have eigenvalues equal or greater to one are retained. This means that these components are accounting for a greater amount of variance than have been contributed by one variable. On the other hand, the components with eigenvalues less than 1 (or average eigenvalue) are accounting for less variance than have been contributed by one variable (Hatcher and O'Rourke, 2013). Table 5.4 provides the eigenvalue table from the analysis of components with an average eigenvalue of 1.0.

The eigenvalue for the first component is 3.14, while for second component is 1.95. This shows that the first component accounts for a relatively large amount

Table 5.4. Eigenvalue table of components

Component	1	2	3	4	5	6	7	8	9	10	11	12	13	14
Eigenvalue	3.14	1.95	1.42	1.35	1.15	0.99	0.96	0.84	0.77	0.73	0.65	0.60	0.22	0.18

of variance (as expected), while the later components account for relatively small amounts. With the eigenvalue-one criterion, the first five components must be retained for interpretation.

5.3.1.2 THE SCREE TEST

The Scree test (Cattell, 1966) plots the eigenvalues in descending order of their magnitude against their component, determining where they level off. The break between the level of the eigenvalues indicates the number of meaningful components to retain (D'agostino and Russell, 2005). The components that appear before the break are assumed to be meaningful and are retained for interpretation. If the Scree plot displays several large breaks, the last break before the level off indicates the retained components. Fig. 5.3 presents the Scree plot from a Principal Component Analysis of 15 variables for the Zagros dataset. With this plot, there is a relatively large break between components 1, 2 & 3, and relatively small breaks between 4 and 5. The last major break is between 12 and 13. In this dataset, as often the case, it is difficult to determine exactly where the breaks in the Scree plot exist.

5.3.1.3 PROPORTION OF VARIANCE

This technique retains those components whose cumulative percentage of variance exceeds a certain value. The cumulative percentage of variance that accounted by few meaningful components should be equal to 70 - 80 percent of the total variance (Pett et al., 2003; Hatcher and O'Rourke, 2013; Garson, 2013), although as little as 50% of the variance explained is considered acceptable (Beavers et al., 2013). This study assumes a cutoff of 60%. The proportion of the total variance explained by each component can be calculated as the eigenvalue for each component divided by the sum of all eigenvalues of the correlation matrix.

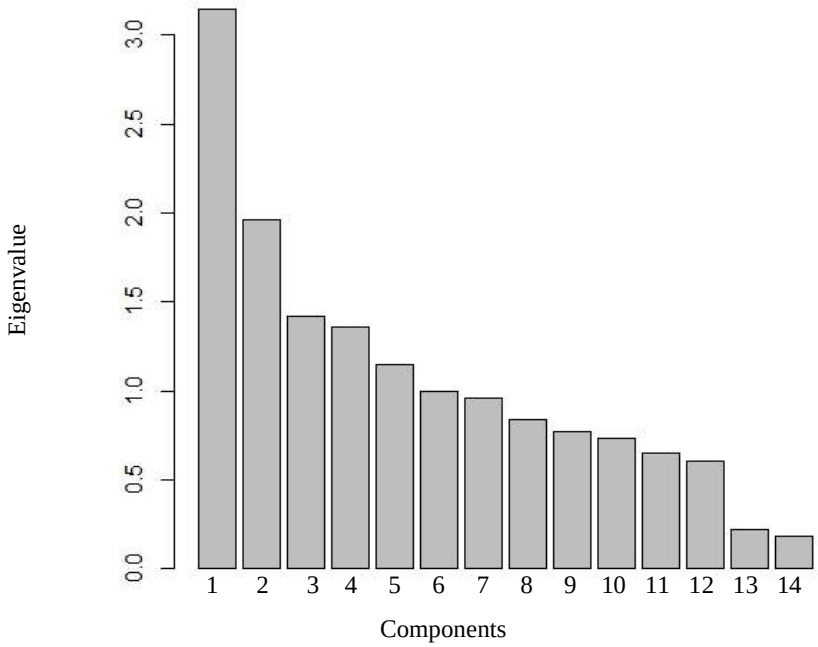

Fig. 5.3. Scree plot of the landslide database with 15 variables.

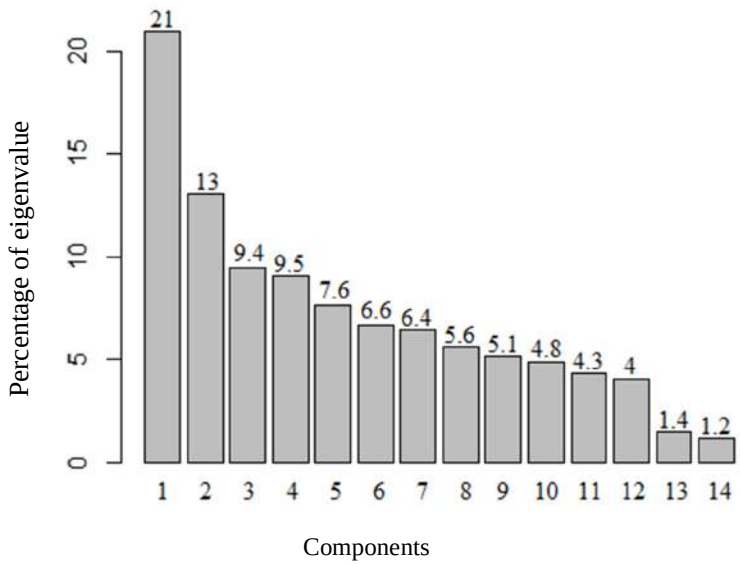

Fig. 5.4. Proportion of variance for 14 components.

In PCA each variable contributes one unit of variance to the analysis. The sum of the eigenvalues of the correlation matrix is equal to the total number of variables. The percentage of variance accounted for each component for this study are presented in Fig. 5.4. Approximately 60% off the total variance is accounted for by the first five components.

5.3.1.4 INTERPRETING THE ROTATED SOLUTION

This technique determines what variables are measured by each of the retained components. For this, the variables that demonstrate high loadings for a

Table 5.5. Loading value of variables in first five components. The highlighted numbers indicate loading values larger than the threshold (0.4). Stars indicate the variables that are selected for the rest of the processes.

No	Variable		Comp1	Comp2	Comp3	Comp4	Comp5
1	Volume	*	0.12	0.10	-0.35	-0.35	0.48
2	Carbonate	*	0.76	0.29	0.01	-0.35	-0.36
3	Fine clastics		-0.50	-0.44	-0.46	0.13	-0.15
4	Evaporite		-0.41	0.37	0.57	0.26	0.37
5	Coarse clastics		-0.16	-0.58	-0.24	0.12	0.42
6	ME.curvaetur		-0.14	-0.13	-0.22	0.25	0.04
7	Dis.Basement fault		0.70	-0.50	0.13	0.26	0.04
8	Dis.drainage		0.25	0.36	-0.03	0.32	-0.07
9	Dis.fault	*	0.06	0.07	-0.58	0.16	-0.28
10	Dis.fold		0.39	-0.26	0.13	-0.08	0.41
11	Dis.river		0.62	-0.50	0.18	0.34	-0.05
12	Pre.slope	*	0.20	0.28	0.02	0.62	-0.05
13	ME.relief		0.45	0.43	-0.36	-0.10	0.41
14	ME.slope		-0.01	0.46	-0.34	0.49	0.19
15	ME.elevation	*	0.87	0.02	-0.11	0.00	0.08

given component have to be identified (Hatcher and O'Rourke, 2013). The factor loading has to be larger than 0.40 (Stevens, 1986). For a given variable if the loading value is larger than 0.40 on more than one component, that variable is removed and the process is repeated for remaining variables (Hatcher and O'Rourke, 2013).

Table 5.5 represents the loadings of variables in each component. The 2, 3, 4, 5, 7, 11, 13 and 15 load on component 1, while the rest of the variables load on other components. The variables 6 and 8 do not load on the first five components while 3, 4, 7, 11, 13 and 14 load on more than one component; therefore they have to be dropped from the dataset.

5.3.2 RESULTS OF SECOND ANALYSIS

The eigenvalue table for retained variables is presented in table 5.6. The component 1, 2, and 3 demonstrated eigenvalues greater than 1 so are

Table 5.6. Eigenvalue of first five components.

Component	1	2	3	4	5
Eigenvalue	1.6373	1.1369	1.0044	0.7934	0.428

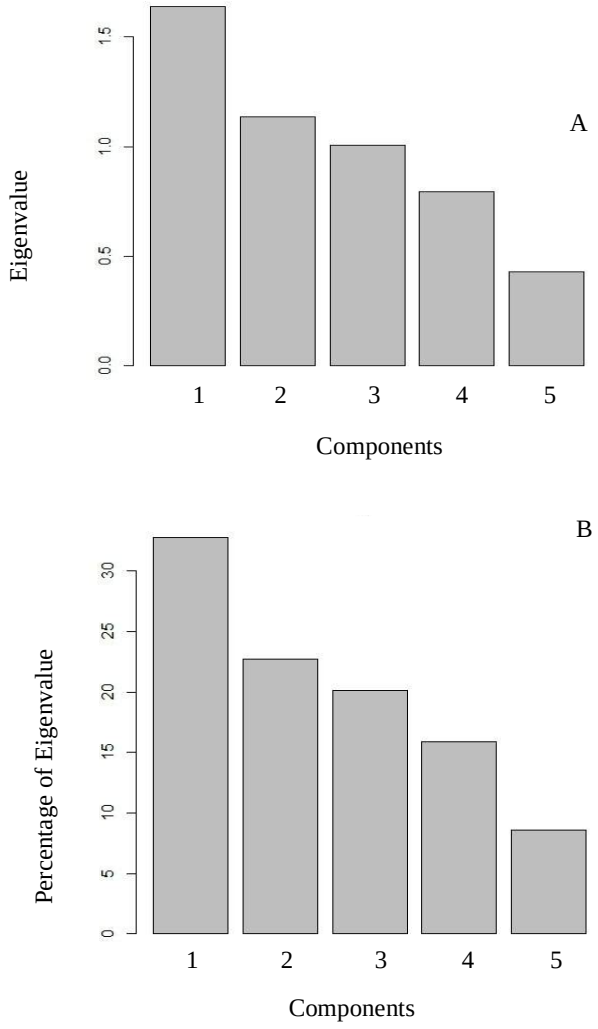

Fig. 5.5. A) The scree plot. B) The proportion of variance.

Table 5.7. Percentage of eigenvalue of first five components presented in Fig. 5.5 B.

Component	1	2	3	4	5
Percentage of eigenvalue	32.7	22.7	20	15.8	8.5

retained for further interpretation.

The Scree plot (Fig. 5.5A) shows that there are two main breaks in the data following component 1 and 4. The proportion of variance in Fig. 5.5B and table 5.7 shows that first three components explain 75% of variance of the dataset.

The results from the three tests (eigenvalue-one, Scree plot and Propagation of variance) all indicate that the three first components are an appropriate representation of variability in the Zagros landslide dataset.

The loading values of the variables for the first three components are presented in table 5.8. Variable 2 and variable 5 in table 5.8 display significant loading for component one. Variable 1 and 4 show meaningful loading for component 2 and the variable 3 shows meaningful loading in component three.

Correlation circles plot all variables against two principal components, which are represented on the X and Y axes (the horizontal axis shows the first component and the vertical axis shows the second component). The angle between vectors gives the degree of correlation (0° = highly correlated, 90° = uncorrelated and 180° = negatively correlated), while the vector length indicates the strength of the relationship (Buehler et al., 2011). Fig. 5.6 illustrates correlation circles of five variables in two dimensions. The carbonate lithology and elevation of landslides are loaded in component 1 while the volume of landslides and pre-slope loads in component two.

The lengths of the arrows indicate that the carbonate lithology, volume, elevation and pre-slope of landslides are strongly correlated. The distance to faults is not strongly correlated with other variables. The carbonate lithology and elevation of landslides shows a high degree correlation. The volume and pre-slope of landslides show a negative correlation. The distance to faults shows a slight negative correlation to the volume of landslides.

Fig. 5.6A shows the data plotted in the PC coordinate system. Each quadrant of Fig. 5.6B represents a group of landslides that have similar characteristics. The geographic distribution of landslides with similar characteristics may uncover new evidence that could lead to better understanding about large landslides in the region.

Table 5.8. The highlighted numbers indicate loading values larger than the threshold.

No	Variable	Comp1	Comp2	Comp3
1	Volume	0.1598	0.7711	-0.271
2	Carbonate	0.8476	0.0991	0.1439
3	Dis.fault	0.1899	-0.121	-0.937
4	Pre.slope	0.3238	-0.717	-0.101
5	ME.elevation	0.8674	0.0555	0.1519

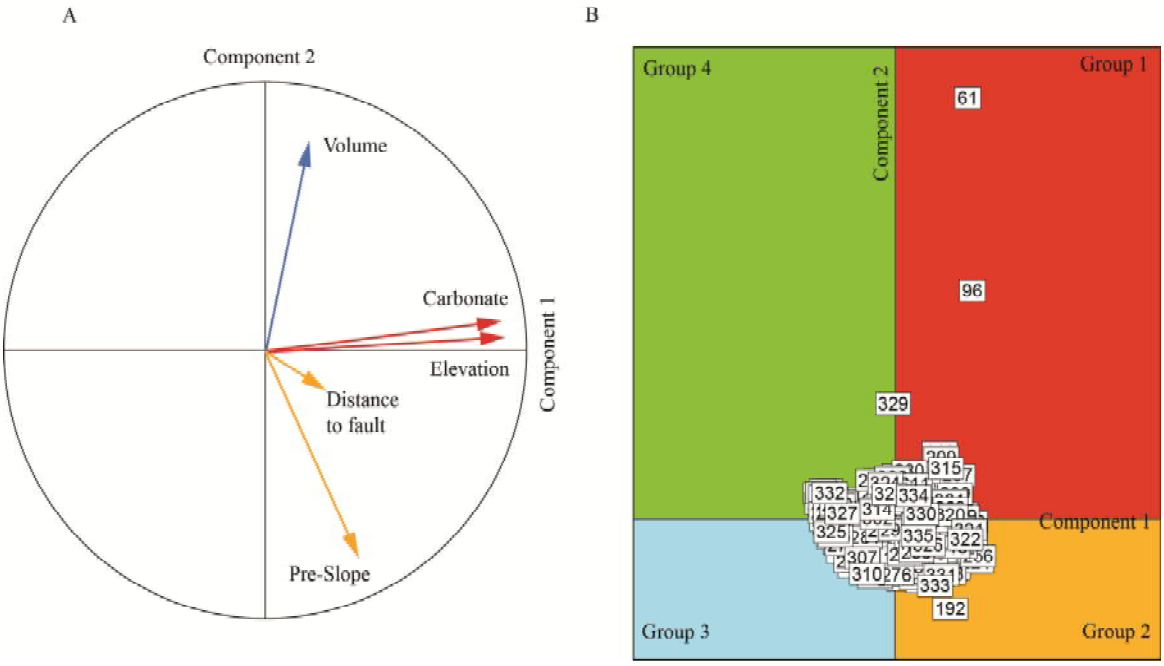

Fig. 5.6. A) The correlation circle of five variables in two dimensions. B) Transformed coordinate of landslides record for the Zagros database.

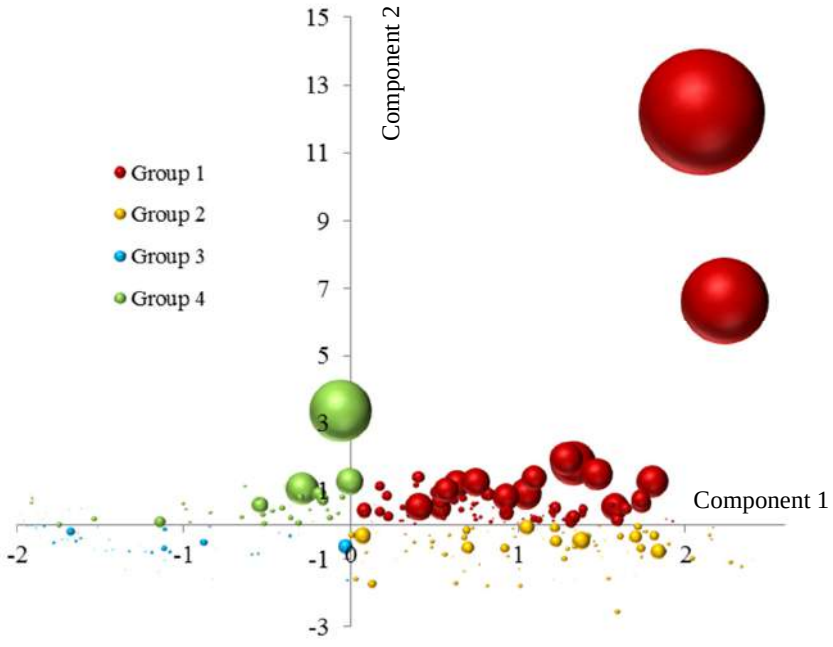

Fig. 5.7. Landslides of group1 include the largest volume of landslides, while group 3 include the smallest landslides of the mountain belt.

Table 5.9. Summarized information of 4 different categorized groups resulting from PCA.

Group number	Frequency	Volume % of total	Mean volume (m^3)	Average pre-slope	Average elevation (m)	Lithology
1	85	80 %	9.17×10^8	14°	1824	All in carbonates.
2	100	5.4 %	5.22×10^7	28°	1655	Mostly in carbonates (83 of total).
3	67	1 %	1.47×10^7	23°	512	Fine clastic and evaporites.
4	83	13 %	1.60×10^8	11.7°	617	36% carbonates, 37 % fine clastics, 16% evaporites and 6 % coarse clastics.

Group 1 where both components are positive (shown in red) includes relatively large volume landslides (Fig. 5.7) that occurred mostly in carbonate rocks at high elevations and with gentle pre-slopes. This group includes 85 landslides (25% of database) and constitutes 80% of the total mass failure volume. By plotting these landslides on a geographic map, one sees that they are mainly located between the active Main Recent Fault (MRF) and the Main Zagros Reverse Fault (MZRF) in the north and the Zagros Mountain Frontal Fault (ZMFF) in the south (Fig. 5.8). In addition, the geographic size distribution shows that the large landslides of this group occur close to the Balarud fault and the northern segment of the Kazerun strike slip fault (Fig. 5.8). Group 2 (shown in orange) characterized by positive component 1 and negative component 2 includes relatively small landslides with steep slope prior to mass failure. It includes highly elevated carbonate rocks, which are located far from major faults (Fig. 5.8) and its large landslides occur near the intersection of the Zagros Mountain Frontal Fault and the Balaroud and Kazerun faults. Group 3 whose components are both negative (shown in blue) includes landslides in relatively weak evaporite and clastic rocks with smallest volume, lowest elevation and relatively steep slopes prior to mass failure that are distant from the MRF and MZRF faults in the eastern sector and are close to the High Zagros Fault (HZF) in the west (Fig. 5.8). The largest landslides of this group occur close to the northern termination of the Kazerun Fault. This group contains 67 landslides (20% of the landslide inventory) and constitutes 1% of the total volume of the mass movements. Group 4 where component 1 is negative and component 2 is positive (shown in green) includes relatively large landslides that occur at relatively small distances to the Zagros Foredeep Fault in the eastern sector and the Zagros Mountain Frontal Fault towards the west. The largest landslides of this group occur close to the Main Recent Fault (Fig. 5.8).

In general, the geographic map (Fig. 5.8) shows that large landslides of the different groups occur in places where carbonate rocks have larger outcrop and occur at high elevation close to the Zagros Mountain Frontal Fault, delimited by the Balaroud and Kazeroun strike slip faults towards the west and east, respectively. Small landslides of the different groups occur mainly in the evaporitic and clastic rocks at lower elevations (Fig. 5.8) towards the west of the Balaroud fault and east of the Kazerun strike slip fault (Fig. 5.8). A summary of the four groups is presented in the table 5.9.

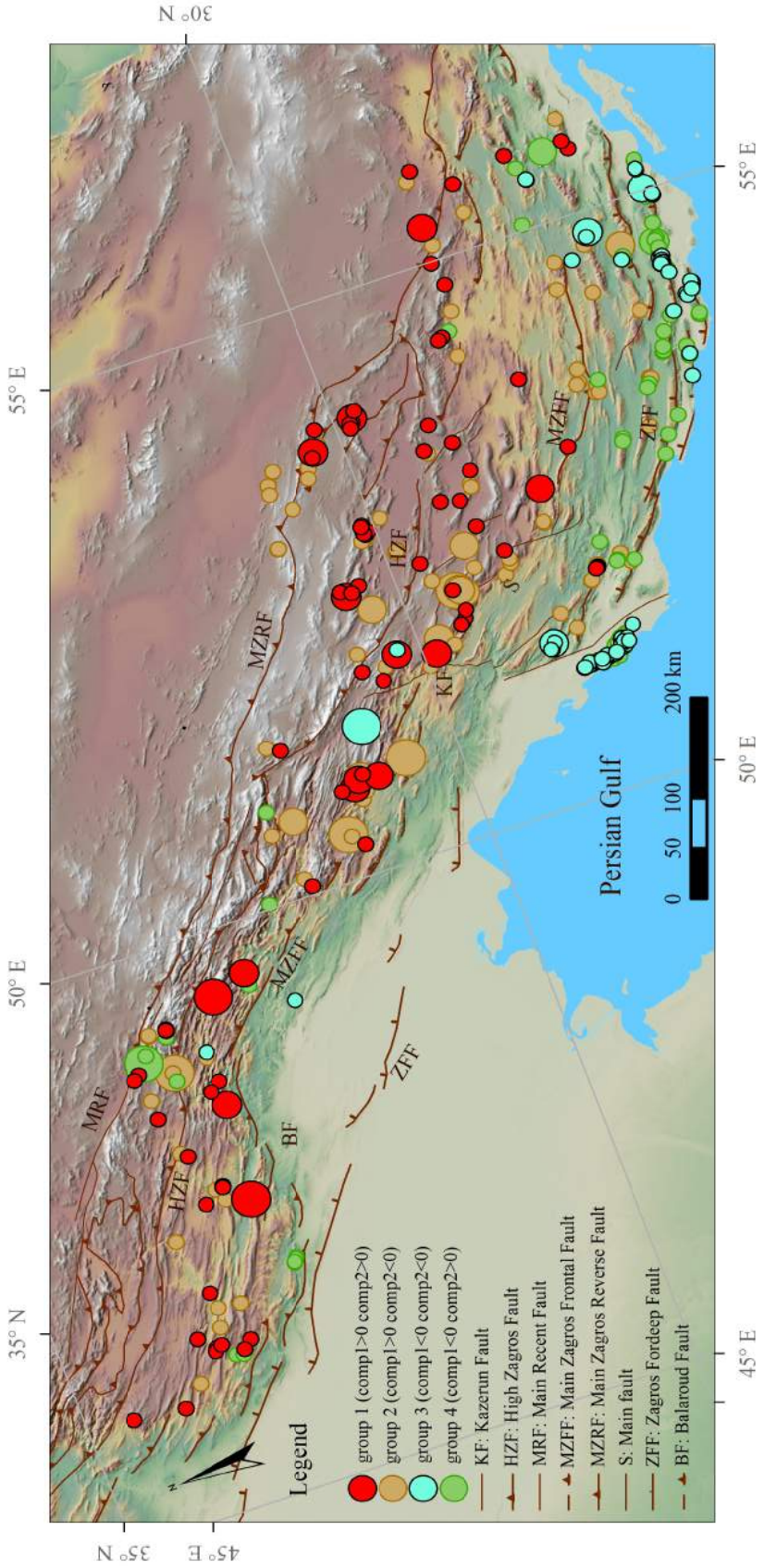
30° N
55° E
50° E
45° E
35° N
Legend
group 1 (comp1>0 comp2>0)
group 2 (comp1>0 comp2<0)
group 3 (comp1<0 comp2<0)
group 4 (comp1<0 comp2>0)
KF: Kazerun Fault
HZF: High Zagros Fault
MRF: Main Recent Fault
MZFF: Main Zagros Frontal Fault
MZRF: Main Zagros Reverse Fault
S: Main fault
ZFF: Zagros Fordeep Fault
BF: Balaroud Fault
Persian Gulf
0 50 100 200 km
MRF
HZF
BF
MZFF
ZFF
MZRF
KF
S

5.4 COMPARISON OF LANDSLIDES PROPERTIES BETWEEN THE EASTERN (FARS) AND WESTERN (LORESTAN) ZAGROS

Based on our investigation on the pattern of landslides that have been discussed in chapter 3, the landslide characteristics vary markedly between the eastern and western sides of the Zagros region. Because of this, PCA has also been applied separately for the Fars and Dezful regions. First, to investigate normality of the variables on both sides of the mountain belt, the Shapiro test has been applied. The results are represented in the table 5.10 and confirm that all variables in this dataset are non parametric.

To compare the similarity between the two groups of samples, the Wilcoxon test is applied. This method measures the difference between two groups compared to the difference within the groups; the ratio between these two numbers is designated W. The p-value is the probability that the pattern of data in the sample could be produced by random data. A p-value less than 0.05 indicates that the null hypothesis should be rejected, meaning that there is only a 5% chance that there is no real difference. Results of the Wilcoxon test on our data set are represented in table 5.11. The results reveal that the p-value is more than 0.05 for some variables (indicated with a star). Therefore, the null hypothesis can be accepted for these variables, meaning that the characteristics of these variables are the same in both regions. Variables that have a p-value less than 0.05, show different characteristics in western and eastern sides of the Zagros.

The frequency and volume distributions of eight variables from different populations in the Lorestan

Table 5.11. Result of Wilcoxon test reveals that 8 variables of 17 variables are not from the same population. The star indicates the variables that are from the same population.

Variables	p-value	W
Volume	6.476E-10	5113
Area	8.378E-10	5143
Mean relief	3.39E-11	4782
Mean elevation	3.675E-7	5917
Carbonate	0.00031	7080
Dis.fault *	0.8891	9760
Mean slope *	0.3562	8978
Dis.fold *	0.8913	9758
Dis.drainage *	0.7272	9914
Dis Basement fault	0.0000047	6292
Mean curvature *	0.1707	8649
Coarse clastic *	0.2205	9035
Fine clastic *	0.05009	110180
Dis.river	0.004123	11767
Evaporite	0.0000032	11988
Pre.slope *	0.3838	10297

Table 5.10. Result of Shapiro test reveals that distribution of the dataset in Fars and Lorestan region are non-parametric

Variables	Lurestan		Fars	
	W	P - Value	W	P - Value
Volume	0.2312	2.20E-16	0.3314	2.20E-16
Carbonate	0.7963	9.81E-09	0.7778	2.20E-16
Fine clastic	0.6745	1.60E-11	0.7696	2.20E-16
Evaporite	-	-	0.5342	2.20E-16
Clastic rockes	0.5176	3.30E-14	0.4796	2.20E-16
Mean curvature	0.9143	9.73E-05	0.8774	1.23E-13
Dis Basement fault	0.8717	2.04E-06	0.6265	2.20E-16
Dis.drainage	0.8331	1.10E-07	0.8795	1.66E-13
Dis.fault	0.825	6.34E-08	0.8767	1.13E-13
Dis.fold	0.6438	4.13E-12	0.5554	2.20E-16
Dis.river	0.8717	2.05E-06	0.7016	2.20E-16
Pre.slope	0.9557	0.01103	0.9764	0.000252
Mean relief	0.9588	0.01668	0.9681	1.44E-05
Mean Slope	0.9499	0.005276	0.9595	1.09E-06
Mean elevation	0.9842	0.049	0.8964	2.15E-12
Area	0.3116	2.20E-16	0.4364	2.20E-16

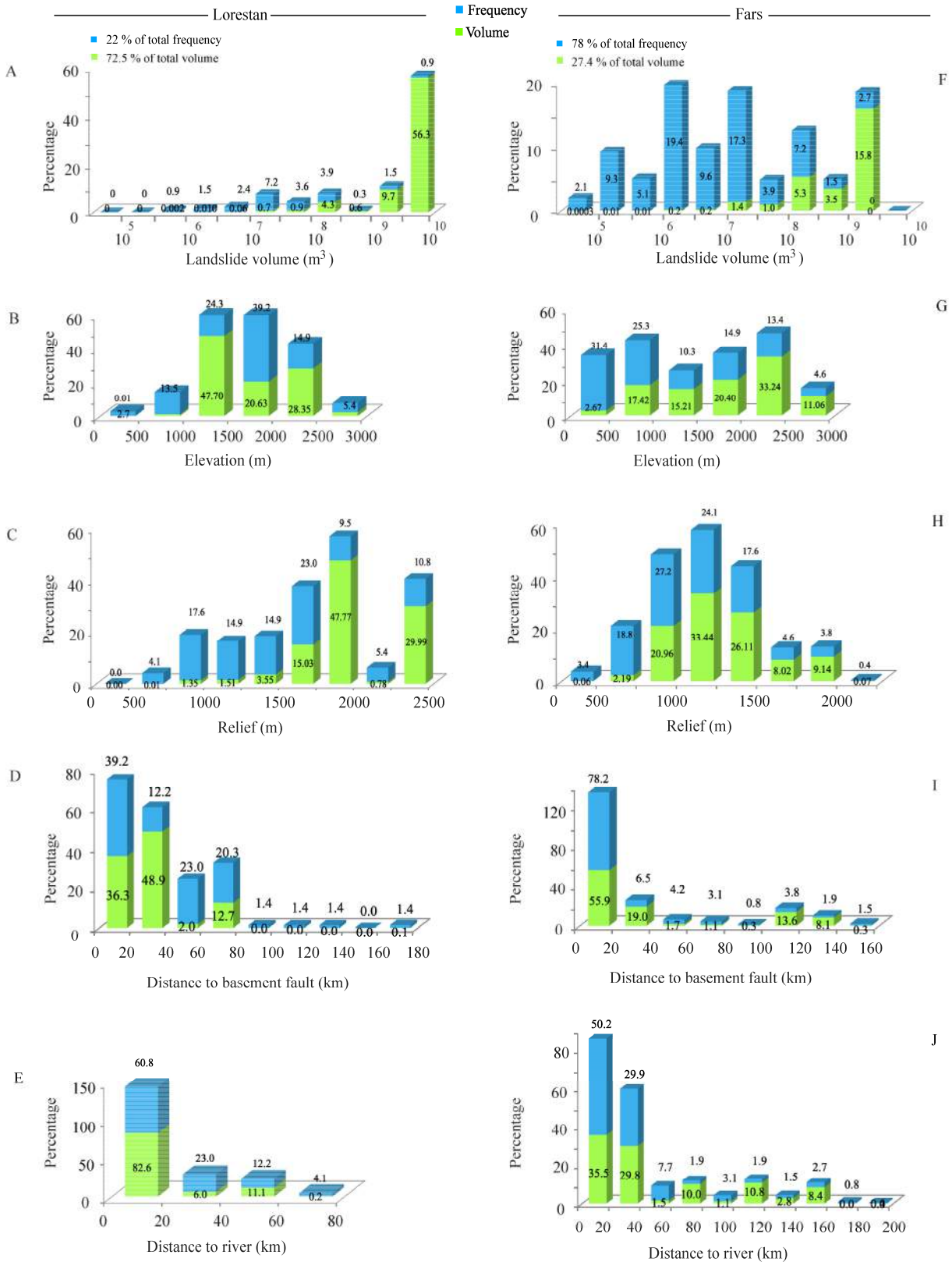

Fig. 5.9. Comparison of the volume and frequency distribution of variables that show different statistical characteristics in western and eastern parts of the Zagros region that have been presented in table 5.11.

and Fars regions are shown in Fig. 5.9. For comparison purposes, histograms of the variables that are not from the same population are represented in Fig. 5.9. The ranges of intensive peaks of their distribution are presented in the table 5.12.

The Lorestan region accounts for 72% of the total volume of mass movements in the Zagros mountain belt. Fig. 5.9A shows the size of landslides in terms of frequency and volume in the Lorestan region; 66% of the total volume of mass failures had volumes larger than 10^9 m^3. The distribution changes in the Fars region, where 78% of the landslides by frequency moved 27.4% of total volume of mass movements (Fig. 5.9F).

The volume of landslides in the Lorestan region is concentrated at higher elevations, while they are spread more uniformly than in the Fars region (Fig. 5.9 B and G). In the Lorestan province landslides mostly occurred in high local relief, while local relief is generally lower in the Fars region (Fig. 5.9 C and H). The distance to basement faults in the Lorestan region is two times more compared to in the Fars region (Fig. 5.9 D and I). Landslides are more intensive close to the river channel in the Lorestan region, while they are more uniformly spread in the Fars region (Fig. 5.9 E and J). Landslides occur in four lithologies in the Fars region (i.e., carbonate, evaporite, fine clastic and coarse clastic) but are most abundant in coarse clastics and evaporites, while in the Lorestan region landslides do not occur in evaporites but mainly involve carbonate rocks.

The results of the statistical comparison between the two populations of landslides for the Lorestan and Fars regions reveal that landslides have different characteristics. To investigate the correlation of variables in both regions a correlation analysis has been applied, the results of which are represented in tables 5.13 and 5.14. Except for the landslide area and volume that are well correlated in both regions, elevation and relief show a good correlation (0.62) in the Lorestan region. A significant difference between the Lorestan and Fars databases is the lack of evaporites in landslides of the Lorestan region. Elevation, topographic relief and carbonate rocks (0.26, 0.23 and 0.22 respectively) have a weak but real positive correlation with volume in the Fars region. Relief shows a weak positive correlation (0.22) with the volume of landslides while Pre slope shows a weak negative correlation (0.25) with landslide volumes in the Lorestan region.

Table 5.12. The range of intense peaks of landslides distribution in the Lorestan and Fars regions.

		Intensive peak	
Variables	Unit	Lorestan	Fars
Volume	m^3	5×10^9- 10^{10}	5×10^8- 10^{10}
Mean elevation	m	1000 - 2500	500 - 3000
Mean relief	m	1500 - 2500	750 - 1500
Dis Basement fault	km	0 - 40	0 - 20
Dis.river	km	0 - 20	0 - 40
Lithology		Carbonate Fine clastic Coarse clastic	Carbonate Fine clastic Coarse clastic Evaporite

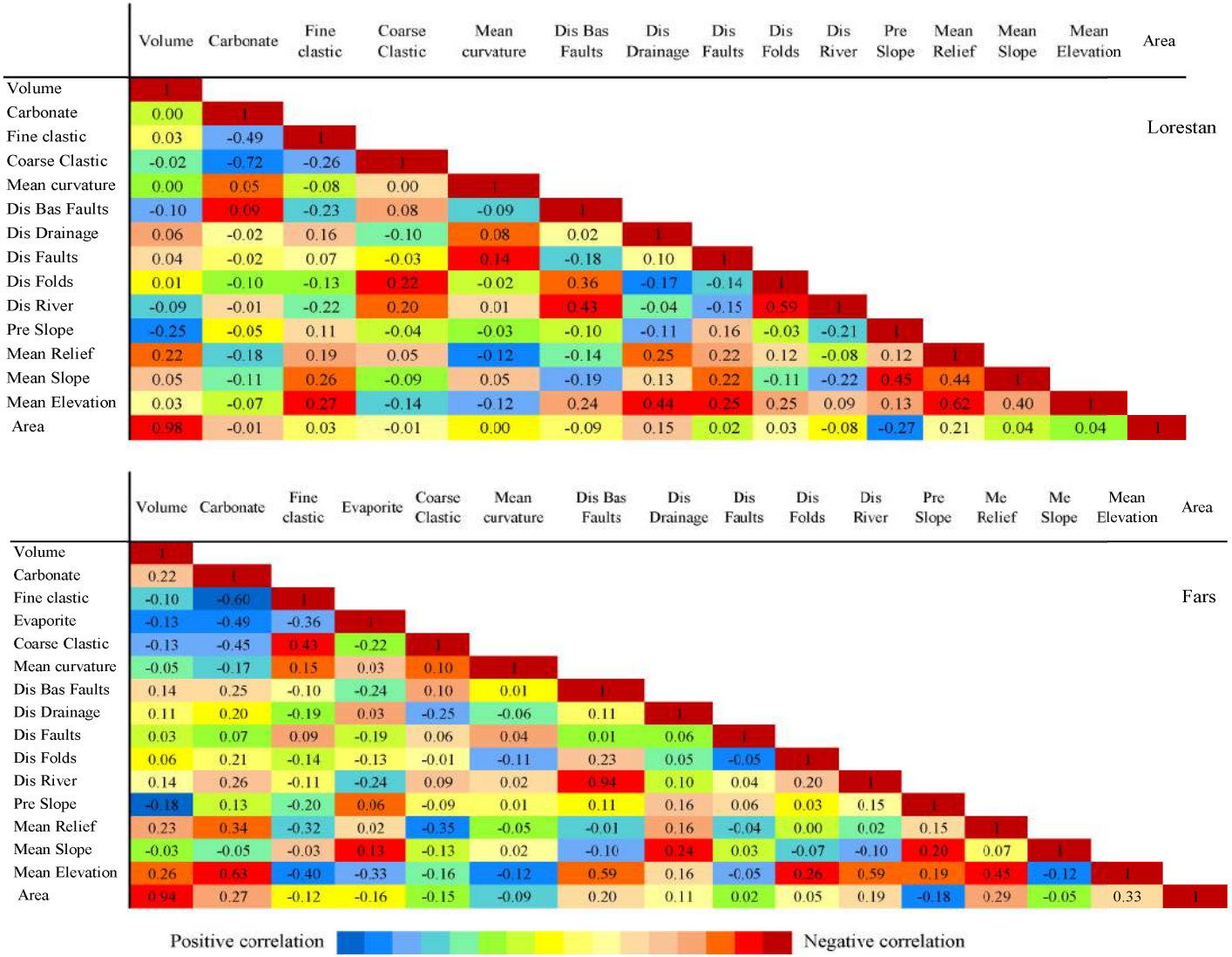

Table. 5.13. Linear correlation analysis results for the Lorestan and Fars region. Red colours shows positive correlation and blue colours shows negative correlation.

Table. 5.14. Results of correlation test between volume and other variables in the Lorestan and Fars regions.

	Fars		Lorestan	
	P-value	correlation	P-value	correlation
Area	2.2E-16	0.94	2.2E-16	0.98
Carbonate	0.0004	0.22	0.9950	0.00
Coarse Clastic	0.0434	-0.13	0.8474	-0.02
Dis Bas Faults	0.0191	0.14	0.3810	-0.10
Dis Drainage	0.0725	0.11	0.6092	0.06
Dis Faults	0.5736	0.03	0.7450	0.04
Dis Folds	0.3220	0.06	0.9019	0.01
Dis River	0.0223	0.14	0.4245	-0.09
Evaporite	0.0408	-0.13	-	-
Mean curvature	0.4102	-0.05	0.9975	0.00
Mean Elevation	1.719E-05	0.26	0.7691	0.03
Mean Relief	0.0002	0.23	0.0614	0.22
Mean Slope	0.6594	-0.03	0.6598	0.05
Fine clastic	0.1096	-0.10	0.8166	0.03
Pre Slope	0.0030	-0.18	0.0304	-0.25

5.4.1 PRINCIPAL COMPONENT ANALYSIS OF THE LORESTAN REGION

The results of three tests (eigenvalue-one, Scree plot and Propagation of variance) all indicate that the three first components are an appropriate representation of the variability of landslides for the Lorestan region, explaining 71.4% of variance of the dataset. Variables that have a meaningful loading for the three first components (i.e., volume, curvature, distance to fold, Pre slope and Mean slope) are shown in table 5.15.

Fig. 5.10A illustrates correlation circles of the five retained variables against the first two principal components in the Lorestan region. The mean slope and pre slope of landslides load in component 1 while the volume of landslides and distance to folds load in component two. The lengths of the arrows indicate that mean slope, pre slope, volume and distance to folds are strongly correlated. The mean curvature is not strongly correlated with other variables. The mean slope and pre slope of landslides also shows a high degree of correlation. The volume and distance to folds show a negative correlation. Mean curvature shows a slight positive correlation to the volume of landslides. Fig. 5.10B shows the data of the Lorestan region that are plotted in the PCA coordinate system, which enable us to separate the landslides into four main groups.

Table. 5.15. Loading value of the first three components in the Lorestan dataset. The highlighted numbers indicate loading value larger than the threshold ± 0.40.

	Comp1	Comp2	Comp3
Volume	-0.354	0.8032	-0.136
ME.curvatur	0.1326	0.2093	0.9687
Dis.fold	-0.219	-0.444	0.1147
Pre.slope	0.8574	-0.164	-0.058
ME.slope	0.7659	0.3926	-0.133

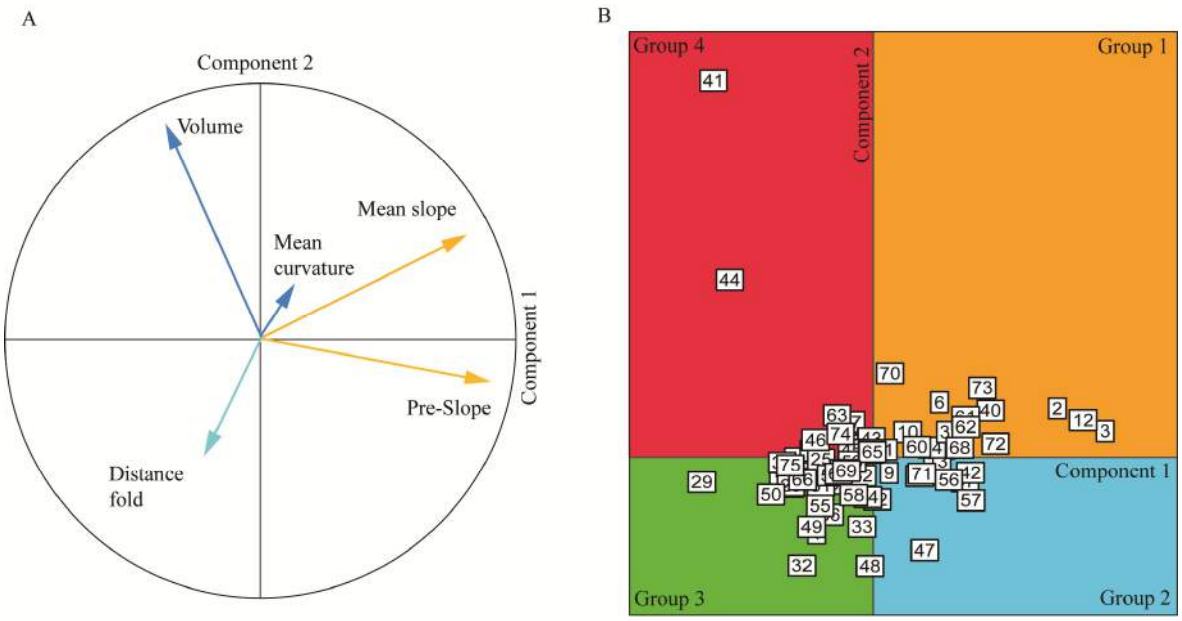

Fig. 5.10. A) The correlation circle of five variables of Lorestan dataset in two dimension. B) Transformed coordinate of landslides record.

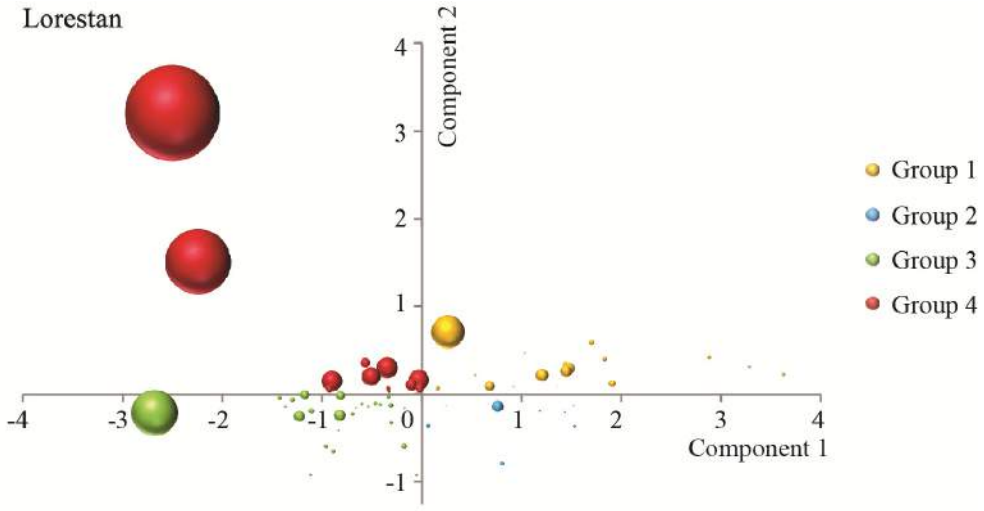

Fig. 5.11. The volume distribution of four groups of landslides within Lorestan region in PCA coordinate. The size of circles represent the relative size of landslides.

Fig. 5.11 represents the relative volume distribution of landslides of the Lorestan region in PCA coordinate. Group 1 includes landslides with steep mean slopes and contains 6% of the total volume of landslides. Group 2 includes small landslides that occurred on steep pre slopes, and contains 0.6% of the total volume of landslides. Group 3 includes landslides that occurred far from fold axes and contains 10% of the total volume of landslides. Samples that are located in group 4 have the largest average volume and include 55% of the total volume of landslides. The geographic distribution of landslides is concentrated mainly between the MZFF and HZF faults (Fig. 5.12).

5.4.2 PRINCIPAL COMPONENT ANALYSIS OF THE FARS REGION

The first components are meaningful components and account for 72% of the variance of database. Carbonate, coarse clastics and elevation have meaningful loading values in the first component while the pre slope has a meaningful loading in the second component (table 5.16)

Table 5.16. The loading value of two first components the Fars dataset. The loading values larger than threshold (± 0.40) is highlighted.

	Comp1	Comp2
Carbonate	0.89	0.19
Coarse clastics	-0.63	-0.27
Pre.slope	0.35	-0.92
ME.elevation	0.79	-0.03

Fig 5.13 shows a correlation circle of four retained variables against the first two components in the Fars region. Carbonate rocks has a strong positive correlation with elevation, while they have a negative correlation with coarse clastics (Fig. 5.13A). The pre slope of landslides is negatively correlated with the other three variables. The distribution of landslides in the PCA coordinate framework is plotted in Fig. 5.13B. Landslides that have positive values in both components (group 1), occur mostly at high elevations and within carbonate rocks. Group 2 includes landslides with steeper pre slopes and group 3 mostly contains coarse clastic rocks at lower elevation and with non-carbonate rocks. Group 4 contains landslides with gentler pre slope.

The volume distribution of landslides of the Fars region is shown in PCA coordinates in Fig. 5.14. Group 1 includes largest landslides (20% of total volume of landslides) that occurred in high elevation carbonate rocks, while group 3 includes the smallest volume of landslides (0.5% of the total volume of landslides) and occurred mostly in coarse clastic and evaporite rocks.

The geographic distribution of the largest landslides are concentrated in two main areas in the Fars region. In the western section of the region mostly large landslides occurred between MZRT and MZFF faults, while they show a cluster in eastern section of the region between the ZFF and MZRF faults (Fig. 5.15).

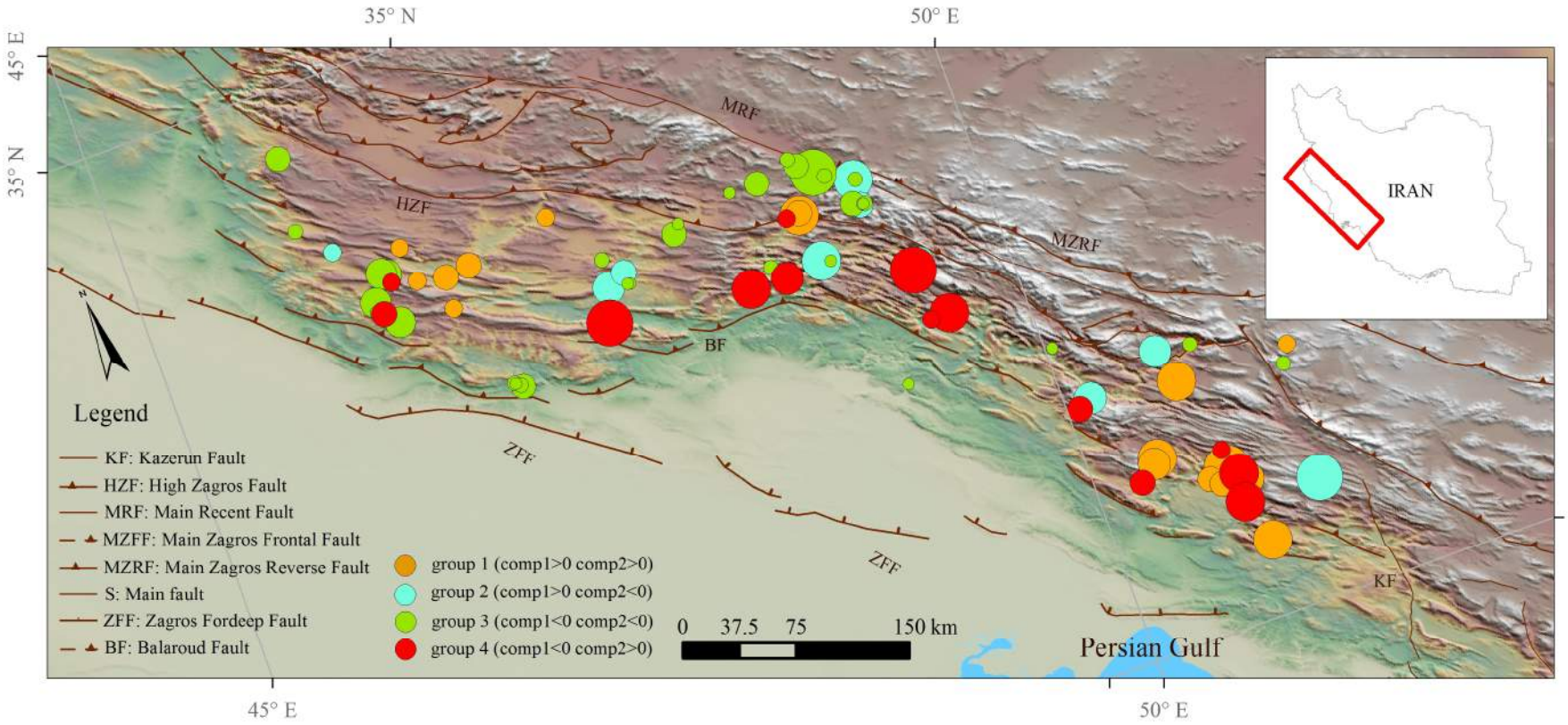

Fig. 5.12. Size distribution of four groups of landslides within the Lorestan region. The size of circles represent the relative size of landslides.

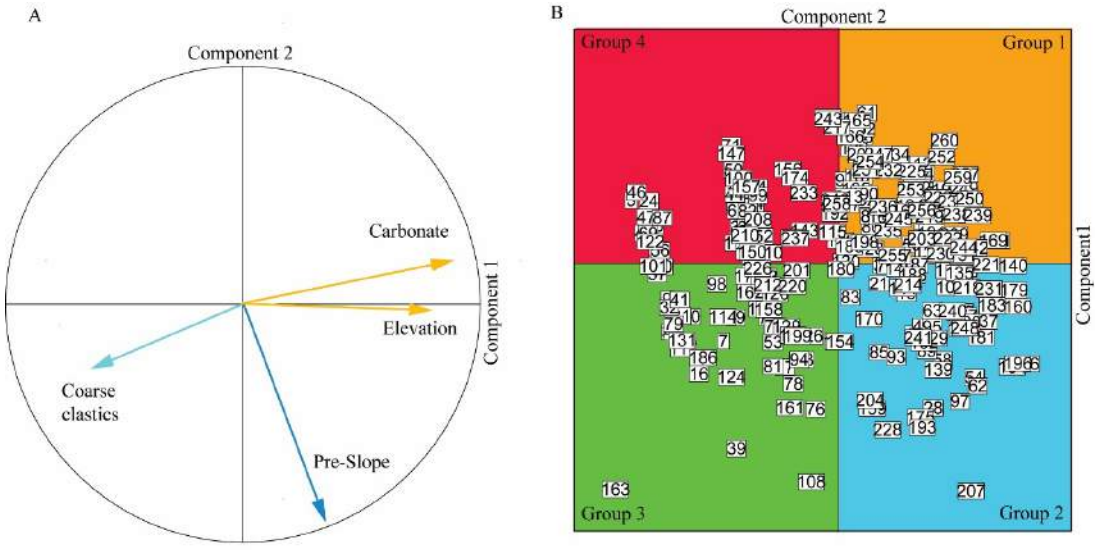

Fig. 5.13. The correlation circle of four variables in the Fars dataset. B) Transformed coordinates of the landslide record.

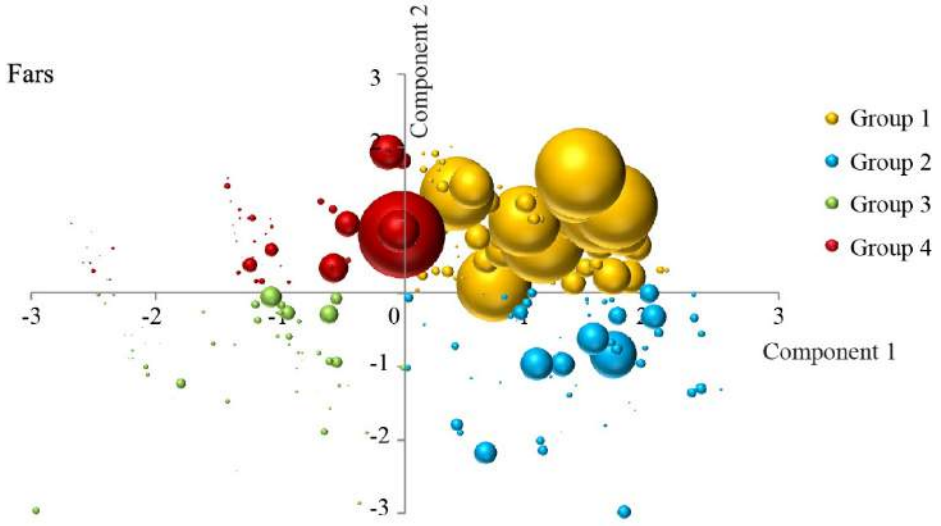

Fig. 5.14. Volume distribution of four groups of landslides of the Fars region in PCA coordinate. The size of circles represents the relative size of landslides.

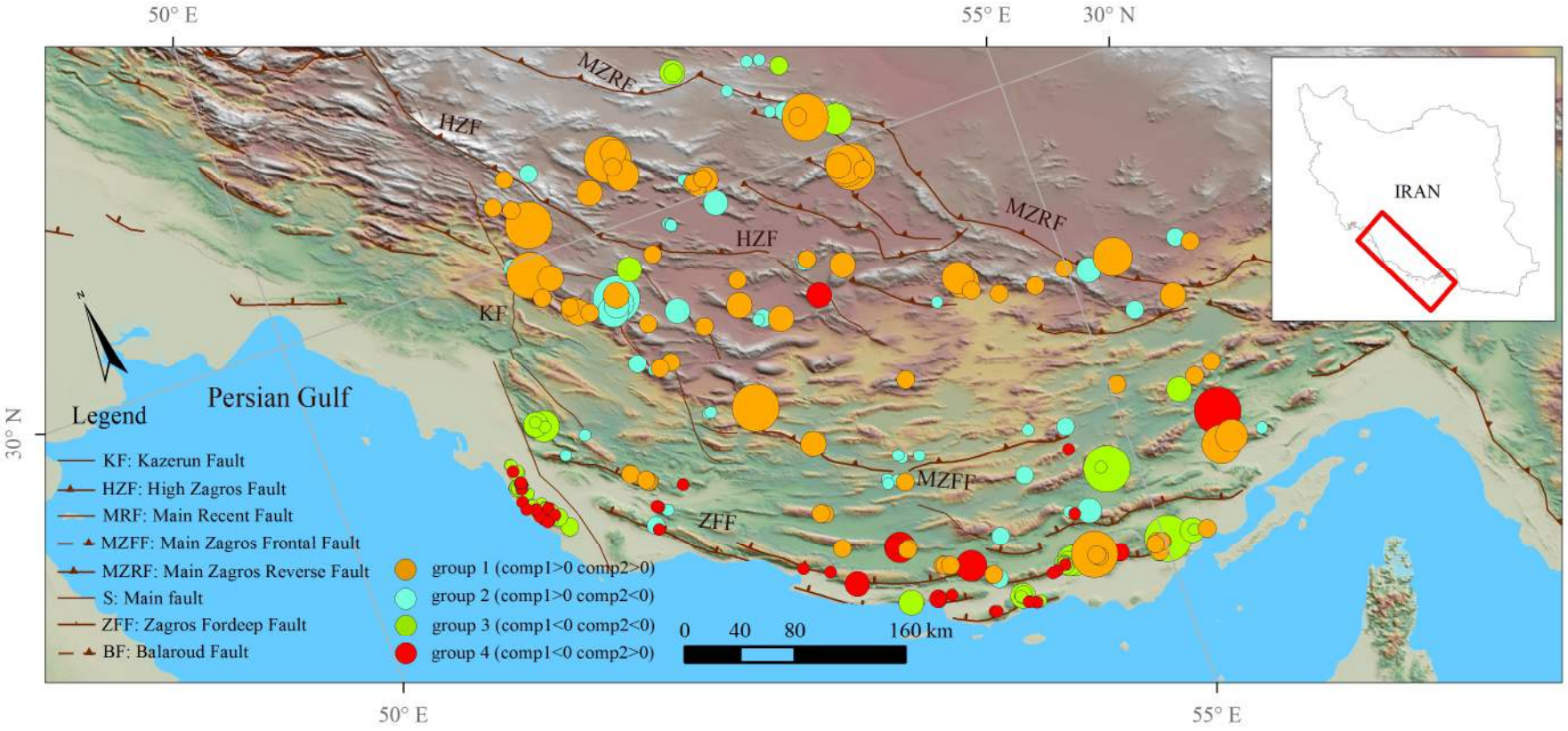

Fig. 5.15. Size distribution of four groups of landslides of the Fars region. The size of circles represents relative size of landslides. Group 1 include the largest landslide.

5.5 CONCLUSIONS

Principle Component Analysis (PCA) enabled us to better understand the link between causative factors and landslide occurrence in the Zagros region. The results of PCA show that lithology and elevation are the most influential geological and morphological parameters controlling the magnitude of large deep-seated landslides ($>10^4 m^3$). It also indicates that larger landslides are most frequent on gentle slopes (7-15°) and toward the northern part of the region.

The geographic distribution of landslides with similar characteristics displays meaningful clusters. The largest landslides occurred towards the north and northwest where topography is higher and carbonate rocks have extensive outcrops, whereas the small landslides occur mainly in the evaporitic and clastic rocks towards the south which are generally at lower elevation. The results of a statistical comparison between the two populations of landslides in the Lorestan and Fars regions reveals that landslides have different properties across the Zagros region. In the Lorestan area, almost all landslides occurred in carbonates and fine clastic rocks. The largest landslides (55% of total volume of landslides) occurred close to fold axes on gently sloping surfaces. In the Fars region, 20% of landslides occurred in highly elevated carbonate rocks. More frequent small landslides occurred in evaporite and fine clastic rocks at lower elevation. On the basis of these results, we conclude that geology exerts a dominant control on the size and distribution of landslides in the Zagros.

Chapter 6

DISCUSSION AND CONCLUSION

This study provides the first comprehensive investigation into the statistical characteristics of large landslides in the Zagros mountain belt. It produced not only a new landslides dataset, but also presents an overview of the spatial distribution of landslides, an investigation of the area-volume scaling and a study of the probability density distribution of landslide volumes. In addition, this study established the causes and nature of large landslides in the Zagros mountain fold-thrust belt. Here, I summarize the major conclusions.

The volume measurements were performed by three-dimensional geometrical modelling of each individual landslide. Area-volume relationship of the large deep-seated landslides shows a power law behaviour with a scaling exponent of $\alpha = 1.49$. By comparison with existing databases (e.g. (Simonett, 1967; Rice et al., 1969; Rice and Foggin, 1971; Abele, 1974; Innes, 1983; Whitehouse, 1983; Martin et al., 2002; Haflidason et al., 2005; Korup, 2005; Ten Brink et al., 2006; Katz et al., 2008; Guzzetti et al., 2009) we conclude that this scaling exponent is mainly related to the thickness of landslides rather than any physical processes. Results of the probability distribution of landslides, spanning six order of magnitude in volume ($10^4 < V_L < 10^{10}$ m^3), show the highest probability of occurrence is approximately 10^7 m^3 in the Zagros region.

The volume of landslides and their frequency have different distribution patterns. Landslides with large volume are developed mostly in carbonate rocks and show an intense clustering in the Lorestan region, whereas more frequent small landslides are developed in low strength lithologies (evaporite and coarse clastic rocks) that are concentrated in the Fars region especially near the Persian Gulf coast line. The probability density of landslide volumes in both regions is presented in Fig. 6.1. The density of landslides in the Fars region is high compared with the Lorestan region. Conversely, smaller volume landslides are more probable in the Fars region, whereas larger volume of landslides are more probable in the Lorestan region.

The geographic distribution of landslides with similar characteristics (identified with PCA) in the eastern (Fars) and western (Lorestan) sectors of the Zagros region reveals groups 3 and 4 in the Lorestan and group 1 in the Fars region which coincide with clustered areas identified in average volume density (Fig. 6.2). These groups together involved 86.5% of the total volume and 38% of total frequency of landslides and they occurred mainly in carbonate rocks with mean relief more than 1200 m and on slopes with an average of 14°.

Groups 1 and 2 in the Lorestan region and groups 2, 3, and 4 in the Fars region are located in the clustered area of density distribution of landslides frequency (Fig. 6.3).

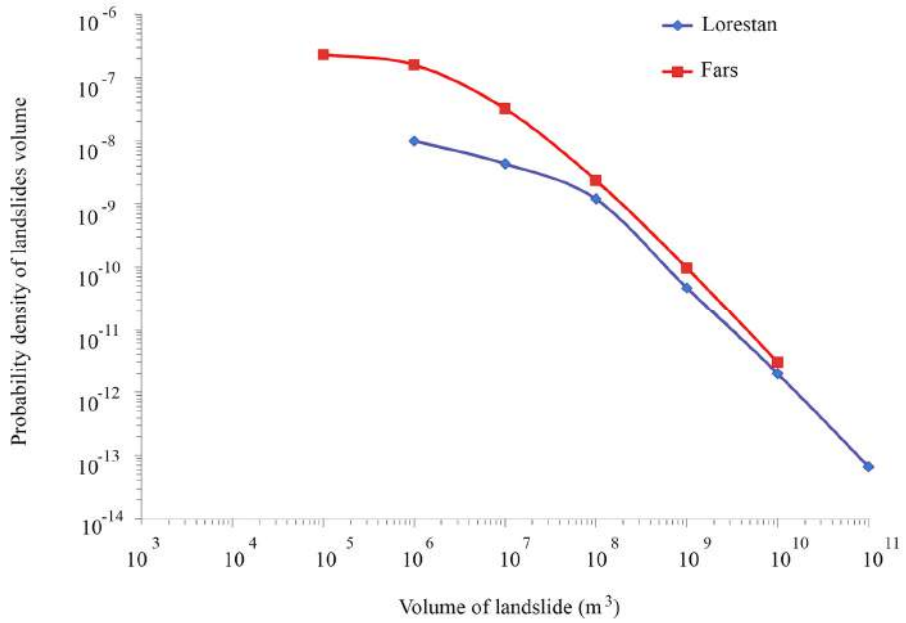

Fig. 6.1. Comparison of probability density of landslides volume in the Lorestan and Fars regions.

These groups 13.5% of landslides by volume and 62% of landslides by frequency. Compared to the others groups mentioned above, they are relatively small and occurred on the steeper slopes (24°) often near the Persian Gulf coastline are in fine grain clastic and evaporite rocks.

We have statistically identified the most important parameters that impact on the frequency and volume of landslides. The landslide frequency increases close to fluvial channel, active faults, on fold limbs, in unconsolidated rocks and on steeper slops. The magnitude of large deep-seated landslides is strongly correlated with high strength lithologies (such as thick carbonate units), high average topographic relief and high elevation, conditions that are most commonly encountered in the northern part of the Zagros.

The spatial distribution of human settlements and their geographical location that coincide with clustered zones of large landslides (>10^4 m^3) is shown in the Fig. 6.4 and 6.5. Of the total 415 settlements (i.e., city, town, village) in the Zagros, 65 of them coincide with the Frequent Zone of large landslides (>10^4 m^3) that contain more than 2 landslides per 1023 km^2. This includes 4 cities, 18 towns and 43 villages and their access roads (Fig.6.4). Three towns (Zaghe and Sepiddasht in Lorestan province and Kalameh in Bushehr province) and a village (Sivand in the Fars province) are located less than 2 km distance from landslides (Fig.6.5). Reactivation of old landslides near these settlements in response to grading activities, climate change or seismic shaking could cause significant damage and fatalities.

21 settlements that contain 2 cities, 15 towns and 4 villages are located in large volume zone (>$7.2\times10^5 m^3$). 109 roads in the Zagros region intersect the large landslide zone and in 16 sections of roads, landslides are less than 2 km from main roads (Fig.6.6).

Seven settlements coincide with both the frequent and large volume zones (Fig.6.7) making them especially vulnerable to landslide risk.

These preliminary findings emphasise the importance of landslides study in the Zagros region. Our preliminary investigation show that large landslides in the Zagros region are not related to the frequency of the historical/recorded earthquakes with magnitude of $M_W \leq 7$. Most likely, intense precipitation during the early to mid Holocene was the main trigger of large landslide in the Zagros region. Most of the large Zagros landslides occurred when the thick carbonate units (often the Asmari limestone) slid off fine clastic formations (Pabdeh-Gurpi marls). This situation would be favored by rapid drainage of surface runoff water in the carbonates and generation of high pore fluid pressures in the underlying low permeability marls, that is likely to have occurred following extreme rainfall events and anomalously wet periods.

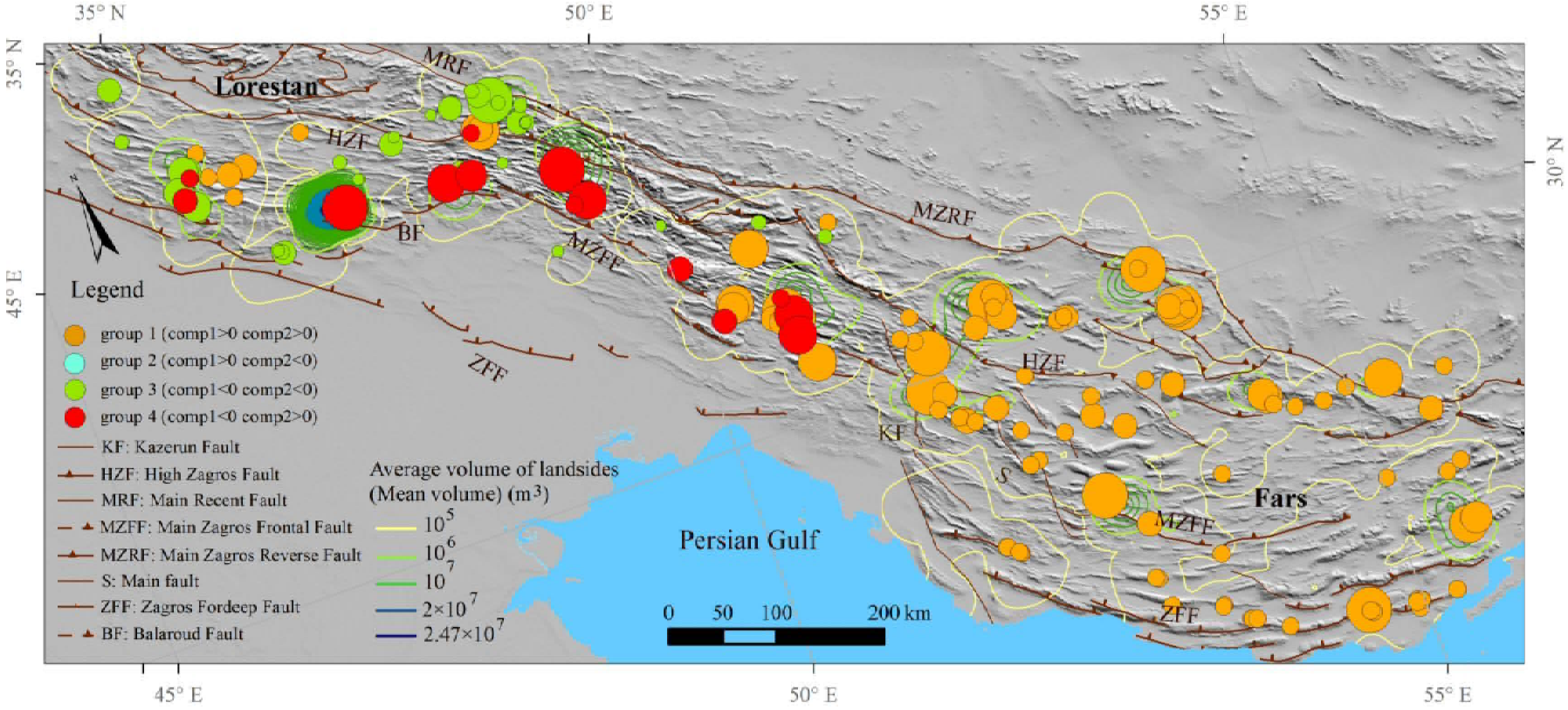

Fig. 6.2. Density distribution of landslide volumes combined with results of PCA.

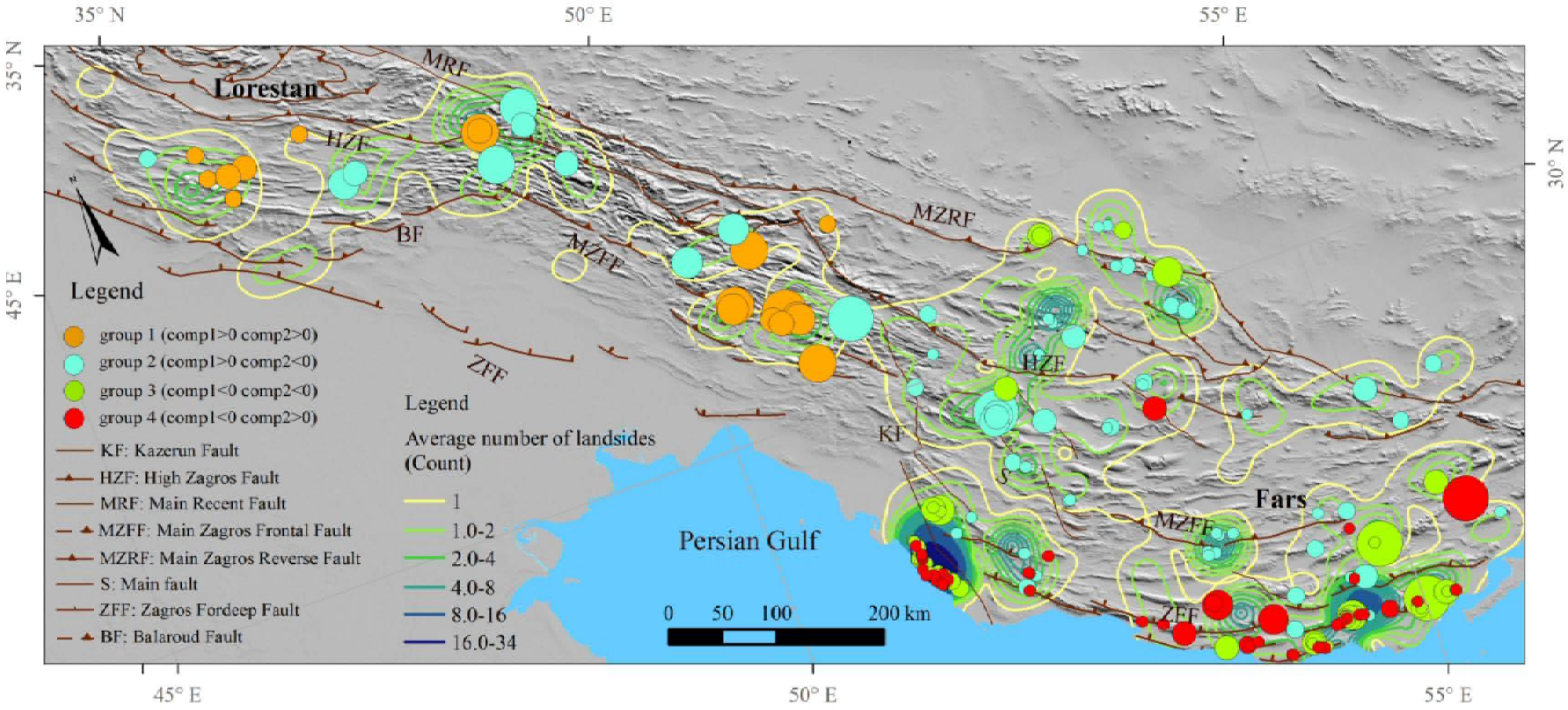

Fig. 6.3. Density distribution of landslides frequency superimposed on results from PCA analysis.

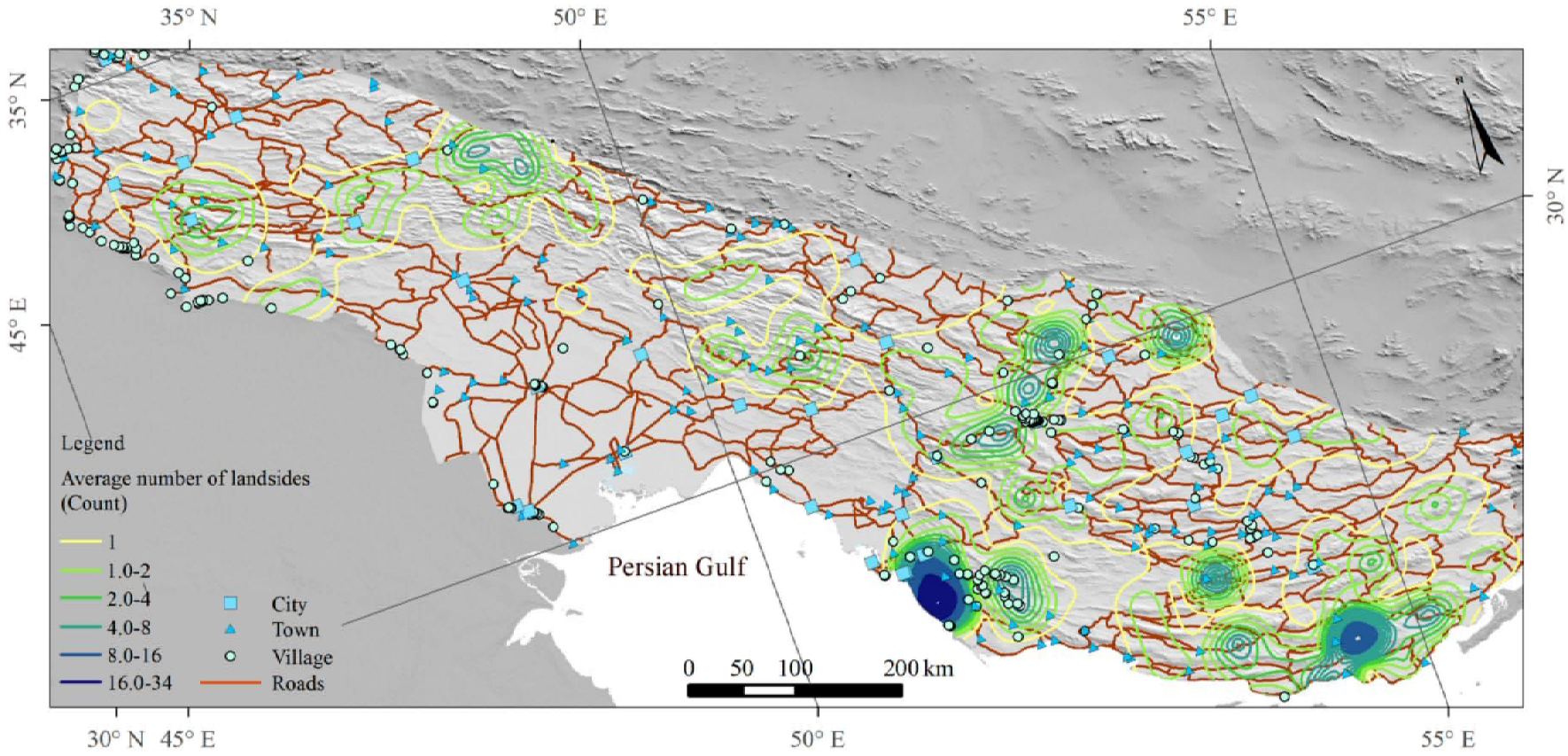

Fig. 6.4. Landslide frequency superposed on settlements and roads in the Zagros region. 170 cities, towns and villages coincide with the zone that contains at least one landslide per 1023km^2 area.

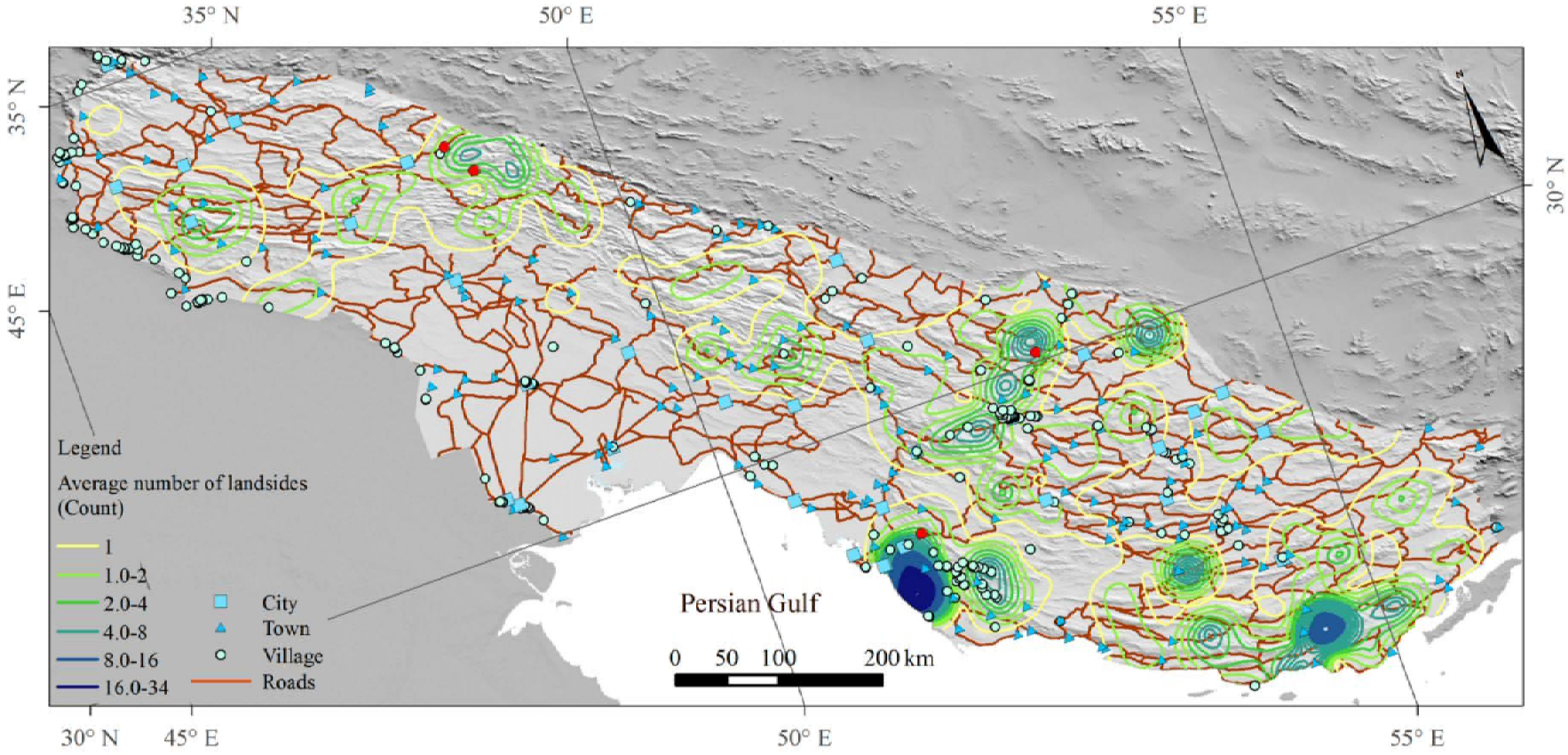

Fig. 6.5. Location of four settlements within 2 km distance from Large landslides (>$10^4 m^3$).

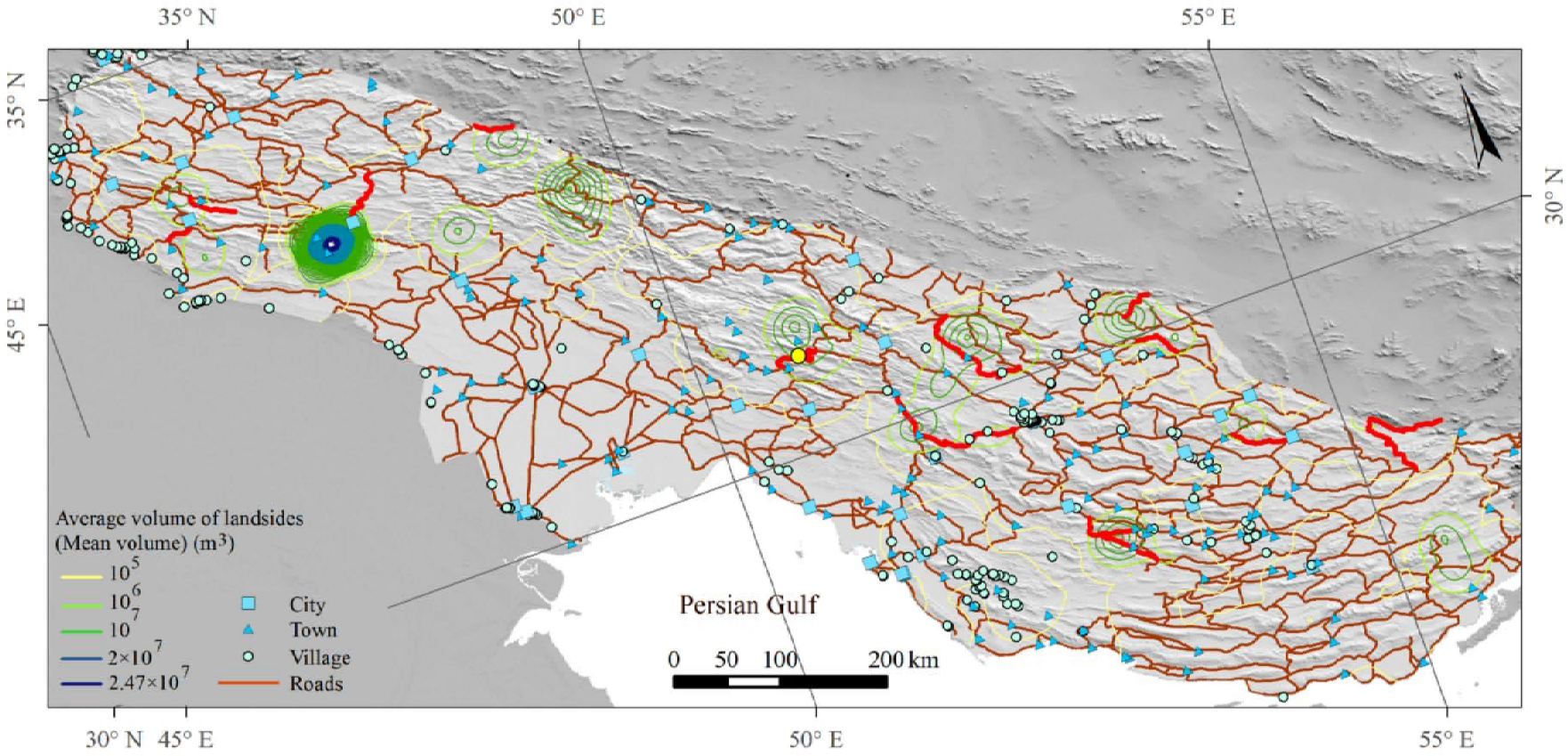

Fig. 6.6. 260 cities are within the large landslide zone that include landslides larger than 105m 3 per 1023 km^2. 16 sections of the roads are within 2 km distance from main roads, shown in red. The Sarfariab village in the Kohgiluyeh-va-Boyer Ahmad province is located within 5 km distance from a large landslide, shown in yellow.

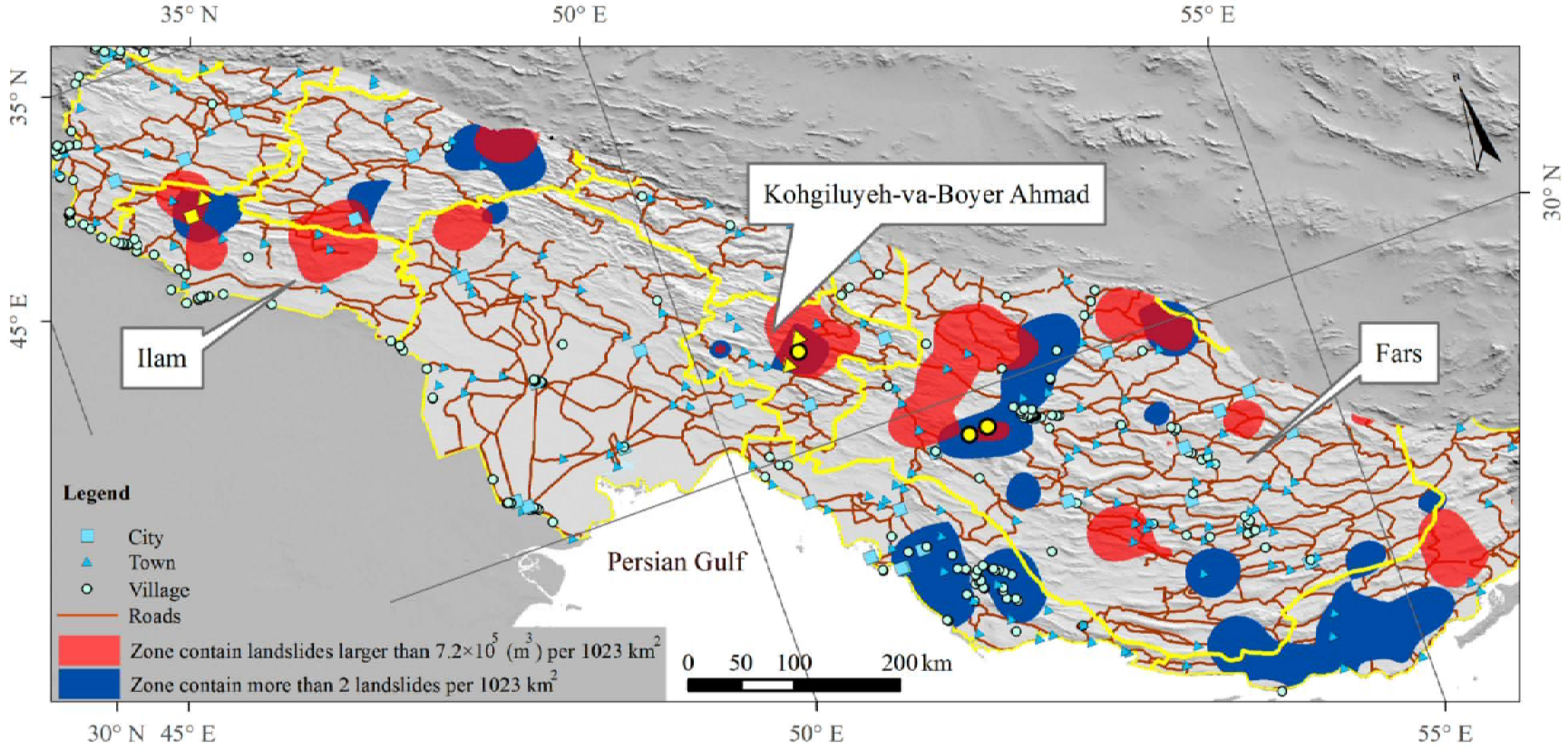

Fig. 6.7. Seven human settlements in the Zagros coincide with both frequent and large landslide zones, that include a city (Ilam in the Ilam province), 3 towns (Sarableh in the Ilam province, Abadeh and Choram in Kohgiluyeh-va-Boyer Ahmad Province) and three villages (Sarfariyab in the Kohgiluyeh-va-Boyer Ahmad province, Nasim abad and Dashtarjan in the Fars province) that are shown in yellow.

We suspect that the Zagros region, in presence of the water, is sensitive for the occurrence of large landslides. More dating studies on landslides in the future are required to test this hypothesis.

6.1 OUTLOOK

The results presented in this thesis suggest further research is necessary to complete the database of the smaller landslides ($<10^4 m^3$). We have predicted that the landslide inventory of the Zagros region, is missing almost 2000 landslides smaller than $10^4 m^3$ (Stark and Hovius, 2001; Malamud et al., 2004; Newman, 2005; White et al., 2008; Brunetti et al., 2009; Guzzetti et al., 2009b). To meaningfully assess the landslide hazard in the study area more detailed study with higher resolution data is needed.

In addition, geomorphological evidences suggest that most large landslides are probably prehistoric events (Crozier, 1986). Except for a single rock avalanche (Seymareh), there is no dating study on the occurrence of the large landslides in the Zagros region. Knowing the accurate age of large landslides is important in order to understand the temporal probability of the large events and to identify the main trigger of these mass movements. We believe that many of the largest landslides possibly occurred during a specific time period due to their similar morphology. We suspect that this period could coincide with a time of pronounced climate change. If true, the dating of lake deposits related to large mass movements can be very useful to answer this question.

Appendix

A: Landslide inventory of the Zagros mountain belt include 335 medium-large size landslide records and 29 columns. Dis indicates distance from, ME indicates Mean.
a 1,Fars; 2, Lorestan.
b ES, Earth slide; RS, Rock slide; S, Slump; DS, Debris slide.
c b, Beneath surface; t, Top surface.
d S, Source area; d, Debris area

		Location						Volume measurements error																			
		UTM coordinate			Geographic coordinate																						
Name	Region [a]	Long (E°)	Lat (N°)	Zone	Long (E°)	Lat (N°)	Volume (m^3)	Negative error (%)	Positive error (%)	Area (m^2)	ME-Elevevation (m)	ME-Relief (m)	ME-Curvature	Aspect	ME-Slope (Degree)	Pre-Slope (Degree)	Carbonate %	Fine clastic %	Evaporite %	Coarse clastic %	Dis-Fold (m)	Dis-fault (m)	Dis-B-Fault (m)	Dis-River (m)	Dis-Drainage (m)	Slide type [b]	Constructed surface [c]	Position [d]
L1	2	312185.4498	3709557.176	39	48.97795	33.50909	60,482,600	10	20	1,343,530	1994.582	1523.04	0.078189	NE	18.06	14	50	50	0	0	30954.22	1551.54	73652.48	62941.981	571.03778	ES	b	s
L2	2	190623.4012	3679054.672	38	47.681184	33.206178	17,348,800	5	10	680,573	1130.53	1364.11	-0.056317	E	20.12	27	75	0	0	25	19.110704	5857.566	3480.276	3627.5096	378.24921	ES	b	s
L3	2	201216.1001	3677046.62	39	47.795318	33.191071	967,077	5	10	78,350	916.9464	726.223	-0.020998	S	9.703	13	100	0	0	0	3233.8926	2222.707	4390.102	7047.7371	694.32585	ES	b	d
L4	2	202383.7413	3676563.606	39	47.807983	33.187043	1,120,670	5	5	172,811	917.8672	677.342	0.002125	SW	6.13	13	100	0	0	0	3420.797	2383.701	5117.532	8167.9874	717.8611	ES	b	d
L5	2	192868.9633	3698043.787	38	47.698798	33.377814	38,911,200	5	5	991,903	1421.613	963.621	-0.127624	NE	17.37	15	75	0	0	25	155.49629	10508.98	8585.289	13137.744	232.5389	S	b	s
L6	2	479249.5804	3422697.582	39	50.782782	30.937517	3,879,690,000	5	5	20,398,000	2489.182	2293.65	-0.011393	SW	26.59	14	60	40	0	0	424.38176	6678.979	10162.5	6336.3342	4701.2113	RS	t	s
L7	2	487310.7115	3414049.098	39	50.867274	30.859593	143,248,000	5	10	1,782,980	2654.342	2473.7	-0.123549	SW	30.11	28	60	40	0	0	1509.7784	8771.31	6267.293	7277.5768	1062.4969	RS	t	s
L8	2	488534.9603	3411652.833	39	50.880106	30.837983	92,872,700	5	5	1,218,010	2373.692	2449.98	0.011424	SW	35.92	17	60	40	0	0	2053.8502	7122.802	4650.323	6946.5171	1026.1616	RS	t	s
L9	2	482571.3527	3397574.916	39	50.817983	30.710878	1,169,470,000	5	5	7,964,950	1504.589	1800.44	0.078346	NW	17.21	13	90	10	0	0	4711.2091	2065.47	10617.06	8018.6072	3018.8868	S	t	s
L10	2	468162.4235	3419491.451	39	50.666822	30.908341	44,134,300	5	5	877,707	1502.84	1187.85	-0.004904	NE	35.2	31	60	40	0	0	1333.5892	2229.495	1937.496	7013.487	1066.3575	RS	t	s
L11	2	473799.4969	3413811.461	39	50.725959	30.857227	34,650,000	5	5	866,245	1649.983	1255.5	0.002903	NE	31.42	43	60	40	0	0	220.77632	1219.106	252.0417	1608.7412	1646.3731	RS	t	s
L12	2	489761.9351	3367823.651	39	50.893372	30.442493	428,623,000	5	10	1,486,650	1968.04	2231.21	-0.023588	NW	27.63	24	80	20	0	0	563.42477	774.6701	31803.92	16817.903	1853.1697	S	t	s
L13	2	172710.305	3737523.561	38	47.468017	33.727281	10,042,100	5	5	218,956	1500.932	883.75	0.189185	NW	23.06	20	100	0	0	0	1111.3199	13238.53	31438.2	5829.1451	1947.9393	ES	b	s
L14	2	106305.7341	3704245.714	38	46.76763	33.405401	1,588,460	5	5	149,583	2097.221	1859.85	-0.013248	N	21.73	26	0	100	0	0	429.38793	9228.665	42164.3	15288.13	1592.5625	DS	b	s
L15	2	80103.76377	3735941.599	38	46.471819	33.680473	24,464,100	5	5	1,736,670	1799.883	1356.76	0.064675	SE	13.99	17	80	15	0	5	1350.0891	2579.15	68556.97	12477.557	816.92051	ES	b	s
L16	2	56700.32007	3768844.622	38	46.203665	33.966696	4,389,740	5	5	254,499	1384.433	886.505	-0.000572	S	14.63	24	100	0	0	0	1709.3632	414.8902	105256	7330.172	817.05529	S	b	s
L17	2	91750.58816	3754950.645	38	46.588321	33.855948	11,386,500	5	10	684,379	1826.411	1201.82	0.042173	E	21.16	19	50	0	0	50	418.16614	3561.82	87582.5	30223.948	2265.2684	ES	b	s
L18	2	123203.1734	3727016.307	38	46.939305	33.616329	46,090,900	5	5	898,240	1002.833	1008.4	0.012191	NE	20.59	17	100	0	0	0	4224.1965	2407.837	57956.89	324.77375	760.1728	RS	b	s
L19	2	109290.7027	3725358.396	38	46.790445	33.596406	28,622,600	5	5	1,169,590	1340.565	1013.65	0.02149	SW	32.25	38	100	0	0	0	614.06747	9867.651	62486.36	5332.1455	1598.3439	RS	t	s
L20	2	93647.34031	3730449.812	38	46.620002	33.636349	8,613,250	5	5	311,945	1327.106	1721.88	0.001462	NE	21.35	24	100	0	0	0	1206.411	6277.018	63386.39	21341.125	349.91213	RS	t	s
L21	2	76099.72421	3709096.182	38	46.441483	33.437521	291,523,000	5	10	5,184,490	1394.46	950.839	0.003095	NE	13.04	10	100	0	0	0	1759.3008	2852.832	42544.61	1181.1432	1263.0741	S	b	s
L22	2	69708.48618	3718080.521	38	46.368642	33.515748	161,061,000	5	5	3,876,720	1438.886	1050.98	0.066531	NE	12.44	12	100	0	0	0	1224.1811	3232.507	52886.73	1057.8557	1344.6992	ES	b	s
L23	2	66366.14618	3720339.87	38	46.331678	33.53471	19,986,000	6	6	625,887	1561.581	1040.15	-0.013026	NE	10.05	11	0	100	0	0	1241.5105	303.4276	56095.59	1519.5803	2077.0417	S	b	s
L24	2	122273.6614	3642605.277	38	46.96441	32.85652	703,228	5	10	85,745	495.7813	885.476	0.014304	SW	8.129	12	85	15	0	0	650.32224	94.26647	3237.437	48998.335	768.00602	ES	b	s
L25	2	121728.6898	3643085.686	38	46.958404	32.860655	44,897,000	10	15	1,014,460	534.733	873.604	-0.056857	SW	11.22	18	85	15	0	0	784.16826	21.30044	3374.401	49074.548	709.35664	ES	b	s

		Location						Volume measurements error																			
		UTM coordinate			Geographic coordinate																					
Name	Region [a]	Long (E°)	Lat (N°)	Zone	Long (E°)	Lat (N°)	Volume (m^3)	Negative error (%)	Positive error (%)	Area (m^2)	ME-Elevation (m)	ME-Relief (m)	ME-Curvature	Aspect	ME-Slope (Degree)	Pre-Slope (Degree)	Carbonate %	Fine clastic %	Evaporite %	Coarse clastic %	Dis-Fold (m)	Dis-fault (m)	Dis-B-Fault (m)	Dis-River (m)	Dis-Drainage (m)	Slide type [b]	Constructed surface [c]	Position [d]
L26	2	124578.0366	3640378.609	38	46.98988	32.837274	34,959,100	5	5	1,355,920	537.8993	907.58	-1.03E-09	SW	10.29	11	85	15	0	0	122.60579	277.3867	3165.537	48643.701	1140.9072	RS	b	s
L27	2	125669.7491	3639071.852	38	47.002044	32.825888	96,776,400	5	5	2,020,160	557.3578	924.488	0.001728	SW	10.35	11	100	0	0	0	76.588824	319.077	2991.078	48359.816	836.48751	RS	b	s
L28	2	311218.2262	3642882.115	39	48.981392	32.907883	1,359,630	5	10	95,569	697.1945	1565.75	0.005812	W	13.18	20	0	0	0	100	3784.8335	19254.03	12965.56	115.89734	2.760949	ES	b	d
L29	2	306424.4689	3645117.639	39	48.929692	32.927197	63,311,000	5	5	1,609,730	1279.562	1672.38	-0.003379	NW	10.77	27	85	15	0	0	4584.6161	19607.15	10644.78	3187.1402	411.88692	DS	b	d
L30	2	278739.9894	3652772.558	39	48.631969	32.990935	27,333,700	5	5	548,557	1578.969	1573.25	0.017558	NE	13.46	16	85	15	0	0	3637.6565	7692.259	17977.26	12184.917	2368.0935	S	b	s
L31	2	284979.0109	3642207.461	39	48.701161	32.896958	455,369,000	5	5	3,502,050	889.5389	1505.58	0.059323	NE	17.12	17	90	10	0	0	3152.9626	1499.904	6774.435	1699.6891	735.00937	ES	b	s
L32	2	264147.1976	3644014.36	39	48.47816	32.90895	1,487,370,000	5	5	7,865,520	1649.125	1715.54	-0.022661	SW	20.78	12	85	15	0	0	959.08468	2843.836	10931.24	22243.134	1330.5362	RS	t	s
L33	2	358355.0069	3622671.891	39	49.488329	32.73276	10,271,300	5	5	861,340	1271.446	2272.05	0.001077	SW	16.97	35	60	0	0	40	2911.5037	7726.448	363.8232	742.78874	1022.3568	DS	b	s
L34	2	352461.3086	3617564.513	39	49.426259	32.685931	15,328,100,000	5	5	34,045,200	2443.834	2480.21	-0.066726	NE	18.7	5	85	15	0	0	2197.9481	9501.005	5128.961	6497.937	1219.9381	S	t	s
L35	2	351869.8067	3582799.679	39	49.425431	32.372355	58,475,700	5	10	1,249,440	770.9053	1392.52	0.172489	NE	11.66	18	85	15	0	0	3204.892	812.8714	12345.52	26296.967	568.2522	DS	b	d
L36	2	362701.9571	3582752.663	39	49.540547	32.373316	1,446,020,000	5	5	13,687,100	1502.283	1357.75	0.000455	E	16.05	11	100	0	0	0	2781.6449	3838.594	21213.5	20121.015	3861.2076	RS	t	s
L37	2	339017.4572	3687548.433	39	49.270642	33.315045	54,871,100	5	5	977,022	2394.111	2133.44	0.023618	SW	14.89	35	100	0	0	0	22234.358	412.6005	64138.44	46594.347	339.46918	S	b	d
L38	2	340305.1783	3687166.75	39	49.284538	33.311796	30,568,000	5	5	610,672	2436.762	2088.83	-0.20342	SW	19.19	25	100	0	0	0	22734.393	70.54098	63850.32	45355.029	300.24555	DS	b	s
L39	2	324968.7569	3696515.626	39	49.118052	33.393692	43,426,800	5	5	1,139,860	1900.942	1614.52	0.022479	NW	15.28	15	0	0	0	100	22801.004	1864.703	64721.76	54096.195	884.34481	S	b	s
L40	1	732436.5749	3248630.855	39	53.394052	29.345365	7,607,990	5	10	335,509	2067.774	924.02	0.087204	NW	15.94	30	100	0	0	0	5036.6498	4274.648	42318.8	47293.596	3043.8953	S	b	d
L41	2	337800.6742	3670306.326	39	49.260658	33.15941	8,313,560	5	5	477,989	1873.007	1492.86	-0.006671	NE	20.17	25	92	8	0	0	7728.4774	8709.562	46928.3	31670.352	449.4695	S	b	s
L42	2	338730.1012	3670338.266	39	49.270615	33.159837	14,156,300	5	5	381,069	1846.255	1534.04	-0.017023	NE	18.62	17	92	8	0	0	8304.3581	9240.631	46985.38	31966.78	406.34338	S	b	s
L43	2	340386.2556	3670036.984	39	49.288421	33.157366	47,555,000	10	15	624,333	1885.111	1518.42	0.085915	NE	17.32	15	92	8	0	0	9041.8169	9916.177	46729.02	32218.19	316.142	DS	b	s
L44	2	339412.6318	3670402.766	39	49.27792	33.16052	7,884,500	5	5	300,630	1827.717	1537.52	0.066833	NE	14.15	15	92	8	0	0	8760.3411	9668.274	47068.32	32238.746	333.51984	DS	b	s
L45	2	409796.1698	3536791.092	39	50.045408	31.963529	7,044,770	5	5	316,951	812.3944	1832.52	-0.147427	E	11.79	18	70	30	0	0	2921.9133	3663.048	39450.03	3939.1847	416.91019	ES	b	s
L46	1	735369.0511	3251109.276	39	53.424763	29.367169	41,796,200	5	10	1,127,670	1929.883	1009.86	-0.019034	NW	11.4	17	100	0	0	0	1320.0183	6143.39	46138.55	50697.924	777.25018	S	b	d
L47	2	420144.4779	3497206.496	39	50.158151	31.607208	17,786,500	5	5	407,724	2526.769	2498.18	-0.05168	NE	20.34	30	80	20	0	0	4868.9029	5734.708	29763.46	6318.2622	2351.2418	S	b	s
L48	2	463592.8327	3511461.491	39	50.615646	31.738015	31,040,200	5	5	899,743	2207.162	1944.03	-0.020769	SW	26.95	30	70	30	0	0	19451.362	1675.376	43268.83	10531.391	701.68045	S	b	s
L49	2	483680.9353	3508019.296	39	50.827774	31.707422	40,442,200	5	10	1,390,680	1476.488	2166.23	0.001312	W	15.97	19	20	0	0	80	11690.803	400.0858	48604.65	1302.1997	1106.2416	DS	b	s
L50	2	469238.1003	3487894.837	39	50.675981	31.525558	305,675,000	5	10	2,726,640	1909.609	1221.68	0.023893	NE	18.52	24	100	0	0	0	237.71673	11470.55	23846.07	11180.697	1513.3884	RS	t	s
L51	2	441238.0697	3441751.179	39	50.383782	31.108151	91,865,100	5	5	1,556,250	2381.94	1737.22	0.098689	SW	25.3	24	60	40	0	0	1793.3004	22193.19	7074.061	18621.111	1330.9776	RS	t	s
L52	2	443726.4551	3444375.434	39	50.409729	31.13195	434,299,000	5	5	3,910,120	2254.693	1847.68	0.014981	NE	26.09	25	60	40	0	0	1813.0011	23230.86	10633.87	21166.846	1951.6197	RS	t	s
L53	2	412464.8799	3492689.736	39	50.077602	31.565902	288,947,000	5	10	2,068,210	1901.712	2312.41	0.039669	SW	23.8	5	80	20	0	0	3958.7361	296.0616	20859.1	14648.798	610.55199	RS	b	s

		Location						Volume measurements error																		
		UTM coordinate			Geographic coordinate																				
Name	Region [a]	Long (E°)	Lat (N°)	Zone	Long (E°)	Lat (N°)	Volume (m^3)	Negative error (%)	Positive error (%)	Area (m^2)	ME-Elevation (m)	ME-Relief (m)	ME-Curvature	Aspect	ME-Slope (Degree)	Pre-Slope (Degree)	Carbonate %	Fine clastic %	Evaporite %	Coarse clastic %	Dis-Fold (m)	Dis-fault (m)	Dis-B-Fault (m)	Dis-River (m)	Dis-Drainage (m)	Slide type [b]	Constructed surface [c]	Position [d]
L54	2	431282.4476	3432793.731	39	50.279996	31.026792	217,305,000	5	5	2,853,390	1540.457	1720.62	-0.00789	SW	19.89	16	100	0	0	0	3426.4532	16604.05	5879.9	12879.616	1995.4886	RS	t	s
L55	2	479736.2901	3435311.012	39	50.787625	31.051339	8,654,080	5	5	333,923	2155.162	1570	-0.018866	NE	18.47	17	70	30	0	0	954.48465	6345.464	21288.31	3819.3625	895.98958	RS	t	s
L56	2	49373.80057	3839715.493	38	46.087644	34.600396	89,917,000	5	5	1,654,180	2163.603	1402.05	-0.03615	SW	14.54	11	100	0	0	0	6671.205	12343.66	175863.6	72811.063	2533.2483	S	b	d
L57	2	42273.19944	3790831.403	38	46.036541	34.15807	20,442,800	5	5	523,386	1504.212	1089.01	-0.069546	SW	16.34	15	100	0	0	0	3324.2162	2265.229	130585.5	24364.985	386.94524	RS	b	s
L58	2	535109.465	3486528.57	39	51.369762	31.513107	2,680,570	5	5	158,156	2676.864	1344.04	0.190639	NW	18.3	30	60	0	0	40	5991.685	4619.182	82476.48	46423.804	1513.8448	S	b	s
L59	2	529612.3868	3475047.817	39	51.311526	31.409676	32,626,400	5	5	1,239,360	2711.758	1428.33	0.013071	SE	11.97	19	60	0	0	40	996.51273	2254.167	75360.59	33877.34	4442.0665	S	b	s
L60	1	570942.6418	3377773.288	39	51.739508	30.530222	49,627,500	5	5	780,251	2162.281	1162.52	0.119353	NW	20.42	19	90	10	0	0	5742.3633	3773.073	12830.73	21735.443	487.85216	S	b	s
L61	1	586520.3635	3376029.833	39	51.90173	30.513469	24,181,800	5	5	886,109	2186.574	874.144	0.408439	E	14.85	21	50	50	0	0	1578.5021	2691.596	13098.76	30553.678	511.38985	ES	b	s
L62	1	558281.97	3361604.082	39	51.606635	30.385002	4,476,020	5	10	340,735	1988.093	1598.91	-0.001755	SW	17.39	20	80	20	0	0	2094.0405	2723.826	6843.064	4964.4329	650.58668	RS	b	s
L63	1	568632.0263	3355298.376	39	51.713945	30.327559	9,692,090	5	5	412,607	2432.412	1400.81	-0.008392	NW	16.13	21	80	20	0	0	43.445045	4569.428	5512.189	7342.0011	1336.8509	S	b	s
L64	1	575831.576	3340953.403	39	51.787799	30.197688	1,480,280,000	5	5	12,752,100	1811.786	1723.68	0.024931	SW	14.93	20	50	50	0	0	1505.0513	1346.187	6141.043	1826.508	1843.0453	RS	b	s
L65	1	579637.5766	3339385.245	39	51.827217	30.183294	2,257,840	5	5	110,641	1942.84	1587.54	0.04264	NW	14.67	23	0	100	0	0	720.68254	248.6069	10224.69	1820.5914	1865.2221	S	b	d
L66	2	527170.8159	3396177.505	39	51.283721	30.698086	408,113,000	5	5	4,560,980	1941.957	1093.78	-0.072579	NE	17.52	28	0	100	0	0	1011.0485	3108.829	8352.08	1286.0038	1045.6853	RS	b	s
L67	1	636337.0397	3366559.854	39	52.419579	30.423413	2,028,590,000	5	5	12,838,500	2494.149	920.873	-0.066709	NW	12.14	12	90	10	0	0	1666.3195	2132.178	33938.9	63703.03	3118.6858	S	b	s
L68	1	637910.2462	3360520.308	39	52.435158	30.368749	15,061,500	5	5	913,823	2623.467	1112.79	0.0518	NW	15.28	20	100	0	0	0	510.82449	4036.986	31474.44	62534.289	1655.8327	S	b	s
L69	1	642232.546	3352289.703	39	52.479009	30.293998	292,081,000	5	5	4,656,830	2244.758	1405.43	-0.060161	NW	13.05	21	100	0	0	0	2022.0206	2842.273	32028.21	64035.222	1418.4429	S	b	s
L70	1	641382.6054	3370401.195	39	52.472621	30.457484	260,296,000	5	5	4,383,400	2467.017	947.743	-0.070115	NE	15.2	17	100	0	0	0	4306.6119	2197.675	40255.6	69971.526	1168.6703	S	b	s
L71	1	618819.2057	3348154.675	39	52.23513	30.259216	127,781,140	5	5	2,629,490	1904.049	1227.54	-0.026854	SE	14	20	50	50	0	0	2459.3594	9188.556	8729.025	40364.223	563.85495	RS	b	s
L72	1	684132.8706	3326360.993	39	52.910014	30.054492	39,384,000	5	5	1,092,000	1918.229	1043.49	0.036103	NE	20.45	13	80	20	0	0	1724.5822	2904.427	74692.86	84025.91	851.2749	RS	b	s
L73	1	690446.1443	3329772.737	39	52.976081	30.084295	90,728,500	5	5	2,080,540	2230.448	941.939	-0.054272	NE	14.41	16	70	30	0	0	1009.2328	2113.378	80196.65	90776.027	2145.4956	RS	b	s
L74	1	689064.6628	3331108.333	39	52.961992	30.096556	26,792,700	5	5	748,579	2190.753	934.053	-0.076964	NE	13.84	18	70	30	0	0	323.64466	1828.781	78614.32	90782.323	1965.6981	RS	b	s
L75	1	686019.0358	3330638.347	39	52.930319	30.092785	39,400,400	5	5	1,600,980	1873.078	943.694	-0.04793	NW	14.54	19	75	25	0	0	2309.9358	1528.374	75686.76	88028.761	1185.4166	RS	b	s
L76	1	683066.9883	3330584.403	39	52.89969	30.092745	28,398,400	5	5	914,500	1819.438	999.786	0.131789	SE	11.11	15	75	25	0	0	2451.7702	1184.542	72788.95	85622.455	566.7548	RS	b	s
L77	1	681879.7002	3329621.127	39	52.887211	30.084234	66,717,400	5	5	2,554,160	1914.385	1049.03	-0.041099	E	12.05	16	75	25	0	0	2967.5925	535.8556	71800.81	84094.521	735.33676	RS	b	s
L78	1	679188.457	3330360.772	39	52.859423	30.091303	7,099,800	5	5	460,882	2399.66	1134.41	0.039997	E	13.24	23	75	25	0	0	1993.7986	1825.134	69017.65	82419.645	1351.2412	RS	b	s
L79	1	677371.1314	3334868.619	39	52.841327	30.132229	2,768,200	5	5	299,549	2311.138	1102.21	-0.126778	S	12.45	23	70	30	0	0	2041.6755	54.3911	66500.49	83935.267	1523.0211	S	b	s
L80	1	750921.8294	3357807.348	39	53.609767	30.326098	20,260,500	5	5	587,731	2760.849	870.777	0.021773	NW	13.06	26	100	0	0	0	8560.6512	1873.875	140220	149490.14	603.03332	RS	b	s
L81	1	721116.7723	3384837.202	39	53.30573	30.575635	7,989,630	5	5	389,430	2870.594	881.938	-0.130948	NE	14.48	23	100	0	0	0	2301.0851	2270.71	117213.6	149001.33	239.76258	RS	b	s

		Location						Volume measurements error																			
		UTM coordinate			Geographic coordinate																					
Name	Region [a]	Long (E°)	Lat (N°)	Zone	Long (E°)	Lat (N°)	Volume (m^3)	Negative error (%)	Positive error (%)	Area (m^2)	ME-Elevevation (m)	ME-Relief (m)	ME-Curvature	Aspect	ME-Slope (Degree)	Pre-Slope (Degree)	Carbonate %	Fine clastic %	Evaporite %	Coarse clastic %	Dis-Fold (m)	Dis-fault (m)	Dis-B-Fault (m)	Dis-River (m)	Dis-Drainage (m)	Slide type [b]	Constructed surface [c]	Position [d]
L82	1	762440.3114	3348661.846	39	53.727173	30.241217	2,149,870,000	5	10	23,524,600	2655.677	1096.01	-0.053406	NE	13.93	7	80	20	0	0	6023.6518	1458.123	139818.7	147890.5	1418.7785	ES	b	s
L83	1	692301.7503	3410745.845	39	53.010263	30.814257	12,623,100	5	10	591,541	2565.405	1149.81	0.116874	NE	16.67	28	10	45	0	45	5225.0586	10907.07	105173.2	134483.07	1252.5928	S	b	s
L84	1	692818.3327	3410261.957	39	53.015569	30.809809	4,008,050	5	5	302,876	2597.801	1125.9	0.054434	NE	16.84	37	10	45	0	45	5141.8145	10312.01	105263.4	134648.36	814.96928	S	b	s
L85	1	780508.9168	3340466.869	39	53.912561	30.163317	35,315,300	5	5	1,213,160	2437.956	917.459	-0.171791	S	12.89	20	50	0	0	50	2887.6757	383.7968	142042.4	150746	2482.9333	S	b	s
L86	1	746503.2977	3399093.223	39	53.573642	30.699191	6,984,030	5	5	357,762	1938.545	1124.34	-0.009072	SE	15.68	24	100	0	0	0	11132.638	10329.7	146062.4	177717.45	279.48893	RS	b	s
L87	1	767268.2843	3342059.463	39	53.775622	30.180651	12,397,700	5	5	544,726	2761.172	1000.3	0.093176	SW	15.78	28	100	0	0	0	8289.7058	576.2325	136417.5	145461.75	3270.4114	S	b	s
L88	1	757062.6608	3390263.959	39	53.681588	30.617375	5,316,960	5	5	255,543	2137.543	734.301	0.161792	N	15.53	23	0	50	0	50	10856.578	4834.888	152952.7	180399.2	2292.1984	S	b	s
L89	1	738603.4073	3400688.69	39	53.491599	30.715182	576,046	5	5	133,841	2296.088	1256.35	-0.083668	NW	15.19	26	100	0	0	0	11974.231	10103.06	139436.4	170939.4	1374.6619	S	b	s
L90	1	786648.9727	3300020.727	39	53.965384	29.797368	55,262,200	5	5	1,449,460	2349.487	1460.99	0.06778	W	19.96	17	100	0	0	0	1563.7544	4063.004	101296.4	119174.43	1130.7118	S	b	s
L91	1	785726.08	3301076.637	39	53.956127	29.807098	22,654,200	5	5	805,641	2290.75	1554.89	0.02276	W	14.69	28	100	0	0	0	1358.9031	4835.711	102396.2	119476.07	1402.0088	S	b	s
L92	1	780905.0861	3303953.279	39	53.907054	29.834132	1,915,210,000	5	10	17,463,700	2435.862	1512.84	-0.040826	SW	13.78	12	100	0	0	0	4274.3969	8590.436	105628.2	119091.5	3568.0331	S	b	s
L93	1	777306.5596	3305199.236	39	53.870174	29.846177	723,198,000	5	5	7,849,680	2393.962	1493.97	-0.005773	SW	12.4	15	100	0	0	0	6033.3959	7310.986	107274	118208	1500.7579	S	b	s
L94	1	776838.8837	3307640.173	39	53.865967	29.868283	702,409,000	5	5	6,337,040	2674.095	1439.88	-0.067618	SW	20.06	13	85	15	0	0	4226.2704	8614.931	109755	120053.19	2537.2275	S	b	s
L95	1	774715.2625	3309488.06	39	53.844478	29.885414	23,084,400	5	5	584,187	2586.005	1454.5	-0.083164	SW	21.77	35	90	10	0	0	3665.4358	8297.224	111880	120584.12	2165.0935	S	b	s
L96	1	772704.1409	3308343.856	39	53.823385	29.875548	171,022,000	5	5	2,644,270	2272.414	1575.33	-0.08392	SW	14.99	15	90	10	0	0	5646.3128	6041.379	111065.1	118603.88	915.08056	DS	b	d
L97	1	856745.2958	3013555.552	40	54.60063	27.198557	132,257,000	5	5	2,512,720	664.4457	1916.98	0.078628	NW	14.83	42	60	20	20	0	5052.6884	1408.157	5668.296	14311.066	467.37059	RS	b	d
L98	1	755684.5711	3239018.285	39	53.631077	29.254188	96,980,200	5	5	1,693,590	1807.616	1597.97	-0.066402	NE	12.18	20	100	0	0	0	6741.5667	1719.831	49481.79	52182.088	1887.7305	S	b	d
L99	1	735313.8224	3223930.227	39	53.418421	29.122091	164,717,000	5	5	2,484,900	1923.289	1186.59	-0.186786	NE	12.64	7	60	10	0	30	14410.53	703.281	28562.3	27640.962	2928.7976	RS	b	s
L100	1	707620.5577	3216695.503	39	53.132634	29.061668	103,756,000	5	5	1,593,190	2105.593	1250.14	-0.068759	S	17.27	17	100	0	0	0	1434.7766	4165.609	13095.71	9124.5229	414.4081	ES	b	s
L101	1	696520.5255	3221362.848	39	53.019498	29.105532	30,829,000	5	5	1,092,170	2484.208	1415.01	0.00429	S	12.96	35	100	0	0	0	490.76284	4610.102	2282.202	10074.349	1193.4414	ES	b	s
L102	1	693737.8989	3221210.064	39	52.990891	29.104581	4,319,000	5	5	361,897	2108.603	1473.73	-0.238152	SE	15.15	23	80	0	20	0	2331.8671	3165.634	728.0423	8547.9504	2591.8825	DS	b	s
L103	1	685205.286	3235696.123	39	52.905662	29.236528	114,726,000	10	10	2,818,160	1906.238	1257.43	-0.031037	NE	13.66	11	80	0	20	0	1967.3557	2847.606	15974.81	11170.314	3309.5632	S	b	s
L104	1	689290.325	3253275.505	39	52.95069	29.394494	5,785,270	5	5	402,497	1868.806	1074.95	-0.277904	S	12.68	19	80	0	20	0	1377.363	4295.199	29523.29	28266.916	1376.4224	ES	b	s
L105	1	643761.9445	3291152.522	39	52.486657	29.742267	8,114,550	5	5	367,537	1778.485	538.868	-0.101446	NE	12.61	17	100	0	0	0	4097.669	3759.329	28924.1	31413.795	2396.907	RS	b	s
L106	1	733965.8056	3250279.823	39	53.410141	29.359951	22,454,600	5	5	650,288	1942.137	980.954	-0.074128	NW	12.78	32	100	0	0	0	2787.7845	5631.783	44512.7	49390.877	829.30955	S	b	d
L107	1	661033.132	3306094.453	39	52.667435	29.874933	892,261	5	5	102,871	1618.027	577	-0.023329	NE	11.49	37	100	0	0	0	4558.0955	6661.659	51436.56	53652.941	1499.3694	S	b	d
L108	1	660804.6176	3306427.771	39	52.66512	29.877969	1,348,010	5	5	134,273	1646.125	577	-0.246389	NE	14.64	38	100	0	0	0	4521.9867	6949.249	51548.7	53625.357	1760.4436	S	b	s
L109	1	660737.576	3306739.512	39	52.664473	29.88079	200,526	5	5	40,863	1628.883	601.453	-0.198838	NE	13	37	100	0	0	0	4375.1317	7148.729	51746.79	53727.903	2058.6735	S	b	s

		Location						Volume measurements error																			
		UTM coordinate			Geographic coordinate																					
Name	Region [a]	Long (E°)	Lat (N°)	Zone	Long (E°)	Lat (N°)	Volume (m^3)	Negative error (%)	Positive error (%)	Area (m^2)	ME-Elevevation (m)	ME-Relief (m)	ME-Curvature	Aspect	ME-Slope (Degree)	Pre-Slope (Degree)	Carbonate %	Fine clastic %	Evaporite %	Coarse clastic %	Dis-Fold (m)	Dis-fault (m)	Dis-B-Fault (m)	Dis-River (m)	Dis-Drainage (m)	Slide type [b]	Constructed surface [c]	Position [d]
L110	1	660639.8369	3307360.545	39	52.663554	29.886405	3,903,060	5	5	172,345	1634.083	607.5	0.12615	NE	15.21	31	100	0	0	0	4054.9601	7524.285	52164.19	53967.706	2668.664	S	b	s
L111	1	659898.4208	3308200.497	39	52.656004	29.894079	9,478,000	5	5	280,012	1660.418	607.5	-0.012941	NE	16.71	29	100	0	0	0	4091.6138	7724.782	52341.56	53789.137	2789.5536	S	b	s
L112	1	659358.9527	3308527.023	39	52.650467	29.897095	3,917,730	5	5	252,168	1680.618	607.016	-0.047228	NE	15.88	29	100	0	0	0	4156.6891	7703.065	52250.85	53516.077	2679.493	S	b	s
L113	1	691879.2853	3311496.602	39	52.987655	29.919236	84,555,900	5	5	997,011	1921.305	959.198	0.009795	NE	26.35	26	100	0	0	0	2447.7782	2065.502	70785.59	78888.264	628.1014	RS	b	s
L114	1	611869.764	3219971.427	39	52.149664	29.103255	59,920,000	5	5	785,903	1746.14	1831.68	-0.059263	SW	21.38	24	60	40	0	0	1351.701	5169.285	3552.288	15530.397	2073.8652	RS	b	s
L115	1	659715.2493	3229428.101	39	52.642578	29.183459	4,178,290	5	5	388,906	1615.328	776.752	-0.058971	NE	7.395	11	100	0	0	0	3244.1301	471.0397	3559.641	1776.1734	246.21991	RS	b	s
L116	1	646883.8263	3246607.076	39	52.512934	29.340009	161,596,000	5	5	1,947,510	2317.202	1180.21	-0.002268	SW	17.75	26	100	0	0	0	2117.0385	3289.552	3871.897	6800.9676	3961.8298	ES	b	s
L117	1	620371.1904	3211770.487	39	52.236132	29.028474	8,850,550	5	5	460,184	1840.415	1659.27	-0.091531	SW	9.232	24	50	50	0	0	2879.1308	1509.327	5648.2	26042.328	3524.7687	ES	b	d
L118	1	626499.9147	3286585.966	39	52.307655	29.70295	13,126,500	5	5	480,680	2233.424	1126.83	-0.05502	NE	15.7	27	0	0	0	100	2978.5974	7421.217	14428.4	14006.705	1087.6563	S	b	s
L119	2	76819.29839	3743639.754	38	46.432827	33.748383	366,852,000	5	5	6,929,960	1776.321	1379.25	-0.189824	NE	13.55	12	100	0	0	0	172.68946	221.1687	76534.94	15906.059	1208.0109	ES	b	d
L120	1	626486.4268	3244726.527	39	52.302669	29.325257	8,549,780	5	5	481,624	2320.013	1321.29	-0.120966	SW	17.83	19	80	20	0	0	4011.4732	16083.32	8493.602	12176.422	12.270294	S	b	s
L121	1	608310.7089	3261382.953	39	52.117154	29.477255	271,733,000	5	5	3,102,290	1978.851	1487.96	-0.150603	SW	16.83	28	80	20	0	0	5934.8805	2242.538	4583.005	4691.388	889.54418	S	b	d
L122	1	611533.8231	3264777.087	39	52.150739	29.507599	153,778,000	5	5	3,133,420	2171.953	1412.61	-0.142513	E	18.1	30	50	50	0	0	1793.0573	760.6345	9246.715	3352.5209	1662.3973	S	b	s
L123	1	612925.3002	3265846.97	39	52.165203	29.517128	282,404,000	5	5	3,740,930	1891.231	1371.42	-0.13816	E	16.2	30	50	50	0	0	1826.078	1217.49	10210.91	2615.2492	620.18337	S	b	s
L124	1	612632.9575	3269130.229	39	52.162526	29.54678	586,958,000	5	5	5,689,170	2123.589	1253.76	-0.011071	E	23.15	30	80	20	0	0	2781.93	600.7589	7861.65	5368.0479	603.21136	S	b	s
L125	1	613525.4363	3271687.295	39	52.172002	29.569772	245,786,000	5	5	2,908,910	2078.207	1178.54	-0.069439	E	19	17	100	0	0	0	5265.6927	80.60846	5309.209	4326.0828	687.18698	ES	b	s
L126	1	557247.8351	3315714.296	39	51.593385	29.970948	24,187,700	5	5	525,085	1312.782	1246.06	-0.187657	SW	14.2	24	85	15	0	0	1044.9727	2461.278	3664.378	23041.467	3242.3566	S	b	s
L127	1	566219.2405	3306437.865	39	51.685796	29.886785	1,871,550,000	5	10	16,256,500	1790.259	1917.7	-0.172377	SW	27.12	16	85	15	0	0	421.97488	6905.745	7107.182	22658.551	1049.2358	RS	b	s
L128	1	585002.9803	3272374.612	39	51.877632	29.578247	174,430,000	5	5	3,891,510	1402.646	1897.44	-0.362899	SW	17.02	18	70	30	0	0	5239.8997	1440.083	1996.083	19739.146	148.43961	DS	b	d
L129	1	593858.842	3266218.276	39	51.968526	29.522057	19,911,800	5	5	768,319	1988.808	2184.2	-0.081209	SW	9.004	13	80	20	0	0	6164.2317	1654.328	5682.743	19751.439	916.72879	DS	b	s
L130	1	587403.464	3269309.411	39	51.902168	29.55042	163,849,000	5	5	2,849,080	1484.859	1964.05	-0.028225	SW	16.68	11	80	20	0	0	4620.2856	543.9701	152.3283	21238.373	628.58857	DS	b	d
L131	1	583104.0473	3274964.6	39	51.858226	29.601748	70,922,600	5	5	1,664,900	1422.965	1927.99	0.202618	SW	13.9	16	80	20	0	0	6368.1476	4530.289	3264.856	18625.402	386.16692	DS	b	d
L132	1	568708.5192	3287880.098	39	51.71039	29.71918	5,384,660	5	5	230,590	1600.419	1308.3	0.049717	NE	11.15	22	100	0	0	0	3496.3904	16154.27	8358.92	18843.608	2348.7503	S	b	s
L133	1	577874.1068	3299290.453	39	51.805972	29.821605	155,865,000	5	5	2,257,400	2037.77	1903.61	-0.213442	SW	19.36	21	80	20	0	0	2471.5186	6517.037	5476.264	9014.4859	1776.9397	S	b	s
L134	1	805328.6101	3191293.321	40	54.12834	28.81305	3,318,410	5	5	179,915	1611.194	1122.51	-0.012474	NE	19.03	26	100	0	0	0	1562.9813	2361.504	4091.207	30919.644	728.69483	S	b	s
L135	1	823097.1643	3203423.615	40	54.313618	28.918015	369,682,000	5	5	6,137,790	2052.01	1412.62	0.013454	NE	12.27	21	100	0	0	0	6897.7346	99.24471	25018.88	32033.763	2290.8811	S	b	s
L136	1	824970.3337	3199352.688	40	54.33163	28.880859	391,919,000	5	5	5,215,060	1880.043	1480.48	0.060366	NE	17.85	16	60	40	0	0	8673.1181	453.2523	23266.31	27688.566	524.25215	DS	b	s
L137	1	828479.8249	3191473.537	40	54.36527	28.80897	14,024,500	5	5	447,365	1359.122	1415.47	-0.063507	W	12.71	11	60	40	0	0	13380.817	1881.531	19796.26	19460.539	251.12379	DS	b	s

		Location																								
		UTM coordinate			Geographic coordinate			Volume measurements error																		
Name	Region [a]	Long (E°)	Lat (N°)	Zone	Long (E°)	Lat (N°)	Volume (m^3)	Negative error (%)	Positive error (%)	Area (m^2)	ME-Elevation (m)	ME-Relief (m)	ME-Curvature	Aspect	ME-Slope (Degree)	Pre-Slope (Degree)	Carbonate %	Fine clastic %	Evaporite %	Coarse clastic %	Dis-Fold (m)	Dis-fault (m)	Dis-B-Fault (m)	Dis-River (m)	Dis-Drainage (m)	Slide type [b]	Constructed surface [c]	Position [d]
L138	1	844652.7395	3183142.504	40	54.52818	28.729684	892,938	5	5	80,657	1112.675	909.379	-0.727094	W	18.85	21	100	0	0	0	11563.359	5724.422	18451.07	18765.68	2535.7483	S	b	s
L139	1	868359.2988	3180217.316	40	54.769497	28.696792	2,434,320	5	5	198,533	2244.572	1768.03	0.200602	SE	10.22	11	75	25	0	0	1747.4797	2177.627	3976.347	35319.254	372.99554	DS	b	s
L140	1	889170.3783	3185541.441	40	54.983868	28.738636	28,679,900	5	5	980,208	2003.71	1237.92	-0.090724	NE	14.29	14	100	0	0	0	15849.196	3978.85	2336.435	30860.362	1023.918	ES	b	s
L141	1	701485.5479	3123520.021	39	53.053212	28.222157	180,965,000	5	5	2,906,910	985.4228	936.843	-0.143345	NE	13.3	16	90	10	0	0	2648.0492	2975.907	502.0363	4368.9049	1637.2853	S	b	s
L142	1	770604.7068	3145350.18	39	53.762064	28.406607	6,299,390	5	5	431,870	1902.162	1268.21	-0.256778	NE	15.93	14	85	15	0	0	2875.7105	3504.575	1481.898	59654.73	329.49801	DS	b	s
L143	1	903747.7558	3178827.108	40	55.130402	28.673711	96,546,200	5	5	1,113,760	2382.339	886.94	-0.146066	W	14.43	23	100	0	0	0	11210.453	1548.409	12492.01	15103.49	2244.9944	S	b	s
L144	1	924112.8218	3140911.11	40	55.3243	28.325927	19,619,900	5	5	371,313	2378.41	1822.19	-0.139891	W	22.23	28	70	0	30	0	1060.648	3826.3	4270.143	17816.688	331.12058	ES	b	d
L145	1	950467.9911	3142243.855	40	55.59285	28.329145	103,603,000	5	5	1,730,290	1819.951	1614.01	0.082241	NE	16.84	15	100	0	0	0	3808.1092	7616.402	74.82506	13630.064	2157.9333	ES	b	s
L146	1	921080.0654	3182679.397	40	55.308732	28.702863	1,178,330,000	5	5	6,125,990	2081.06	1137.98	-0.105899	SW	15.22	10	100	0	0	0	27641.264	639.2872	21060.54	14848.324	1384.2938	ES	b	s
L147	1	963208.7088	3182129.483	40	55.738435	28.683515	35,468,900	5	5	836,362	1856.681	912.281	0.003339	NE	20.54	30	95	5	0	0	41465.232	464.3159	38692.61	26800.983	1270.198	S	b	s
L148	1	971445.5599	3175899.305	40	55.819881	28.624504	4,014,070	5	5	237,819	1514.44	719.051	-0.089646	E	16.76	18	100	0	0	0	36727.597	3124.619	36850.71	23972.548	2706.6617	S	b	d
L149	1	898723.6983	3093606.737	40	55.049915	27.907935	3,303,780	5	5	175,004	711.2154	393.898	-0.016742	NE	7.762	19	60	0	40	0	10615.075	707.6701	3049.776	31503.291	787.26527	S	b	d
L150	1	948360.0855	3081962.138	40	55.548474	27.787419	43,993,400	5	5	421,886	1175.205	1517.42	-0.019617	NW	10.34	9	75	0	25	0	1920.0354	4821.796	2960.727	12955.444	88.71196	ES	b	s
L151	1	935458.6405	3076056.338	40	55.415764	27.738507	10,962,300	5	5	412,749	880.8947	1891.73	-0.012274	SE	30.1	30	30	0	70	0	2373.002	486.4723	3354.093	25211.091	1000.5417	S	b	s
L152	1	936181.402	3076240.101	40	55.423142	27.739927	10,592,000	5	5	252,389	836.4556	1904.75	0.043094	SE	23.3	30	30	0	70	0	2533.0468	658.7403	4081.078	24477.974	398.89636	S	b	s
L153	1	979879.0549	3031583.214	40	55.847331	27.323359	7,723,340	5	5	137,179	1107.196	1443.03	-0.128082	SE	23.17	36	95	5	0	0	2274.7395	4681.831	9639.064	11362.602	6307.6448	S	b	s
L154	1	951713.8077	3029203.08	40	55.562704	27.311515	888,051,000	5	10	6,877,130	641.2119	1308.58	0.035751	SW	28.53	12	100	0	0	0	978.26837	19020.9	17990.72	22705.786	3515.608	S	t	s
L155	1	959581.1933	3032745.382	40	55.643293	27.340775	519,642,000	5	5	4,630,620	948.5526	1349.41	0.023607	NW	14.2	10	100	0	0	0	2475.4185	13820.31	10640.8	19185.672	5850.1042	ES	b	s
L156	1	955682.2243	3053104.785	40	55.611628	27.525288	1,997,320,000	10	15	7,506,510	1038.978	1165.5	0.126059	NW	15.05	14	50	30	20	0	3182.7688	4907.852	2385.491	21912.376	636.75235	S	b	s
L157	1	961431.6324	3088209.755	40	55.683141	27.839205	6,987,430	5	5	159,816	1256.492	1316.71	0.033171	NE	28.02	10	100	0	0	0	2415.9685	3744.578	10091.19	4393.0612	3451.8739	ES	b	s
L158	1	835410.6235	3083118.805	40	54.404887	27.830826	1,079,650	5	5	68,958	1118.352	645.17	0.115467	SW	24.91	35	100	0	0	0	6979.6051	1580.211	10342.41	32653.119	1770.2182	S	b	s
L159	1	858976.6876	3076769.462	40	54.641824	27.767519	18,385,700	5	5	684,533	995.3049	1526.19	-0.004047	SE	34.51	41	75	0	25	0	252.37766	6800.696	12859.48	25753.914	4421.8342	ES	b	s
L160	1	538064.1268	3203578.368	39	51.390649	28.959653	24,015,200	5	5	816,933	610.0241	923.985	-0.154626	SW	18.61	25	0	70	0	30	5962.6357	9751.096	9144.818	45415.464	492.2489	RS	b	s
L161	1	594744.8513	3117544.244	39	51.965198	28.180227	17,889,600	5	5	680,245	403.8518	1048.68	-0.037753	SW	21.89	11	50	50	0	0	2806.9058	11136.83	9819.75	7222.2759	2824.8917	S	b	d
L162	1	538254.1886	3205245.308	39	51.392656	28.974692	515,780	5	5	72,130	784.92	889.292	0.005631	NE	10.48	36	0	70	0	30	6697.8678	10030.91	9531.839	44055.374	899.57727	S	b	s
L163	1	542546.6174	3200763.835	39	51.436545	28.934108	58,144,900	5	5	797,578	487.8699	841.22	-0.075735	SE	17.52	22	0	20	80	0	8774.2387	14075.03	13260.64	50103.694	355.80438	RS	b	s
L164	1	593631.6929	3118423.944	39	51.953929	28.188246	11,411,100	5	5	626,206	310.6255	1046.31	0.13946	SW	22.08	10	50	50	0	0	2151.5903	10239.13	8409.806	7303.5287	3161.7986	S	b	d

		Location						Volume measurements error																			
		UTM coordinate			Geographic coordinate																					
Name	Region [a]	Long (E°)	Lat (N°)	Zone	Long (E°)	Lat (N°)	Volume (m^3)	Negative error (%)	Positive error (%)	Area (m^2)	ME-Elevevation (m)	ME-Relief (m)	ME-Curvature	Aspect	ME-Slope (Degree)	Pre-Slope (Degree)	Carbonate %	Fine clastic %	Evaporite %	Coarse clastic %	Dis-Fold (m)	Dis-fault (m)	Dis-B-Fault (m)	Dis-River (m)	Dis-Drainage (m)	Slide type [b]	Constructed surface [c]	Position [d]
L165	1	543009.6896	3199799.513	39	51.441259	28.925389	1,371,670	5	5	159,419	453.8333	831.068	0.084594	NE	8.507	27	0	0	100	0	8185.5883	14485.51	13605.7	51167.681	505.5198	RS	b	s
L166	1	549378.6014	3175258.99	39	51.505528	28.703659	15,819,000	5	5	589,425	1077.025	1798.1	-0.035292	NE	20.05	28	50	50	0	0	2122.6386	6424.624	9698.534	29177.435	2133.3131	ES	b	s
L167	1	565169.853	3184414.432	39	51.667714	28.785593	268,053	5	5	55,036	768.0789	985.486	0.021924	NE	26.18	25	80	20	0	0	5217.0787	6039.04	3938.455	39615.807	556.3187	DS	b	s
L168	1	584403.6848	3146424.358	39	51.861958	28.441597	2,886,180	5	5	226,362	732.9127	1036.23	0.010695	SW	21.78	21	85	15	0	0	1690.1161	7042.728	2508.386	16485.227	310.46435	ES	b	s
L169	1	583852.9649	3147204.097	39	51.856391	28.44867	5,863,820	5	5	310,930	651.2696	1048.88	0.005703	SW	12.71	21	85	15	0	0	1859.6487	7056.731	3017.567	16386.289	181.19584	ES	b	s
L170	1	592590.2806	3138933.983	39	51.944953	28.373437	2,659,160	5	5	189,031	818.9536	1070.51	0.051952	NE	13.82	17	85	15	0	0	769.91939	7516.115	2478.769	11522.247	1082.6362	RS	b	s
L171	1	594183.0798	3136996.945	39	51.96105	28.355841	14,187,600	5	5	393,909	1037.271	1109.48	0.023437	NE	15.12	17	85	15	0	0	136.16143	6874.517	4693.622	10170.682	1316.3412	ES	b	s
L172	1	593395.7416	3137502.569	39	51.953057	28.360461	13,356,200	5	5	525,829	1054.501	1090.44	-0.02273	NE	20.92	17	85	15	0	0	83.544534	6824.921	3999.773	10362.909	1643.3574	ES	b	s
L173	1	595352.7326	3137015.144	39	51.972985	28.355921	1,574,870	5	5	92,569	874.3603	1073.71	-0.012243	NE	17.5	23	85	15	0	0	837.27612	7572.601	4972.847	10617.755	640.39817	RS	b	s
L174	1	596181.032	3136594.466	39	51.981401	28.352063	493,106	5	5	44,629	813.75	1100.49	-0.027458	NE	29.55	23	85	15	0	0	982.71168	7715.07	4475.437	10531.171	1302.8992	RS	b	s
L175	1	514637.6847	3174546.578	39	51.14985	28.69809	487,147	5	5	85,392	152.9194	418.081	-0.003414	W	17.91	22	0	70	0	30	973.91414	5202.878	17751.69	34861.536	235.57103	RS	b	s
L176	1	518526.5429	3149379.423	39	51.189255	28.470869	18,879	5	5	2,700	436	782.75	-0.003574	SW	20.07	23	0	100	0	0	884.06681	4447.859	14259.29	9417.9223	720.5128	DS	b	s
L177	1	527502.229	3135069.925	39	51.280603	28.341544	1,865,480	5	5	108,326	407.6757	749.546	-0.145775	NE	25.96	27	0	0	100	0	409.52651	2386.397	4316.892	7799.1233	152.56294	RS	b	s
L178	1	519971.553	3145978.254	39	51.203957	28.440147	184,006	5	5	17,029	443.6667	767	0.095353	SW	21.08	16	0	0	100	0	861.23559	1513.615	12582.86	5807.54	59.226202	ES	b	s
L179	1	513198.1789	3164626.916	39	51.134999	28.608567	90,432	5	5	23,726	234.2778	696.5	0.013002	NW	18.01	26	0	85	0	15	1939.33	529.1888	19516.43	25538.4	223.02012	ES	b	d
L180	1	520484.4574	3143110.687	39	51.209144	28.414254	9,561,400	5	5	316,195	361.9035	751.87	0.109908	SW	8.6	18	0	0	100	0	1492.9143	842.9619	11873.16	2901.7265	236.68504	RS	b	s
L181	1	514303.5349	3148298.463	39	51.146102	28.461165	36,547	5	5	11,012	50.75	716	0.024731	SW	19.06	6	0	70	0	30	5197.4919	5662.521	18397.57	10310.902	67.971297	ES	b	d
L182	1	521868.9161	3138498.564	39	51.223192	28.3726	5,306,160	5	5	239,522	302.5142	767	0.001921	SW	7.116	18	0	0	100	0	2633.3813	172.0988	10173.52	1646.7032	123.28779	RS	b	s
L183	1	512842.7095	3163517.375	39	51.131351	28.598555	1,374,210	5	5	174,840	300.1953	712.25	0.031753	SW	13.93	14	0	70	0	30	2353.2252	706.8497	19908.17	24591.458	207.75631	ES	b	s
L184	1	513709.404	3182209.055	39	51.14044	28.767264	717,273	5	5	79,313	198.8167	358	-0.108005	NW	14.7	22	0	70	0	30	730.99443	869.124	17748.13	42570.67	455.19307	ES	b	s
L185	1	524262.5264	3134616.741	39	51.247539	28.337517	185,681	5	10	31,858	358.4167	767	-0.058932	SW	22.64	19	0	0	100	0	2596.4716	841.2098	7517.567	6128.8993	251.33152	ES	b	s
L186	1	525362.5225	3135003.239	39	51.25877	28.340985	719,797	5	10	62,587	413.6667	767	-0.241657	SW	17.16	8	0	0	100	0	1455.3375	311.1729	6446.886	6374.1601	59.782388	ES	b	s
L187	1	524133.2379	3135862.768	39	51.246246	28.348767	3,246,490	5	5	124,174	467.75	767	-0.097005	SW	12.26	9	0	0	100	0	2061.6814	784.8853	7732.591	4972.9812	153.2469	ES	b	s
L188	1	522479.7368	3137019.762	39	51.229397	28.359241	428,529	5	5	93,829	303.4412	746.545	-0.085226	SW	22.04	12	0	0	100	0	2876.831	722.0483	9462.04	3230.5227	371.66218	ES	b	s
L189	1	521593.4935	3140204.625	39	51.220413	28.388004	712,269	5	5	50,624	430.75	767	-0.0523	SW	14.12	10	0	0	100	0	1985.3195	47.60379	10566.1	97.670019	122.3922	ES	b	s
L190	1	520918.9877	3140306.503	39	51.21353	28.388935	610,186	5	5	90,599	319.8281	767	0.141379	SW	16.63	11	0	0	100	0	2509.5293	615.3455	11246.03	154.90857	151.30899	ES	b	s
L191	1	514243.7989	3177113.868	39	51.14585	28.721268	5,263,620	5	5	261,255	200.0368	358.187	-0.030695	SW	15.97	11	0	70	0	30	1135.8709	2648.695	17893.38	37458.24	304.57961	RS	b	s
L192	1	514702.4659	3177646.075	39	51.150554	28.726066	380,450	5	5	60,278	231.7632	358	-0.004297	SW	14.34	19	0	70	0	30	587.74259	2426.626	17368.26	37907.211	554.53981	RS	b	s
L193	1	514235.9172	3181600.9	39	51.145826	28.761769	104,551	5	5	29,607	230.9318	358	-0.02631	SW	13.3	18	0	70	0	30	324.36975	68.61552	17306.82	41886.333	163.4626	S	b	s

		Location					Volume measurements error																			
		UTM coordinate			Geographic coordinate																					
Name	Region [a]	Long (E°)	Lat (N°)	Zone	Long (E°)	Lat (N°)	Volume (m^3)	Negative error (%)	Positive error (%)	Area (m^2)	ME-Elevevation (m)	ME-Relief (m)	ME-Curvature	Aspect	ME-Slope (Degree)	Pre-Slope (Degree)	Carbonate %	Fine clastic %	Evaporite %	Coarse clastic %	Dis-Fold (m)	Dis-fault (m)	Dis-B-Fault (m)	Dis-River (m)	Dis-Drainage (m)	Slide type [b]	Constructed surface [c]	Position [d]
L194	1	527762.365	3137969.216	39	51.283327	28.36771	1,401,000	5	5	116,894	283.0427	754.554	-0.044925	NE	23.44	13	0	100	0	0	2133.7479	3127.004	4257.586	6568.0996	49.443232	DS	b	s
L195	1	517150.6592	3176034.453	39	51.175599	28.711489	122,062	5	10	19,766	233.8214	346	0.062665	NE	13.37	18	0	70	0	30	1525.0455	5291.524	15155.12	35993.088	61.213638	S	b	s
L196	1	520628.8628	3140023.437	39	51.210563	28.386384	388,822	5	10	50,638	260.6447	767	-0.050879	SW	20.79	15	0	0	100	0	2904.3199	929.2139	11515.91	209.53681	42.36538	ES	b	s
L197	1	517261.958	3150776.489	39	51.176357	28.483498	371,206	5	5	29,507	281.6042	789	-0.024928	SW	14.19	20	0	100	0	0	1512.6572	6048.505	15617.33	11106.947	717.83174	S	b	s
L198	1	513393.5188	3153958.971	39	51.136872	28.51227	1,472,690	5	5	66,600	203.0595	789	0.047176	SW	17.34	10	0	70	0	30	4194.1855	10262.11	19671.79	15566.759	587.57861	RS	b	s
L199	1	513740.5663	3164247.068	39	51.140542	28.605132	4,348,500	5	5	187,763	342.9301	697.129	-0.167929	SW	17.19	23	0	85	0	15	1379.4667	1098.466	18986.81	25019.162	199.62045	ES	b	s
L200	1	513626.3059	3164787.421	39	51.13938	28.610011	6,782,880	5	5	337,110	309.5887	696.5	-0.027217	SW	10.57	23	0	70	0	30	1519.3335	944.1125	19083.26	25569.993	597.87639	ES	b	s
L201	1	529392.5946	3141136.061	39	51.300044	28.39626	13,182	5	5	9,196	120.625	735.25	-0.029809	NE	12.97	15	0	70	0	30	5168.5398	6267.616	2849.933	7904.1561	199.48646	ES	b	s
L202	1	536560.1511	3125806.282	39	51.372728	28.257702	4,615,490	5	5	221,109	290.6719	496	-0.096227	NE	16.19	24	0	70	0	30	1906.3933	9016.557	2041.088	7758.3332	284.46356	S	b	d
L203	1	531784.3897	3135006.403	39	51.324291	28.340874	3,249,640	5	5	124,533	139.7	656.602	0.040952	NE	10.52	14	0	70	0	30	4039.6216	6245.917	40.56722	9902.8016	127.36217	DS	b	s
L204	1	527307.9701	3141066.239	39	51.278762	28.395675	3,046,220	5	5	172,710	389.6089	753.702	0.008328	NE	18.65	19	0	85	0	15	3349.1692	4911.867	4924.76	5831.4112	254.99598	DS	b	s
L205	1	529785.0905	3137527.851	39	51.303958	28.363681	372,978	5	5	33,116	252.8269	735.25	0.014856	NE	17.07	8	0	70	0	30	3635.3978	4978.587	2209.211	8627.4706	96.479624	ES	b	s
L206	1	528520.2702	3140144.931	39	51.291115	28.387333	1,971,990	5	5	88,584	235.3083	756	-0.025249	NE	13.62	21	0	70	0	30	3908.986	4953.595	3651.733	6965.6686	289.31262	ES	b	s
L207	1	525160.275	3139215.727	39	51.256798	28.379014	2,242,540	5	5	114,725	477.2313	766.866	-0.209963	NE	25.08	13	0	0	100	0	553.53291	2425.964	6939.542	3716.0618	305.21171	ES	b	s
L208	1	525488.135	3138995.112	39	51.26014	28.377016	771,431	5	5	62,151	460.0938	752.63	0.071916	NE	18.73	22	0	0	100	0	719.71883	2275.321	6597.23	4089.7844	240.68944	ES	b	s
L209	1	523661.2425	3142133.656	39	51.241558	28.405381	1,466,310	5	5	95,442	437.4572	763.785	-0.013734	NE	22.06	21	0	0	100	0	782.60008	2276.809	8636.492	2917.6398	214.71802	ES	b	s
L210	1	517542.5596	3174327.104	39	51.179585	28.696073	1,056,970	5	5	82,193	175.2308	344.016	-0.201886	NE	23.2	15	0	70	0	30	1938.1172	6793.921	14855.6	34256.08	1603.0451	S	b	s
L211	1	518552.3889	3158292.984	39	51.189662	28.551328	209,202	5	5	54,302	456.0789	759.711	0.000015	NE	16.23	27	0	70	0	30	1879.6232	8356.209	14373.27	18203.47	429.75277	S	b	s
L212	1	516498.7158	3157829.003	39	51.168661	28.547168	1,108,870	5	5	77,649	573.2241	783.774	0.090252	NE	25.85	23	0	85	0	15	224.93422	7445.075	16441.08	18107.419	1819.4181	ES	b	s
L213	1	527530.0122	3142615.518	39	51.281066	28.409655	638,088	5	5	56,289	189.9375	755.013	0.061399	NE	18.48	5	0	70	0	30	4341.561	5982.958	4810.233	6477.4481	988.72477	DS	b	d
L214	1	515654.8871	3163204.515	39	51.160108	28.5957	2,613,140	5	5	114,245	533.2866	765.89	0.002991	NE	14.8	8	0	70	0	30	293.07635	3177.589	17107.79	23535.743	213.25011	ES	b	s
L215	1	516182.9924	3163448.426	39	51.165513	28.597895	373,650	5	5	24,869	413.4167	751.639	0.130011	NE	15.18	20	0	70	0	30	865.21929	3625.318	16571.95	23667.409	27.847855	ES	b	s
L216	1	516678.5783	3164034.214	39	51.17059	28.603177	41,198	5	5	12,267	407.8333	697.042	0.040244	NE	17.05	18	0	70	0	30	1490.7913	4044.169	16057.39	24155.06	79.353024	ES	b	s
L217	1	516219.121	3164079.685	39	51.165891	28.603593	540,430	5	5	70,840	461.42	699.667	0.041279	NE	14.52	18	0	70	0	30	1057.0328	3582.598	16515.1	24280.619	312.8567	ES	b	s
L218	1	516210.7042	3165353.182	39	51.165823	28.615088	347,760	5	5	52,253	374.0132	681.309	0.000533	NE	12.75	6	0	70	0	30	1035.1857	2972.959	16481.66	25534.733	173.6507	ES	b	s
L219	1	516515.6492	3165770.308	39	51.168949	28.618849	447,535	5	5	46,297	347.7969	678.344	0.095391	NE	10.48	9	0	70	0	30	1319.9175	3061.598	16163.17	25894.33	316.96003	ES	b	s
L220	1	515945.651	3167364.813	39	51.16314	28.633249	1,039,650	5	5	76,825	342.5096	655.828	0.01806	NE	9.386	12	0	70	0	30	674.62273	2327.395	16680.46	27561.759	136.20373	S	b	s
L221	1	516283.229	3167449.289	39	51.166595	28.634008	331,462	5	5	47,349	317.6471	647.776	0.019635	NE	16.87	12	0	70	0	30	1007.7942	2675.134	16340.29	27588.822	131.39634	S	b	s
L222	1	516602.3673	3167588.237	39	51.169862	28.635258	48,359	5	5	14,132	264.75	616.45	0.174321	NE	15.86	12	0	70	0	30	1319.9525	3017.02	16016.75	27676.846	33.351745	S	b	s

		Location						Volume measurements error																			
		UTM coordinate			Geographic coordinate																					
Name	Region [a]	Long (E°)	Lat (N°)	Zone	Long (E°)	Lat (N°)	Volume (m^3)	Negative error (%)	Positive error (%)	Area (m^2)	ME-Elevevation (m)	ME-Relief (m)	ME-Curvature	Aspect	ME-Slope (Degree)	Pre-Slope (Degree)	Carbonate %	Fine clastic %	Evaporite %	Coarse clastic %	Dis-Fold (m)	Dis-fault (m)	Dis-B-Fault (m)	Dis-River (m)	Dis-Drainage (m)	Slide type [b]	Constructed surface [c]	Position [d]
L223	1	516311.7799	3167637.662	39	51.16689	28.635708	203,544	5	5	28,339	310.6389	639.111	0.113859	NE	13.27	19	0	70	0	30	1027.3408	2748.106	16305.56	27770.239	46.891492	ES	b	s
L224	1	515447.3175	3161486.768	39	51.157962	28.580197	255,544	5	5	42,074	582.0893	787	-0.071307	NE	16.65	20	0	70	0	30	334.70989	3902.957	17371.7	21910.067	1053.7404	S	b	s
L225	1	525944.6974	3144686.077	39	51.264927	28.428378	83,769	5	5	18,203	336.2	751.5	0.085751	SW	28.75	14	0	70	0	30	4057.923	4277.589	6534.745	6337.7507	143.10358	DS	b	s
L226	1	524343.5164	3148336.54	39	51.248655	28.46136	1,502,890	5	5	93,267	314.0682	697	-0.01008	NE	11.7	14	0	70	0	30	4081.8408	5041.864	8384.184	8681.6671	499.16993	ES	b	s
L227	1	525929.6234	3144837.102	39	51.264777	28.429741	183,019	5	5	28,725	313.825	751.5	0.004796	SW	15.27	14	0	70	0	30	4123.2528	4288.44	6560.212	6437.2717	33.741608	DS	b	s
L228	1	527411.9752	3143712.76	39	51.279887	28.419562	527,096	5	5	88,890	133.6129	754.545	0.011318	NE	17.59	10	0	70	0	30	4808.9118	5703.643	5003.757	6874.0032	119.64605	ES	b	s
L229	1	588910.6292	3105842.538	39	51.904881	28.075013	40,075,000	5	5	766,133	708.1299	1061.83	-0.090191	SW	14.71	38	50	30	20	0	1984.7913	5417.703	1041.721	18700.854	1359.9345	S	b	s
L230	1	589993.429	3102303.992	39	51.915629	28.043001	11,409,300	5	5	444,582	529.0767	1045.3	-0.039842	SW	17.1	5	85	15	0	0	573.85164	3391.361	1606.846	20790.971	826.04485	S	b	s
L231	1	856193.2565	3060431.847	40	54.608782	27.621062	9,028,650	5	5	396,751	1192.748	1366.7	0.046098	SE	17.84	16	0	100	0	0	249.20574	9483.24	3117.94	10347.886	1959.2133	S	b	s
L232	1	824080.172	3052771.824	40	54.281824	27.560104	27,973,500	5	5	903,509	1088	1263.12	0.114131	S	16.98	42	70	0	30	0	2138.0309	703.1776	8627.932	5129.8574	653.89446	S	b	s
L233	1	876170.0815	3038105.487	40	54.803888	27.414539	91,222,000	5	5	1,557,090	941.313	1188.46	0.028553	SW	20.27	22	0	20	80	0	1625.222	9586.074	13498.15	31062.786	2864.1649	S	b	s
L234	1	872630.7561	3040520.425	40	54.768901	27.437265	349,157	5	5	52,328	1083.294	1201.12	0.02053	S	16.76	28	0	20	80	0	94.456383	5857.703	10321.63	26801.319	197.61733	ES	b	s
L235	1	866087.009	3044829.023	40	54.704127	27.477855	2,954,650	5	5	155,620	1244.116	1235.95	0.026519	NW	18.58	40	100	0	0	0	1184.2151	4993.249	4427.328	19017.115	1672.5295	S	b	s
L236	1	866092.9365	3045169.161	40	54.70429	27.480918	1,349,240	5	5	95,485	1177.044	1257.31	0.00446	NW	18.12	29	100	0	0	0	1524.307	4910.495	4479.633	18877.919	1341.7959	S	b	s
L237	1	844298.2398	3017346.675	40	54.476254	27.235891	11,883,500	5	5	325,691	706.553	1776.21	0.059209	N	11.1	39	50	0	50	0	2070.0409	3351.467	3949.66	16536.346	506.91092	S	b	s
L238	1	847182.8709	3014934.469	40	54.504654	27.213428	4,447,870	5	5	257,438	1046.145	1775.17	0.023084	NE	14.86	17	40	60	0	0	3047.1743	4524.524	3852.666	14518.724	271.34128	S	b	s
L239	1	796892.2477	3016624.058	0	53.99801	27.240439	44,918,900	5	5	577,040	1016.297	1437.01	-0.005635	S	14.01	51	100	0	0	0	1207.0258	8476.869	7433.741	17025.694	409.76944	ES	b	s
L240	1	738980.9475	3078726.006	39	53.425969	27.811888	231,955	5	5	28,318	731.7955	744.955	0.109946	SW	29.94	32	100	0	0	0	2326.2535	568.5541	2615.277	24372.169	1133.5692	DS	b	s
L241	1	739368.8887	3081856.534	39	53.430533	27.840054	2,664,240	5	5	175,155	878.2462	717.563	0.009148	NE	16.31	34	100	0	0	0	647.29473	1701.536	1646.574	27302.289	1930.1812	ES	b	s
L242	1	745368.9227	3078768.839	39	53.490775	27.81112	435,071	5	10	55,884	965.3696	723.821	0.05389	NE	22.44	25	100	0	0	0	595.58054	3877.225	6121.375	25590.381	1452.5542	RS	b	s
L243	1	746084.8549	3078548.31	39	53.497991	27.809	621,237	5	5	87,398	916.7419	720.175	-0.077591	NE	24.52	31	100	0	0	0	725.55348	3805.752	6144.413	25203.695	1313.699	DS	b	s
L244	1	763682.792	3090651.012	39	53.679157	27.914791	2,872,670	5	5	159,554	1090.129	1010	-0.01236	SW	20.86	31	100	0	0	0	3710.8956	7157.678	10014.14	38383.965	1590.6481	DS	b	s
L245	1	750737.2045	3095770.317	39	53.548816	27.963454	2,814,750	5	5	191,232	1170.558	1089.54	-0.049203	SW	25.76	33	60	0	40	0	5344.25	576.7901	5580.059	41762.406	1940.8467	S	b	s
L246	1	752430.3936	3093269.083	39	53.56548	27.940578	6,852,110	5	5	212,208	864.6058	1089.87	0.025533	SW	23.18	33	100	0	0	0	6516.1369	13.9117	8412.827	39248.671	357.39353	ES	b	s
L247	1	749570.0164	3075731.709	39	53.532751	27.782953	1,291,390	5	5	103,073	922.9257	731.345	-0.044279	SW	13.04	5	100	0	0	0	266.56937	2438.486	7937.384	21832.089	910.34055	ES	b	s
L248	1	729907.5992	3034957.2	39	53.325567	27.418667	78,516,600	5	5	2,173,110	752.805	654.367	0.001152	SW	16.47	6	80	20	0	0	1696.0415	10773.08	5090.989	4040.0857	863.04371	ES	b	s
L249	1	732964.8072	3032093.204	39	53.355922	27.392313	332,778,000	5	5	4,185,770	629.3189	656.136	-0.013334	SW	11.37	5	80	20	0	0	645.11779	14852.53	2452.675	4599.7466	853.65901	ES	b	s
L250	1	737967.835	3029732.678	39	53.40602	27.370157	35,063,600	5	5	746,662	701.3649	708.472	-0.029832	SW	12.68	20	80	20	0	0	967.73632	19871.67	455.5282	5489.1965	507.43912	ES	b	s
L251	1	737109.2798	3028753.687	39	53.397155	27.361476	18,570,700	5	5	554,954	573.0535	703.037	-0.0681	SW	16.33	20	80	20	0	0	302.79533	20033.37	582.2861	4257.7177	348.91719	ES	b	s

		Location						Volume measurements error																			
		UTM coordinate			Geographic coordinate																					
Name	Region [a]	Long (E°)	Lat (N°)	Zone	Long (E°)	Lat (N°)	Volume (m^3)	Negative error (%)	Positive error (%)	Area (m^2)	ME-Elevevation (m)	ME-Relief (m)	ME-Curvature	Aspect	ME-Slope (Degree)	Pre-Slope (Degree)	Carbonate %	Fine clastic %	Evaporite %	Coarse clastic %	Dis-Fold (m)	Dis-fault (m)	Dis-B-Fault (m)	Dis-River (m)	Dis-Drainage (m)	Slide type [b]	Constructed surface [c]	Position [d]
L252	1	784834.9767	2991498.395	39	53.870587	27.016433	13,604,700	5	5	356,453	710.7614	969.727	-0.020467	NE	17.53	6	100	0	0	0	980.05178	7635.581	4537.622	9035.6509	1190.5549	ES	b	d
L253	1	755579.3704	3009844.301	39	53.579794	27.187602	59,036,600	5	5	1,001,430	852.8811	1081.52	-0.087902	NE	16.22	14	70	30	0	0	1609.9134	782.3992	17647.84	7465.8027	1402.008	ES	b	s
L254	1	756756.2146	3009242.464	39	53.591538	27.181955	33,209,300	5	5	1,119,310	771.1407	1082.16	-0.000949	NE	17.34	15	70	30	0	0	1265.3764	382.1663	18120.22	7871.7982	429.07322	ES	b	s
L255	1	760265.63	3008029.76	39	53.626674	27.170358	22,548,000	5	5	1,010,750	752.7799	876.233	-0.032833	NE	14.4	15	85	15	0	0	1563.9629	493.4073	19108.86	8571.1751	1675.2599	ES	b	s
L256	1	772882.4588	3002749.399	39	53.752722	27.120299	475,691,000	5	5	5,998,440	804.3535	1083.63	-0.03904	NE	13.84	14	60	40	0	0	4703.2819	1899.25	20120.41	7404.809	1157.2058	ES	b	s
L257	1	747444.2405	2987242.139	39	53.493223	26.985219	4,987,340	5	5	183,441	143.7386	1080.75	0.038505	S	14.72	17	0	100	0	0	3402.6191	5628.043	37308.03	31392.203	1131.5831	ES	b	s
L258	1	787453.6902	2987562.851	39	53.896042	26.980406	21,598,600	5	5	874,445	802.6057	1045.76	0.064914	SW	21.55	22	50	0	50	0	1621.4825	5426.764	503.3008	9771.7692	382.41186	S	b	s
L259	1	779385.5199	2965721.686	39	53.809958	26.785093	1,509,650	5	5	136,838	495.8469	733.653	-0.00219	NE	17.34	5	0	100	0	0	2374.9039	5989.969	317.9456	32282.242	498.79633	S	b	s
L260	1	777948.2416	2966162.105	39	53.795613	26.78935	9,228,570	5	5	364,385	452.5515	729.783	-0.004672	NW	12.83	6	0	100	0	0	2436.1417	6461.557	1180.45	32607.74	340.68412	S	b	s
L261	1	745822.1501	2988098.51	39	53.477061	26.993232	54,614,500	5	5	1,169,960	310.969	1075.97	-0.047757	S	16.43	16	0	100	0	0	2413.3041	6130.036	39131.6	30900.735	1063.9063	RS	b	s
L262	1	754963.2075	2987503.306	39	53.568976	26.986214	2,756,490	5	5	236,189	533.4265	1076.38	0.00622	SW	21.67	10	0	100	0	0	1204.0885	7440.213	30415.23	29444.919	1777.8745	S	b	s
L263	1	799193.8886	2971001.73	40	54.010227	26.828609	3,878,990	5	5	146,462	262.4279	681.915	-0.000939	E	12.29	25	0	100	0	0	3045.5256	7551.344	14225.03	21342.041	128.44089	S	b	s
L264	1	797266.0556	2970126.149	40	53.990645	26.821125	348,720	5	5	56,171	410.5595	717.75	0.056817	N	23.75	28	0	100	0	0	2240.5797	8631.924	15246.05	22409.958	1499.2373	S	b	d
L265	1	798744.0882	2970200.127	40	54.005516	26.821477	11,617,900	5	5	311,505	388.0876	708.273	0.005247	E	13.76	25	0	100	0	0	2260.7971	8397.216	15038.73	22172.799	21.901037	S	b	s
L266	1	801739.8311	2964873.603	40	54.034341	26.77281	148,986	5	10	35,551	351.3409	798.125	0.043257	S	26.61	20	0	100	0	0	2589.2976	4009.708	19289.94	27415.119	4203.023	S	b	s
L267	1	801144.2585	2964668.878	40	54.02831	26.771092	282,886	5	10	37,760	326.3077	749.833	0.050285	S	23.65	16	0	100	0	0	2993.0832	3695.942	19728.81	27644.626	4574.8019	S	b	s
L268	1	805138.2325	2963098.998	40	54.068047	26.756074	1,603,980	5	5	170,455	346.0151	798.5	0.005926	SW	25.62	26	0	100	0	0	3034.2722	2910.515	15456.4	29028.211	5239.2252	S	b	s
L269	1	807307.1145	2962284.052	40	54.08963	26.748253	789,342	5	10	44,650	311.6912	798.5	0.042669	SE	21.92	29	0	0	100	0	3021.5531	2520.878	13153.28	29936.566	5400.8069	S	b	s
L270	1	808695.8269	2963049.285	40	54.103763	26.754848	215,976	5	5	32,491	408.8958	798.5	0.019841	SW	25.97	32	0	0	100	0	1811.1196	3535.162	12259.98	29319.4	4274.3265	S	b	s
L271	1	805838.6133	2962619.793	40	54.074964	26.751601	1,282,940	5	5	159,919	382.2458	798.5	-0.018144	SW	30.39	15	0	100	0	0	3231.9798	2572.559	14615.08	29520.534	5382.0708	S	b	s
L272	1	821724.7294	2978993.676	40	54.238685	26.895648	356,453	5	10	50,711	651.8421	1193.75	0.011721	SE	20.44	18	0	0	100	0	3445.8614	2215.903	7838.308	14561.459	720.74887	S	b	s
L273	1	824794.5153	2979542.974	40	54.269689	26.899888	1,646,150	5	5	223,914	638.9344	1193.65	0.033697	SE	19.51	12	0	0	100	0	2976.2892	2241.328	5347.677	14741.571	1370.8849	S	b	s
L274	1	830814.8876	2981873.776	40	54.330832	26.919481	4,025,930	5	5	224,865	658.3494	1382.19	0.035803	S	15.93	18	0	0	100	0	803.16407	2447.621	1029.362	14580.365	1695.3111	S	b	s
L275	1	830730.9688	2981361.597	40	54.329852	26.914884	5,396,730	5	5	258,485	576.5335	1383.76	-0.018301	SW	19.22	23	0	0	100	0	1312.9825	2165.98	872.8744	15095.017	1445.4396	S	b	s
L276	1	831821.5776	2981606.613	40	54.340883	26.916834	2,850,790	5	5	194,617	706.8007	1376.9	0.055364	SW	21.56	31	0	0	100	0	1096.4702	1667.041	10.54808	14851.422	2538.5283	S	b	s
L277	1	830174.8972	2982802.199	40	54.324642	26.928001	6,137,740	5	5	307,852	632.7117	1354.91	0.048893	SW	20.94	27	0	0	100	0	141.62171	3567.763	2019.717	13688.174	1681.53	S	b	s
L278	1	830400.8945	2983424.826	40	54.327079	26.933559	606,160	5	10	75,580	797.875	1371.88	-0.053432	W	18.19	31	0	0	100	0	758.14717	3622.092	2099.337	13050.791	2293.4729	S	b	s

		Location						Volume measurements error																			
		UTM coordinate			Geographic coordinate																					
Name	Region [a]	Long (E°)	Lat (N°)	Zone	Long (E°)	Lat (N°)	Volume (m^3)	Negative error (%)	Positive error (%)	Area (m^2)	ME-Elevevation (m)	ME-Relief (m)	ME-Curvature	Aspect	ME-Slope (Degree)	Pre-Slope (Degree)	Carbonate %	Fine clastic %	Evaporite %	Coarse clastic %	Dis-Fold (m)	Dis-fault (m)	Dis-B-Fault (m)	Dis-River (m)	Dis-Drainage (m)	Slide type [b]	Constructed surface [c]	Position [d]
L279	1	830330.9097	2983892.801	40	54.3265	26.937794	1,830,970	5	5	139,926	769.0931	1360.93	-0.024314	W	15.42	37	0	0	100	0	1227.7874	3148.952	2373.165	12588.832	2576.2688	S	b	s
L280	1	829774.6446	2982249.156	40	54.320471	26.923111	1,872,810	5	5	112,767	486.3214	1340.36	-0.039487	SW	21.75	34	0	0	100	0	400.80408	3465.799	2126.993	14162.804	1004.5043	S	b	s
L281	1	833725.8677	2981726.77	40	54.360061	26.917462	16,232,600	5	5	664,108	713.5184	1372.79	0.01311	SW	15.25	28	0	0	100	0	960.11432	1849.879	1634.116	14925.871	4382.4121	RS	b	s
L282	1	892166.2056	2969246.073	40	54.943512	26.789826	5,009,340	5	5	201,644	493.1007	1037.93	-0.033167	SE	14.97	22	70	0	30	0	1990.4259	2521.827	5182.821	19393.361	3589.4302	S	b	s
L283	1	837177.055	2980416.424	40	54.394406	26.904821	17,379,800	5	5	546,049	458.7564	1352.36	-0.046423	S	23.44	21	0	0	100	0	2229.8655	403.3623	5305.04	17088.439	893.9112	RS	b	s
L284	1	836311.0605	2983032.977	40	54.386405	26.928613	37,291,200	5	5	1,089,700	1098.154	1355.53	-0.004895	S	18.03	20	0	0	100	0	376.34375	1036.098	3350.506	14334.202	3362.8139	RS	b	s
L285	1	841838.1569	2981317.384	40	54.441509	26.911805	3,191,640	5	5	229,542	739.5241	1331.8	-0.005598	S	16.95	11	0	0	100	0	931.69404	3637.043	7323.014	18322.223	2592.5933	S	b	s
L286	1	845252.4359	2980415.217	40	54.475583	26.902833	1,356,250	5	5	115,738	770.1488	1275.6	-0.016089	S	13.33	10	0	0	100	0	1417.2464	4643.008	7135.194	19107.891	666.94543	S	b	s
L287	1	849434.3993	2977759.848	40	54.516876	26.877862	2,515,300	5	5	110,856	657.7927	1345.2	-0.000609	S	16.56	33	70	0	30	0	3648.9124	3174.453	4364.882	21238.232	1509.81	S	b	s
L288	1	851294.2287	2982300.711	40	54.536842	26.918315	1,429,930,000	5	10	9,091,820	750.54	1257.75	0.039092	NE	14.54	11	100	0	0	0	1255.7161	1330.678	7015.995	16555.514	1998.7333	S	b	s
L289	1	852318.2622	2981196.525	40	54.546824	26.908106	4,819,010	5	5	258,412	667.9763	1258.66	-0.085472	E	11.93	8	100	0	0	0	610.2055	44.50523	7720.269	17328.643	2433.4913	S	t	s
L290	1	853858.9702	2979470.926	40	54.561822	26.892166	13,886,200	5	5	474,101	504.9292	1227.25	0.02609	E	13.3	8	100	0	0	0	196.9648	2176.944	5952.61	18717.782	2865.7205	S	b	s
L291	1	867575.5345	2977641.403	40	54.699124	26.872135	45,282,100	5	5	810,263	623.6364	1052.54	0.012337	NW	10.66	14	0	20	80	0	7288.2898	5886.243	3743.435	17653.534	1896.4128	S	b	s
L292	1	728323.0355	2991878.99	39	53.301543	27.030326	13,091,400	5	5	514,521	122.3178	513.5	0.009617	S	13.43	23	0	100	0	0	1268.0529	4137.073	29715.28	33260.372	2723.1544	RS	b	s
L293	1	891280.5633	2968928.355	40	54.934525	26.787212	9,377,770	5	5	302,720	410.683	1039.07	0.008316	S	18.83	22	0	0	100	0	2250.0885	2339.026	5482.31	20219.205	3147.4044	S	b	s
L294	1	892770.2262	2969179.999	40	54.949554	26.789061	1,681,780	5	5	104,731	370.9551	1038.73	-0.084748	S	18.26	22	0	0	100	0	2127.3457	2366.866	5261.269	19053.735	3247.0959	S	b	s
L295	1	891031.7982	2975433.681	40	54.934054	26.845878	2,738,150	5	5	162,974	862.0792	882.642	0.000678	NE	21.4	12	70	0	30	0	4257.6856	3631.702	1026.75	14934.02	2597.6394	RS	b	s
L296	1	891608.7113	2976153.828	40	54.940072	26.852203	782,399	5	5	91,303	649.853	886.765	0.006531	NE	14.08	16	0	0	100	0	4938.9357	4296.78	1734.914	14028.743	2064.9568	RS	b	s
L297	1	892240.1762	2977020.047	40	54.946684	26.859828	26,367,200	5	5	581,539	486.4123	898.68	-0.001395	NE	15.34	15	100	0	0	0	5676.8429	5143.232	2588	12970.805	1341.8527	RS	b	s
L298	1	895060.7447	2975903.636	40	54.974657	26.848978	4,114,690	5	5	289,269	703.0324	938.357	-0.000738	NE	20.79	7	100	0	0	0	4082.4158	3318.475	1413.981	12594.261	2366.2806	RS	b	s
L299	1	895820.1139	2975663.428	40	54.982207	26.846599	10,426,600	5	5	565,625	750.5229	945.893	-0.025158	NE	10.94	7	100	0	0	0	3720.636	2608.455	1158.25	12238.355	2906.803	RS	b	s
L300	1	899797.2886	2976272.774	40	55.022335	26.850955	118,512,000	5	10	1,826,330	384.5848	903.166	-0.015366	NE	10.12	20	0	20	80	0	4590.1218	2821.714	1692.97	9157.3709	2595.2029	RS	t	s
L301	1	916635.0649	2976479.883	40	55.19145	26.847903	17,139,300	5	5	459,274	175.7831	840.558	-0.019509	N	16.77	21	0	20	80	0	3524.4861	8158.713	2213.751	3616.7234	3054.623	RS	b	d
L302	1	917987.7974	2976511.341	40	55.20504	26.847783	2,087,500	5	5	103,396	193.5833	843.412	-0.010634	N	15.63	32	0	20	80	0	3503.0221	6805.748	916.0744	3108.2502	1797.5774	S	b	d
L303	1	924559.4542	2975478.445	40	55.270655	26.836503	11,567,700	5	5	612,661	571.2709	860.641	-0.04842	SW	20.56	10	0	20	80	0	2268.276	243.9168	5697.466	5050.4714	354.13562	RS	b	s
L304	1	926218.8664	2974639.884	40	55.287025	26.828448	3,553,440	5	5	272,243	578.9257	861	-0.02715	SW	13.32	6	100	0	0	0	1745.1855	1279.029	7518.184	5804.1208	1018.5787	RS	b	s
L305	1	614045.3955	3126820.969	39	52.162695	28.262424	649,176	5	5	91,537	247.9265	884.227	-0.070437	NE	11.57	8	0	70	0	30	4313.3082	4408.197	7025.36	10089.375	116.00967	ES	b	s
L306	2	67912.66321	3726970.757	38	46.345075	33.594946	277,236,000	10	15	3,711,320	1343.491	958.41	-0.070032	NW	15.7	12	60	40	0	0	229.18413	1122.751	61915.38	717.7458	828.08696	S	b	s

		Location																								
		UTM coordinate			Geographic coordinate			Volume measurements error																		
Name	Region [a]	Long (E°)	Lat (N°)	Zone	Long (E°)	Lat (N°)	Volume (m^3)	Negative error (%)	Positive error (%)	Area (m^2)	ME-Elevation (m)	ME-Relief (m)	ME-Curvature	Aspect	ME-Slope (Degree)	Pre-Slope (Degree)	Carbonate %	Fine clastic %	Evaporite %	Coarse clastic %	Dis-Fold (m)	Dis-fault (m)	Dis-B-Fault (m)	Dis-River (m)	Dis-Drainage (m)	Slide type [b]	Constructed surface [c]	Position [d]
L307	1	624420.5684	3211312.561	39	52.277657	29.023953	7,611,580	5	5	306,755	1811.095	1405.42	-0.021867	NE	15.91	21	80	20	0	0	6504.7008	5407.966	8577.278	28122.155	1568.1389	DS	b	d
L308	1	632312.499	3212825.633	39	52.358859	29.036811	25,929,100	5	5	681,426	1893.638	997.861	-0.041316	NE	13.11	16	50	35	0	15	10505.17	4051.432	15753.42	27606.358	1068.3908	ES	b	d
L309	1	644406.5682	3169619.406	39	52.477514	28.64564	8,921,480	5	5	354,511	767.0504	1039.58	0.004032	SW	17.3	24	100	0	0	0	6835.9719	1956.549	4251.85	37328.909	56.832586	S	b	d
L310	1	645815.023	3169539.124	39	52.49191	28.644758	226,506	5	5	37,266	780.5577	1046.21	-0.040845	SW	10.75	27	100	0	0	0	6202.4317	2770.511	5417.985	37483.646	203.89505	S	b	s
L311	1	674000.5949	3161788.876	39	52.779008	28.571352	1,354,960,000	5	10	13,705,100	1470.52	1285.77	-0.084477	SW	19.17	14	95	5	0	0	1454.9656	9372.449	15744.67	33809.283	1069.4503	S	b	s
L312	1	599362.2427	3113218.309	39	52.011863	28.140843	359,532	5	5	57,216	721.9868	1001.41	-0.051297	NW	14.89	41	100	0	0	0	4183.0426	11798.32	11055.42	6647.6041	2018.8891	S	b	s
L313	1	758184.951	3350885.524	39	53.683539	30.262175	5,200,560	5	5	244,100	2694.217	1088.81	-0.044233	SW	11.13	20	100	0	0	0	8025.4624	1257.844	139890.2	147345.64	1548.784	S	b	s
L314	1	742390.8372	3360912.233	39	53.52183	30.35583	2,602,820	5	5	182,403	2699.981	1071.58	-0.020498	SW	28.37	35	100	0	0	0	9243.3907	2995.838	132109.6	148278.87	3489.4338	S	b	s
L315	1	697312.0725	3045250.232	39	52.997706	27.516645	1,984,620	5	5	159,220	456.2924	1390.5	0.012676	SW	18.41	19	100	0	0	0	3334.3554	9371.376	2854.843	880.95406	1167.3113	ES	b	d
L316	1	699013.9909	3017217.273	39	53.010348	27.263469	219,391,000	5	5	4,267,170	338.0993	1251.33	0.013354	SW	9.589	18	40	60	0	0	646.97983	2626.828	258.4092	21214.326	77.05684	RS	b	s
L317	1	685054.3497	3031701.692	39	52.871591	27.396121	8,635,790	5	5	279,145	540.315	1273.37	-0.024246	SW	12.63	17	40	60	0	0	835.18004	3731.543	13703.4	16547.248	2208.1878	S	b	s
L318	1	669336.8003	3040365.018	39	52.713896	27.476341	27,954,000	5	5	688,978	121.998	1298.36	-0.034185	SW	20.04	17	88	12	0	0	694.03897	1577.807	23083.41	19088.568	1822.3569	RS	t	s
L319	1	691739.7293	3074281.846	39	52.945947	27.779383	7,310,150	5	5	410,912	1183.169	1077.81	-0.053207	SW	19.9	8	70	0	30	0	395.84567	3656.978	34.26867	8680.1718	549.83345	S	b	s
L320	1	693827.9353	3072972.013	39	52.966917	27.767265	23,131,600	5	5	797,331	1018.156	993.287	-0.005379	SW	16.57	13	70	0	30	0	667.57245	5063.695	2499.151	8556.4845	1792.897	S	b	s
L321	2	326814.9617	3548101.171	39	49.165512	32.055877	5,176,080	5	10	175,848	180.0858	561.638	-0.030866	NE	16.21	17	0	20	0	80	3579.4587	3359.697	6547.444	15992.133	23.127754	ES	b	d
L322	2	319736.027	3701325.044	39	49.060854	33.436182	7,486,820,000	10	15	35,178,200	1824.022	1625.79	-0.064218	NW	9.645	10	10	0	0	90	25308.346	3418.956	67422.47	57964.88	1889.7924	S	b	s
L323	2	334033.1096	3672746.062	39	49.219828	33.180836	71,946,000	5	5	1,972,230	1748.236	1834.98	-0.010717	SW	17.88	16	5	5	0	90	7450.6739	8259.149	49265.18	33268.088	749.18786	DS	b	d
L324	2	79263.80653	3742002.676	38	46.459914	33.734636	422,538,000	5	5	6,173,900	1638.306	1491.79	-0.025044	NE	8.91	19	100	0	0	0	1493.8491	841.1845	74666.04	16142.276	1863.524	ES	b	s
L325	2	308983.4166	3715352.898	39	48.942257	33.560764	21,780,300	5	5	662,516	1723.35	1171.25	-0.00778	SW	18.34	14	70	0	0	30	35926.852	1560.787	78921.58	67514.754	1151.5091	S	b	s
L326	2	288477.4194	3707650.335	39	48.72332	33.487477	87,634,800	5	10	3,112,410	1982.541	848.812	0.004166	N	14.15	24	100	0	0	0	17590.837	7648.838	71439.14	47642.972	1073.5364	ES	b	s
L327	2	239510.2358	3701568.89	39	48.198534	33.421892	712,510	5	5	123,552	1219.978	862.574	-0.003836	NW	9.778	26	90	0	0	10	3017.239	3145.293	49862.53	3122.28	266.79314	DS	b	s
L328	2	235255.286	3696381.182	39	48.154347	33.374116	61,120,800	5	10	1,774,640	1461.803	916.368	0.009615	NE	13.59	7	100	0	0	0	4359.0897	642.136	43491	9785.7945	765.33942	DS	b	s
L329	2	272519.9953	3708422.935	39	48.551502	33.491166	1,106,600	5	5	114,986	1620.327	1092.67	-0.015007	NE	10.05	21	100	0	0	0	9640.013	1564.073	73974	31833.352	66.133771	DS	b	s
L330	2	296806.1052	3679063.812	39	48.819345	33.231433	7,787,370	5	5	232,153	1385.933	1412.9	0.030403	SW	16.46	18	0	0	0	100	1403.6022	85.29722	42154.34	29375.864	566.95272	DS	b	s
L331	2	304016.8096	3678128.225	39	48.896885	33.224332	536,678,000	20	30	2,665,070	1275.405	1739.75	0.036876	SW	21.98	26	50	0	0	50	215.40087	1690.494	41372.82	30640.353	730.84823	S	b	s
L332	2	304291.1817	3679563.724	39	48.899519	33.237321	67,052,000	5	5	1,193,950	1342.326	1699.6	0.005915	SW	30.44	24	50	0	0	50	176.96244	786.2257	42829.74	32095.162	716.11635	S	b	s
L333	2	183736.7823	3656979.718	38	47.615057	33.005415	32,061,100,000	5	5	104,000,000	1164.938	1840.45	0.041431	NE	21.22	11	80	20	0	0	4253.1878	5455.564	21117.85	3268.4518	827.82983	RS	t	s
L334	2	201543.2976	3684870.501	39	47.796253	33.261623	8,639,060	5	10	335,515	795.588	917.254	-0.002524	S	18.63	34	100	0	0	0	2138.8138	5208.939	8856.31	125.66569	368.9058	S	b	s
L335	2	484858.3894	3416860.902	39	50.841582	30.884936	1,441,240,000	5	5	10,978,400	2697.902	2478.82	-0.025608	SW	18.57	18	60	40	0	0	1071.5108	9310.009	7719.335	8390.224	3662.3731	RS	t	s

References

Abele, G., 1974, Bergstürze in den Alpen, ihre Verbreitung, Morphologie und Folgeerscheinungen.

Alavi, M., 2004, Regional stratigraphy of the Zagros fold-thrust belt of Iran and its proforeland evolution: American Journal of Science, v. 304, no. 1, p. 1–20, doi: 10.2475/ajs.304.1.1.

Alcántara-Ayala, I., and Goudie, A.S., 2010, Geomorphological Hazards and Disaster Prevention: Cambridge University Press.

Alexander, D.C., 1993, Natural Disasters: CRC Press.

Alexander, D.E., 2004, Natural hazards on an unquiet Earth, *in* Matthews, J.A. ed., Unifying Geography: Common Heritage, Shared Future, Routledge, London, p. 266–282.

Alimohammadi, B., 2005, landslide zonation map in the Barmahan catchment, Neishabur: Ferdowsi university of Mashhad.

Alipoor, R., Zaré, M., and Ghassemi, M.R., 2012, Inception of activity and slip rate on the Main Recent Fault of Zagros Mountains, Iran: Geomorphology, v. 175–176, p. 86–97, doi: 10.1016/j.geomorph.2012.06.025.

Allen, M.B., Saville, C., Blanc, E.J.-P., Talebian, M., and Nissen, E., 2013, Orogenic plateau growth: Expansion of the Turkish-Iranian Plateau across the Zagros fold-and-thrust belt: Tectonics, v. 32, no. 2, p. 171–190, doi: 10.1002/tect.20025.

Antonini, G., Ardizzone, F., Cardinali, M., Galli, M., Guzzetti, F., and Reichenbach, P., 2002, Surface deposits and landslide inventory map of the area affected by the 1997 Umbria-Marche earthquakes: Bollettino della Società Geologica Italiana, v. 121, no. 1, p. 843–853.

ArcGIS Blog Understanding curvature rasters,.

ArcGIS Desktop.

Authemayou, C., Bellier, O., Chardon, D., Malekzade, Z., and Abassi, M., 2005, Role of the Kazerun fault system in active deformation of the Zagros fold-and-thrust belt (Iran): Comptes Rendus Geoscience, v. 337, no. 5, p. 539–545, doi: 10.1016/j.crte.2004.12.007.

Azañón, J.M., Azor, A., Pérez-Peña, J.V., and Carrillo, J.M., 2005, Late Quaternary large-scale rotational slides induced by river incision: The Arroyo de Gor area (Guadix basin, SE Spain): Geomorphology, v. 69, no. 1–4, p. 152–168, doi: 10.1016/j.geomorph.2004.12.007.

Babakan, S., Zare, M., and Memarian, H., 2009, SEISMO-GEOTECHNICAL ZONATION MAPPING OF SOUTHERN CASPIAN SEA COASTLINE: v. 43, no. 3, p. 229–238.

Bailey, T.C., and Gatrell, A.C., 1998, Interactive Spatial Data Analysis: Buch: Longman Scientific & Technical.

Barnard, P.L., Owen, L.A., Sharma, M.C., and Finkel, R.C., 2001, Natural and human-induced landsliding in the Garhwal Himalaya of northern India: Geomorphology, v. 40, no. 1–2, p. 21–35, doi: 10.1016/S0169-555X(01)00035-6.

Baum, R.L., Harp, E.L., and Hultman, W.A., 2000, Map Showing Recent and Historic Landslide Activity on Coastal Bluffs of Puget Sound Between Shilshole Bay and Everett, Washington:.

Bayer, R., Chery, J., Tatar, M., Vernant, P., Abbassi, M., Masson, F., Nilforoushan, F., Doerflinger, E., Regard, V., and Bellier, O., 2006, Active deformation in Zagros—Makran transition zone inferred from GPS measurements: Geophysical Journal International, v. 165, no. 1, p. 373–381, doi: 10.1111/j.1365-246X.2006.02879.x.

Beavers, A.S., Lounsbury, J.W., Richards, J.K., Huck, S.W., Skolits, G.J., and Esquivel, S.L., 2013, Practical Considerations for Using Exploratory Factor Analysis in Educational Research:.

Beniston, M., Stoffel, M., and Hill, M., 2011, Impacts of climatic change on water and natural hazards in the Alps: Can current water governance cope with future challenges? Examples from the European "ACQWA" project: Environmental Science & Policy, v. 14, no. 7, p. 734–743, doi: 10.1016/j.envsci.2010.12.009.

Berberian, M., 1995, Master "blind" thrust faults hidden under the Zagros folds: active basement tectonics and surface morphotectonics: Tectonophysics, v. 241, no. 3–4, p. 193–224, doi: 10.1016/0040-1951(94)00185-C.

Berger, W.H., 1990, The younger dryas cold spell—a quest for causes: Global and Planetary Change, v. 3, no. 3, p. 219–237, doi: 10.1016/0921-8181(90)90018-8.

Bishop, M.P., Shroder Jr., J.F., and Colby, J.D., 2003, Remote sensing and geomorphometry for studying relief production in high mountains: Geomorphology, v. 55, no. 1–4, p. 345–361, doi: 10.1016/S0169-555X(03)00149-1.

Bobek, H., 1963, Nature and implications of Quaternary Climatic changes in Iran, *in* Changes of climate, UNESCO and the World Meteorological Organization, p. 403–413.

Bolourchi, M.J., and Ansari, F., 1998, Rock avalanche of Abikar- Karkan-e-olya village (Chahar Mahaal and Bakhtiari province):.

Bouchon, M., 1973, Effect of topography on surface motion: Bulletin of the Seismological Society of America, v. 63, no. 2, p. 615–632.

Brabb, E., 1991, The world landslide problem: Episodes, v. 14, p. 52–61.

Brabb, E.E., and Harrod, B.L. (Eds.), 1989, Landslides Extent & Econ Significance: Taylor & Francis.

Brardinoni, F., and Church, M., 2004, Representing the landslide magnitude–frequency relation: Capilano River basin, British Columbia: Earth Surface Processes and Landforms, v. 29, no. 1, p. 115–124, doi: 10.1002/esp.1029.

Brunetti, M.T., Guzzetti, F., and Rossi, M., 2009, Probability distributions of landslide volumes: Nonlinear Processes in Geophysics, v. 16, p. 179–188.

Buehler, D.M., Versteegh, M.A., Matson, K.D., and Tieleman, B.I., 2011, One Problem, Many Solutions: Simple Statistical Approaches Help Unravel the Complexity of the Immune System in an Ecological Context: PLoS ONE, v. 6, no. 4, p. e18592, doi: 10.1371/journal.pone.0018592.

Burns, S.J., Matter, A., Frank, N., and Mangini, A., 1998, Speleothem-based paleoclimate record from northern Oman: Geology, v. 26, no. 6, p. 499–502, doi: 10.1130/0091-7613(1998)026<0499:SBPRFN>2.3.CO;2.

Burroughs, S.M., and Tebbens, S.F., 2001, Upper-truncated Power Laws in Natural Systems: pure and applied geophysics, v. 158, no. 4, p. 741–757, doi: 10.1007/PL00001202.

Burt, J.E., and Barber, G.M., 1996, Elementary Statistics for Geographers: Guilford Press.

Cattell, R.B., 1966, The Scree Test For The Number Of Factors: Multivariate Behavioral Research, v. 1, no. 2, p. 245–276, doi: 10.1207/s15327906mbr0102_10.

Charman, J.H., and Griffiths, J.S., 1993, Natural Disasters: Protecting Vulnerable Communities : Proceedings of the Conference Held in London, 13-15 October 1993 (P. A. Merriman & C. W. A. Browitt, Eds.): Thomas Telford.

Chen, W.-F., and Duan, L. (Eds.), 2014, Bridge Engineering Handbook, Second Edition: Substructure Design: CRC Press.

Chen, Z., Zhang, J.-M., Ho, K., Wu, F.-Q., and Li, Z.-K., 2008, Landslides and Engineered Slopes. From the Past to the Future, Two Volumes + CD-ROM: Proceedings of the 10th International Symposium on Landslides and Engineered Slopes, 30 June - 4 July 2008, Xi'an, China: CRC Press.

Chu, D., and Gordon, R.G., 1998, Current plate motions across the Red Sea: Geophysical Journal International, v. 135, no. 2, p. 313 – 328, doi: 10.1046/j.1365-246X.1998.00658.x.

Clark, P.J., and Evans, F.C., 1954, Distance to Nearest Neighbor as a Measure of Spatial Relationships in Populations: Ecology, v. 35, no. 4, p. 445–453, doi: 10.2307/1931034.

Coe, J.A., Godt, J.W., Baum, R.L., Bucknam, R.C., and Michael, J.A., 2004, Landslide susceptibility from topography in Guatemala, *in* Landslides: Evaluation and Stabilization/Glissement de Terrain: Evaluation et Stabilisation, Set of 2 Volumes, CRC Press, p. 69–78.

Colman-Sadd, S.P., 1978, Fold Development in Zagros Simply Folded Belt, Southwest Iran: AAPG Bulletin, v. 62, no. 6, p. 984–1003.

Cressie, N.A.C., 1991, Statistics for spatial data: J. Wiley.

Crozier, M.J., 1986, Landslides: Causes, Consequences and Environment: Routledge Kegan & Paul, London; New York.

Cruden, D.., and Varnes, D.., 1996, Landslides: investigation and mitigation (A. K. Turner & R. L. Schuster, Eds.): National Academy Press.

D'agostino, R.B., and Russell, H.K., 2005, Scree Test, *in* Encyclopedia of Biostatistics, John Wiley & Sons, Ltd.

Dai, F.., and Lee, C.., 2002, Landslide characteristics and slope instability modeling using GIS, Lantau Island, Hong Kong: Geomorphology, v. 42, no. 3–4, p. 213–228, doi: 10.1016/S0169-555X(01)00087-3.

Davis, L.L., and West, L.R., 1973, Observed effects of topography on ground motion: Bulletin of the Seismological Society of America, v. 63, no. 1, p. 283–298.

Densmore, A.L., Anderson, R.S., McAdoo, B.G., and Ellis, M.A., 1997, Hillslope Evolution by Bedrock Landslides: Science, v. 275, no. 5298, p. 369–372, doi: 10.1126/science.275.5298.369.

Densmore, A.L., Ellis, M.A., and Anderson, R.S., 1998, Landsliding and the evolution of normal-fault-bounded mountains: Journal of Geophysical Research: Solid Earth, v. 103, no. B7, p. 15203–15219, doi: 10.1029/98JB00510.

Dussauge, C., Grasso, J.-R., and Helmstetter, A., 2003, Statistical analysis of rockfall volume distributions: Implications for rockfall dynamics: Journal of Geophysical Research: Solid Earth, v. 108, no. B6, p. n/a–n/a, doi: 10.1029/2001JB000650.

Dussauge-Peisser, C., Helmstetter, A., Grasso, J.-R., Hantz, D., Desvarreux, P., Jeannin, M., and Giraud, A., 2002, Probabilistic approach to rock fall hazard assessment: potential of historical data analysis: Natural Hazards and Earth System Sciences, v. 2, no. 1/2, p. 15–26, doi: 10.5194/nhess-2-15-2002.

Dykes, A.P., and Warburton, J., 2008, Characteristics of the Shetland Islands (UK) peat slides of 19 September 2003: Landslides, v. 5, no. 2, p. 213–226, doi: 10.1007/s10346-008-0114-7.

Earickson, R.J., and Harlin, J.M., 1994, Geographic Measurement and Quantitative Analysis: Prentice Hall, New York : Toronto : New York.

Ebdon, D., 1985, Statistics in Geography Second Edition: A Practical Approach: Wiley-Blackwell, Oxford Oxfordshire ; New York, NY, USA.

Erismann, T.H., and Abele, G., 2001, Dynamics of Rockslides and Rockfalls: Springer.

Faris, F., and Wang, F., 2014, Stochastic analysis of rainfall effect on earthquake induced shallow landslide of Tandikat, West Sumatra, Indonesia: Geoenvironmental Disasters, v. 1, no. 1, p. 1–13, doi: 10.1186/s40677-014-0012-3.

Ferrigno, J.G., 1988, Glaciers of the Middle East and Africa - GLACIERS OF IRAN: , p. 31–47.

Fleitmann, D., 2001, Annual to Millennial Indian Ocean Monsoon Variability Recorded in Holocene and Pleistocene Stalagmites from Oman:.

Fleitmann, D., Burns, S.J., Mudelsee, M., Neff, U., Kramers, J., Mangini, A., and Matter, A., 2003, Holocene Forcing of the Indian Monsoon Recorded in a Stalagmite from Southern Oman: Science, v. 300, no. 5626, p. 1737–1739, doi: 10.1126/science.1083130.

Forests, range and watershed management organization of Iran.

Galli, M., Ardizzone, F., Cardinali, M., Guzzetti, F., and Reichenbach, P., 2008, Comparing landslide inventory maps: Geomorphology, v. 94, no. 3–4, p. 268–289, doi: 10.1016/j.geomorph.2006.09.023.

Garson, G.D., 2013, Factor Analysis: Statistical Associates Publishers.

Geli, L., Bard, P.-Y., and Jullien, B., 1988, The effect of topography on earthquake ground motion: A review and new results: Bulletin of the Seismological Society of America, v. 78, no. 1, p. 42–63.

Getis, A., 1991, Spatial interaction and spatial autocorrelation: a cross product approach: Environment and Planning A, v. 23, no. 9, p. 1269–1277.

Getis, A., and Ord, J.K., 1992, The Analysis of Spatial Association by Use of Distance Statistics: Geographical Analysis, v. 24, no. 3, p. 189–206, doi: 10.1111/j.1538-4632.1992.tb00261.x.

Ghazipour, N., and Uromeihy, A., 2007, The use of Cone-Fall Theory for Evaluation of Rock-Fall Hazard along the Chaloos-Road(Pol-e-Zanguleh – Marzan-Abad): Journal of Geosciences, v. 17, no. 66, p. 160–169.

Griffiths, H.I., Schwalb, A., and Stevens, L.R., 2001, Evironmental change in southwestern Iran: the Holocene ostracod fauna of Lake Mirabad: The Holocene, v. 11, no. 6, p. 757–764, doi: 10.1191/09596830195771.

Grunert, J., CARLS, H.-G., and PREU, C., 1978, Rezente Vergletscherungen in zentraliranischen Hochgebirgen: Issuu, v. 28, p. 148–166.

Grützner, C., Fernández-Steeger, T.M., Reicherter, K.R., Müller, D., Rodríguez Bouzo, L., and Silva, P.G., 2008, Historic and prehistoric landslides and rock falls in the Bolonia Bay region/SW Spain:.

Guzzetti, F., Ardizzone, F., Cardinali, M., Rossi, M., and Valigi, D., 2009a, Landslide volumes and landslide mobilization rates in Umbria, central Italy: Earth and Planetary Science Letters, v. 279, no. 3–4, p. 222–229, doi: 10.1016/j.epsl.2009.01.005.

Guzzetti, F., Ardizzone, F., Cardinali, M., Rossi, M., and Valigi, D., 2009b, Landslide volumes and landslide mobilization rates in Umbria, central Italy: Earth and Planetary Science Letters, v. 279, no. 3-4, p. 222–229, doi: 10.1016/j.epsl.2009.01.005.

Guzzetti, F., Ardizzone, F., Cardinali, M., Rossi, M., and Valigi, D., 2009c, Landslide volumes and landslide mobilization rates in Umbria, central Italy: Earth and Planetary Science Letters, v. 279, no. 3–4, p. 222–229, doi: 10.1016/j.epsl.2009.01.005.

Guzzetti, F., Carrara, A., Cardinali, M., and Reichenbach, P., 1999a, Landslide hazard evaluation: a review of current techniques and their application in a multi-scale study, Central Italy: Geomorphology, v. 31, no. 1–4, p. 181–216, doi: 10.1016/S0169-555X(99)00078-1.

Guzzetti, F., Malamud, B.D., Turcotte, D.L., and Reichenbach, P., 2002, Power-law correlations of landslide areas in central Italy: Earth and Planetary Science Letters, v. 195, no. 3–4, p. 169–183, doi: 10.1016/S0012-821X(01)00589-1.

Guzzetti, F., Mondini, A.C., Cardinali, M., Fiorucci, F., Santangelo, M., and Chang, K.-T., 2012, Landslide inventory maps: New tools for an old problem: Earth-Science Reviews, v. 112, no. 1–2, p. 42–66, doi: 10.1016/j.earscirev.2012.02.001.

Guzzetti, F., Reichenbach, P., and Wieczorek, G.F., 1999b, Rockfall hazard and risk assessment in the Yosemite Valley, California, USA: Nat. Hazards Earth Syst. Sci., v. 3, no. 6, p. 491–503, doi: 10.5194/nhess-3-491-2003.

Hack, J.T., and Goodlett, J.C., 1960, Geomorphology and forest ecology of a mountain region in the central Appalachians: United States Geological Survey PP - 347.

Haflidason, H., Lien, R., Sejrup, H.P., Forsberg, C.F., and Bryn, P., 2005, The dating and morphometry of the Storegga Slide: Marine and Petroleum Geology, v. 22, no. 1–2, p. 123–136, doi: 10.1016/j.marpetgeo.2004.10.008.

Hampton, M.A., Lee, H.J., and Locat, J., 1996, Submarine landslides: Reviews of Geophysics, v. 34, no. 1, p. 33–59, doi: 10.1029/95RG03287.

Harp, E.L., and Jibson, R.W., 1996, Landslides triggered by the 1994 Northridge, California, earthquake: Bulletin of the Seismological Society of America, v. 86, no. 1B, p. S319–S332.

Harrison, J.V., and Falcon, N.L., 1938, An Ancient Landslip at Saidmarreh in Southwestern Iran: The Journal of Geology, v. 46, no. 3, p. 296–309, doi: 10.2307/30081302.

Hart, A.B., 2004, LANDSLIDE INVESTIGATION IN THE RÍO AGUAS CATCHMENT, SOUTHEAST SPAIN:.

Hatcher, L., and O'Rourke, N., 2013, A Step-by-step Approach to Using SAS for Factor Analysis and Structural Equation Modeling: SAS Institute.

Hayashi, J.N., and Self, S., 1992, A comparison of pyroclastic flow and debris avalanche mobility: Journal of Geophysical Research: Solid Earth, v. 97, no. B6, p. 9063–9071, doi: 10.1029/92JB00173.

Hewitt, K., Clague, J.J., and Orwin, J.F., 2008, Legacies of catastrophic rock slope failures in mountain landscapes: Earth-Science Reviews, v. 87, no. 1–2, p. 1–38, doi: 10.1016/j.earscirev.2007.10.002.

Hoelzmann, P., Gasse, F., Dupont, L.M., Salzmann, U., Staubwasser, M., Leuschner, D.C., and Sirocko, F., 2004, Palaeoenvironmental changes in the arid and sub arid belt (Sahara-Sahel-Arabian Peninsula) from 150 kyr to present, *in* Battarbee, R.W., Gasse, F., and Stickley, C.E. eds., Past Climate Variability through Europe and Africa, Developments in Paleoenvironmental Research 6, Springer Netherlands, p. 219–256.

Hovius, N., Stark, C.P., and Allen, P.A., 1997, Sediment flux from a mountain belt derived by landslide mapping: Geology, v. 25, no. 3, p. 231–234, doi: 10.1130/0091-7613(1997)025<0231:SFFAMB>2.3.CO;2.

Hungr, O., Leroueil, S., and Picarelli, L., 2013, The Varnes classification of landslide types, an update: Landslides, v. 11, no. 2, p. 167–194, doi: 10.1007/s10346-013-0436-y.

Imaizumi, F., and Sidle, R.C., 2007, Linkage of sediment supply and transport processes in Miyagawa Dam catchment, Japan: Journal of Geophysical Research: Earth Surface, v. 112, no. F3, p. n/a–n/a, doi: 10.1029/2006JF000495.

Innes, J.L., 1983, Lichenometric dating of debris-flow deposits in the Scottish Highlands: Earth Surface Processes and Landforms, v. 8, no. 6, p. 579–588, doi: 10.1002/esp.3290080609.

International Institute of Earthquake Engineering and Seismology - Geotechnical Engineering Research International Institute of Earthquake Engineering and Seismology - Geotechnical Engineering Research,.

Iverson, R.M., 1997, The physics of debris flows: Reviews of Geophysics, v. 35, no. 3, p. 245–296, doi: 10.1029/97RG00426.

Iverson, R.M., Schilling, S.P., and Vallance, J.W., 1998, Objective delineation of lahar-inundation hazard zones: v. 110, no. 8, p. 972–984.

Jackson, J.A., 1980, Reactivation of basement faults and crustal shortening in orogenic belts: Nature, v. 283, no. 5745, p. 343–346, doi: 10.1038/283343a0.

Jibson, R.W., Harp, E.L., Schulz, W., and Keefer, D.K., 2004, Landslides Triggered by the 2002 Denali Fault, Alaska, Earthquake and the Inferred Nature of the Strong Shaking: Earthquake Spectra, v. 20, no. 3, p. 669–691, doi: 10.1193/1.1778173.

J. S. Scheingross, B.M.M., 2013, Fault-zone controls on the spatial distribution of slow-moving landslides: Geological Society of America Bulletin, v. 125, no. 3-4, p. 473–489, doi: 10.1130/B30719.1.

Kaiser, H.F., 1960, The Application of Electronic Computers to Factor Analysis: Educational and Psychological Measurement, v. 20, no. 1, p. 141–151, doi: 10.1177/001316446002000116.

Katz, O., Aharonov, E., and Morgan, J.K., 2008, Controls on landslides size-distribution: relationships between area and volume of landslides in homogeneous material from slope-stability and discrete element calculations: AGU Fall Meeting Abstracts, v. -1, p. 06.

Keefer, D.K., 1984, Landslides caused by earthquakes: Geological Society of America Bulletin, v. 95, no. 4, p. 406–421, doi: 10.1130/0016-7606(1984)95<406:LCBE>2.0.CO;2.

Keefer, D.K., 1994, The importance of earthquake-induced landslides to long-term slope erosion and slope-failure hazards in seismically active regions: Geomorphology, v. 10, no. 1–4, p. 265–284, doi: 10.1016/0169-555X(94)90021-3.

Kehl, M., 2009, Quaternary climate change in Iran - the state of knowledge.: Erdkunde, v. 63, no. 1, p. 1–17, doi: 10.3112/erdkunde.2009.01.01.

Kharazipour, A., 2008, Review of Forests, Wood Products and Wood Biotechnology of Iran and Germany: Universitätsverlag Göttingen.

Khoshbakht, K., 2006, Agrobiodiversity of Plant Genetic Resources in Savadkouh, Iran, with Emphasis on Plant Uses and Socioeconomic Aspects: kassel university press GmbH.

Komak panah, A., Montazeralghaem, S., and Chodani, A., 1994, Landslide zonation in Iran, landslide and a review of landslides in iran.: International Institute of earthquake engineering and seismology (IIEES).

Korup, O., 2005, Distribution of landslides in southwest New Zealand: Landslides, v. 2, no. 1, p. 43–51, doi: 10.1007/s10346-004-0042-0.

Korup, O., Clague, J.J., Hermanns, R.L., Hewitt, K., Strom, A.L., and Weidinger, J.T., 2007, Giant landslides, topography, and erosion: Earth and Planetary Science Letters, v. 261, no. 3–4, p. 578–589, doi: 10.1016/j.epsl.2007.07.025.

Korup, O., Densmore, A.L., and Schlunegger, F., 2010, The role of landslides in mountain range evolution: Geomorphology, v. 120, no. 1–2, p. 77–90, doi: 10.1016/j.geomorph.2009.09.017.

Lacoste, A., Vendeville, B.C., and Loncke, L., 2011, Influence of combined incision and fluid overpressure on slope stability: Experimental modelling and natural applications: Journal of Structural Geology, v. 33, no. 4, p. 731–742, doi: 10.1016/j.jsg.2011.01.016.

Landslide.blogfa.com Landslide profesional website,.

Larsen, I.J., Montgomery, D.R., and Korup, O., 2010, Landslide erosion controlled by hillslope material: Nature Geoscience, v. 3, no. 4, p. 247–251, doi: 10.1038/ngeo776.

Larsen, M.C., and Torres-Sanchez, A.J., 1996, Geographic relations of landslide distribution and assessment of landslide hazards in the Blanco, Cibuco, and Coamo basins, Puerto Rico: United States Geological Survey WRI - 95-4029.

Larsen, M.C., and Torres-Sanchez, A.J., 1998, The frequency and distribution of recent landslides in three montane tropical regions of Puerto Rico:.

Lee, S., and Pradhan, B., 2006, Probabilistic landslide hazards and risk mapping on Penang Island, Malaysia: Journal of Earth System Science, v. 115, no. 6, p. 661–672, doi: 10.1007/s12040-006-0004-0.

Lee, J., and Wong, D.W.S., 2001, Statistical Analysis with ArcView GIS: John Wiley & Sons.

Legorreta Paulin, G., 2007, Assessment of landslides susceptibility: STATE UNIVERSITY OF NEW YORK AT BUFFALO.

Legros, F., 2002, The mobility of long-runout landslides: Engineering Geology, v. 63, no. 3–4, p. 301–331, doi: 10.1016/S0013-7952(01)00090-4.

Malamud, B.D., Turcotte, D.L., Guzzetti, F., and Reichenbach, P., 2004, Landslide inventories and their statistical properties: Earth Surface Processes and Landforms, v. 29, no. 6, p. 687–

Martin, Y., Rood, K., Schwab, J.W., and Church, M., 2002, Sediment transfer by shallow landsliding in the Queen Charlotte Islands, British Columbia: Canadian Journal of Earth Sciences, v. 39, no. 2, p. 189–205, doi: 10.1139/e01-068.

McClusky, S., Reilinger, R., Mahmoud, S., Ben Sari, D., and Tealeb, A., 2003, GPS constraints on Africa (Nubia) and Arabia plate motions: Geophysical Journal International, v. 155, no. 1, p. 126–138, doi: 10.1046/j.1365-246X.2003.02023.x.

McEwen, A.S., 1989, Mobility of large rock avalanches: Evidence from Valles Marineris, Mars: Geology, v. 17, no. 12, p. 1111–1114, doi: 10.1130/0091-7613(1989)017<1111:MOLRAE>2.3.CO;2.

McQuarrie, N., 2004, Crustal scale geometry of the Zagros fold–thrust belt, Iran: Journal of Structural Geology, v. 26, no. 3, p. 519–535, doi: 10.1016/j.jsg.2003.08.009.

Miller, S.A., 2007, Geographical information systems (GIS) applied to landslide hazard mapping and evaluation in north-east Wales [Ph.D.]: University of Liverpool.

Miller, F.P., Vandome, A.F., and McBrewster, J., 2010, Causes of Landslides: Alphascript Publishing.

Mitchell, A., 2005, ESRI Guide to GIS Analysis, Volume 2: Spatial Measurements and Statistics: Esri Pr.

Moeyersons, J., Trefois, P., Nahimana, L., Ilunga, L., Vandecasteele, I., Byizigiro, V., and Sadiki, S., 2010, River and landslide dynamics on the western Tanganyika rift border, Uvira, D.R. Congo: diachronic observations and a GIS inventory of traces of extreme geomorphologic activity: Natural Hazards, v. 53, no. 2, p. 291–311, doi: 10.1007/s11069-009-9430-z.

Montgomery, D.R., and Brandon, M.T., 2002, Topographic controls on erosion rates in tectonically active mountain ranges: Earth and Planetary Science Letters, v. 201, no. 3-4, p. 481–489.

Moore, I.D., Grayson, R.B., and Ladson, A.R., 1991, Digital terrain modelling: A review of hydrological, geomorphological, and biological applications: Hydrological Processes, v. 5, no. 1, p. 3–30, doi: 10.1002/hyp.3360050103.

Muscheler, R., Kromer, B., Björck, S., Svensson, A., Friedrich, M., Kaiser, K.F., and Southon, J., 2008, Tree rings and ice cores reveal 14C calibration uncertainties during the Younger Dryas: Nature Geoscience, v. 1, no. 4, p. 263–267, doi: 10.1038/ngeo128.

Nettleton, W.D., and Chadwick, O.A., 1996, Late Quaternary, redeposited loess-soil developmental sequences, South Yemen: Geoderma, v. 70, no. 1, p. 21–36, doi: 10.1016/0016-7061(95)00063-1.

Newman, M.E.J., 2005, Power laws, Pareto distributions and Zipf's law: Contemporary Physics, v. 46, no. 5, p. 323–351, doi: 10.1016/j.cities.2012.03.001.

Ohlmacher, G.C., 2007, Plan curvature and landslide probability in regions dominated by earth flows and earth slides: Engineering Geology, v. 91, p. 117–134, doi: 10.1016/j.enggeo.2007.01.005.

Ohlmacher, G.C., and Davis, J.C., 2003, Using multiple logistic regression and GIS technology to predict landslide hazard in northeast Kansas, USA: Engineering Geology, v. 69, no. 3–4, p. 331–343, doi: 10.1016/S0013-7952(03)00069-3.

Othman, A.A., and Gloaguen, R., 2013, River Courses Affected by Landslides and Implications for Hazard Assessment: A High Resolution Remote Sensing Case Study in NE Iraq–W Iran:.

Pachur, H.-J., and Hoelzmann, P., 1991, Paleoclimatic implications of late quaternary lacustrine sediments in Western Nubia, Sudan: Quaternary Research, v. 36, no. 3, p. 257–276, doi: 10.1016/0033-5894(91)90002-M.

Pearce, C., Seidenkrantz, M.-S., Kuijpers, A., Masse, G., Reynisson, N.F., and Kristiansen, S.M., 2013, Ocean lead at the termination of the Younger Dryas cold spell: Nature Communications, v. 4, p. 1664, doi: 10.1038/ncomms2686.

Pelletier, J.D., 1997, Scale-invariance of soil moisture variability and its implications for the frequency-size distribution of landslides: arXiv:physics/9705035,.

Pett, M.A., Lackey, N.R., and Sullivan, J.J., 2003, Making Sense of Factor Analysis: The Use of Factor Analysis for Instrument Development in Health Care Research: SAGE Publications, Inc, Thousand Oaks, Calif.

Pias, M.J., 1972, Signification geologique pedologique et paleoclimatique de formations paleolacustres et detaiques au Seistan (Afghanistan meridional), *in* Comptes rendus hebdomadaires des séances de l'Académie des sciences., D.sciences naturelles, Gauthier-Villars (Paris), p. 1143–1146.

Pinet, P., and Souriau, M., 1988, Continental erosion and large-scale relief: Tectonics, v. 7, no. 3, p. 563–582, doi: 10.1029/TC007i003p00563.

Pirouz, M., 2013, The geometry and sedimentary record of tectonics in the Neogene Zagros foreland basin: University of Geneva.

Pirouz, M., Simpson, G., Bahroudi, A., and Azhdari, A., 2011, Neogene sediments and modern depositional environments of the Zagros foreland basin system: Geological Magazine, v. 148, no. 5-6, p. 838–853, doi: 10.1017/S0016756811000392.

Prellwitz, R.W., Koler, T.E., and Steward, J.E., 1994, Slope stability reference guide for national forests in the United States (D. E. Hall, M. T. Long, & M. D. Remboldt, Eds.): For sale by U.S. G.P.O., Supt. of Docs, Washington, DC.

Rajabi, A.M., Mahdavifar, M.R., Khamehchiyan, M., and Gaudio, V.D., 2011, A new empirical estimator of coseismic landslide displacement for Zagros Mountain region (Iran): Natural Hazards, v. 59, no. 2, p. 1189–1203, doi: 10.1007/s11069-011-9829-1.

Ramsey, L.A., Walker, R.T., and Jackson, J., 2008, Fold evolution and drainage development in the Zagros mountains of Fars province, SE Iran: Basin Research, v. 20, no. 1, p. 23–48, doi: 10.1111/j.1365-2117.2007.00342.x.

Al-Rawi, Y.T., Al-Tawash, B.S., and Al-Ameri, T.K., 2005, POLLEN EVIDENCE OF LATE QUATERNARY VEGETATION AND INFERRED CLIMATIC CHANGES OF LAKE RAZZAZA, WESTERN IRAQI DESERT: Iraq Academic Scientific Journals, v. 1, no. 2, p. 1–13.

Reid, L.M., and Page, M.J., 2002, Magnitude and frequency of landsliding in a large New Zealand catchment: Geomorphology, v. 49, no. 1–2, p. 71–88, doi: 10.1016/S0169-555X(02)00164-2.

Reneau, S.L., and Dietrich, W.E., 1987, The importance of hollows in debris flow studies; Examples from Marin County, California: Reviews in Engineering Geology, v. 7, p. 165–180, doi: 10.1130/REG7-p165.

Rice, R.M., Crobett, E.S., and Bailey, R.G., 1969, Soil Slips Related to Vegetation, Topography, and Soil in Southern California: Water Resources Research, v. 5, no. 3, p. 647–659, doi: 10.1029/WR005i003p00647.

Rice, R.M., and Foggin, G.T., 1971, Effect High Intensity Storms on Soil Slippage on Mountainous Watersheds in Southern California: Water Resources Research, v. 7, no. 6, p. 1485–1496, doi: 10.1029/WR007i006p01485.

Richard Dixon Oldham, 1899, ... Report on the Great Earthquake of 12th June 1897: K. Paul, Trench, Trübner & co.

Roberts, N.J., and Evans, S.G., 2013, The gigantic Seymareh (Saidmarreh) rock avalanche, Zagros Fold–Thrust Belt, Iran: Journal of the Geological Society, v. 170, no. 4, p. 685–700, doi: 10.1144/jgs2012-090.

Royston, J.P., 1982, An Extension of Shapiro and Wilk's W Test for Normality to Large Samples: Applied Statistics, v. 31, no. 2, p. 115, doi: 10.2307/2347973.

Safavi, S.M., and Mirsaneii, R., 2009, Landslide distribution map of Tehran province, *in* CIVILICA,.

Sassa, K., 1998, Environmental Forest Science: Proceedings of the IUFRO Division 8 Conference Environmental Forest Science, Held 19-23 October 1998, Kyoto Universisty, Japan: Springer.

Schuster, R., and Fleming, R., 1986, ECONOMIC LOSSES AND FATALITIES DUE TO LANDSLIDES.: United States Geological Survey, 11–28 p.

Shah, B.V., 1983, Is the environment becoming more hazardous? A global survey 1947 to 1980: Disasters, v. 7, no. 3, p. 202–209, doi: 10.1111/j.1467-7717.1983.tb00822.x.

Shapiro, S.S., and Wilk, M.B., 1965, An Analysis of Variance Test for Normality (Complete Samples): Biometrika, v. 52, no. 3/4, p. 591, doi: 10.2307/2333709.

Shayan, S., 2006, New Geomorphologic Observation on Dating an Old Grand Landslide, Seimareh (Kabir-Kuh), Zagros Mountains, Southwest Iran: Islamic sciences and the humanities, , no. 131, p. 71–92.

Shirani, K., and Seif, A., 2012, Landslide hazard zonation by using statistical methods (Pishkuh region in Fereydonshahe province): v. 22, no. 85, p. 149–158.

Shoaei, Z., Ghayoumian, J., and Sassa, K., 1998, The largest debris flow in the world, Seimareh landslide, western Iran., *in* Kluwer Academic Publishers, p. 553–561.

Simonett, D.., 1967, Landslide distribution and earthquakes in the Bewani and Torricelli Mountains, New Guinea, in: Landform studies from Australia and New Guinea; (J. N. Jennings & J. A. Mabbutt, Eds.): Australian National University Press, Canberra.

Singer, S.F., and Avery, D.T., 2007, Unstoppable Global Warming: Every 1,500 Years: Rowman & Littlefield Publishers.

Smith, S.L.J., 2010, Practical Tourism Research: CABI.

Stark, C.P., and Hovius, N., 2001, The characterization of landslide size distributions: Geophysical Research Letters, v. 28, no. 6, p. 1091–1094, doi: 10.1029/2000GL008527.

Stevens, J., 1986, Applied Multivariate Statistics for the Social Sciences: L. Erlbaum Associates Inc., Hillsdale, NJ, USA.

Stevens, L.R., Ito, E., Schwalb, A., and Wright Jr., H.E., 2006, Timing of atmospheric precipitation in the Zagros Mountains inferred from a multi-proxy record from Lake Mirabad, Iran: Quaternary Research, v. 66, no. 3, p. 494–500, doi: 10.1016/j.yqres.2006.06.008.

Stevens, L.R., Wright, H.E., and Ito, E., 2001, Proposed changes in seasonality of climate during the Lateglacial and Holocene at Lake Zeribar, Iran: The Holocene, v. 11, no. 6, p. 747–755, doi: 10.1191/09596830195762.

Takezawa, nagazumi, Uchida, T., and Ishizuka, T., 2012, Window size of slope relief on susceptibility of earthquake induced landslides:.

Talebian, M., and Jackson, J., 2004, A reappraisal of earthquake focal mechanisms and active shortening in the Zagros mountains of Iran: Geophysical Journal International, v. 156, no. 3, p. 506–526, doi: 10.1111/j.1365-246X.2004.02092.x.

Tatar, M., Hatzfeld, D., and Ghafory-Ashtiany, M., 2004, Tectonics of the Central Zagros (Iran) deduced from microearthquake seismicity: Geophysical Journal International, v. 156, no. 2, p. 255–266, doi: 10.1111/j.1365-246X.2003.02145.x.

Ten Brink, U.S., Geist, E.L., and Andrews, B.D., 2006, Size distribution of submarine landslides and its implication to tsunami hazard in Puerto Rico: Geophysical Research Letters, v. 33, no. 11, p. n/a–n/a, doi: 10.1029/2006GL026125.

Turner, A.K., and Schuster, R.L., 1996, Landslides: investigation and mitigation: National Academy Press.

VanDen Eeckhaut, M., Poesen, J., Govers, G., Verstraeten, G., and Demoulin, A., 2007, Characteristics of the size distribution of recent and historical landslides in a populated hilly region: Earth and Planetary Science Letters, v. 256, no. 3–4, p. 588–603, doi: 10.1016/j.epsl.2007.01.040.

Varnes, D.J., 1978, SLOPE MOVEMENT TYPES AND PROCESSES: Transportation Research Board Special Report, , no. 176.

Varnes, D.J., and Slopes, I.A. of E.G.C. on L. and O.M.M. on, 1984, Landslide hazard zonation: a review of principles and practice: Unesco.

Vernant, P., Nilforoushan, F., Hatzfeld, D., Abbassi, M.R., Vigny, C., Masson, F., Nankali, H., Martinod, J., Ashtiani, A., Bayer, R., Tavakoli, F., and Chéry, J., 2004, Present-day crustal deformation and plate kinematics in the Middle East constrained by GPS measurements in Iran and northern Oman: Geophysical Journal International, v. 157, no. 1, p. 381–398, doi: 10.1111/j.1365-246X.2004.02222.x.

Wagner, W., and Geyh, M.A., 1999, Application of environmental isotope methods for groundwater studies in the ESCWA region (Economic and Social Commission for Western Asia): Bundesanstalt für Geowissenschaften und Rohstoffe und den Staatlichen Geologischen Diensten in der Bundesrepublik Deutschland.

Walpersdorf, A., Hatzfeld, D., Nankali, H., Tavakoli, F., Nilforoushan, F., Tatar, M., Vernant, P., Chéry, J., and Masson, F., 2006, Difference in the GPS deformation pattern of North and Central Zagros (Iran): Geophysical Journal International, v. 167, no. 3, p. 1077–1088, doi: 10.1111/j.1365-246X.2006.03147.x.

Wang, Y., Li, Z., and Liu, S., 2013, A new model for optimizing relief window size, *in* p. 876817–876817–6.

White, E.P., Enquist, B.J., and Green, J.L., 2008, On estimating the exponent of power-law frequency distributions: Ecology, v. 89, no. 4, p. 905–912, doi: 10.1890/07-1288.1.

Whitehouse, I.E., 1983, Distribution of large rock avalanche deposits in the central Southern Alps, New Zealand: New Zealand Journal of Geology and Geophysics, v. 26, no. 3, p. 271–279, doi: 10.1080/00288306.1983.10422240.

Wieczorek, G.F., Snyder, J.B., Alger, C.S., and Issacson, K.A., 1992, Rock falls in Yosemite Valley, California: United States Geological Survey OFR - 92-387.

Witherick, M., Nagle, G., and Witherick, M.E., 1998, Skills and Techniques for Geography A-Level: Nelson Thornes.

Wright, H.E., 1961, Pleistocene glaciation in Kurdistan: Eiszeitalter und Gegenwart, v. 12, no. Godwin P46.1A, p. 131–164.

Xie, M., Esaki, T., Zhou, G., and Mitani, Y., 2003, Three-dimensional stability evaluation of landslides and a sliding process simulation using a new geographic information systems component: Environmental Geology, v. 43, no. 5, p. 503–512, doi: 10.1007/s00254-002-0655-3.

Yarahmadi, A. mohamad, Moghimi, E., Servati, M.R., and Kardavani, P., 2012, Geomorphologic Evidences of the influence of Glacier Sediments in Lake Formation Case Study: the Formation of Gahar Lake, in Iran: International research Journal of Applied and Basic Sciences, v. 3, no. 2, p. 224–233.

Van Zeist, W., 1967, Late quaternary vegetation history of western Iran: Review of Palaeobotany and Palynology, v. 2, no. 1–4, p. 301–311, doi: 10.1016/0034-6667(67)90159-5.

Zevenbergen, L.W., and Thorne, C.R., 1987, Quantitative analysis of land surface topography: Earth Surface Processes and Landforms, v. 12, no. 1, p. 47–56, doi: 10.1002/esp.3290120107.